DEVELOPMENT OF NANOPOROUS ALUMINUM PILLARED MONTMORILLONITE AND COPPER-DOPED ALUMINUM PILLARED MONTMORILLONITE FOR DYE-CONTAINING WASTEWATER TREATMENT

PRATYAPORN TEPMATEE

A THESIS SUBMITTED IN PARTIAL FULFILLMENT
OF THE REQUIREMENT FOR THE DEGREE OF
DOCTOR OF PHILOSOPHY IN NANOSCIENCE AND NANOTECHNOLOGY
COLLEGE OF NANOTECHNOLOGY
KING MONGKUT'S INSTITUTE OF TECHNOLOGY LADKRABANG
2015

KMITL-2015-NT-D-001-011

DEVELOPMENT OF NANOPOROUS ALUMINUM PILLARED MONTMORILLONITE AND COPPER-DOPED ALUMINUM PILLARED MONTMORILLONITE FOR DYE-CONTAINING WASTEWATER TREATMENT

PRATYAPORN TEPMATEE

A THESIS SUBMITTED IN PARTIAL FULFILLMENT
OF THE REQUIREMENT FOR THE DEGREE OF
DOCTOR OF PHILOSOPHY IN NANOSCIENCE AND NANOTECHNOLOGY
COLLEGE OF NANOTECHNOLOGY
KING MONGKUT'S INSTITUTE OF TECHNOLOGY LADKRABANG
2015
KMITL-2015-NT-D-001-011

การพัฒนาแร่ดินเหนียวอะลูมินัมพิลลาร์มอนต์มอริลโลไนต์และแร่ดินเหนียวอะลูมินัมพิลลาร์มอนต์มอริลโลไนต์เจือคอปเปอร์ที่มีรูพรุนระดับนาโนสำหรับการบำบัดน้ำเสียปนเปื้อนสีย้อม

DEVELOPMENT OF NANOPOROUS ALUMINUM PILLARED MONTMORILLONITE AND COPPER-DOPED ALUMINUM PILLARED MONTMORILLONITE FOR DYE-CONTAINING WASTEWATER TREATMENT

ปรัชญาพร เทพมะที
PRATYAPORN TEPMATEE

วิทยานิพนธ์นี้เป็นส่วนหนึ่งของการศึกษาตามหลักสูตรปริญญาปรัชญาดุษฎีบัณฑิต
สาขาวิชานาโนวิทยาและนาโนเทคโนโลยี
วิทยาลัยนาโนเทคโนโลยีพระจอมเกล้าลาดกระบัง
สถาบันเทคโนโลยีพระจอมเกล้าเจ้าคุณทหารลาดกระบัง
พ.ศ. 2558
KMITL-2015-NT-D-001-011

หัวข้อวิทยานิพนธ์	การพัฒนาแร่ดินเหนียวอะลูมินัมพิลลาร์มอนต์มอริลโลไนต์และแร่ดินเหนียวอะลูมินัมพิลลาร์มอนต์มอริลโลไนต์เจือคอปเปอร์ที่มีรูพรุนระดับนาโนสำหรับการบำบัดน้ำเสียปนเปื้อนสีย้อม
นักศึกษา	นางสาวปรัชญาพร เทพมะที
รหัสประจำตัว	52670154
ปริญญา	ปรัชญาดุษฎีบัณฑิต (ปร.ด.)
สาขาวิชา	นาโนวิทยาและนาโนเทคโนโลยี
พ.ศ.	2558
อาจารย์ที่ปรึกษาวิทยานิพนธ์	ผศ.ดร.ปุณณมา ศิริพันธ์โนน

บทคัดย่อ

งานวิจัยนี้ทำการเตรียมแร่ดินเหนียวอะลูมินัมพิลลาร์ (Alpill-MMTs) โดยดัดแปรโครงสร้างของแร่ดินเหนียวโซเดียมมอนต์มอริลโลไนต์ (Na^{+}-MMT) ด้วยสารละลายอะลูมินัม พอลิออกโซแคตไอออน (AlOH) และเจือคอปเปอร์(II)ออกไซด์ลงในแร่ดินเหนียว Alpill-MMTs (Cu-Alpill-MMTs) ในการเตรียมสารตั้งต้น AlOH จะได้ Al_{13}^{7+} พอลิออกโซแคตไอออนที่มีโครงสร้างแบบ ε-Al_{13} Keggin จากการเตรียมทั้งสองเทคนิค โดยเทคนิคปั่นกวนที่อุณหภูมิ 60 องศาเซลเซียส เป็นเวลา 24 ชั่วโมง และเทคนิคอัลตราโซนิคกำลังสูงที่อุณหภูมิห้อง เป็นเวลา 30 นาที เมื่อใช้อัตราส่วนโดยโมลระหว่าง OH/Al เท่ากับ 2.4 ในการศึกษาผลสภาวะที่ใช้ได้แก่ วิธีการอินเตอร์คาเลชัน (เทคนิคการปั่นกวนและเทคนิคอัลตราโซนิค) ในการเตรียม ได้แก่ วิธีการผสม (เทคนิคการปั่นกวนและเทคนิคอัลตราโซนิค) อุณหภูมิในการทำปฏิกิริยา (อุณหภูมิห้องและ 60 องศาเซลเซียส) และระยะเวลาที่ใช้ในการทำปฏิกิริยา (10, 20, 30 และ 60 นาที) ต่อประสิทธิภาพการอินเตอร์คาเลชันและลักษณะของ Alpill-MMTs พบว่า Alpill-MMT-2.4-Ultra มีปริมาณ Al_2O_3 สูงกว่า Alpill-MMT-2.4-Str และมีรูพรุนหลายขนาดในช่วง 3.8 – 30 นาโนเมตร เป็นผลให้มีพื้นที่ผิวจำเพาะสูงกว่า แต่ใช้ระยะเวลาในการสังเคราะห์ที่สั้นกว่า ทั้งนี้ Alpill-MMT-2.4-Str และ Alpill-MMT-2.4-Ultra ประกอบด้วย ε-Al_{13} Keggin ที่จัดเรียงตัวแบบไม่เป็นระเบียบและไม่สม่ำเสมอในระหว่างชั้นของ MMT จึงเกิดลักษณะโครงสร้างแบบ House of card

เมื่อนำแร่ดินเหนียวดัดแปรด้วย AlOH (AlOH-MMT) และ Alpill-MMTs มาเจือด้วยคอปเปอร์ (II) โดยใช้วิธีการดูดซับร่วมกับอัลตราโซนิค และวิธีการทำให้เปียกชุ่ม โดยวิธีแรกจะนำแร่ดินเหนียว AlOH-MMT และ Alpill-MMTs มาแช่ในสารละลาย $CuSO_4 \cdot 5H_2O$ เข้มข้น 0.4 โมล/ลิตรเป็นเวลา 30 นาที ในเครื่องอัลตราโซนิคพลังงานสูง จากนั้นนำไปเผาแคลไซน์ที่อุณหภูมิ 500 องศาเซลเซียส ได้เป็น Cu-ads-Alpill-MMT1 และ Cu-ads-Alpill-MMT2 ตามลำดับ ส่วนในวิธีทำให้เปียกชุ่มจะปรับเปลี่ยนปริมาณของคอปเปอร์ (II) ที่ใช้ในการเจือใน AlOH-MMT คือ 4, 7, 10 และ 13 เปอร์เซ็นต์โดยน้ำหนัก (wt%) และเมื่อนำไปเผาแคลไซน์ได้เป็น Cu-im-Alpill-MMTs จากการตรวจพิสูจน์เอกลักษณ์พบว่า Cu-Alpill-MMT1 และ Cu-im-Alpill-MMT-13wt% มีปริมาณ CuO แทรกตัวภายในรูพรุนมากที่สุด จึงส่งผลให้มีค่าพื้นที่ผิวจำเพาะ และปริมาตรรูพรุนต่ำที่สุด

ในการศึกษาประสิทธิภาพของสารดูดซับ Alpill-MMTs และ Cu-ads-Alpill-MMTs ในการกำจัดสารถูกดูดซับสีย้อม 2 ชนิด คือ Basic Yellow 1 (BY1) และ Reactive orange 16 (RO16) พบว่าแร่ดินเหนียว Alpill-MMTs และ Cu-ads-Alpill-MMTs มีความสามารถในการกำจัดสีย้อม BY1 สูง (>90 เปอร์เซ็นต์) แต่ความสามารถในการกำจัดสีย้อม RO16 ต่ำ (<5 เปอร์เซ็นต์) พฤติกรรมการดูดซับสีย้อม BY1 ของ Alpill-MMTs สอดคล้องกับสมการจลนศาสตร์แบบ Pseudo-second-order และไอโซเทอมการดูดซับแบบแลงเมียร์ ซึ่งแสดงถึงลักษณะการดูดซับทางเคมีที่เป็นการดูดซับแบบชั้นเดียว ภายหลัง Regeneration ด้วยความร้อนพบว่าประสิทธิภาพการดูดซับของ Alpill-MMTs มีค่าลดลงเล็กน้อย แต่ยิ่งผ่านการดูดซับและ Regeneration ซ้ำในจำนวนรอบที่มากขึ้นค่าความสามารถในการดูดซับก็จะลดลงตามไปด้วย สำหรับการดูดซับแบบกะ Alpill-MMT2.4-Ultra มีค่าเปอร์เซ็นต์การกำจัดและค่าความสามารถในการดูดซับ BY1 สูงที่สุด เมื่อนำสารดูดซับ Alpill-MMT2.4-Ultra ไปทำการดูดซับสีย้อม BY1 ที่ความเข้มข้น 300 มิลลิกรัม/ลิตร ในระบบการดูดซับแบบต่อเนื่อง พบว่าสารดูดซับมีค่าความสามารถในการดูดซับสีย้อม BY1 ต่ำกว่าระบบการดูดซับแบบกะเพียงเล็กน้อย

ในการศึกษาประสิทธิภาพการกำจัดสีย้อม RO16 ของ Cu-ads-Alpill-MMTs และ Cu-im-Alpill-MMTs ด้วยปฏิกิริยาเฟนทอน (Cu-Alpill-MMT/H_2O_2) และเฟน ทอนเชิงแสง (Cu-Alpill-MMT/H_2O_2/UV) พบว่าในปฏิกิริยาเฟนทอนเชิงแสงมีประสิทธิภาพในการกำจัดสีย้อมได้ 100 เปอร์เซ็นต์ แม้จะใช้ระยะเวลาในการทำปฏิกิริยาสั้นกว่าปฏิกิริยาเฟนทอนถึง 6 เท่า ซึ่ง Cu-Alpill-MMT1 มีประสิทธิภาพในการกำจัดที่สูงกว่า Cu-Alpill-MMT2 และ Cu-im-Alpill-MMTs นอกจากนี้ Cu-Alpill-MMT1 Cu-Alpill-MMT2 Cu-im-Alpill-MMT-10wt% และ Cu-im-Alpill-MMT-13wt% สามารถยับยั้งการเจริญเติบโตของเชื้อ *Eschericia coli* ATCC®25922 ได้เมื่อทดสอบตามมาตรฐาน JIS L1902:1998 (เชิงคุณภาพ) โดย Cu-im-Alpill-MMT-13wt% แสดงพื้นที่ปลอดเชื้อที่กว้างที่สุด

คำสำคัญ : โครงสร้างพิลลาร์ ตัวดูดซับ ปฏิกิริยาออกซิเดชัน มอนต์มอริลโลไนต์ วัสดุรูพรุนระดับนาโน

Thesis Title	Development of nanoporous aluminum pillared montmorillonite and copper-doped aluminum pillared montmorillonite for dye-containing wastewater treatment
Student	Miss Pratyaporn Tepmatee
Student ID	52670154
Degree	Doctor of Philosophy
Program	Nanoscience and Nanotechnology
Year	2015
Thesis Advisor	Asst. Prof. Dr. Punnama Siriphannon

ABSTRACT

This research prepared aluminum pillared montmorillonite (Alpill-MMTs) by structural modification of sodium montmorillonite (Na^+-MMT) with aluminum polyoxocation (AlOH) and doped the copper (II) oxide into the Alpill-MMT (Cu-Alpill-MMTs). In the preparation of AlOH precursor, the Al_{13}^{7+} polyoxocation having ε-Al_{13} Keggin structure was obtained in both stirring technique at 60°C for 24 hrs and high power ultrasonic at room temperature for 30 min using the molar ratio of OH/Al=2.4. The effects of preparation conditions, i.e. intercalation method (conventional stirring and ultrasonic assisted methods), reaction temperatures (room temperature and 60 °C) and reaction time (10, 20, 30 and 60 min), on the intercalation efficiency and characters of Alpill-MMTs were investigated. The characterization results indicated that the ultrasonic product of Alpill-MMT-2.4-Ultra possessed high content of Al_2O_3 with multiple pore sizes in the range of 3.8 – 30 nm, resulting in higher specific surface area (SSA) than that of Alpill-MMT-2.4-rt-Str stirring product, but it could be obtained in shorter processing time. Both of Alpill-MMT-2.4-rt-Str and Alpill-MMT-2.4-Ultra were composed of the random orientation and inhomogeneous distribution of ε-Al_{13} Keggin ions in the interlayer space of MMT, resulting in the house of card structure.

The AlOH modified MMT (AlOH-MMT) and Alpill-MMTs were doped with copper (II) ion by ultrasonic assisted adsorption and impregnation methods. In the ultrasonic assisted adsorption, the AlOH-MMT and Alpill-MMT precursors were soaked in 0.4 mol/l $CuSO_4 \cdot 5H_2O$ solution for 30 min with high power ultrasonic treatment. The Cu(II) doped products were calcined at 500°C in order to obtain the Cu-ads-Alpill-MMT1 and Cu-ads-Alpill-MMT2, respectively. In the impregnation method, the AlOH-

MMT was impregnated with the $CuSO_4 \cdot 5H_2O$ solution using various copper (II) loading, i.e. 4, 7, 10 and 13 wt%, and then calcined to obtained Cu-im-Alpill-MMTs. It was found that the Cu-ads-Alpill-MMT1 and Cu-im-Alpill-MMT-13wt% possessed the highest CuO content in their porous structures, resulting in the lowest of SSA and pore volume.

Efficiencies of dye removal of Alpill-MMTs and Cu-ads-Alpill-MMTs adsorbents were studied using 2 types of dye adsorbates, i.e. Basic Yellow 1 (BY1) and Reactive orange 16 (RO16). The Alpill-MMTs and Cu-ads-Alpill-MMTs exhibited high BY1 removal (>90%), but they hardly removed RO16 (<5%). The BY1 adsorption behavior of Alpill-MMTs was corresponded to pseudo-second-order kinetic equation and Langmuir adsorption isotherm, representing the chemisorption of monolayer adsorbate on the adsorbent. After thermal regeneration, the adsorption capacities of Alpill-MMTs were slightly decreased. The higher numbers of adsorption and regeneration, the lower adsorption capacities were obtained. The Alpill-MMT-2.4-Ultra exhibited the highest percentage of BY1 removal and adsorption capacity in the batch adsorption system. When the Alpill-MMT2.4-Ultra was used for removal 300 mg/l BY1 in the continuous adsorption system, the BY1 adsorption capacity was slightly lower than that in the batch adsorption system.

The efficiencies of Cu-ads-Alpill-MMT and Cu-im-Alpill-MMT for RO16 removal were studied using Fenton reaction (Cu-Alpill-MMT/H_2O_2) and photo-Fenton reaction (Cu-Alpill-MMT/H_2O_2/UV). The removal efficiency in the photo-Fenton reaction was 100% even using 6-fold shorter reaction time than the Fenton reaction, in which the Cu-ads-Alpill-MMT1 exhibited higher removal efficiency than the Cu-ads-Alpill-MMT2 and Cu-im-Alpill-MMTs. In addition, the Cu-ads-Alpill-MMT1, Cu-ads-Alpill-MMT2, Cu-im-Alpill-MMT-10wt% and Cu-im-Alpill-MMT-13wt% could inhibit the growth of *Eschericia coli* ATCC®25922 under JIS L 1902: 1998 (Qualitative) test method, in which the Cu-ads-Alpill-MMT1 presented the largest inhibition zone.

Keywords : Adsorbent, Catalytic oxidation reaction, Montmorillonite, Nanoporous materials, Pillared structure

Acknowledgment

The author would like to take this opportunity to express sincere thanks to their advisors and people who gave useful advice and full support in this research.

The author wishes to express them deep gratitude to Asst. Prof. Dr. Punnama Siriphannon for her valuable advice and encouragement throughout this research. It goes without saying to the special project committees, Prof. Dr. Jiti Nukeaw, Assoc. Prof. Dr. Wisanu Pecharapa, Asst. Prof. Dr. Apiluc Eiad-Ua and Asst. Prof. Dr. Dujreutai Pongkao Kashima for reading and criticizing the manuscript.

Special thanks to Development and Engineering (RD&E) fund through The National Nanotechnology Center (NANOTEC), Thailand (P-11-00225) to King Mongkut's Institute of Technology Ladkrabang (KMITL) for financial support from the research. We would like to thank the Scientific Instruments Service Center, Faculty of Science, KMITL, for XRD and XRF analyses. In addition, thanks also of College of KMITL Nanotechnology, KMITL, for instrument process and instrument analysis.

Miss Pratyaporn Tepmatee

CONTENT

CONTENT (CONT.)

CONTENT (CONT.)

CONTENT (CONT.)

LIST OF TABLES

LIST OF TABLES (CONT.)

LIST OF TABLES (CONT.)

LIST OF FIGURES

LIST OF FIGURES (CONT.)

LIST OF FIGURES (CONT.)

LIST OF FIGURES (CONT.)

Abbreviations

ABS	: Absorbencies
ε-Al_{13}-Keggin	: ε-Aluminum-Keggin
^{27}Al NMR	: ^{27}Al Nuclear magnetic resonance spectrometer
AlOH	: Aluminum polyoxocation
AlOH-MMT	: Aluminum polyoxocation montmorillonite
Alpill-MMT	: Aluminum pillared montmorillonite
Alpill-MMT-Str	: Aluminum pillared montmorillonite preparation by convention stirring method
Alpill-MMT-Ultra	: Aluminum pillared montmorillonite preparation by ultrasonic assisted method
BY 1	: Basic Yellow 1
CDBA	: Cetyl dimethyl benzyl ammonium chloride
CEC	: Cation exchange capacity
CR	: Congo red
CTAB	: Cetyl trimethyl ammonium bromide
Cu-Alpill-MMT	: Aluminum pillared montmorillonite doped copper
Cu-ads-Alpill-MMT	: Aluminum pillared montmorillonite doped copper preparation by ultrasonic assisted adsorption method
Cu-im-Alpill-MMT	: Aluminum pillared montmorillonite doped copper preparation by impregnation method
CWPO	: Catalytic Wet Peroxide Oxidation
BDDT	: Brunauer-Deming-Dewing-Teller
BET	: Brunauer-Emmett-Teller
BJH	: Barrett-Joyner-Halenda
d_{001}	: Basal spacing
E.coli	: Eschericia coli
IUPAC	: International Union of Pure and Applied Chemistry
Na^{+}-MMT	: Sodium-Montmorillonite
RO16	: Reactive orange 16
SEM-EDX	: Scanning electron microscope and energy dispersive spectroscopy
SSA	: Specific surface area
TOC	: Total organic carbon analyzer
UV-Vis	: UV-VIS spectrophotometer
XRD	: X-ray diffractrometer
XRF	: X-ray fluorescence spectroscopy

Chapter 1
Introduction

1.1 Introduction

Textile industry is a vast multi-sector industry ranging from production of yarn from plants or chemicals, weaving, bleaching, dyeing and finishing for properties' modification and the subsequent manufacture of clothing and apparels. Textile manufacturing industry, therefore, consumes high quantities of water and chemicals; consequently, it is one of the largest sources of water pollution. The excessive chemicals may contaminate to the public water system, in which some residual chemicals are toxic and harmful to living organisms and environment. Dyeing wastewater is one of the most important water pollution because dyes can create unsightly appearance and severely affect the aquatic life due to the reduction of light penetration and their toxicity [1-3].

Several treatment processes for dye removal have extensively been applied such as membrane filtration [4-5], ozone treatment [6-7], biodegradation [8-9] and ion exchange [10-11], however, their high cost and operation difficulty are the most important limitations. Adsorption is one of the most attractive methods because it possesses higher efficiency in dye removal from wastewater than the biological method and flexibility in design and operation than other methods. In the adsorption process, the contaminants in the wastewater will be adsorbed on the surface of adsorbents, in which several kinds of adsorbents have been developed such as fly ash [12], zeolite [13], chitosan [14], clay [15], activated carbon [16], etc. The activated carbon is the most popular adsorbent in various industries because it shows high surface area, resulting in high adsorption capacity. However, it is difficult to separate and regenerate the used activated carbon by chemical and thermal processes, leading to loss of adsorbent and high operating costs.

From this point of view, various natural adsorbents have been developed due to their availability and low costs. Clay minerals are one of the most attractive natural adsorbents for physicochemical treatment of wastewater since they possess not only the lamellar structure with high surface area providing a large number of adsorption sites, but also good thermal stability [17–19] and regenerability [20]. Although the application of clay adsorbents for residual dye removals from textile industrial effluents has attracted the attention due to their abundant resources and inexpensive, the adsorption capacities of clays for organic dye molecules might be limited by their small basal spaces. In order to improve the dye adsorption

efficiencies of clays, the interlayer spaces of clays have been modified by intercalation with large organic and/or inorganic molecules, such as chitosan [21], cetyltrimethylammonium bromide [22], hexadecyltrimethylammonium [23], polydiallydimethyl-ammonium [24], aluminum oxide [25–30], iron oxide [31], silica [32], etc. Although the organic intercalated clays exhibited high adsorption capacities for dye removals, the inorganic oxide intercalated clays owned various merits, e.g. multi-charged centers, high surface areas, large interlayer spaces, thermal stabilities, regenerability, etc [25].

In the present study, we have been interested in the aluminum oxide intercalated montmorillonite commonly known as aluminum pillared montmorillonite (Alpill-MMT) because the intercalated aluminum oxide possesses not only the previously described merits of inorganic oxide, but also the chemical stability and inertness [28]. It was, therefore, the structure and adsorption ability of Alpill-MMT would not change during adsorption treatment and/or after regeneration. In the previous studies, the Alpill-MMT was conventionally prepared by slow adding the base-hydrolyzed Al_{13} polyoxocations ($[AlO_4Al_{12}(OH)_{24}(OH_2)_{12}]^{7+}$, Al_{13}^{7+}) into the montmorillonite suspension. The Al_{13}^{7+} ions could intercalate into the interplanar spacing of MMT via cation exchange reaction and finally were calcined to form stable aluminum oxide pillared MMT [26-27, 29-30]. This conventional pillaring method requires long processing time especially in the base hydrolysis and intercalation steps and high quantity of water for MMT swelling. To overcome these drawbacks, the high power ultrasonic has been used in this research to accelerate the preparation of base hydrolyzed Al_{13}^{7+} and promote the simultaneous diffusion of Al_{13}^{7+} into the interlayer spacing of MMT, simplifying and shortening the intercalation process of MMT. The effects of ultrasound on structures of base hydrolyzed Al_{13}^{7+} ions and Alpill-MMT were investigated.

In addition, we have been interested in enhancing the decolorization efficiency of the Alpill-MMT by doping with copper (II) in the present study because the copper (II) could not only act as catalyst in advanced oxidation processes (AOPs) [33-34], but also antibacterial agent [35-36]. The AOPs are one of the most attractive and effective method for wastewater treatment because the AOPs have the ability to generate the highly reactive hydroxyl radicals (HO•) in which they can attack a wide variety of organic contaminants in wastewater, resulting in decolorization, degradation and mineralization to CO_2 and H_2O [37-39]. The copper (II) was selected as dopant in this work because it was claimed to have greater catalytic activity for AOPs than iron catalysts in some researches [40-41]. The decolorization activities of copper doped Alpill-MMT (Cu-Alpill-MMT) for basic and reactive dyes were

investigated in comparison with those of the starting Na^{+}-MMT and Alpill-MMT using three different treatment systems, i.e. batch adsorption, Fenton and photo Fenton.

1.2 Objectives

1.2.1 To study the effect of preparation parameters on structure and properties of aluminum pillared montmorillonite (Alpill-MMT) and aluminum pillared montmorillonite doped copper (Cu-Alpill-MMT)

1.2.2 To study the mechanisms and capabilities of Alpill-MMT and Cu-Alpill-MMT for dye removals

1.2.3 To determine the antibacterial activities of Alpill-MMT and Cu-Alpill-MMT

1.3 Scope of study

1.3.1 Preparation of aluminum pillared montmorillonite (Alpill-MMTs) nanoporous adsorbents from sodium montmorillonite (Na^{+}-MMT) and aluminum polyoxocations (Al_{13}^{7+}) solution using various parameters as follows:

- Molar ratio of OH/Al, i.e. 2.0 and 2.4
- Preparation method of aluminum polyoxocations, i.e. conventional stirring method and ultrasonic assisted method
- Reaction temperature of conventional stirring method, i.e. room temperature and 60 °C
- Reaction time of ultrasonic assisted method, i.e. 10, 20, 30 and 60 min

1.3.2 Preparation of copper doped aluminum pillared montmorillonite (Cu-Alpill-MMT) from Alpill-MMTs and copper solution various parameters as follows:

- Type of precursor, i.e. AlOH-MMT and Alpill-MMT
- Preparation method of Cu-Alpill-MMT, i.e. ultrasonic assisted adsorption and impregnation
- Weigh percent of copper dopant in impregnation method, i.e. 4, 7, 10 and 13 wt.%

1.3.3 Characterization of Alpill-MMTs and Cu-Alpill-MMTs by various techniques, i.e. X-ray fluorescence spectrometry (XRF), X-ray diffractometry (XRD), nitrogen adsorption, scanning electron microscope and energy dispersive spectroscopy (SEM-EDX)

1.3.4 Study on the mechanisms and capabilities of Alpill-MMT and Cu-Alpill-MMT for dye removals under various treatment systems as follows:

- Type of adsorbent, i.e. Alpill-MMTs and Cu-Alpill-MMTs
- Treatment method, i.e. Adsorption: batch and continuous method
  Catalytic oxidation: Fenton and photo Fenton reaction
- Type of dye solution, i.e. basic yellow 1 (BY1) and reactive orange 16 (RO16)
- Contact time in batch adsorption process
- Initial concentration in batch adsorption process
- Reaction time of Fenton and photo Fenton processes

1.3.5 Study on the thermal regeneration of the Alpill-MMT adsorbent

1.3.6 Study on the antibacterial activities of Alpill-MMT and Cu-Alpill-MMT

1.4 Expected Results

1.4.1 High efficiencies and economic nanoporous absorbents/catalysts can be produced from domestic clay minerals. These are value-adding of domestic clay minerals and reducing the import of expensive adsorbents.

1.4.2 These nanoporous clay absorbents/catalysts can be applied for treatment of textile industrial wastewater containing not only cationic dye molecules, but also anionic and reactive dye molecules.

1.4.3 Mechanisms of nanoporous clay absorbents/catalysts in dye removals can be applied for development of various wastewater treatment systems in order to eliminate the organic contaminants.

Chapter 2
Theory and Literature Review

2.1 Clay minerals

Clay has been used to indicate fine particle with a grain size less than 2 μm. Clay is an important group of the phyllosilicate minerals, which composes of tetrahedral sheets of SiO_4 bonded with (Al, Mg, Fe)$(O,OH)_6$ octahedral sheets. The different arrangements of tetrahedral and octahedral layers lead to different classes of clay minerals which are classified into two main groups i.e. 1:1 and 2:1 as shown in Figure 2.1 [42]. The 1:1 arrangement has 1 tetrahedral sheet linked to 1 octahedral sheet, such as kaolinite. On the other hand, the 2:1 family comprises of 2 tetrahedral sheets sandwiching a center octahedral sheet, in which they bond together by oxygen ions that belong to both sheets. The clay minerals classified to 2:1 family are illite, smectite, vermiculite and chlorite.

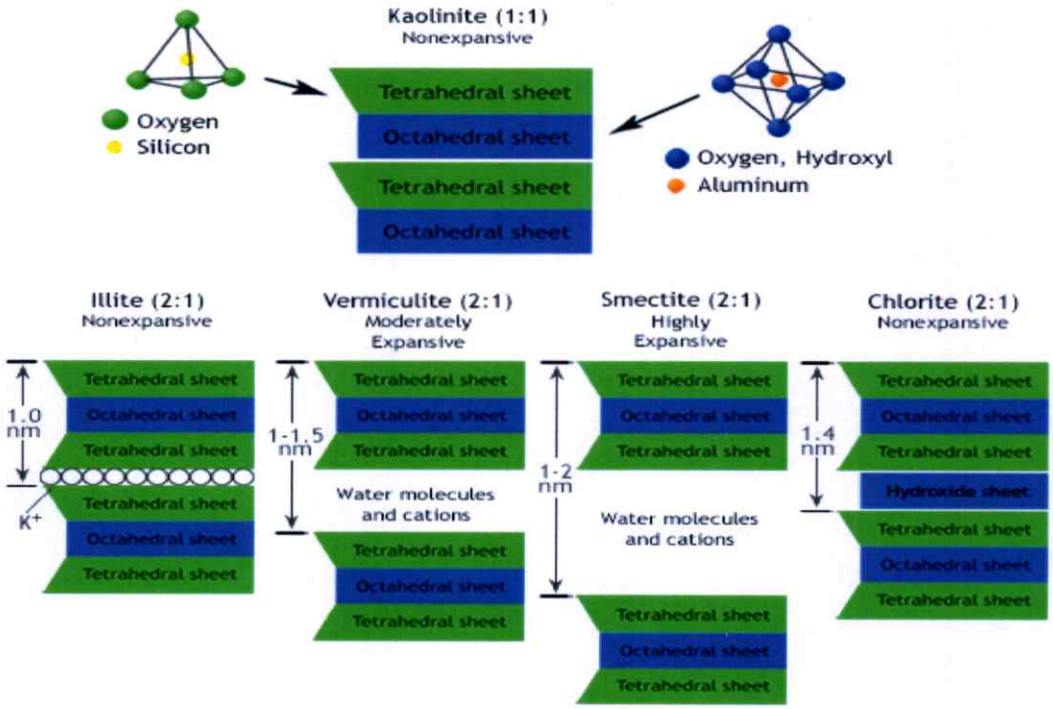

Figure 2.1 Structural arrangements of several clay minerals [43]

Generally, the 2:1 structure has a negative charge on the surface of clay layers that must be balanced externally by cations. The quantity of balancing cations holded the interlayer spacing of clay is called cation exchange capacity (CEC), usually measured in milliequivalents per 100 g of dried clay.

Differences in the charge of the clay layers, deficiency and interlayer cations result in different physical and chemical properties of clay minerals, such as thermal stability and swelling behavior, etc. Table 2.1 summarizes the common properties of some common clay minerals.

Table 2.1 Classification and properties of clay minerals [44]

Type	Species	Water swelling	CEC	Chemical formula
1:1	Kaolinite	Poor	Low	$Al_4Si_4O_{10}(OH)_8$
2:1	Illite	Poor	Low	$(K,H_3O)(Al,Mg,Fe)_2(Si,Al)_4O_{10}[(OH)_2,(H_2O)]$
	Vermiculite	Good	High	$(Mg,Fe^{+2},Al)_3(Al,Si)_4O_{10}(OH)_2{\cdot}4H_2O$
	Smectite	Good	High	$(Na, Ca)(Al,Mg)_6(Si_40_{10})_3(OH)_{6-n}H_{20}$
	Chlorite	Poor	Low	$(Mg,Fe)_3(Si,Al)_4O_{10}(OH)_2(Mg,Fe)_3(OH)_6$

The 2:1 clay family has better property than that of 1:1 arrangement. It possesses higher exchange ability of interlayer cations and more expanding ability than other clay minerals when water penetrating into the interlayer spacing. Hence, the structure of 2:1 clay family could be easily modified and improved their properties. Montmorillonite (MMT) is a member of the 2:1 smectite family which is hydrated sodium calcium aluminum magnesium silicate hydroxide $(Na,Ca)_{0.33}(Al,Mg)_2(Si_4O_{10})(OH)_2{\cdot}nH_2O$ as shown in Figure 2.2 (a). The common balancing cations in the MMT structure are sodium, calcium, magnesium and potassium. However, the exact ratio of cations varies with source of clay minerals. The crystalline structure of MMT is a stack of flake-shaped particles of about 1 nm thickness as shown in Figure 2.2 (b). The MMT has been found in numerous locations around the world, e.g. North America, China, Japan, France, etc. In Thailand, it has been discovered in Chaibadan, Lopburi.

The main properties of MMT are high specific surface area (SSA) and high CEC, therefore, the MMT has been used in a wide range of industrial applications, such as nanocomposite materials [45-46], ceramics [47,44], oil drilling [48], paper industries [49], decolorizing agents [50], ion exchanger, heterogeneous catalysis, etc [51].

Moreover, the negative charge surface of MMT could easily attract with a positive charge elements. Therefore, the MMT has been widely used as adsorbent for wastewater treatment applications [52-53].

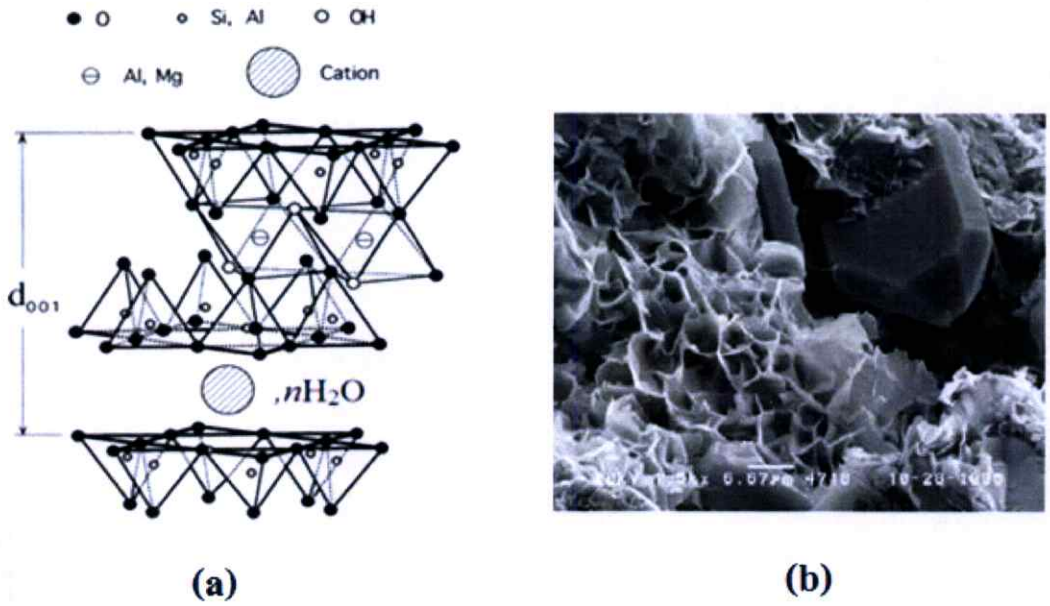

Figure 2.2 Basic structure (a) and flake-like shape (b) of montmorillonite (MMT) [54]

In addition, the MMT structure could be modified in order to improve their properties by ion exchange between the interlayer cations and other larger cations, usually known as cationic exchange reaction or intercalation process [55].

2.2 Intercalation process

Intercalation is the process of inserting atoms or molecules (guest chemical species) between layers in host materials with layered structure. The interlayer of MMT clay can be efficiently intercalated with various organic and inorganic compounds in order to increase its pore size and surface area. The intercalated process is easily achieved by machanical stirring of clay suspension with guest ions dissolved in water. The organic intercalation such as chitosan [21], starch [56], cetyltrimethylammonium [57], hexadecyltrimethylammonium [58], polydially-dimethyl ammonium, hydrazine, urea, formamide, acetamide, dimethyl sulfoxide, acetate [59], etc. has been reviewed. These organic molecules intercalated clay are suitably applied as adsorbent, filler and thickener, however, they are insusceptibity for high temperature applications (>250 °C) [60]. In order to overcome the disadvantage of organic intercalate clay, the inorganic molecules known as

polyoxocations are intercalated into the MMT interlayers for improvement the thermal property. In addition, the inorganic intercalated clay possesses many advantages, e.g. multi-charged centers, high surface areas, large interlayer spaces and regenerability [61]. Hence, the inorganic intercalated clays are more attractive than the organic intercalated clays. Various inorganic intercalating molecules were studied, e.g. aluminum oxide [61-65], iron oxide [66], silica [67], etc., commonly called as pillaring agents. The pillaring agents, i.e. bulky inorganic polyoxocations can be exchanged with interlayered cations of clays. These inorganic polyoxocations convert to metal oxide clusters by dehydration and dehydroxylation after calcination process. These metal oxide clusters (known as pillars) bond with surface oxygens in clay layer, which generate a two-dimensional porous network on interlayer space. The pillared structure can increase the basal spacing (d_{001}) of the clays layers and the thermal stability, preventing the collapse of the interlayer space and generating a stable porous structure [68]. The metal oxide intercalated clays are called as pillared clays (PILCs). Figure 2.3 shows the preparation process of PILCs. The PILCs, properties strongly depend on the synthesis parameters, such as the type of starting clay, type of inorganic pillaring solution, conditions of intercalation, drying and calcination processes, etc. The inorganic pillaring solutions have been produced through the partial base hydrolysis of Al, Mg, Fe, Cr, Ni, Bi, Si and Zr salts [69-70].

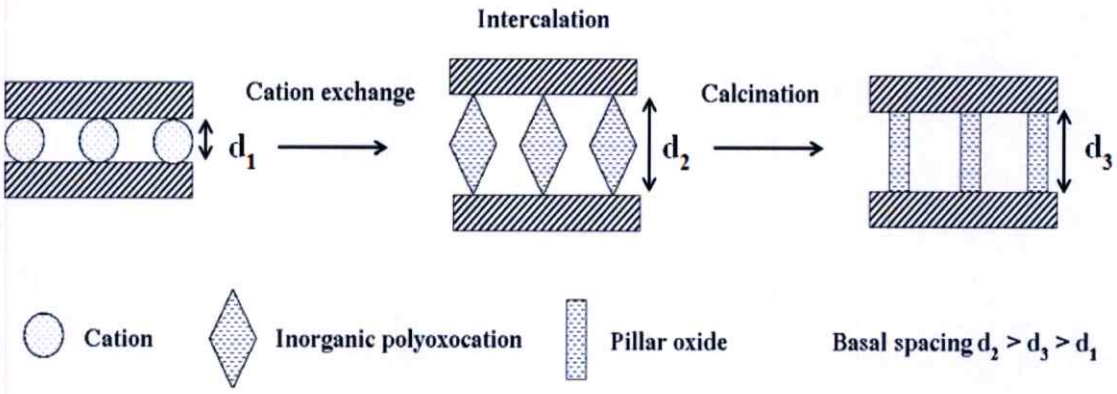

Figure 2.3 Schematic representation of the pillaring process [55].

However, the aluminum pillaring agent is most widely used because the aluminum chemistry is defined as better chemical composition, structure and charge than that of other cations [57]. Moreover, the functional groups of solution were simply studied by using spectroscopy, such as nuclear magnetic resonance (NMR).

2.3 Aluminum pillared montmorillonite

The Al_{13} polyoxocation is one of the most attractive agents, in which it was firstly studied by Johansson in 1960. The merit of Al_{13} polyoxocation is presence of stable uniform size than other pillar species, leading to obtain a homogeneous distribution of the Al_{13} polyoxocation between clay layers. Having a high surface area and porosity, this material is commonly used as catalysts support and selective adsorbents. From this point of view, our study has been focused on the synthesis of Al_{13} polyoxocation as a pillaring agent. In general terms, the experimental procedure for the synthesis of aluminum pillared montmorillonite (Alpill-MMT) can be represented by two experiments.

2.3.1 Synthesis of aluminum pillaring solution

The pillaring solution of Al_{13} polyoxocation is commonly prepared through hydrolysis reaction between base and Al^{3+} solutions. The structures of Al_{13} polyoxocation depend on the concentration of base solution adding into the Al^{3+} solutions. Normally, three types of the Al_{13} polyoxocation structure have been discussed in the reviews. In the low base concentration system, two minor polynuclear species $Al_2(OH)_2(H_2O)_4^{4+}$ and $Al_3(OH)_4(H_2O)_9^{5+}$ are formed by hydrolysis and polymerization of Al^{3+}. The large $[Al_{13}O_4(OH)_{24}(H_2O)_{12}]^{7+}$ polyoxocation species are formed in the neutral solution systems [71-73]. Finally, the flocculation of hydroxide is obtained at high concentration of base system. Most found structure is the $[AlO_4Al_{12}(OH)_{24}(H_2O)_{12}]^{7+}$ species (Al_{13}^{7+} polyoxocation) which is commonly called Al_{13}-Keggin structure model [74]. The Al_{13}-Keggin contain a central tetrahedral aluminum ($Al(O)_4$) unit surrounded by twelve aluminum octahedral ($Al(O)_6$) units, having an ionic radius in solution of ~ 1.3 nm [75]. Figure 2.4 shows various familiar isomers of Al_{13}-Keggin.

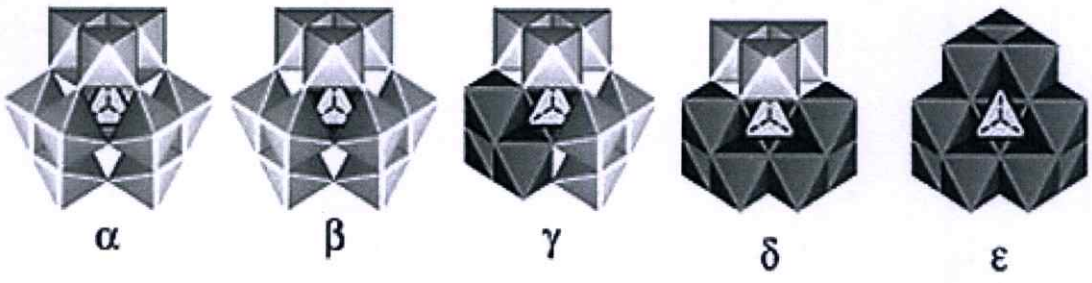

Figure 2.4 Keggin isomers of Al_{13} polyoxocation species [74].

Among these Al_{13}-Keggin isomer structures, the most studied structure is the ε-isomer (ε-Al_{13}-Keggin), consisting of four planar trimeric $Al_3(OH)_6$ groups that linked to

the central $Al(O)_4$ site via four μ_4-*O* as shown in figure 2.5 (a). The molecule has *12* η-OH_2 sites and two structurally distinct sets of 12 μ_2-*OH* at the shared edges of $Al(O)_6$ octahedral [74]. The structure of ε-Al-Keggin in pillaring solution was analyzed by ^{27}Al NMR, in which four peaks of the chemical shifts were observed. The chemical shift at δ 0 ppm corresponded to hexaaqua Al^{3+} and from of monomer, i.e. $Al(H_2O)_6^{3+}$, $Al(OH)(H_2O)_5^{2+}$ and $Al(OH)_2(H_2O)_4^{+}$. The $Al_2(OH)_2(H_2O)_8^{4+}$ dimer and few $Al_3(OH)$ trimer were obtained at δ 3–5 ppm. The peak of tridecamer, $AlO_4Al_{12}(OH)_{24}(H_2O)_{12}^{7+}$, or ε-$Al_{13}$-Keggin was showed at δ 62.5 ppm and the $Al(OH)_4^-$ anion was assigned at δ 80 ppm [76]. Moreover, the literature, the signal at δ 64.5 and δ 70 ppm respectively corresponded to δ-Al_{13} and Al_{30} structure, [77] as shown in Figure 2.5 (b).

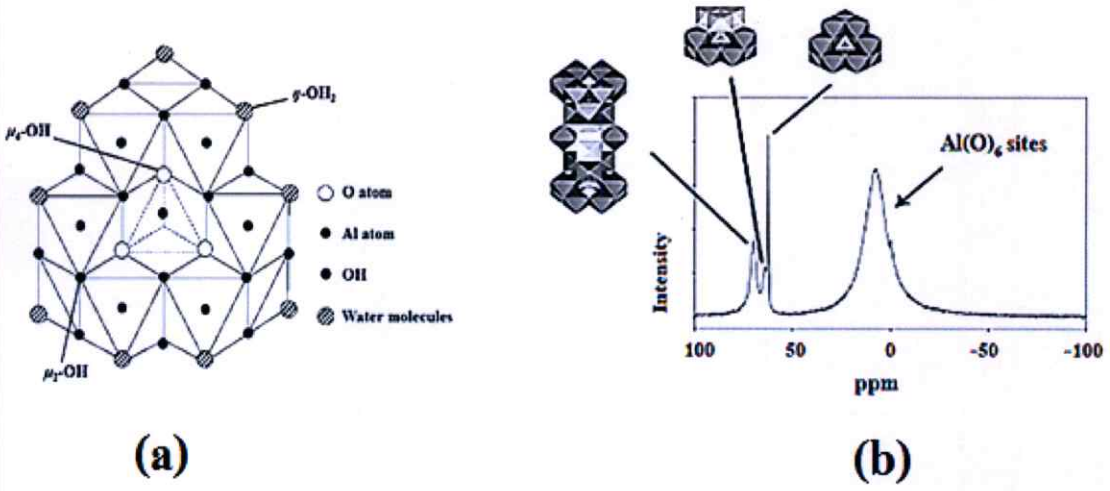

Figure 2.5 Structure of ε-Al_{13} Keggin (a) and ^{27}Al NMR spectrum of the large aluminum molecules ε-Al_{13}, δ-Al_{13} and Al_{30} (b) [74]

Literature reviews

The structures of pillaring solutions are mainly depended on the preparation parameters, such as OH/Al molar ratio, heat treatment, reaction time and mixing methods, etc. Thomas J. P. *et al* [78] studied on the effect of OH/Al molar ratios. The Al-pillaring solution was prepared at 25 °C by adding NaOH solution to $AlCl_3$ solution using various OH/Al molar ratios, i.e., 0.0, 1.0, 1.5, 2.25 and 2.42. The ^{27}Al NMR spectrum of Al^{3+} starting solution showed a single sharp line at δ 0.0 ppm. In contrast, the pillaring solution showed the chemical shift at δ 62.8 ppm, corresponded to ε-Al_{13} Keggin structure. The intensity of ε-Al_{13} Keggin peak increased with increasing of the OH/Al molar ratios from 1.0 to 2.42. However, the precipitation of aluminum hydroxide was obtained in some studies when the OH/Al molar ratio was higher than 2.5, such as the titration between $Al(NO_3)_3$ /or $Al_2(SO_4)_3$ and NaOH under various OH/Al ratios by Jim D. and John G. [79].

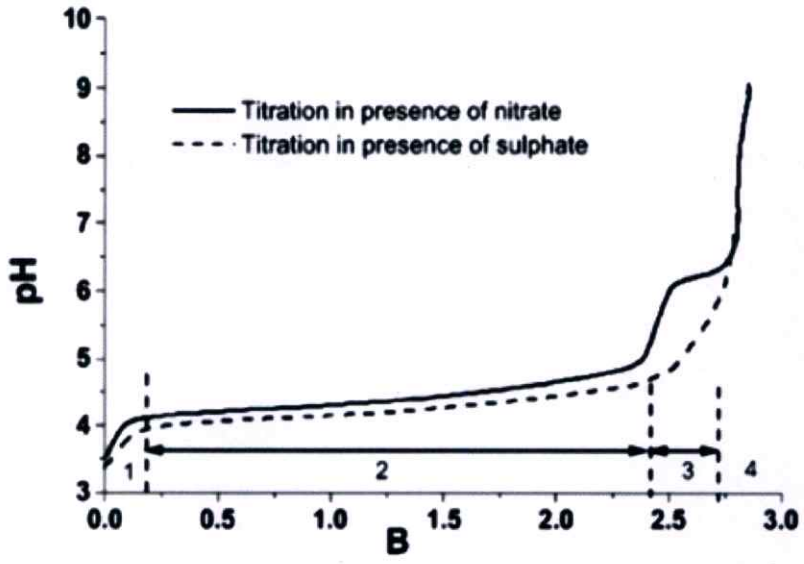

Figure 2.6 Titration curves between $AlCl_3$ and NaOH under various OH/Al ratios [62].

Figure 2.6 shows the titration curves of $AlCl_3$ and NaOH, in which it can be observed 4 main regions. In region 1, the pH of solution was rapidly increased because of the base neutralization of free acid, which produced by spontaneous hydrolysis. The pH of mixture in the region 2 was slowly increased in between 0.3 and 2.4 of the OH/Al molar ratios, corresponded to the formation of dimeric, trimeric and Al_{13} polyoxocation. The increasing of OH/Al molar ratios in the region 3 from 2.4 to 2.8 would increase the pH of solution from 4.5 to 6.2, producing the amorphous $Al(OH)_3$ and rapid precipitation. In the region 4, the positive charge on the surface of colloid hydroxide particles was reduced, thus the aluminum hydroxide flocculation would form. In addition, Baoyou S. *et al.* [80] studied on the structure of Al pillaring species in the solid state by adding Na_2SO_4 solution into the Al pillaring solution at the OH/Al molar ratio of 2.4. The XRD pattern proved that the solid-state Al pillaring species mainly consisted of well-formed crystalline solid as shown in Figure 2.7 (a), corresponding to the matter with tetrahedral structure as observed in SEM images from Figure 2.7 (b). The existence of Al_{13}-Keggin structure in the precipitate was also confirmed by solid state ^{27}Al NMR. There was only one peak at chemical shift of 61.5 ppm, which was attributed to the resonance of the central Al atom within the ε-Al_{13}-Keggin structure.

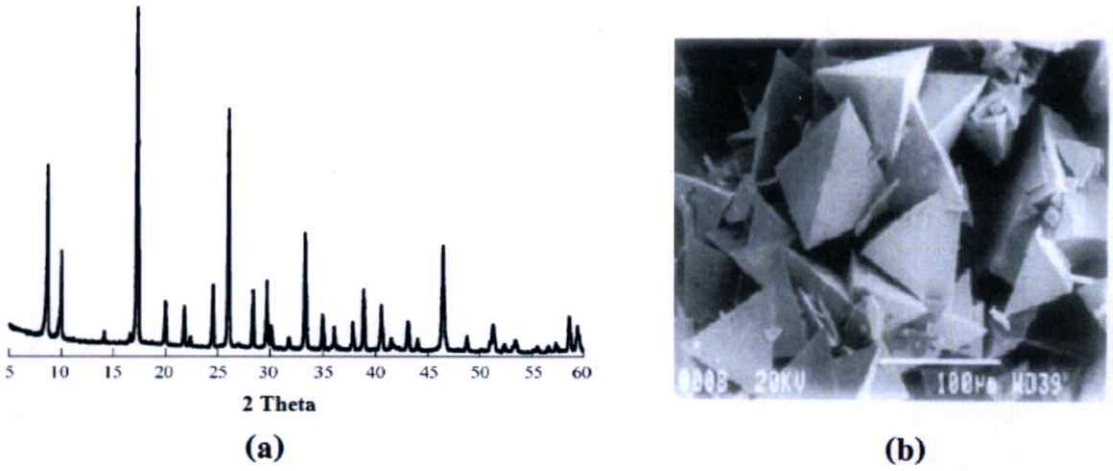

Figure 2.7 XRD pattern of Al_{13}-$(SO_4)_n$ precipitate (a) and SEM image of ε-Al_{13}-Keggin precipitate (b) [30].

Wei-Zi W. and Pa H. H. [81] studied on the effect of reaction time on the structure of pillaring solution, which were prepared by adding 0.1 mol/L NaOH to 0.1 mol/L $AlCl_3$ and then stirring for various aging periods from 1 to 120 h. The fraction of ε-Al_{13} Keggin slowly increased with increasing reaction time to 80 h and then became constant for longer reaction time. Moreover, Wallace O. *et al.* [82] prepared Al pillaring solution by adding NaOH to $AlCl_3$ solution at the OH/Al molar ratio of 2.25. The reaction time at 4 h showed the maximum amount of ε-Al_{13}-Keggin structure and then it transformed to $Al_{24}O_{72}$ structure after aging longer than 2 days.

Lionel A. and Francis T. [83] studied on the effect of reaction time and reaction temperature on the structure of aluminum pillaring solution. The solution was prepared by adding 0.5 mol/L $Al(NO_3)_3 \cdot 9H_2O$ solution into 1.0 M NaOH at 90 °C using OH/Al molar ratio of 2.46 with vigorous stirring. The ^{27}Al NMR spectrum showed the peak at δ 63 and δ 0 ppm. When this solution was heated between 50 and 150 °C or aged during 6-24 months at 20 °C, the ε-Al_{13}- Keggin structure transformed to new aluminum polycations, especially δ-Al_{30}-Keggin as shown in Figure 2.8.

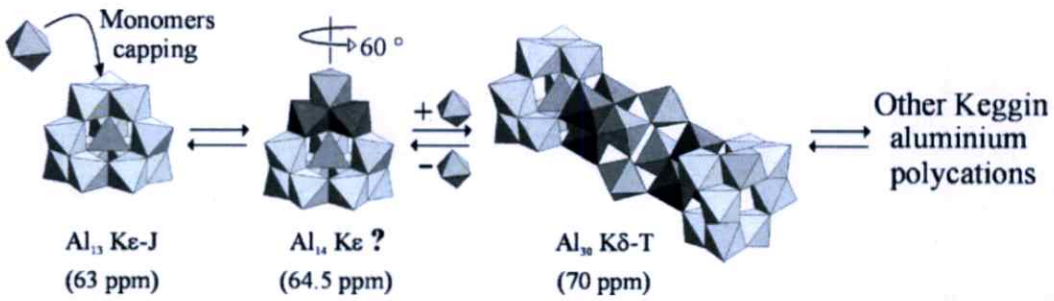

Figure 2.8 Chemical path ways of ε-Al_{13}-Keggin transform to δ-Al_{30}-Keggin [83]

Initially, the ε-Al_{13}-Keggin structure was capped by Al monomer to form an intermediate species ε-Al_{14}-Keggin, which was shown at δ 64.5 ppm of Al^{27}NMR spectrum. It can be assumed that the ε-Al_{14}-Keggin was formed during the first stage of ε-Al_{13}-Keggin transformation and then dimerized and reacted with two other monomers to produce δ-Al_{30}-Keggin. In addition, Zhaoyang C. *et al.* [84] studied on the transformation of ε-Al_{13}-Keggin to δ-Al_{30}-Keggin. The content of δ-Al_{30}-Keggin became higher than that of ε-Al_{13}-Keggin when the Al pillaring solution was heated at 95 °C for more than 12 h.

2.3.2 Synthesis of aluminum pillared montmorillonite

In general, the synthesis of aluminum pillared montmorillonite (Alpill-MMT) has been performed in three main steps as follows. Firstly, a suspension of MMT clay was mixed with the Al pillaring solution. In laboratory preparation, high quantity of water was required for preparing the well dispersed clay. Suspension, therefore, many researches had tried to minimize the water consumption. The intercalation of ε-Al_{13}-Keggin within MMT layers was followed by the cation exchange process. Secondly, the cationic exchanged suspension was filtered, washed and dried, resulting in the intercalated MMT. The washing and drying process play the important roles on the properties of the intercalated MMT, especially in porosity. Washing was commonly performed by filtration or dialysis, while drying could be done at room temperature or in an oven at 50-100 °C. Finally, the intercalated MMT was calcined at high temperature in order to convert the ε-Al_{13}-Keggin to aluminum oxide (Al_2O_3) pillared clusters as shown in the equation (2.1) [85-86] and Figure 2.9. The chemical bond between the pillars and surface oxygens of MMT were formed producing the high permanent individual layer apart. In addition, the increases of micro-porosity and surface area were achieved in the pillared clay; thereby they have the potential for adsorption application.

$$Al_{13}O_4 + (OH)_{28+n}^{(3-n)} \xrightarrow{-H_2O} 6.5Al_2O_3 + (3-n)H^+ \qquad (2.1)$$

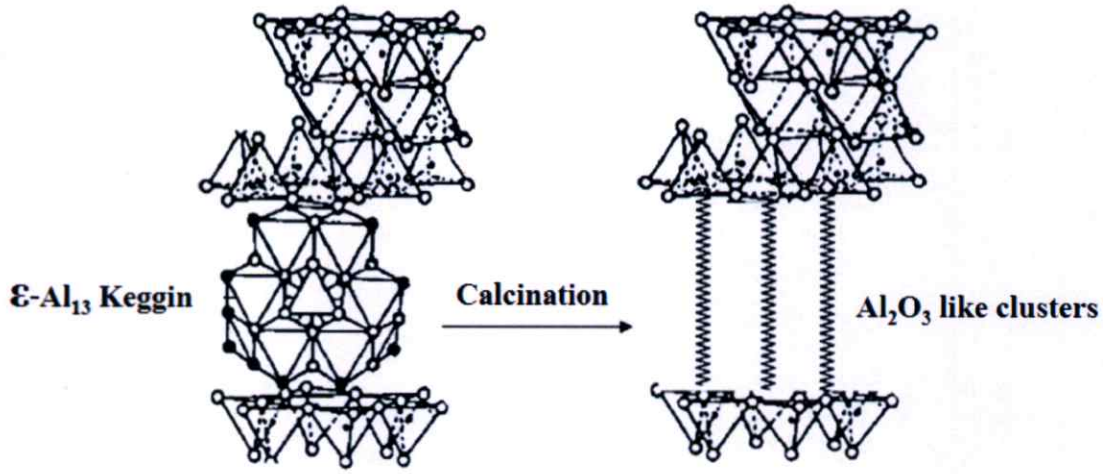

Figure 2.9 Schematic diagrams of Al_{13} intercalated MMT and Al-pillared clay [87]

The arrangement of Al_2O_3 cluster in the clay layers can be divided into two classifies. The first type is a characteristic long range face-to-face stacking of clay layers (lamellar aggregation), resulting in a large micro-porosity as shown in Figure 2.10 (a). On the other hand, house of card aggregation (face-to-edge and edge-to-edge) of clays generate the meso-/macropores present in delaminated structures as shown in Figure 2.10 (b).

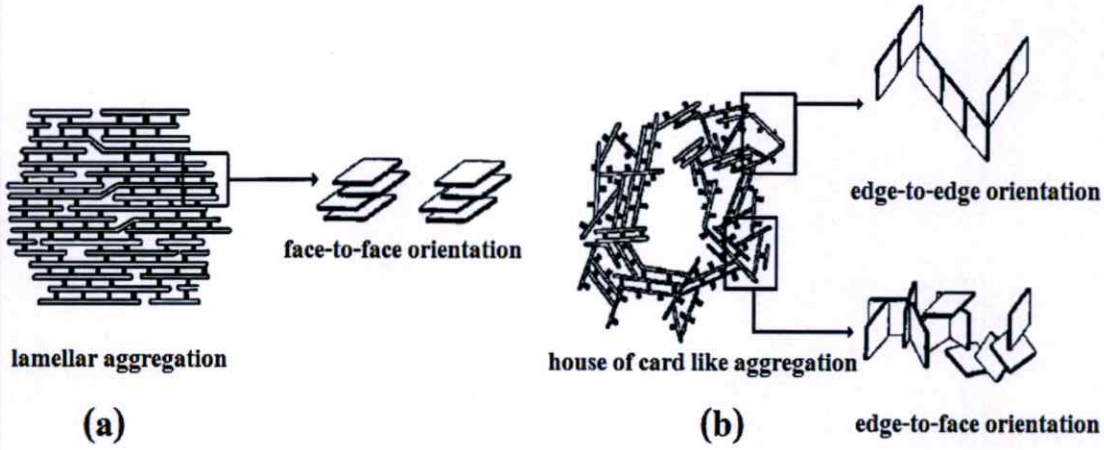

Figure 2.10 Schematic representation of (a) face-to-face and (b) a house of cards like aggregation

In order to tailor Alpill-MMT for their applications the understanding of Alpill-MMT is requires. Moreover, the porosity parameters, such as basal space (d_{001}), pore volume, pore size distribution and surface area must be investigated. In this research, X-ray diffraction (XRD) was used for studying expand of Alpill-MMT layers compared to the starting MMT. The surface area, pore volume and pore size

distribution would be analyzed by gas adsorption technique, in order to support the XRD results. In addition, the effects of preparation parameters on the structure of Alpill-MMT have been investigated.

Literature reviews

Pinnavaia T.J. *et al* [78] studied on the effect of drying process on the structure of Al pillared clays. The freeze-drying and air-drying methods were investigated. Both air-drying and freeze-drying methods lead to products with a range of d_{001} in 18.2-20.5 Å. The air-drying product possessed the pore opening greater than 6.2 Å but less than 9.2 Å. In contrast, the freeze-drying products exhibited a kinetic diameter 10.0 Å. The effect of drying method on pore size was related to layer aggregation in the Al pillared clay. Figure 2.11 show the model of flocculated Al pillared clay. The freeze drying method tend to preserve the structure of flocculated clay, whereas the air-drying method indeed the reorganizing of the delaminated aggregates and optimizing face-to-face aggregation. Moreover, the drying methods the significantly affected catalyst longevity of Al pillared clays. The catalytic activity of air-dried Al pillared clay exhibited decreased with increasing reaction time, but that of the freeze-dried Al pillared clay was stable over the range of investigated reaction time.

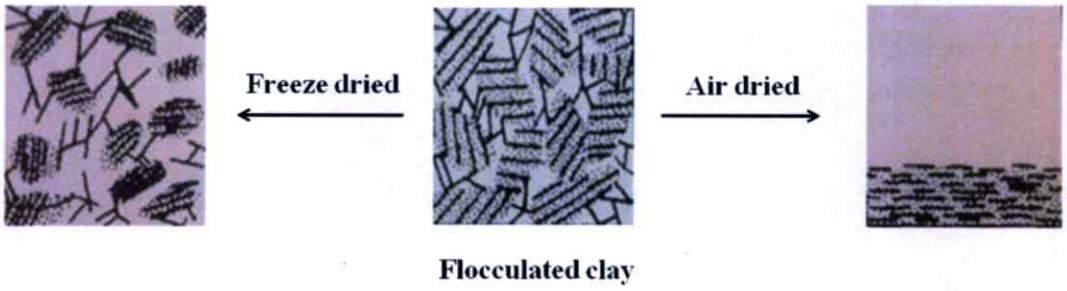

Figure 2.11 Clay aggregations after drying process

Mokaya R. and Jones W. [88] studied on the effect of acid treatment of the starting MMT before preparation of the Al pillared clay by conventional method. The MMT or Al pillared MMT was treated with the concentrated sulphuric acid using 0.35 of acid/clay ratio for 16 h. The acid treated Al pillared MMT possessed higher pore volume and meso-porosity (>50 nm), comparing with the conventional Al pillared MMT. In addition, the increasing amount of acid treatment was led to increase in pore volume and pore diameter (> 40 Å).

Khalaf H. *et al* [89] concerned in the influence of cationic surfactant, i. e. cetyl trimethyl ammonium bromide (CTAB), treatment on the preparation of Al pillared

clay. The Maghnia and Mostaghanem were used as the staring clays from Algeria. All of Al pillared clays were prepared using 1.8 of OH/Al molar ratio, 2 wt. % of CTAB/g clay and 4.0 meq/g of meqAl/g clay. Four difference methods for preparing Al pillared clays were investigated; (1) the Al pillaring solution was firstly added to a stirred clay suspension and then CTAB solution (2.0 wt. %) was added, (2) the CTAB solution was firstly added to a stirred clay suspension and then the Al pillaring solution was added, (3) both solutions were simultaneously added to a stirred clay suspension and (4) a CTAB solution was added to a re-dispersed suspension of Al-hydroxy-montmorillonite. Four methods were compared with the conventional preparation method of Al-pillared clay. The conventional Al-pillared clay possesed 1.8 nm of d_{001}, 200-300 cm^3/g of specific surface area (SSA) and stability at 500°C. The CTAB-modified Al pillared clay obtained by the last method showed higher thermal stability than the other method.

Maes N. *et al* [90] interested on the preparation of pillared clay using various pillaring agents, i. e. Al, Ti, Zr and Fe pillaring agent for improving the properties of clay materials. The Al pillared clay (Al-PILC) had higher crystallinity and SSA than the other. In contrast, the Fe pillared clay (Fe-PILC) exhibited the lowest SSA and micropore volume, in which its adsorption isotherm resembled to non-porous isotherm type. The Ti pillared clay (Ti-PILC) showed distortion in the XRD pattern because the presence of broad range of pore diameter indicated non-uniform sizes of Ti molecules. Moreover, the effects of drying methods, i. e. air-dried and freeze-dried, were investigated. It can be seen that no significant changes in the SSA and micropore volume after air-drying and freeze-drying for Al-PILC, Zr-PILC and Ti-PILC.

Cheng L.S. and Yang R.T. [91] studied on the preparation parameters affected to the structure of the Al pillared clays. The Arizona MMT (CEC = 1.40 meq/g) and Wyoming MMT (CEC = 0.76 meq/g) were used as starting clays. Several of OH/Al molar ratios (0.5, 1.6, 2.2 and 2.5) and calcining temperatures (400 and 600 °C) were investigated. It was observed that the SSA and micropore volume of the Al pillared Arizona MMT was higher than Al pillared Wyoming MMT, while their d_{001} were similar. In addition, the SSA of both samples increased with increasing OH/Al molar ratio during pillaring process. The maximum SSA was obtained at OH/Al = 2.2, and then it declined upon further increasing of OH/Al molar ratio. The interlayer spacing was collapsed at high calcination temperature. Therefore, micropore volume of clay calcined at 600 °C was consistently lower than those clay calcined at 400 °C.

Sanchez A. and Montes M. [92] studied on the influence of preparation parameters on the properties of Al pillared clays. The Spanish clay was used as the starting material, which ground and classified particle size by sieving into four fractions: (1) < 60 μm, (2) 60-100 μm, (3) 100-200 μm, and (4) 200-320 μm. Figure

2.12 shows the scanning electron microscope (SEM) images of the starting clay and Al pillared clays with the particle size smaller than 60 μm and the large particle size of 200-320μm. All Al pillared clays had similar appearance, implying that the particle size of the starting clay had no influence on the properties of Al pillared clays. The Al pillaring solution was prepared by adding NaOH solution to the $AlCl_3$ solution under vigorous stirring at room temperature. The concentration of $AlCl_3$ was varied 0.2, 0.4, 0.8 and 1.5 M. ^{27}Al NMR spectra of the Al pillaring solutions showed slight reduction in quantity of the ε-Al-Kegging structure when increasing $AlCl_3$ concentration. In addition, the SSA and pore volume of all pillared clays also decreased when increasing of $AlCl_3$ concentrations. It can also be seen that the decreasing of SSA and pore volume were due to the decreasing in the corresponding microporous properties (micropore surface area and micropore volume respectively), but the mesoporous properties remaining almost constant.

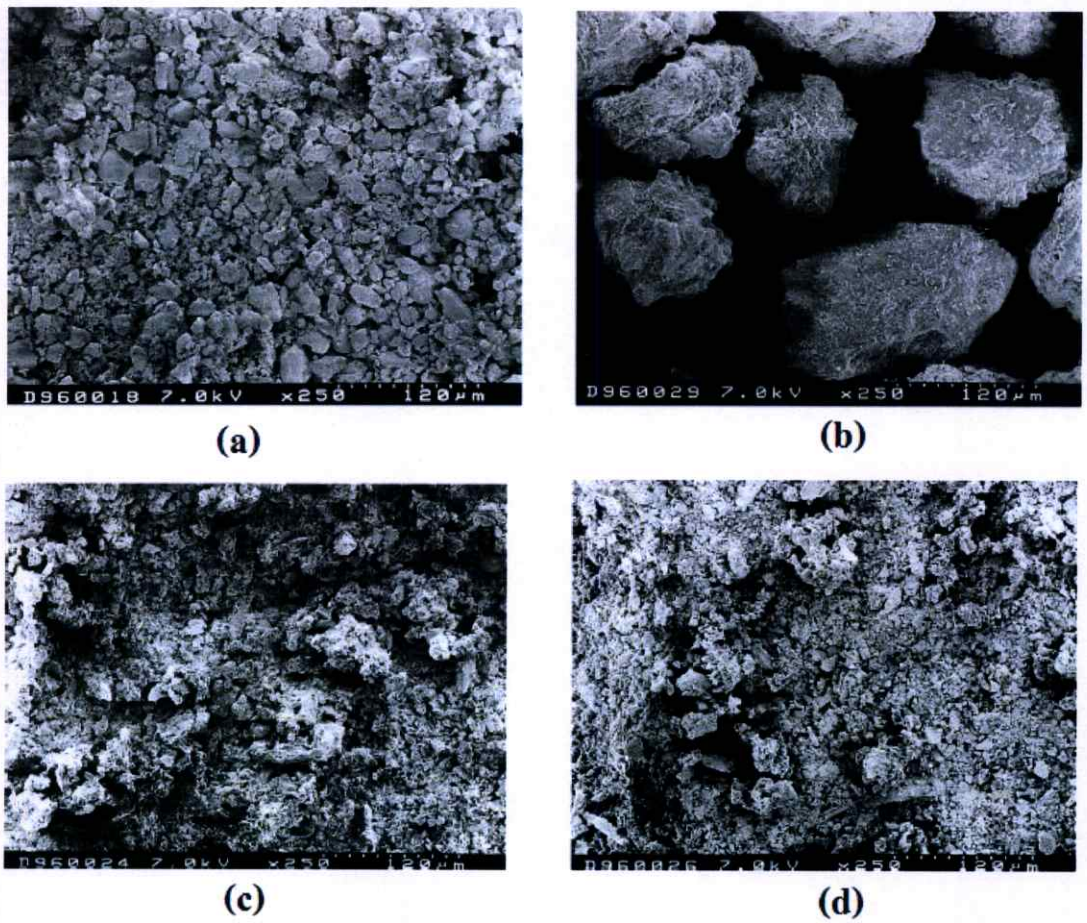

Figure 2.12 SEM micrographs of the starting (a and b) and Al pillared clays (c and d)

Katdare S.K. *et al* studied on the effect of sonication technique on the properties of Al pillared MMT. Moreover, the effect of duration of ultrasonic treatment (2, 5, 10, 20, 40, 60 and 80 min) and type of exchangeable cations (Na^{+}, Ca^{2+} and La^{3+}) were also investigated. The longer duration of ultrasonic treatment, the higher quantity ε-Al_{13}-Keggin was obtained into all Al-pillared clays. From this result, the role of ultrasound was to accelerate the ε-Al_{13}-Keggin diffusion within the clay layers. Moreover, the ultrasonic treatment method could also handle the concentrated clay suspensions, which was the advantage over the conventional preparation method. However, the rate of ε-Al_{13}-Keggin insertion was dependent on the exchangeable cation presented in the clays. For similar duration of ultrasonic treatment ca. 5 min, the ε-Al_{13}-Keggin incorporation in increased in the order of Na^{+}-MMT > Ca^{2+}-MMT > La^{3+}-MMT. The delamination occurred at difference durations of ultrasonic treatment for a given form of clay. The delamination of Na-pillared MMT, Ca-pillared MMT and La-pillared MMT were formed after 20, 60 and 80 min, respectively.

Shin Y-S. *et al* [93] studied on the effect of preparation parameters on the properties of the Al pillared MMT. The Al pillaring solution was aged for 1, 4 and 7 days, respectively. After that the Al pillaring solution was slowly added to MMT suspension with stirring for 24 h at room temperature. The solid products were separated by filtration, and dried at 105 °C and calcined for 3 h at 400, 600 and 760 °C. The starting MMT showed 14.2 Å of d_{001}, but the heating processes reduced the d_{001} value to 9.5 Å. In line with the starting MMT, the d_{001} of Al pillared MMT slightly decreased when increasing the calcined temperature. Whereas, the Al pillaring solution aging for 4 and 7 days remained constant of d_{001}. The longer aging time of Al pillaring solution could increase the SSA and micropore volume of the Al pillared MMT, whereas the mesopore volume actually remained constant.

Jimenez de Haro M.C. *et al* [94] studied on the effect of ultrasonic pretreatment starting of clays on the properties of Al pillared clays. Santa Olalla (SV, high-charge) and Ojen (OV, low-charge) were used as the starting clays. Clay was mixed with hydrogen peroxide (H_2O_2, 30%) solution and deionized water, and then sonicated for 10 -100 h. After that, both of pretreatment clays were reacted with the Al pillaring solution using conventional method. It can be seen that the pretreated OV (36 m^2/g) and SV (54 m^2/g) showed higher SSA than the starting clays (1 m^2/g). The XRD patterns show that the crystal structure of both starting clays remained practically unchanged after sonication. However, the pretreatment produced a significant delamination and decreasing of the particle size and the layer charge. The Al pillared SV showed a d_{001} of 14 Å, whereas that of the Al pillared OV was at 14 and

18 Å. The 18 Å diffraction peak was preserved at high temperatures (550 °C) and it was responsible for the increases of SSA and microporosity.

Olaya A. *et al* [95] studied on the effect of microwave radiation on the properties of Al pillared MMT. The clay suspension were prepared at 2 %, 30%, and dry clay, The Al pillared MMT were synthesized by applying microwave irradiation both during the aging of the Al pillaring solution and in the intercalation process. This method considerably reduced the reaction time and the amount of water when comparing with the conventional method. The intercalation was carried out by direct mixing of the pillaring solution and the clay. The XRD analyses of the cationic exchange capacity and the catalytic assessment in the n-heptane hydroconversion, showed that the solids synthesized exhibited better characteristics and catalytic behavior than the Al pillared MMT obtained through the conventional method of synthesis.

2.4 Synthesis of aluminum pillared montmorillonite doped metals

Since the pillared clays possess high thermal stability, high acidic property, high surface area and porosity, therefore, they can act as the substrates for doping the transition metal in order to create the active site for the catalysis reaction. Normally, Cr, Ag, V, Fe, Mn, Ti, Ce, Pd and Cu have been used as the active components in pillared catalysts [96-98]. The Cu and Fe dopants show high efficiencies for active catalysis of oxidation reactions [99]. However, the Cu catalyst shows a greater rate conversion of the pollutants in solution than the Fe catalysts at the same reaction conditions for the long range of pH [97, 100]. This result indicates the efficiency of Cu for using as degradation catalysis of organic water pollutants, such as phenol [101-102], olive oil mill [103-104] agro food, dyes [105-106], etc., *via* Fenton-like reactions, photo-Fenton reactions, and wet hydrogen peroxide oxidation [107]. In addition, the Cu metallic ions could perform an inhibition of the bacteria growth [108-109], indicating the antibacterial property.

The principle of catalyst preparation is the metal-salt dispersed within the porous support by general methods, such as ionic exchange, deposition, impregnation, co-precipitation [110-111], adsorption from solution, etc. After that, the metal-salt was converted to metal oxide and bonded to the support surface by calcination process. Figure 2.13 demonstrates the feature of copper oxide clusters trapped in the interlayer space of aluminum pillared clay.

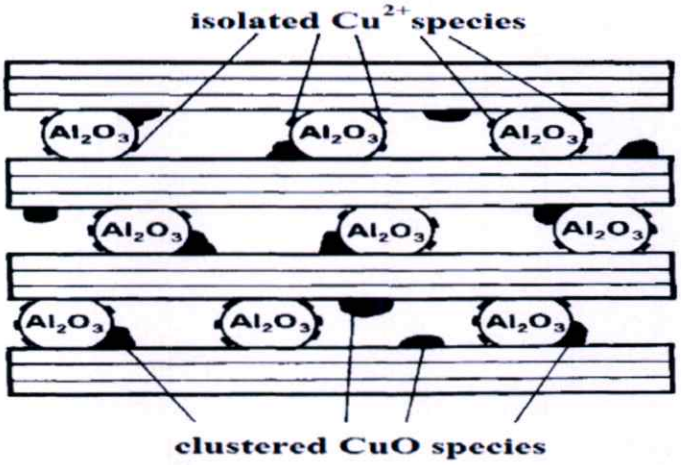

Figure 2.13 Model of copper oxide fixed on aluminum pillared clay [112]

The adsorption process is one of the most effective methods to obtain well dispersion and distribution of catalysts, in which it is on the support and easy to operation when comparing with the other process. Thus, this technique is widely used in the preparation of industrial catalysts. Formality of process is adsorption of metal salts or metal ions from their solutions by either physisorption or chemisorption on the active sites of supports. On the other hand, the impregnation method is also widely used for preparing small quantity of catalysts for basic studies. During impregnation, the metal ion precursor is deposited on the support, using the same volume of metal ion solution as the pore volume of support. Hence, the amount of catalyst in the support can be controlled. In this research, the catalyst preparation was carried out by doping copper ions (Cu^{2+}) into the Al pillared MMT using adsorption and impregnation.

Literature reviews

Frini N. *et al* [113] studied on the effect of intercalation method on the properties of Cu-Al pillared clays. Wyoming MMT (W), Tunisian illite (H) and Algerian bentonite (MR) were used as the starting clay materials. The Al pillaring solution was performed at 40 °C with a OH/(Al+Cu) molar ratio of 2 and at Cu/(Al+Cu) of 0, 5 and 10. The Cu-Al pillared clays were prepared by three methods; (1) conventional method (C method), (2) the dry clay powder was directly dispersed in the diluted pillaring solution (P method) and (3) a concentrated slurry method in which a dialysis bag containing clay-water slurry (33% w/w) was placed in the pillaring solution (CS method). The illustration of the three different methods was shown in Figure 2.14. The results show that the calcinations of modified clays at 300°C led to d_{001} peak of about 1.8 nm. However, the Cu- A1pillared clay (H) is remarkably stable upon ageing (one year) and upon thermal treatment (800°C). The SSA and porosity considerably

increases. It can be note that these surface properties of the Cu-A1 pillared clay were higher than those of the Al pillared clays. The Cu-Al pillared clay (H) preparation by P method showed the maximum pore volume. Moreover, the Cu-Al pillared clay (H) prepared by CS method showed the maximum microporous pore volume. Therefore, the best results were obtained from P and CS method. The Cu-Al pillared clay prepared by P method was much more active for phenol conversion than the D method, which was investigated by Barrault J. *et al* [114].

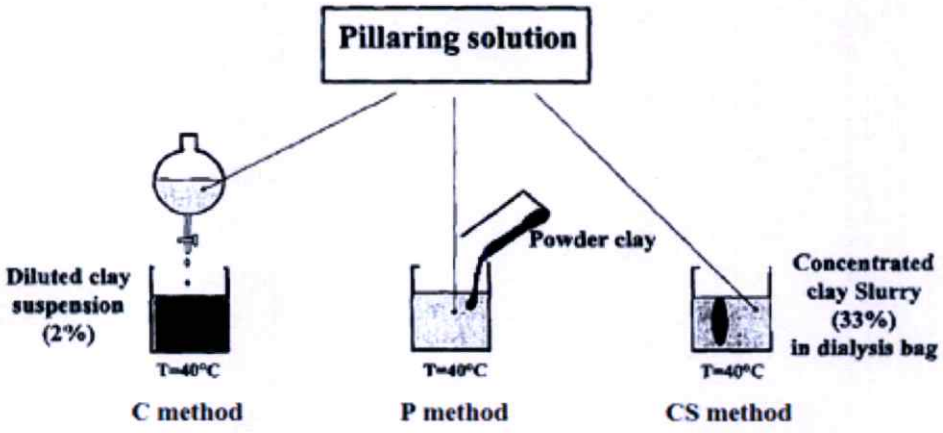

Figure 2.14 Illustration of three methods of intercalation process [113]

Bahranowski K. *et al* [115] studied on the effect of preparation parameters on the physic-chemical and catalytic properties of the Cu-Al pillared clay. The copper solution (0.1 mol/L) was introduced into the Al pillared clay by means of cationic exchange method. The exchanged samples were obtained by varying the weight percentage of copper (Cu), i.e. 1.1, 2.0 and 2.3. The values of d_{001} and the SSA of both Al pillared clay and Cu-Al pillared clay were higher than these of the starting clay. However, the SSA and micropore volume of Al pillared clay and Cu-Al pillared gradually decreased when increasing in Cu content. The copper ions were anchored at the pillars rather than at the surface of clay layer as evidenced by electron spin resonance (ESR) spectra. In addition, the catalytic hydroxylation of phenol was investigated. The Al pillared clay showed certain activity in hydroxylation of phenol, however, the Cu-Al pillared clay clearly improved the catalytic properties. An increase of Cu content did not improve the catalytic performance because the clusters of amorphous CuO might cause a local blocking of the micropores, resulting in obstacle the catalytic activities of some Cu species.

Ramaswamy V. *et al* [116] studied on the effect of immobilization method on the properties of Cu-Al pillared MMT. The Cu-Al pillared MMT was prepared by dispersing 1 g of Al pillared MMT into pyridine solution and then the $CuC_{32}H_2Cl_{14}N_8$ was added into this suspension under sonication for 20 min. The molar ratio of Cu-Cl_{14}Pc / g of Al pillared MMT was varied, i.e. 25, 50 and 70 mg, in order to obtain Cu-Alpill-MMT-25(US), Cu-Alpill-MMT-50(US) and Cu-Alpill-MMT-75(US), respectively. The immobilization of copper on the Al pillared MMT by conventional method was denoted Cu-Alpill-MMT-(S). It can be observed that all of the Cu-Alpill-MMTs were good thermal stability as compared with the Al pillared MMT. The ultrasonic samples had higher CuO content when comparing with the Cu-Alpill-MMT-(S). The higher copper concentration, the lower SSA was obtained. In addition, the size of the agglomeration of Cu-Alpill-MMT-(US) was smaller than that of the Cu-Alpill-MMT-(S). All Cu immobilized samples showed good catalytic activity on hydroxylation of phenol using H_2O_2 as oxidizing agent.

Yuan P. *et al* [117] studied on the effect of synthesis method on the properties of iron pillared MMT (Fepill-MMT). The Fepill-MMT was prepared by adding Na_2CO_3 powder into 0.2 M $Fe(NO_3)_3$ solution and then adding to the clay suspension. The OH/Fe molar ratio was varied range of 0.5-2.5. It was observed that increasing of OH/Fe molar ratio could increase the Fe_2O_3 content in the interlayer of clay. However, the intensity of d_{001} peak decreased with increasing of Fe content in the pillaring solution, resulting in the delamination (edge-to-face and edge-to-edge) of clay stack. The N_2 adsorption/desorption of Fepill-MMT showed type IV of isotherms, suggesting that it was the mesoporous samples. The Fepill-MMT showed high porosity and SSA as compared with the starting MMT. The SSA and the porosity of the laminated Fepill-MMT are 215.7 m^2/g and 0.29 ml/g, respectively. The average pore diameter would decrease when the OH/Fe ratio increased from 0.5 to 1.0. However, the increase of OH/Fe ratio from 1.5 to 2.5 was slightly effected on the pore structure parameters.

Lin Q. *et al* [118] studied on the effect of impregnation method on catalytic activity of Cu-impregnated- Ce-Al pillared clay (Cu-Ce-Alpill-clay). The conversion of nitric oxide (NO) removal from lean-burn gasoline and diesel exhaust were investigated. The Ce-Al pillared clay was prepared by slow adding NaOH solution into $AlCl_3$ + $CeCl_3$ solutions in order to obtain an OH/(Al+Ce) molar ratio of 2.0. This solution was added into clay dispersion and then calcined at 500 °C for 6 hrs. The $Cu(NO_3)_2$ solution impregnated into the Ce-Al pillared clay and evaporated under an infrared lamp, the weight of Cu was varied, i.e. 1, 2, 3 and 5 wt%. The samples were calcined at 500 °C for 6 hrs in order to obtain the Cu-Al-Ce-pillared clay. The Ce-Al pillared clay showed slit-like pore structure and the average pore diameter was in

the range of 9.26-11.35 nm, resulting in a house of cards structure of clay aggregation. The Cu-Al-Ce-pillared clay was significantly active for NO removal. The maximum NO conversion was reached about 56% when using the 2 wt% Cu content at 350 °C of reaction temperature The NO conversion decrease when increasing of Cu content.

Achma R.B. *et al* [119] studied on the effect of preparation parameters on the catalytic activity of Cu-Al pillared clay. The elimination of tyrosol by catalytic wet peroxide oxidation (CWPO) was investigated. The Cu-Al pillared clay was prepared by solid ion exchange method. The Al pillared clay was mixed with $Cu(NO_3)_2$ in agate mortar for 10 min, followed by heating at 300 °C for 3 h under helium atmosphere. The sample was calcined under helium and oxygen atmosphere in order to obtain the Cu_{He}-Al pillared clay and Cu_{Oxy}-Al pillared clay, respectively. Both Cu_{He}-Al pillared clay and Cu_{Oxy}-Al pillared clay does not affect the character of the XRD pattern of Al pillared clay. However, the XRD pattern of Cu_{Oxy}-Al pillared clay was broaded, which indicating the distortion of Cu-Al pillared clay layer was produced by calcined under oxygen flow. In addition, the product calcination under helium flow was more the crystalline than under oxygen flow. The Cu_{He}-Al pillared clay showed more catalytic activity and stability than Cu_{Oxy}-Al pillared clay because the copper species of Cu_{He}-Al pillared clay was wish linked to the internal layer of Al pillared clay.

2.5 Dyes

Dyes are organic compounds with aryl rings structure which have delocalized electrons. Commonly, the dye molecules comprise of two major components, i.e. chromophores and auxochromes. The chromophores are the unsaturated functional groups, such as azo (-N=N-), ethenyl (-C=C-), nitroso (-N=O), carbonyl (-C=O), azomethine (-CH=N-), etc. The color of dye is provided by the presence of chromophore group. The auxochromes are characteristic groups which intensify color and/or improve the dye affinity to substrate. The most effective auxochromes are amino ($-NH_2$), cyano (-CN), acetyl ($-COCH_3$), carboxylic acid (-COOH), hydroxyl (-OH), sulphonic acid ($-SO_3H$) and methoxy ($-OCH_3$) groups.

The common classification of dyes is based on their origins, applications and chemical properties, especially classification by usage in textile industries. In textile industries, they are applied on fibers, such as cotton, wool, nylon, silk, etc. Synthetic dyes are extensively used in the textiles industries because they are easy to use, cheap and wide range of colors. Examples of synthetic dyes are acid, basic, direct,

reactive, vat, sulphur, disperse dyes, etc. In the present study, the basic and reactive dyes were selected as water contaminant models.

2.5.1 Basic dye

The basic dyes are water soluble and yield colored cations in solution, therefore, they are known as cationic dyes. The most popular basic dyes are diazahemicyanine, triarylmethane, cyanine, hemicyanine, thiazine, oxazine, and acridine. They have been commonly applied on paper, polyacrylonitrile, modified nylons, and modified polyesters. This research used basic yellow 1 (BY1) as wastewater model. The chemical formula of BY1 is $C_{17}H_{19}Cl\ N_2S$ as shown in Figure 2.15 and its molecular weight of 318.86 g/mole.

Figure 2.15 Chemical structure of BY1

2.5.2 Reactive dye

Reactive dyes are water soluble and yield colored anions in solution. The principle chemical classes of reactive dyes are azo (including metallized azo), triphendioxazine, phthalocyanine, formazan, and anthraquinone. These chemical classes are used for dyeing and printing of cotton, wool, etc. The reactive dyes are hydrolyzed to extent of 20% while dyeing textile substrates and therefore are discharged into the effluents in unrecoverable form [120]. This reason is the major problems of wastewater treatment before discharge into the nature. Thus, this research used the reactive orange 16 (RO16) as wastewater model, having the chemical formula of $C_{20}\ H_{17}N_3Na_2O_{11}S_3$ as shown in Figure 2.16. Its molecular weight is 617.53702 g/mole.

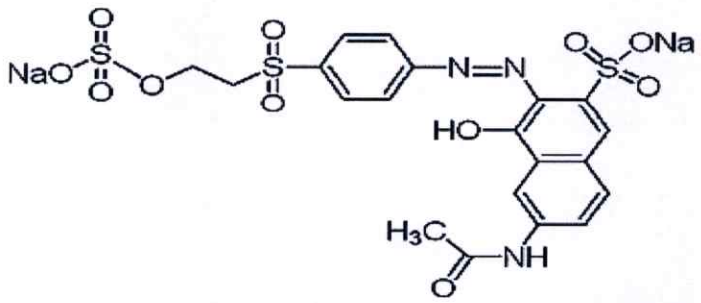

Figure 2.16 Chemical structure of RO16

2.5.3 Dye containing wastewater

The principle processes of textile industries include three main steps, i. e. pretreatment, dyeing/printing and finishing steps. Since, these processes consume large quantities of water creating large volumes of wastewater. Usually, the synthetic dyes are used for dyeing and printing in all of textile industries. The main pollutants in textile wastewater are often rich in color, containing residues of dyes and chemicals, such as complex components, many aerosols, high chroma as well as much more hard-biodegradation materials. The presence of very small amount of dyes in water is highly visible. Therefore the discharges of textile wastewater into the water resource can impede light penetration, damaging the food chain organism and aquatic life. It is important to reduce and remove dye color from wastewater before discharging to the environment.

2.5.4 Dye removal method

Generally, methodologies of dye removals are commonly classified as follow.

- Physical method accomplishes removal of substances by use of naturally occurring forces, such as gravity, electrical attraction, and van der Waal forces. Generally, the mechanisms involved in physical treatment do not change in chemical structure of the target substances [121].

- Chemical method consists of some chemical reaction or reactions, which include chemical coagulation, chemical precipitation, ion exchange, and chemical neutralization and stabilization [121].

- Biological method uses microorganisms, mostly bacteria, in the biochemical decomposition of wastewaters to stable end products. More microorganisms, or sludge, are formed and a portion of the waste is converted to carbon dioxide, water and other end products. Generally, biological treatment methods can be divided into aerobic and anaerobic methods, based on availability of dissolved oxygen [122].

- Physicochemical method is a mixture of unit processes, some physical, others chemical or biological in their action. It has been widely used for wastewater treatment because it has high removal of chroma and suspended substances [122].

Most dyes are non-biodegradable in nature and stable against degradation by sunlight and oxidation. The degradation of dyes in wastewater either traditional chemical or biological process has not been very effective [123]. Therefore, physicochemical processes are generally applied to treat colored wastewater. These processes include flocculation, precipitation, ion exchanging, membrane filtration and ozonation. Hence, one of the powerful physicochemical treatment processes for dry removal from wastewater is adsorption due to its simplicity in design and operation, low cost, insensitivity to toxic substances and great efficiency in the removal of hardly degradable dyes, when compared with the conventional removal methods

[124-125]. In addition, this process can be regenerated, resulting in significant cost saving.

2.6 Adsorption

Adsorption is a physicochemical wastewater treatment process, involving the interphase accumulation of concentration of substances at a surface or interface by physical-chemical force [126]. The adsorbate substance e.g. dye molecules, is attracted to the surface of a solid adsorbent [127]. Classifications of adsorption depend on the nature of attractive force existing between the adsorbate and adsorbent, i.e. physical adsorption (physisorption) and chemical adsorption (chemisorption) [128].

2.6.1 Physical adsorption

Physical adsorption (physisorption) is a process of weak electrostatic interaction between the adsorbate-adsorbent and adsorbate-adsorbate. The common interactions are Van der Waals, hydrogen and dipole-dipole bonds. The physisorption is a non-specific phenomenon bringing about the formation of multi-layers [129]. Since the forces of attraction are weak, the process of physisorption can be easily reversible.

2.6.2 Chemical adsorption

Chemical adsorption (chemisorption) is a process of strong chemical interaction between the adsorbate and adsorbent, i.e. covalent and ionic bonding. Since only one layer of adsorbate can chemically bond to the surface of the adsorbent, therefore chemisorption is restricted to a monolayer adsorption at the specific position on the adsorbent surface, commonly known as adsorption site. For this reason, chemisorption is irreversible and associated with activation energy [129].

The process of dye adsorption can be represented by three main steps [70]. Firstly, the diffusion/convection of dye molecules was through the bulk of solution and dye molecules was through a diffusional boundary layer (film diffusion) into the external surface of the adsorbent particles. Secondly, the diffusion of dye molecules from the surface penetrated into the interior structure of the adsorbent materials. Finally, the adsorption of dye molecules occurred on the surface of the adsorbent materials through molecular interactions [130-134]. The overall adsorption process is illustrated in Figure 2.17.

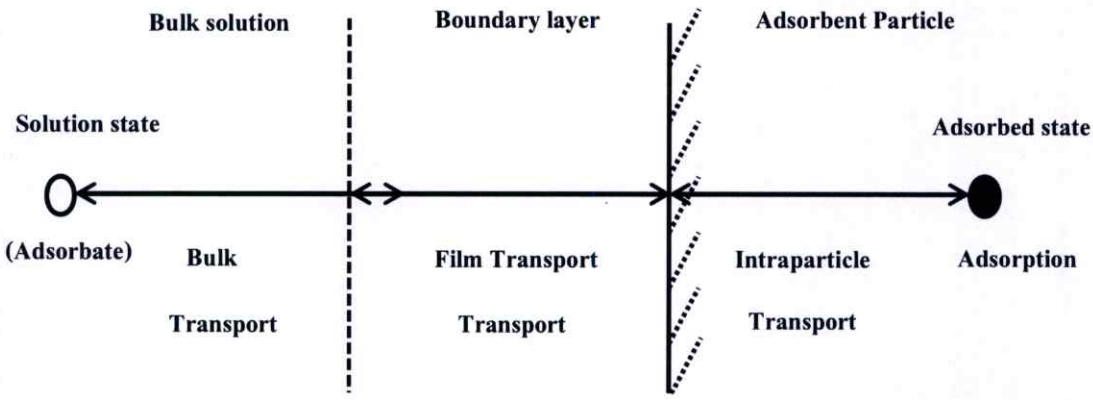

Figure 2.17 Adsorption of dye molecules into the porous adsorbent

The concentrations of dye molecules and agitation may affect the diffusion process in the first step. The second step is usually considered as the rate determining stage, which affects the adsorption of dyes on the substrate. The third step is depended on the nature of the dye molecules, such as anionic and cationic structures.

Moreover, the adsorption ability is influenced by many factors including dye/adsorbent interaction, adsorbent's surface area, particle size, temperature, pH and contact time [135]. The adsorption process can be simply represented in equation (2.2):

$$A + B \rightleftharpoons AB \qquad (2.2)$$

A : adsorbate, B : adsorbent

The AB in the above equation represents the combination of adsorbate and absorbent when the adsorbate bonds with the adsorbent. This equation that governs most adsorbates can be driven to equilibrium. In the reversible reaction, the adsorbate will continue to accumulate on to the surface of the adsorbent until the rate of the forward reaction (adsorption) is equal to the rate of the reverse reaction (desorption). At this point, the adsorption equilibrium has been achieved and further the accumulation of the adsorbate will cease to continue [136]. The adsorption equilibrium can be more or less described by adsorption isotherms.

2.6.3 Adsorption isotherm

An adsorption isotherm is a constant (*iso-*) temperature (*-therm*) equilibrium relationship between the quantity of adsorbate per unit of adsorbent and the equilibrium concentration of adsorbate in the solution. Therefore, the adsorption

behavior of adsorbate on the surface of the adsorbent can be commonly described by Langmuir [137-138] and Freundlich [139-140] equations.

- Langmuir isotherm

The linearized form of Langmuir isotherm has been used to characterize the adsorption process of dye molecules on the adsorbent as expressed in equation (2.3).

$$\frac{C_e}{q_e} = \frac{1}{K_L q_m} + \frac{C_e}{q_m} \qquad (2.3)$$

where q_e is the equilibrium amount of adsorbate adsorbed on the adsorbent (mg/g), C_e is the equilibrium concentration of adsorbate (mg/L), q_m is the maximum amount of adsorbate adsorbed on the adsorbent surface (mg/g) and K_L is a Langmuir constant (L/mg). The q_m and K_L are respectively obtained from slope and intercept of the linear plot of C_e/q_e versus C_e.

The K_L constant represents the energy associated with the adsorption, in which it increases as the strength of adsorption bond increases. The favorable nature of adsorbent on adsorbate can be expressed in term of separation factor (R_L), calculated by the following equation (2.4).

$$R_L = \frac{1}{1+K_L C_I} \qquad (2.4)$$

where C_I is the initial adsorbate concentration range (mg/L), R_L value represents that $R_L > 1$ for unfavorable adsorption, $0 < R_L < 1$ for favorable adsorption and $R_L = 0$ for irreversible adsorption [139, 141].

- Freundlich isotherm

The Freundlich isotherm expresses a multi-site reversible adsorption for heterogeneous surface, which can be written in linearized form as shown in equation (2.5).

$$\log q_e = \log K_F + \frac{1}{n} \log C_e \qquad (2.5)$$

where n and K_F are Freundlich constant respectively related to the adsorption intensity and adsorption capacity of adsorbent (mg/g), obtained from slope of the linear plot of $\log q_e$ versus $\log C_e$. In case of n = 1, it is referred to linear adsorption

and equal adsorption energies for all sites. The value of n between 2 and 10 indicates good adsorption. However, n < 1 shows that the marginal adsorption energy decreased with increasing surface concentration [142-143].

2.6.4 Adsorption kinetic

The kinetic data of adsorption are processed to understand the dynamics of adsorption process in terms of the order of rate constant. It is one of the most important characteristics in defining the efficiency of adsorption [144]. The adsorption kinetics of the heterogeneous adsorption can be expressed by the pseudo-first-order and the pseudo-second-order kinetic models [145-147]. Both models have been widely applied to explain the experimental results obtained from the aqueous pollutants, such as dyes and metal ions [148].

- Pseudo-first-order kinetic equation

$$log(q_e - q_t) = log\, q_e - \frac{tk_1}{2.303} \qquad (2.6)$$

where k_1 is the pseudo-first-order rate constant (min^{-1}), q_e and q_t are the amount of dyes adsorbed per unit amount of adsorbent at equilibrium and at time (t, min), respectively (mg/g). The values of rate constant (k_1) are obtained from the slope of linear plot of log (q_e-q_t) versus t.

- Pseudo-second-order kinetic equation

$$\frac{t}{q_t} = \frac{1}{k_2 q_e{}^2} + \frac{t}{q_e} \qquad (2.7)$$

where k_2 is the pseudo-second-order rate constant (g/mg.min), q_e and q_t are the amount of dyes adsorbed per unit amount of adsorbent at equilibrium and at time (t, min), respectively (mg/g). The values of rate constant (k_2) and q_e are respectively obtained from the intercept and slope of linear plot of t/q_t versus t.

However, there is not only one methodology used for all type of dye wastewater. In the present study, we consider that the contaminants in the textile industrial wastewater is the combination of several dye stuffs even if cationic and anionic dyes. It is, therefore, the adsorption capacities of pillared clay might be limited. In this context, advance oxidation processes (AOP) are considered a highly competitive water treatment technology for the removal of those dyes pollutants

not treatable by conventional techniques due to their high chemical stability and/or low biodegradability [149].

2.7 Advance oxidation processes

One of the most attractive methods for water and wastewater purification, called advanced oxidation processes (AOP) have been studied and developed. The AOP processes mostly use hydrogen peroxide (H_2O_2) as the main oxidizing agent, which generate hydroxyl radicals (HO•) in sufficient quantity to affect water treatment [150]. Many systems are qualified under this broad definition of AOP, included Fenton reaction [151], photo Fenton reaction [152]. These reactions can be divided to two main types as homogeneous and heterogeneous.

- Homogeneous reaction, the catalyst is in the same phase as the reactants. This process requires the advance of separation process to recover the catalyst in order to prevent contamination from the treated water. Disadvantages of this reaction are costly of recovering and enable catalyst reuse.

- Heterogeneous reaction, the catalyst is in a difference phase from the reactants. It is easy to the catalysts from the treated water andable to be reused. In addition, the pillared clays are widely uses as catalyst support because of their high specific surface area.

2.7.1 Fenton reaction

The Fenton reaction has been known since 1894 by Fenton H.J.H. and is currently one of the most powerful oxidizing reactions available. In this reaction, the peroxide is broken down into a hydroxide ion (HO^-) and a hydroxyl free radical (HO•) in the process of transition metal cation catalysts. The hydroxyl free radical is the primary oxidizing species and can be used to oxidize and break apart the organic molecules. The Fenton reaction can be expressed as shown in equation (2.8) [153].

$$M^{n+} + H_2O_2 \longrightarrow M^{(n+1)+} + HO^- + HO\bullet \qquad (2.8)$$

where M is a metal transition. The basic chemistry, as well as applications of Fe^{2+}/H_2O_2 and Fe^{3+}/H_2O_2 are used as catalyst for Fenton reaction wastewater treatment. The reaction between Fe^{2+}/H_2O_2 and Fe^{3+}/H_2O_2 was shown in equation (2.9) and (2.10), respectively.

$$Fe^{2+} + H_2O_2 \longrightarrow Fe^{3+} + HO^- + HO\bullet \qquad (2.9)$$

$$Fe^{3+} + H_2O_2 \longrightarrow Fe^{2+} + H^+ + HOO\bullet \qquad (2.10)$$

In this research, the application of Cu^{2+}/H_2O_2 system is investigation for clay removal. The catalytic reaction between hydrogen peroxide and a Cu^{2+} ion are shown in equation (2.11) and (2.12) [154-155].

$$Cu^{2+} + H_2O_2 \longrightarrow Cu^{+} + HOO\bullet + H^{+} \qquad (2.11)$$

$$Cu^{+} + H_2O_2 \longrightarrow Cu^{2+} + HO\bullet + OH^{-} \qquad (2.12)$$

The Cu^{2+} reacted with the H_2O_2, leading to the formation of strong oxidizing species as shown in the chemical equation (2.11) and (2.12). At the first stage (Eq. (2.11)), the H_2O_2 decomposition with Cu^{2+} resulted in the formation of hydroperoxyl radical (HOO•) and Cu^{+}, then the Cu^{+} reactive intermediate further reacted with the H_2O_2, producing the Cu^{2+} and HO• in the second stage (Eq. (2.12)). These reactive radicals could oxidize organic contaminants in wastewater, resulting in decolorization, degradation and mineralization to CO_2 and H_2O [156-158] as follows in equation (2.13).

$$2R\text{-}H + 2HO\bullet \longrightarrow 2R + 2\,H_2O \qquad (2.13)$$

The rate of degradation of organic pollutant with Fenton like reagents is strongly accelerated by irradiation with UV-Vis light, known as photo-Fenton reaction [149].

2.7.2 Photo Fenton reaction

The oxidizing power of the Fenton system can be greatly enhanced by irradiation with UV or UV-visible light. This is an extension of Fenton process which takes advantage from UV-visible light irradiation at wavelength values higher than 300 nm [100]. The UV-visible irradiation can increase the degradation rate of hydrogen peroxide and the photo-reduction rate of Cu^{2+} ions, which produce new HO• radicals with H_2O_2 according to equation (2.14) and (2.15), respectively. In addition, the UV radiation can induce the formation of more HO• radicals from the decomposition of water molecules in the present of Cu^{2+} as shown in equation (2.16) [159-161].

$$H_2O_2 \xrightarrow{h\nu} 2\,HO\bullet \qquad (2.14)$$

$$Cu^{2+} + H_2O_2 \xrightarrow{h\nu} Cu^{+} + HO\bullet + H^{+} \qquad (2.15)$$

$$Cu^{2+} + H_2O \xrightarrow{h\nu} Cu^{+} + HO\bullet + H^{+} \qquad (2.16)$$

Besides, the Cu^{+} intermediate produced in equation (2.8) and (2.9) can be further reacted with the H_2O_2 as previously shown in equation (2.5). Therefore, the higher quantity of HO• radicals, the faster catalytic oxidation of wastewater is obtained in the photo Fenton system.

Literature reviews

Bouberka Z. *et al* [162] studied on the effect of Al pillared clay on wastewater treatment. Na-bentonite and Al pillared bentonite (Alpill-bentonite) were used as adsorbents. The 0.1 g adsorbent was added to 100 ml of supranol yellow (4GL) solution, using 100 mg/L of initial dye concentration and various adsorption times, i.e. 5, 10, 15, 20, 30, 45, 50, 60, 75 and 120 min. The Na-bentonite and Alpill-bentonite reached their equilibrium in 45 min with 37% of dye removal and 30 min with 60% of dye removal, respectively. Both Na-bentonite and Alpill-bentonite were fitted to pseudo-first-order of kinetic model. The rate constants of Na-bentonite and Alpill-bentonite were 0.078 and 0.079 min^{-1}, respectively. The dye removal percentage decreased with increasing the amount of Na-bentonite. In contrast, the increasing amount of Alpill-bentonite could increase the percentage of dye removal, however, it remained constant after adsorbent dosage of 3 g/L. In the concentration range of 10-100 mg/L, the Alpill-bentonite showed higher adsorption capacity than the Na-bentonite. The Alpill-bentonite was fitted with Langmuir and Freundlich equations, whereas the Na-bentonite was only obeyed to Langmuir equation.

Gurses A. *et al* [163] studied on the effect of MMT on the removal of methylene blue (MB) containing wastewater by adsorption process. The 0.1 g MMT was added to 100 ml of MB solution using various initial MB concentrations, i.e. 10, 20, 30, 40, 50, 60, 70, 80, 90 and 100 mg/L. The increase in initial dye concentration led to an increase in adsorption capacity from 9.2 to 58.3 mg/g for respectively increasing initial concentration from 10 to 100 mg/L. The percentage of dye removal decreased with increasing of adsorption temperature from 20 to 40 °C, however, the adsorption capacity slightly increased when increasing the temperature from 40 to 60 °C. When increasing the adsorbent amount from 0.1 to 0.3 g, the adsorption capacity respectively increased from 57.1 to 66.1 mg/g. The regression coefficient for linear plot of pseudo-second-order was higher than pseudo-first-order. Therefore, the adsorption kinetic of MB sorption on MMT was obeyed to the pseudo-second-order.

Manohar D.M. *et al* [164] studied on the adsorption performance of Al pillared bentonite (Alpill-bentonite) for cobalt (II) removal. The 0.1 g Al pillared bentonite was added to 50 ml of Co(II) solution. The effect of pH, contact time, initial concentration and adsorption isotherm were studied. It was found that the surface charge of Alpill-bentonite was positive at pH below 4.2, thus the Co(II) poorly

adsorbed on the surface of Alpill-bentonite at very low of pH value. The adsorption capacity of Co(II) increased with increasing contact time and reached at the maximum adsorption within 24 h. Moreover, the adsorption capacity increased when increasing the initial Co(II) concentration from 10 to 100 mg/L, whereas the percentage of Co(II) removal decreased with increasing initial concentration. The adsorption isotherm at 30 °C was carried out using various Co(II) concentrations from 10 to 500 mg/L at pH 6. The Alpill-bentonite was fitted with both Langmuir and Freundlich isotherms. The value of 1/n and R_L were between $0.1<1/n<1.0$ and less than 1, respectively, indicating highly favorable adsorption of Co(II) onto the Alpill-bentonite. The kinetic adsorption of Co (II) onto the Alpill-bentonite had two stage; (1) external mass transfer diffusion and (2) intraparticle mass transfer diffusion.

Ntampegliotis K. *et al* [165] studied on the decolorization of dye containing wastewater by Fenton reactions. The procion navy H-exl (PNH), procion crmson H-exl (PCH) and procion yellow H-exl (PYH) were used as pollutant models. The Fe^{3+} or Fe^{2+} and H_2O_2 were used as catalyst and oxidizing agent, respectively. In oxidation experiment, the H_2O_2 was added to dye solution and then quickly added the catalyst to the dye solution. The effect of pH, H_2O_2 concentration, catalyst concentration and catalyst type were investigated. It was observed that the most suitable pH range was in between 3 and 4, while the rate of decolorization rapidly decreased at the pH below 2.0. The decolorization efficiencies of PNH and PCH were optimized when the H_2O_2 concentration was in between 0.2 and 2.0 % (w/w). Moreover, both PNH and PCH dye solutions showed the optimum decolorization rate at the range of $FeCl_3$ concentration between 0.005 and 0.1 % (w/w), whereas the optimum for PYH solution system was at the $FeCl_3$ concentration higher than 0.1 % (w/w). The rate of Fe^{2+} was faster than Fe^{3+} during the early time and then completed within 10 min in the pH range between 3 and 5. When the UV radiation was introduced into the reaction, the rate of decolorization and TOC reduction was faster than the Fenton reaction.

Baskaralingam P. *et al* [166] studied on the effect of organobentonite on the removal of acid red 151 (AR151). The cetyldimethylbenzylammonium chloride bentonite (CDBA-bent) and cetylpyridinium chloride bentonite (CP-bent) were used as adsorbents. In the adsorption experiment, the 0.1 g of adsorbent was added into 50 ml of dye solution. The effects of adsorbent dosage and initial dye concentration were studied. The rate of adsorption increased with increasing of the amount of adsorbent from 0.005 to 0.025 g. The initial dye concentrations used in this study were 60, 80 and 90 mg/L for CDBA-bent and 70, 80 and 100 mg/L for CP-bent. The CP-bent showed higher adsorption capacity than the CDBA-bent at 80 mg/L of initial dye concentration. The adsorption capacity increased when increasing of contact

time and reached equilibrium at 60 and 90 min of CDBA-bent and CP-bent, respectively. Furthermore, the adsorption isotherm and adsorption kinetic were fitted by Langmuir model and pseudo-second-order model, respectively. The higher adsorption capacity of 357.14 mg/g for CDBA-bentonite and 416.66 mg/g for CP-bentonite was obtained from Langmuir equation.

Wang L. and Wang A. [167] studied on the effect of surfactant-modified MMT on the removal of congo red (CR). The cetyltrimethylammonium bromide (CTAB) was used as surfactant in order to intercalated in the MMT, denoted as CTAB-MMT. In the adsorption experiment, 0.05 g of adsorbent was added in to 25 ml of dye solution. The effect of pH (4.0 – 9.0), temperature (30 – 50 °C) and contact time (10 – 900 min) were studied. When the pH value of the dye solution was raised from 4.0 to 9.0, the adsorption capacity reduced slowly from 381 to 344 mg/g. The adsorption capacity increased from 350.13 to 399 mg/g when increasing temperature from 30 to 50°C. The adsorption capacity rapidly increased within 180 min and then reached adsorption equilibrium at 480 min.

Monvisade P. and Siriphannon P. [21] studied on the effect of chitosan intercalated MMT nanocomposites (Chi-MMT) on the removal of basic blue 66 (BB66), basic blue 9 (BB9) and basic yellow 1 (BY1). The Na-MMT, chitosan and Chi-MMT were used as adsorbents. In the adsorption experiment, the 1.0 g of adsorbent was added into 100 ml of 500 mg/L dye solution. After that, the mixture was stirred for 2 h at room temperature and aged overnight. It was observed that the Chi-MMT possessed higher adsorption capacities for BB9 (97%, 48.9 mg/g), BB66 (99%, 49.2 mg/g) and BY1 (92%, 45.9 mg/g) than the Na-MMT and chitosan. However, the adsorption of BB9 and BY1 on chitosan was slightly higher than those of Na-MMT, whereas the excellent adsorption was obtained for BB66. When increasing the initial concentration of basic dye from 500 to 10,000 mg/L, the Chi-MMT obviously showed the distinct adsorption capacities for removal all dyes. The Chi-MMT showed the highest adsorption capacity for BB66, i.e. 977 mg/g.

Giordano L.A. *et al* [168] studied on the catalytic activities of copper zeolite (Cu-Ze) and copper pillared clay (Cupill-clay) for wet hydrogen peroxide catalytic oxidation (WHPCO) of olive oil mill (OMW) containing wastewater. The catalyst was added into waste solution (500 mg/L) and heated to 50 and 80 °C for Cu-Ze and Cupill-clay, respectively. Afterward, the H_2O_2 was continuously feed at 0.5 ml/h into the waste solution. The catalyst/wastewater ratio of Cu-Ze and Cu-PILC was 0.6g/l OMW and 5g/l OMW, respectively. In comparison the overall catalytic performance between Cu-Ze and Cupill-clay, it can be considered that the lower activity of Cupill-clay was compensated by the absence of Cu leaching, which improves the possibility of catalyst reuse. The used Cu-Ze was regenerated and reused at the second

WHPCO reaction cycle for OMW treatment. The percentage of COD reduction slightly decreased from 87.3% to 84.5% in comparison with the first cycle. This result caused by the partial copper leaching after the first reaction cycle. Moreover, both catalysts showed the high conversion in the oxidation of poly-phenols and were able to drastically reduce the chemical oxygen demand (COD), the biochemical oxygen demand (BOD) and the non-biodegradability of the OMW wastewater.

Abdullah A.H. *et al* [169] studied on the effect of activated carbon (AC) and copper oxide doped on activated carbon (Cu-AC) on decolorization of reactive orange 16 (RO16) by adsorption process. 0.5 g of catalysts was added to a beaker containing 1000 ml of 25 mg/L dye solution and then continuously stirred for 6 h. Although the Cu-AC adsorbent showed higher dye adsorption than the AC adsorbent, but the percentage of dye removal was lower than 30% after 6 h of adsorption process. Therefore, the presence of H_2O_2, UV and H_2O_2/UV in the decolorization process was investigated. The effect of H_2O_2 and UV light on the decolorization of RO16 was carried out by adding a fixed amount of 1 M H_2O_2 solution and irradiating the dye solution with UV lamp. However, the system with the corporation of H_2O_2 and UV radiation was faster and higher generated the strongly radical (OH•) than the other systems. The decolorization efficiency of the Cu catalyst under four different conditions was observed to have the following order: Cu-AC/H_2O_2/UV > Cu-AC/H_2O_2 > Cu-AC/UV > Cu-AC/adsorption.

Molu Z.B. and Yurdakoc K. [170] studied on the adsorption capacity of Al pillared clay for trimethoprim (TMP) solution. The Al pillared K10 (Alpill-K10) and Al pillared KSF (Alpill-KSF) were used as adsorbents. The adsorption experiments were carried out in flasks containing 0.01 g of adsorbents and 25 ml of TMP solution. The mixtures were shake and temperature controlled in the water bath. The effect of adsorbents, contact time, adsorption kinetic and adsorption isotherm were investigated. Although the amount of Alpill-K10 in TMP adsorption was lower than that of the Alpill-KSF, but the adsorption capacity exhibited higher than Alpill-KSF. However, the adsorption percentage of Alpill-KSF increased with increasing the amount of adsorbents. The suitable amount of adsorbents on TMP adsorption was 10 and 100 mg of Alpill-K10 and Alpill-KSF, respectively. When increasing the contact time, the adsorption capacities of Alpill-K10 and Alpill-KSF increased and reached the equilibrium after 120 and 240 min, respectively. The adsorption kinetic of all adsorbents corresponded to the pseudo-second-order model with $R^2 > 0.978$. Moreover, the Freudlich isotherm much better fitted than Langmuir isotherm when comparing the value of R^2.

Kaemkit C. *et al* [171] studied on the effect of chitosan intercalated MMT nanocomposites (Chi-MMT) on the removal of basic blue 66 (BB66) and basic yellow

1 (BY1). The Na-MMT, chitosan and Chi-MMT were used as adsorbents. In the adsorption experiment, 0.1 g of adsorbent was added in to 100 ml of 500 mg/L dye solution. After that, the mixture was stirred for 2 h at room temperature and aged overnight. It was observed that the Chi-MMT showed the complete adsorption of BB66 (>99%, 49.8 mg/g) and BY1 (>99%, 49.8 mg/g) over those of Na-MMT and chitosan. The adsorption kinetic of Chi-MMT was carried out using 3000 mg/L of initial BY1 concentration and varying the contact time from 5 to 1440 min. The adsorption capacity increased rapidly within 10 min and then reached equilibrium. The correlation coefficients (R^2) from pseudo-second-order linear plot was higher than pseudo-first-order. Therefore, the kinetic adsorption of Chi-MMT was fitted with pseudo-second-order equation. The adsorption isotherm was carried out varying the initial BY1 concentration from 500 to 7000 mg/L and adsorption time of 1440 min. The adsorption capacity sharply increased from 48.4 to 282.8 mg/g due to the 500 to 4000 mg/L of initial dye concentration, and slightly increased later up to 302.8 mg/g. Moreover, the adsorption isotherm was fitted both Langmuir and Freundlich isotherm models.

Chapter 3
Experimental

3.1 Chemical reagents

Chemical reagents	Grade of purity	Manufactures
1. Mac-gel Montmorillonite (MMT)	Analytical grad	Thai Nippon
2. Aluminum nitrate ($Al(NO_3)_3 \cdot 9H_2O$)	Analytical grad	Rankem
3. Sodium hydroxide (NaOH)	Analytical grad	Labscan
4. Copper (II) sulfate ($CuSO_4 \cdot 5H_2O$)	Analytical grad	Carlo Erba
5. Basic Yellow 1 (BY1, dye content 70%)	Analytical grad	Acros rganics
6. Reactive Orange 16 (RO16, dye content 50%)	Analytical grad	Sigma Aldrich
8. Hydrogen peroxide (H_2O_2, 35 % w/v)	Analytical grad	Fisher chemicals

3.2 Apparatus

Apparatus	Model, Manufactures
1. Nuclear magnetic resonance spectrometer (NMR)	Inova 500, Varian
2. X-ray fluorescence spectrometer (XRF)	SRS 3400, Bruker AG
3. X-ray Diffractrometer (XRD)	D8 Advance, Bruker AG
4. Scanning electron microscope and energy dispersive X-ray microanalysis (SEM-EDX)	JEOL, JSM-5410
5. Gas Adsorption Analyzer	Autosorb-1, Quantachrome

Apparatus	Model, Manufactures
6. UV-VIS Spectrophotometer	Helios omega, Thermo Scientific
7. Total Organic Carbon analyzer (TOC)	TOC-VCPH, Shimadzu
8. Ultrasonic horn	VC-505, Vibra Cell
9. Furnace	Furnace 600, Thermolyne
10. Oven	Isotemp, Fisher Scientific
11. Peristaltic pump	V 77120-52, Cole Parmer
12. Centrifuge machine	Centaur 2, Sanyo
13. Balance	TC-254, Denver Instrument
14. Hot Plate	C-MAG HS 7, Fisher Scientific
15. Thermostat	Euro-ST B, Ika Laboratory Staufen Ltd.
16. UV lamp	TUV TL Mini (254 nm), Philips
17. Sieve	Mesh No. 400, Retsch
18. Mortar and pestle	-
19. Porcelain crucible	-
20. Glassware	-

3.3 Studied factors

The experimental procedures in this thesis were divided into 3 main sections as follow;

3.3.1 Preparation of aluminum pillared montmorillonite

Various preparation conditions were carried out, i.e.

3.3.1.1 Preparation of aluminum polyoxocation solution (AlOH)

- Molar ratio of OH/Al, i.e. 2.0 and 2.4
- Reaction temperature of conventional stirring method, i.e. room temperature and 60 °C

- Preparation method of AlOH solutions, i.e. conventional stirring method and ultrasonic assisted method
- Reaction time of ultrasonic assisted method, i.e. 10, 20, 30 and 60 in

3.3.1.2 Preparation of aluminum pillared montmorillonite (Alpill-MMT)

- Preparation method of Al-pill-MMT, i.e. conventional stirring method and ultrasonic assisted method
- Reaction temperature of conventional stirring method for Alpill-MMT preparation, i.e. room temperature and 60 °C
- Reaction time of ultrasonic assisted method for Alpill-MMT preparation, i.e. 10, 20, 30 and 60 min

3.3.2 Preparation of copper doped aluminum pillared montmorillonite (Cu-Alpill-MMT)

Various preparation conditions were carried out, i.e.

- Preparation method of Cu-Alpill-MMT, i.e. ultrasonic assisted adsorption and impregnation
- Weigh percent of copper dopant in impregnation method, i.e. 4, 7, 10 and 13 wt.%
- Type of precursor, i.e. AlOH-MMT and Alpill-MMT

3.3.3 Waste treatment process of dye solution

Various treatment conditions were carried out, i.e.

- Treatment method, i.e.
  - Adsorption: batch and continuous method
  - Catalytic oxidation: Fenton and photo Fenton reaction
- Type of dye solution, i.e. basic yellow 1 (BY1) and reactive orange 16 (RO16)
- Contact time of BY1 adsorption, i.e. 30, 60, 120, 150, 180, 210, 240, 270 and 300 min
- Initial concentration of BY1 solution in batch adsorption processes, i.e. 50, 100, 300, 500, 700, 1000, 2000 and 3000 mg/l
- Contact time of RO16 adsorption, i.e. 60, 120, 180 and 240 min
- Reaction time of Fenton and photo Fenton process for RO16 removal, i.e. 30, 60, 90, 120, 240 and 360 min

3.3 Experiment

3.4.1 Preparation of montmorillonite

Starting material was a commercial sodium montmorillonite (Na^+-MMT) with the cation exchange capacity of about 1 meq/g. The as-received Na^+-MMT was purified by dispersion in distilled water, sonication for 10 min and further decantation the upper layer of the suspension. The decanted suspension was filter and then dried at 100 °C for 24 hrs. Finally, the Na^+-MMT was characterized by XRF, XRD, and N_2 adsorption. The flow diagram of this stage was shown in the Figure 3.1.

3.4.2. Preparation of aluminum polyoxocation solution (AlOH)

The preparation procedures of aluminum polyoxocation solution (AlOH) were performed using 2 different methods as follow;

A. Conventional stirring method

The AlOH was prepared by slow adding 0.4 M NaOH solution (2 ml/min) into 0.4 M $Al(NO_3)_3 \cdot 9H_2O$ solution, the molar ratio of OH/Al in the solution was varied at 2.0 and 2.4. The mixture was continuously stirred at room temperature for 24 hrs (or/60 °C for 3 hrs and then overnight at room temperature).

B. Ultrasonic assisted method

In this method, the AlOH solution was prepared by mixing 0.4 M NaOH and 0.4 M $Al(NO_3)_3 \cdot 9H_2O$ with a high power ultrasonic probe (20 KHz and 500 W) at room temperature. The reaction time in the solution was varied i.e. 10, 20, 30 and 60 min.

All AlOH preparation conditions were concluded in Table 3.1. The structures of as-prepared solutions were characterized by ^{27}Al-NMR.

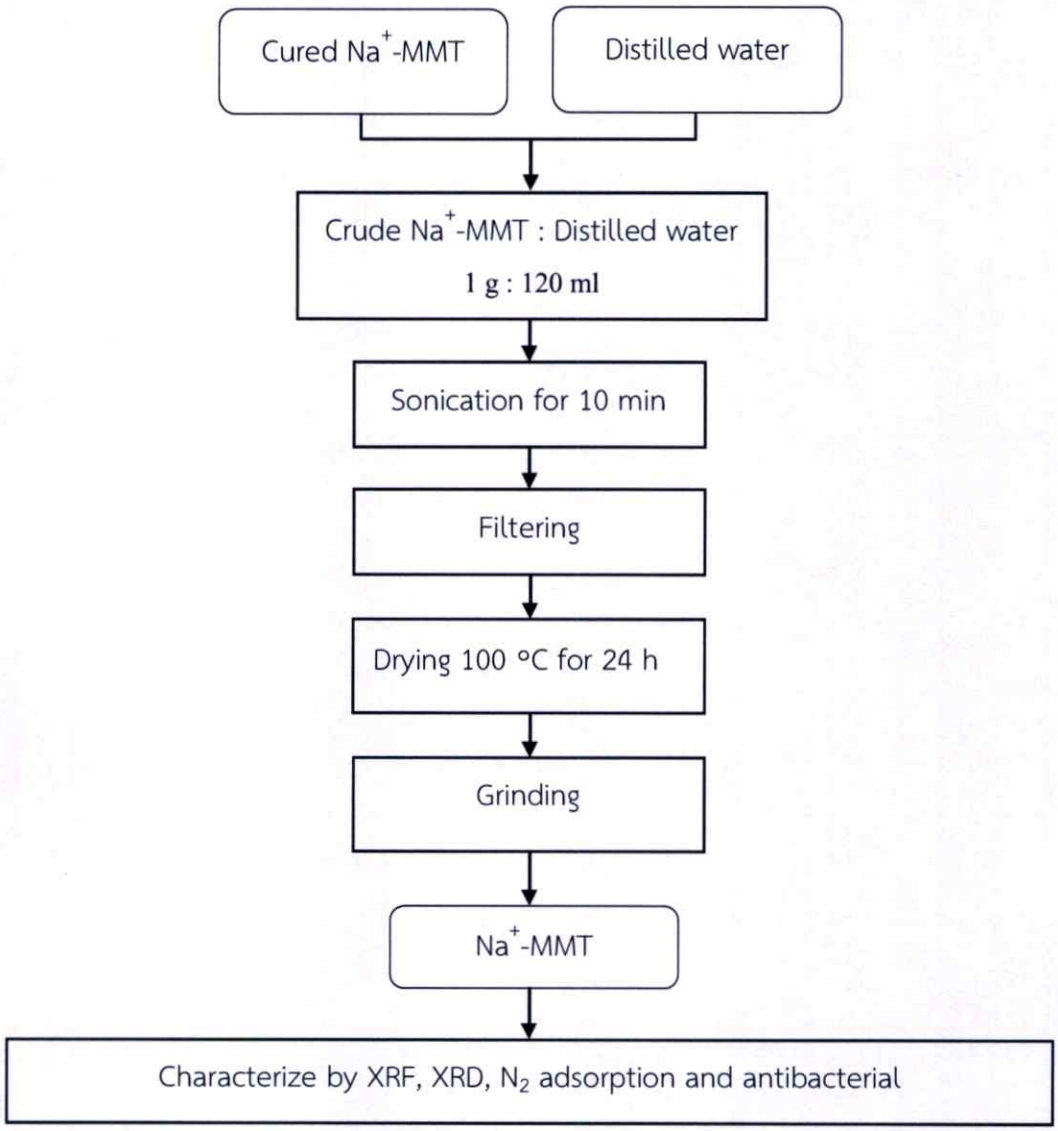

Figure 3.1 Flow diagrams for preparation of Na^+-MMT.

Table 3.1 Preparation conditions of AlOH solution

Sample	OH/Al	Temperature	Reaction time	Method
AlOH-2.0-Str-rt	2.0	Room temperature	24 h	Conventional stirring
AlOH-2.0-Str-60		60 °C		
AlOH-2.4-Str-rt	2.4	Room temperature	24 h	Conventional stirring
AlOH-2.4-Str-60		60 °C		
AlOH-2.4-Ultra-10		Room temperature	10 min	Ultrasonic assisted
AlOH-2.4-Ultra-20			20 min	
AlOH-2.4-Ultra-30			30 min	
AlOH-2.4-Ultra-60			60 min	

3.4.3 Preparation of aluminum pillared montmorillonite (Alpill-MMT)

The preparation procedures of aluminum pillared montmorillonite (Alpill-MMT) were performed using 2 different methods as follow;

A. Conventional stirring method

The AlOH-2.4 solution preparation by conventional stirring method was slowly added (2 ml/min) to the Na^{+}-MMT aqueous suspension, in which the ratio of mmol Al^{3+}/g Na^{+}-MMT was 2.5. The AlOH-MMT suspension was vigorously stirred at room temperature for 24 hrs (or/ 60 °C for 3 hrs and then overnight at room temperature). The modified AlOH-MMT was filtered and washed several times with distilled water. The AlOH-MMT was dried in an oven at 100 °C for overnight and calcined at 500 °C for 2 hrs in order to obtain the aluminum pillared MMT (Alpill-MMT-Str).

B. Ultrasonic assisted method

In this method, the Na^{+}-MMT was added into the AlOH-2.4 solution (ultrasonic assisted method) and then sonicated at room temperature. The reaction time was varied i.e. 10, 20, 30 and 60 min. The mmol Al^{3+}/g Na^{+}-MMT was also maintained at 2.5. The sonicated AlOH-MMT was filtered, washed several times with distilled water, dried at 100 °C for overnight and calcined at 500 °C for 2 hrs in order to obtain the aluminum pillared MMT (Alpill-MMT-Ultra). All Alpill-MMT preparation conditions were concluded in Table 3.2.

Table 3.2 Preparation conditions of Alpill-MMT

Sample	Temperature	Reaction time	Method
Alpill-MMT-2.4-60-Str-rt	Room temperature	24 h	Conventional stirring
Alpill-MMT-2.4-60-Str-60	60 °C		
Alpill-MMT-2.4-30-Ultra-10	Room temperature	10 min	Ultrasonic assisted
Alpill-MMT-2.4-30-Ultra-20		20 min	
Alpill-MMT-2.4-30-Ultra-30		30 min	
Alpill-MMT-2.4-30-Ultra-60		60 min	

Finally, all of Alpill-MMTs were characterized by XRF for measuring the chemical composition of Alpill-MMT powder and measured the basal spacing (d_{001}) by XRD. The specific surface area and pore size diameter were characterized by N_2 adsorption. The flow diagram of Alpill-MMT preparation by conventional stirring and ultrasonic assisted method was shown in the Figure 3.2 and 3.3, respectively.

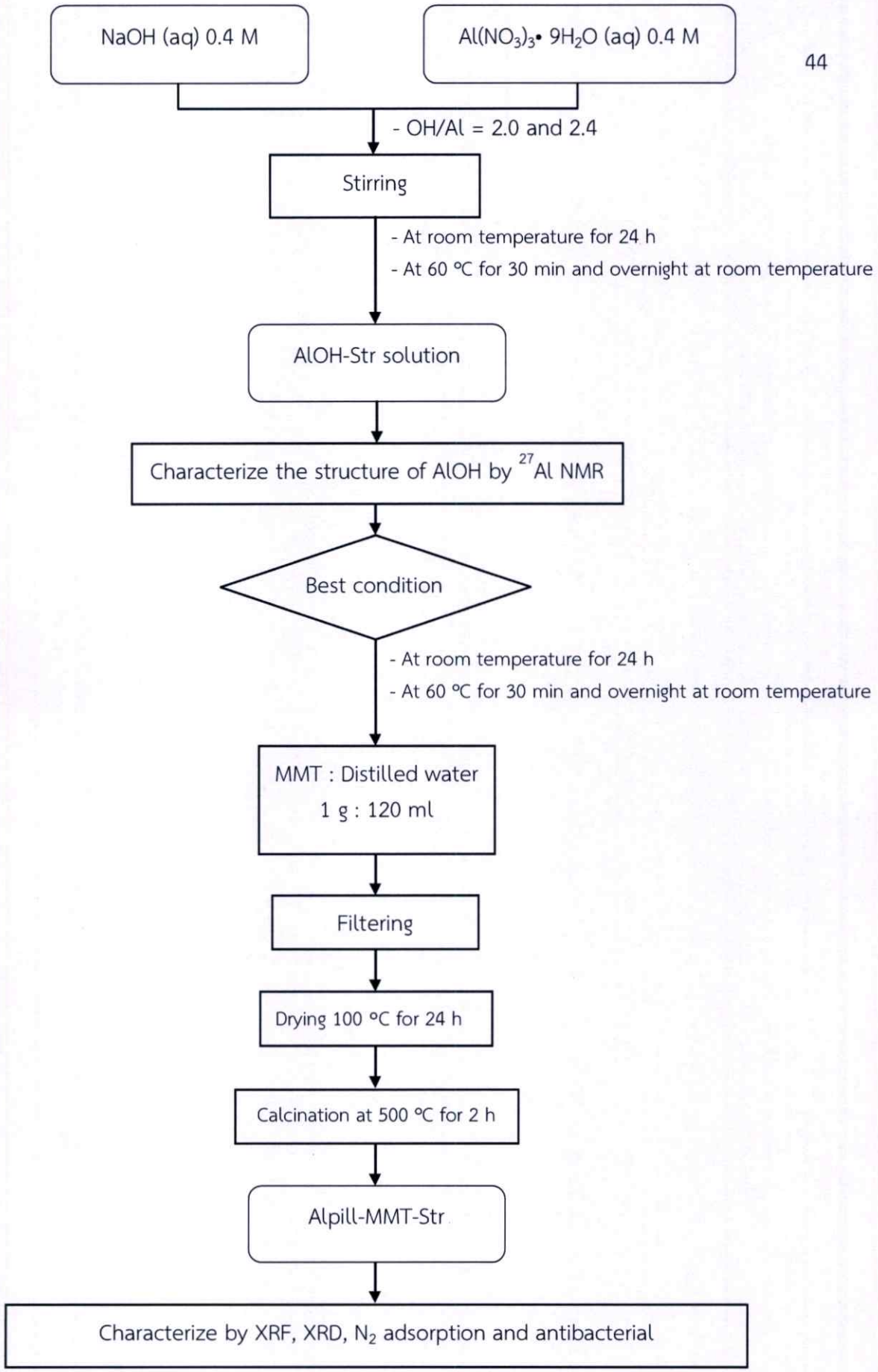

Figure 3.2 Flow diagrams for preparation of Alpill-MMT by conventional stirring method.

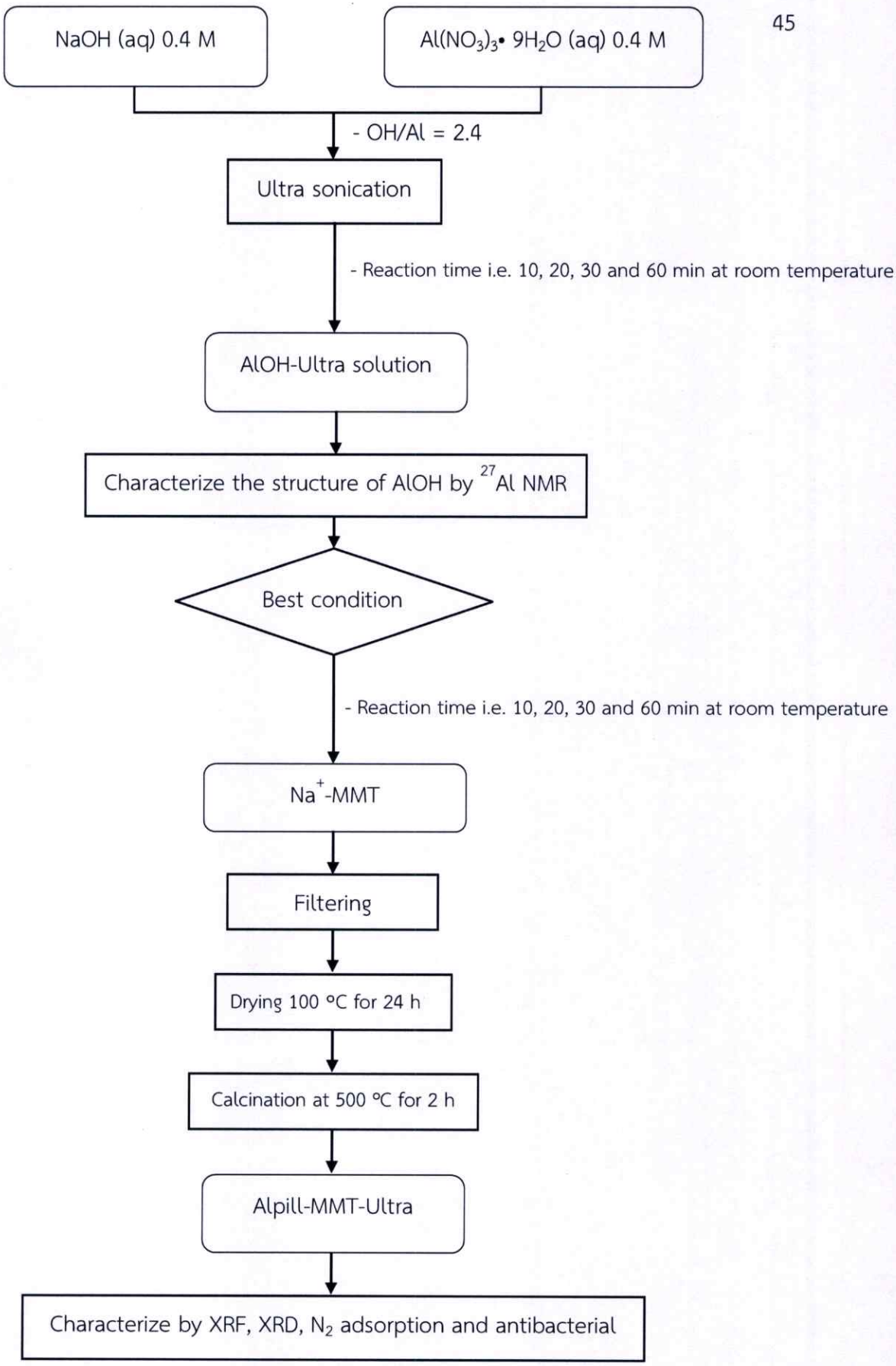

Figure 3.3 Flow diagrams for preparation of Alpill-MMT by ultrasonic assisted method.

3.4.4 Synthesis copper dope Aluminum pillared montmorillonite

A. Adsorption method

The AlOH-MMT /or Alpill-MMT precursor was dispersed in 50 ml an aqueous solution of 0.4 M $CuSO_4 \cdot 5H_2O$. The mixture was treated with a high power sonic probe (20 KHz and 500 W) at room temperature for 30 min. The modified Alpill-MMT was filtered, washed several times with distilled water, dried at 100 °C for overnight and calcined at 500 °C for 2 hrs. The calcined product was described as the copper doped Alpill-MMT (Cu-ads-Alpill-MMT).

B. Impregnation method

The AlOH-MMT was impregnated by $CuSO_4 \cdot 5H_2O$ aqueous solution under various of percent Cu^{2+} in the solution i.e. 4, 7, 11 and 13 wt%. The product was dried at 100 °C for overnight and calcined at 500 °C for 2 h. The calcined product was described as the copper doped Alpill-MMT (Cu-im-Alpill-MMT).

All Cu-Alpill-MMT preparation conditions were concluded in Table 3.3. Finally, all of sample were characterized by XRF for measuring the chemical composition of Cu-Alpill-MMT powder and measured the basal spacing (d_{001}) by XRD. Surface morphologies of the Cu-Alpill-MMTs were investigated by SEM and the elemental distribution of copper on the Cu-Alpill-MMTs surfaces was determined by EDX incorporated with the SEM.

The specific surface area and pore size diameter were characterized by N_2 adsorption. The flow diagram of copper doped Alpill-MMT preparation under adsorption and impregnation method was shown in the Figure 3.4 and 3.5, respectively.

Table 3.3 Preparation conditions of Cu-Alpill-MMT

Sample	Support	Concentration of Cu^{2+}	Method
Cu-ads-Alpill-MMT1	AlOH-MMT	0.4 M	Adsorption
Cu-ads-Alpill-MMT2	Alpill-MMT		
Cu-im-Alpill-MMT-4wt%	Al-OH-MMT	4 wt%	Impregnation
Cu-im-Alpill-MMT-7wt%		7 wt%	
Cu-im-Alpill-MMT-10wt%		10 wt%	
Cu-im-Alpill-MMT-13wt%		13 wt%	

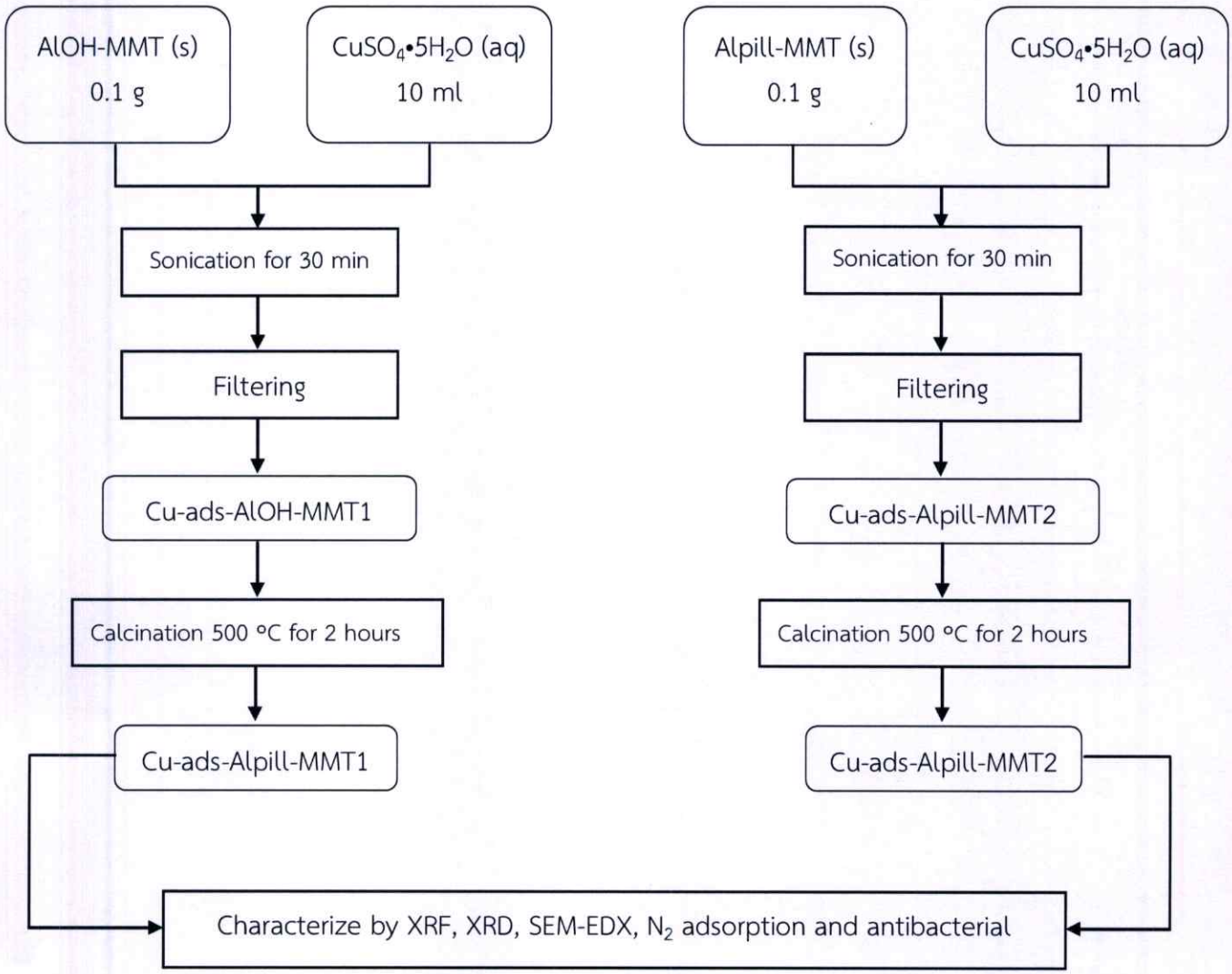

Figure 3.4 Flow diagrams for preparation of Cu-ads-Alpill-MMT by adsorption method.

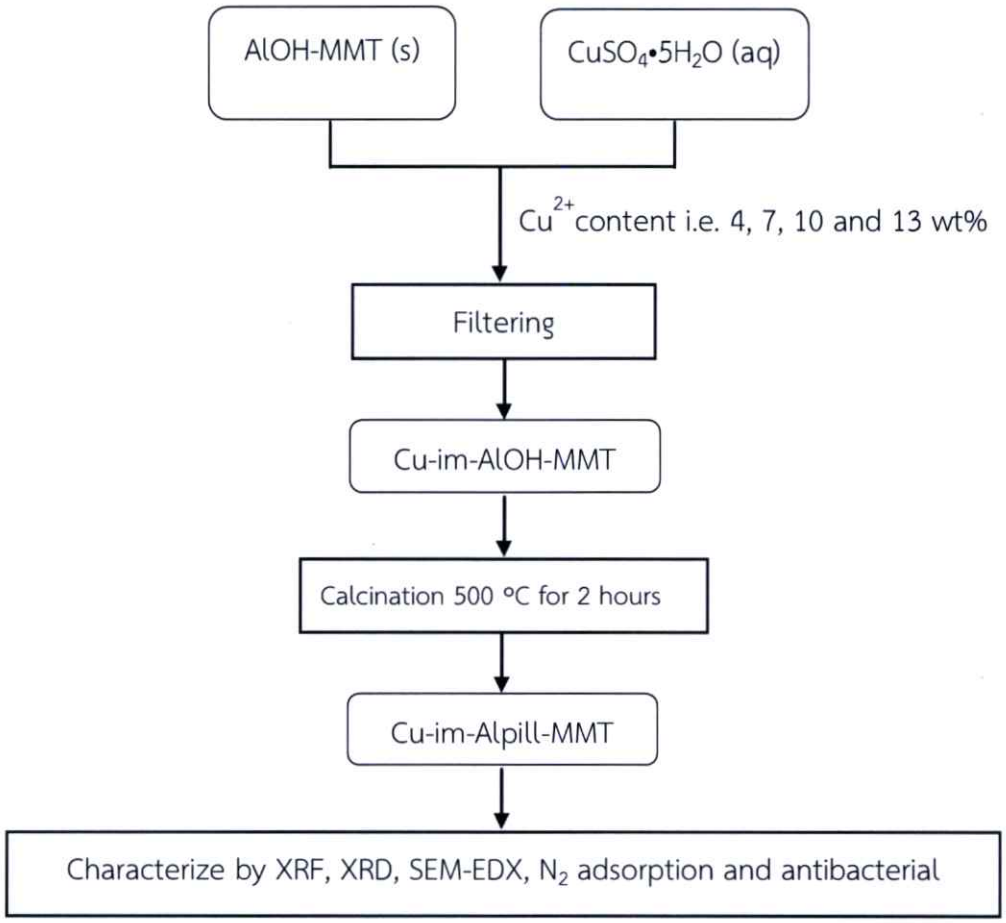

Figure 3.5 Flow diagrams for preparation of Cu-im-Alpill-MMT by impregnation method.

3.5 Waste treatment of dye solution

The experimental procedure in this stage was divided into 2 different methods as follow;

3.5.1 Adsorption method

A. Batch process

The Na^+-MMT, Alpill-MMT-Str, Alpill-MMT-Ultra and Cu-ads-Alpill-MMTs were grinded, sieved through 400 mesh stainless steel, and then used as adsorbents for dye adsorption experiment. In this system, two different kinds of dyes were used as model adsorbates, i.e. Basic Yellow 1 (BY1) and Reactive Orange 16 (RO16). The initial concentrations of dye solutions were fixed. The adsorption was performed by mixing 0.5 g of adsorbent and 50 ml of aqueous dye solution at room temperature

for 120 min. The adsorbent was separated from the dye solution by centrifugation at 5000 rpm for 5 min.

The adsorption time was varied in the range of 30 – 300 min using initial dye concentration of 1000 mg/L in order to determine the adsorption equilibrium. The adsorption was performed by mixing 0.5 g of adsorbent and 50 ml of BY1 aqueous solution at room temperature. The dye solution was separated from the adsorbent by centrifugation at 5000 rpm for 5 min.

The adsorption kinetic of Alpill-MMT-Str and Alpill-MMT-Ultra adsorbents were carried out using initial BY1 concentration of 1000 mg/L with various contact times, i.e. 30, 60, 90, 120, 150, 180, 210, 240, 270 and 300 min. The adsorption was performed by mixing 0.5 g of adsorbent and 50 ml of BY1 aqueous solution at room temperature. The adsorption kinetic data were, therefore, fitted to the equations of pseudo-first-order and pseudo-second-order in order to determine the most suitable model.

The adsorption isotherms of Alpill-MMT-Str and Alpill-MMT-Ultra were determined from the adsorption experiments using various initial BY1 concentrations, i.e. 50, 100, 300, 500, 700, 1000, 2000 and 3000 mg/L. The adsorption was performed by mixing 0.5 g of adsorbent and 50 ml of BY1 aqueous solution at room temperature. The adsorption data were therefore fitted to the Langmuir and Freundlich isotherms in order to find the most suitable model.

The absorbencies of the dye solutions were determined by UV visible spectrophotometry (UV-Vis). In addition, the total organic carbon in the dye solutions before and after adsorption experiment was measured by TOC analyzer (Shimadzu, TOC-VCPH). The flow diagram of batch dye adsorption was shown in the Figure 3.6.

B. Continuous process

The Alpill-MMT-ultra was grinded, sieved through 400 mesh stainless steel, and then used as adsorbent for dye removal under continuous process. The adsorption was performed by packing 1.0 g in glass of Alpill-MMT ultra adsorbent column (diameter = 2 cm and high = 10 cm). The 300 mg/L BY1 solution was continuously fed into column using rate of about 2 ml/min at room temperature. The treated solutions were collected at regular time intervals and the concentration was measured by UV-vis. The flow diagram of continuous dye adsorption was shown in the Figure 3.7.

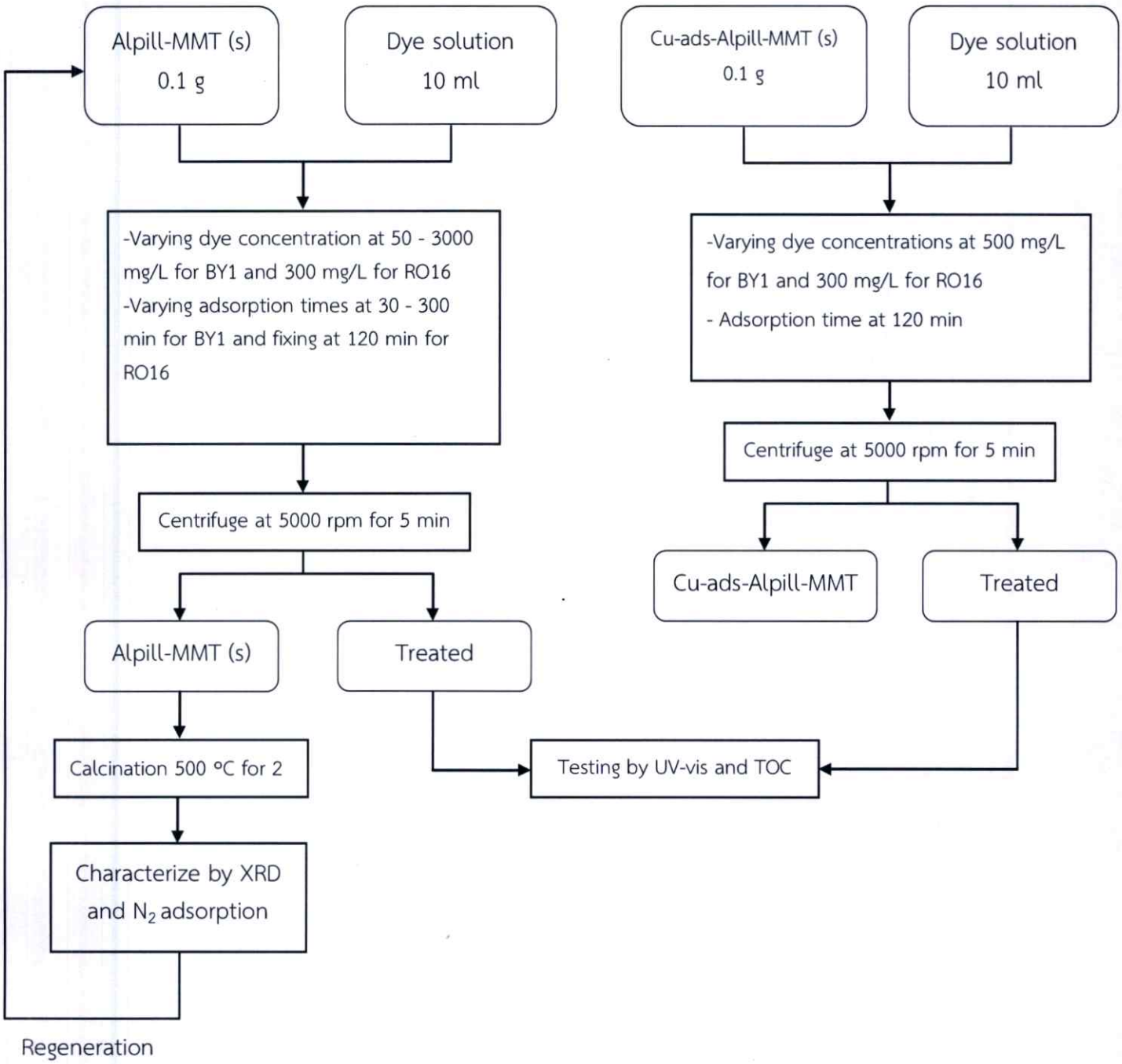

Figure 3.6 Flow diagrams for waste treatment by batch adsorption process

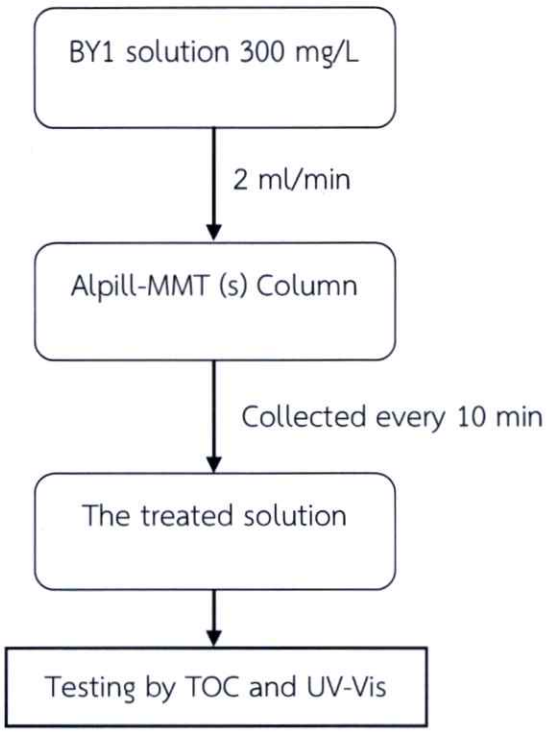

Figure 3.7 Flow diagrams for waste treatment by continuous adsorption process.

3.5.2 Catalytic oxidation process

Catalytic abilities of Alpill-MMT and Cu-Alpill-MMTs for RO16 oxidation were investigated using the Fenton and photo Fenton processes.

A. Fenton process

This process was performed by mixing 0.2 g of Alpill-MMT or Cu-Alpill-MMTs, 20 ml of 300 mg/L RO16 solution and 5 ml of 0.1 M hydrogen peroxide (H_2O_2). The mixture was continuously stirred for various reaction times, i.e. 60, 120, 240 and 360 min. After predetermined reaction time, the catalyst was separated from the mixture solution by centrifugation at 5000 rpm for 5 min. The flow diagram of waste treatment of dye solution was shown in the Figure 3.8.

B. Photo-Fenton process

In this process, the reaction was performed under UV radiation using the similar mixture of Cu-Alpill-MMTs, RO16 and H_2O_2 as prepared for the Fenton process in order to determine the effect of UV radiation on the oxidation efficiency. In this process, the mixture was continuously stirred under 6W UVC-radiation (254 nm; TUV TL Mini, Philips) for various reaction times, i.e. 30, 60, 90, 120, 240 and 360 min. After treatment, the Cu-Alpill-MMT was separated from the mixture solution by centrifugation at 5000 rpm for 5 min. The flow diagram of waste treatment of dye solution was shown in the Figure 3.9.

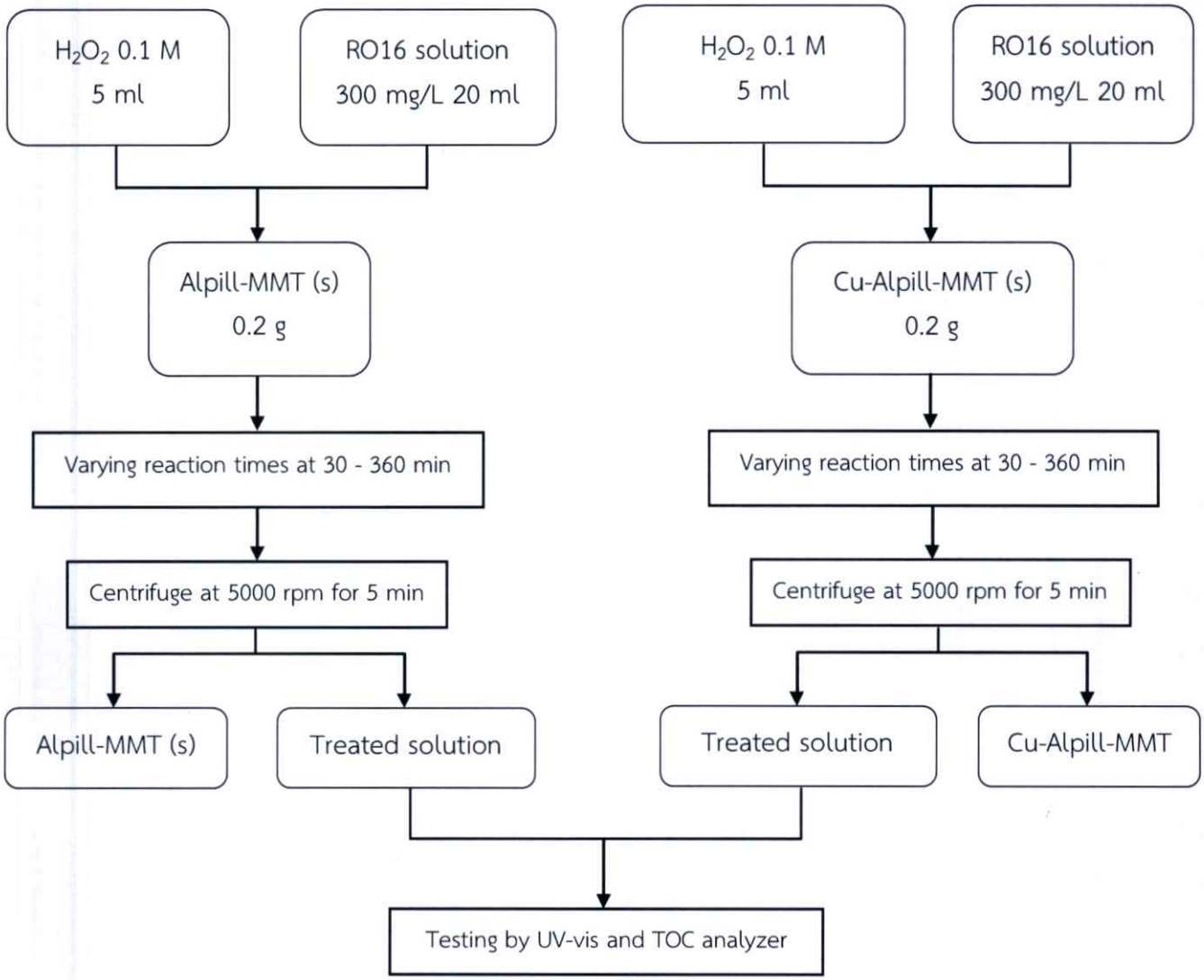

Figure 3.8 Flow diagrams for waste treatment by Fenton reaction.

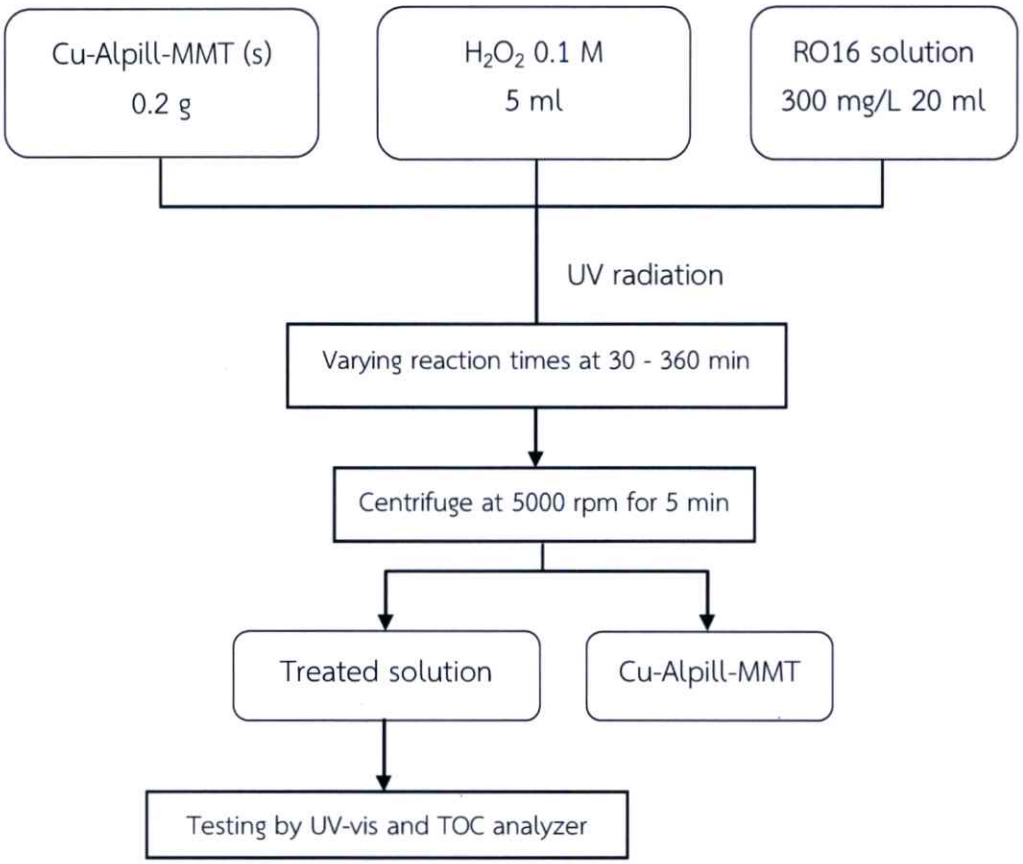

Figure 3.9 Flow diagrams for waste treatment by photo Fenton reaction.

3.6 Regeneration method

After adsorption experiments, the Al-pill-MMT-str and Al-pill-MMT-ultra adsorbents were filtered from the dye solutions and then washed several times with distilled water. The adsorbents were dried at 100 °C for overnight and calcined at 700 °C for 2 h in order to thermally regenerate the adsorbents. The thermally regenerated adsorbents were repeatedly used for the dye adsorption by mixing 0.5 g of adsorbent and 50 ml of BY1aqueous solution using initial dye concentration of 1000 mg/L and contact time of 120 min. In addition, the 2nd-Al-pill-MMTs were thermally regenerate at 700 °C for 2 h after the second adsorption experiment, and then characterized by XRD and N_2 adsorption. A series of regeneration method was shown in Table 3.4.

Table 3.4 Series for regeneration method of Alpill-MMT-Con and Alpill-MMT-Ultra

Samples	Thermally regenerated condition		
	Temperature (°C)	Time (hrs.)	Number of time for calcination
Thermally regenerated 2nd-Al-pillMMT-2.4-60-Str-rt	700	2	3
Thermally regenerated 2nd-Al-pillMMT-2.4-30-Ultra-20			

3.7 Antibacterial activity test

Prior to the antibacterial activity test, 1.5 g of adsorbents was shaped by uniaxial pressing into cylindrical pellet of 1.3 $\pm$ 0.1 cm in diameter. The adsorbent pellet was placed in intimate contact with the surface of agar plate that was inoculated with a cell suspension of *Eschericia coli* (*E.coli*) ATCC®25922 and incubated at 37°C for 24 hrs. This test was performed in triplicate according to the JIS L 1902: 1998 (Qualitative) technique. The presence of and size of any zone of inhibition around the samples was then recorded.

Chapter 4
Results and Discussions

4.1 Preparation of aluminum polyoxocation solutions

Commonly, the aluminum polyoxocation solution (AlOH) has been derived from base-hydrolysis of Al^{3+} solution [1-3], in which various of Al forms Al-OH species were obtained including small/middle/large polymeric AlOH species, such as Al monomeric, $Al_2(OH)_4^{2+}$, $Al_3(OH)_4^{5+}$, $Al_4(OH)_8^{4+}$, $Al_5(OH)_{13}^{2+}$, $Al_6(OH)_{12}^{6+}$, $Al_{10}(OH)_{22}^{8+}$ and $Al_{13}(OH)_{32}^{7+}$ [76]. In this research, the AlOH solutions were prepared by two different methods, i.e. conventional stirring and ultrasonic assisted methods, in order to study the effect of preparation method on the AlOH structures. The as-prepared AlOH solutions were analyzed by ^{27}Al NMR.

4.1.1 Conventional stirring method

The AlOH solutions were prepared using different OH/Al molar ratios (2.0 and 2.4) and reaction temperatures (room temperature and 60 °C). All of the as-prepared AlOH solutions were clear, indicating that there were no $Al(OH)_3$ solid phase formed by partial hydrolysis of Al^{3+} ions. Figure 4.1 shows a strong peak at δ = 63 ppm in the ^{27}Al NMR spectra of all AlOH solutions, corresponding to the chemical shift of $[AlO_4Al_{12}(OH)_{24}(OH_2)_{12}]^{7+}$ tridecamer cation (Al_{13}^{7+} polyoxocation) [77]. This Al_{13}^{7+} polyoxocation is known as ε-Keggin structure, composed of one Al atom occupies a central AlO_4 tetrahedral position and the remaining 12 Al atoms occupy equivalent octahedral positions defined by oxygen, hydroxyl and water ligands as shown in Fig. 4.2 [74, 78]. The pH values of AlOH-2.0-rt-Str, AlOH-2.0-60-Str, AlOH-2.4-rt-Str and AlOH-2.4-60-Str solutions were 4.23, 3.36, 4.33 and 3.43, respectively. By increasing the temperature, the pH of AlOH solution was shifted to the acidic side and the Al_{13}^{7+} polyoxocation species became the predominant species at a given temperature, indicating the kinetics of Al_{13}^{7+} polyoxocation formation was fast [86]. Some research mentioned that the high reaction temperature higher than 80 °C could intensively promote the formation of AlOH species, leading to less Al_{13}^{7+} polyoxocation species [172]. Therefore, the medium high temperature might be favorable for Al_{13}^{7+} polyoxocation formation, therefore the reaction at 60 °C was chosen in this study.

However, the trace signal of $[Al(OH_2)_6]^{3+}$ monomer at δ = 0 ppm was also observed in all samples. The peak intensity of the chemical shift at δ = 0 ppm in both 2.0 and 2.4 OH/Al molar ratios significantly decreased with the increase of reaction temperature used for the base-hydrolysis of Al^{3+} solution. The peak intensity at δ = 0 ppm of the 2.0 OH/Al molar ratio was higher than that of the 2.4 OH/Al molar ratio, indicating that the Al monomeric species (i.e. $Al(OH)_3$, $Al(OH)_2^+$, $Al(OH)^{2+}$ and $[Al(OH_2)_6]^{3+}$) and/or free Al^{3+} ion were mainly obtained in the 2.0 OH/Al molar ratio. By contrast, the higher amount of OH^- in the 2.4 OH/Al molar ratio could promote base-hydrolysis and Al polymerization, therefore, the rate of Al_{13}^{7+} polyoxocation formation in the 2.4 OH/Al molar ratio was faster than that in the 2.0 OH/Al molar ratio.

From the previous results and discussion, the AlOH solution prepared with the OH/Al molar ratio of 2.4 was selected for further preparation of aluminum pillared montmorillonites.

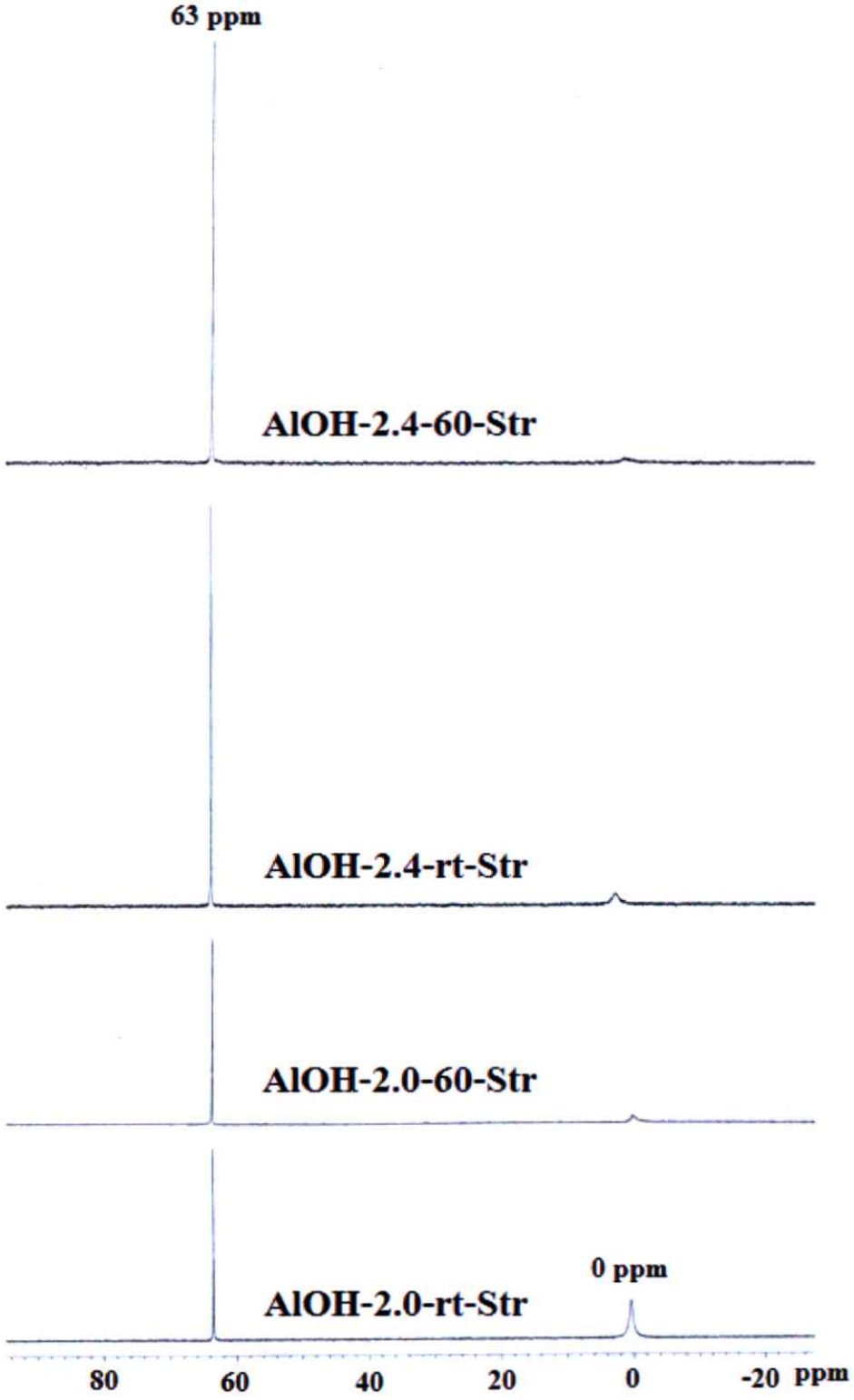

Figure 4.1 ^{27}Al NMR spectra of the AlOH solutions prepared by conventional stirring method

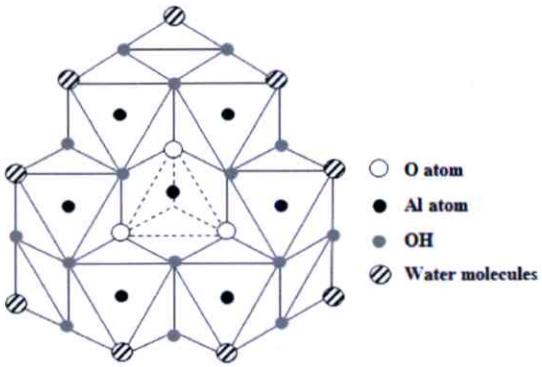

Figure 4.2 Basic structure of Al_{13} ε-Keggin

4.1.2 Ultrasonic assisted method

In this part, the AlOH solution was prepared from the starting precursor with the OH/Al molar ratio of 2.4, in which it was treated with high intensity ultrasonic for various treatment times, i.e. 10, 20, 30 and 60 mins. Figure 4.3 shows the ^{27}Al NMR spectra of the AlOH solutions prepared by ultrasonic assisted methods. The ^{27}Al NMR spectra of all AlOH solutions showed the peak at δ = 0 ppm and δ = 63 ppm, corresponding to the chemical shift of Al monomeric and Al_{13}^{7+} polyoxocation, respectively. The peak intensity at δ = 0 ppm of AlOH-2.4-Ultra-10 was higher than those of AlOH-2.4-Ultra-20, AlOH-2.4-Ultra-30 and AlOH-2.4-Ultra-60, corresponding to the higher amount of Al monomeric species and/or free Al^{3+} ion in the AlOH-2.4-Ultra-10 precursor. The longer ultrasonic treatment time, the lower peak intensity of δ = 0 ppm but the higher peak intensity of δ = 63 ppm were obtained, indicating that the Al_{13}^{7+} polyoxocation was the main component in the AlOH-2.4-Ultra-20, AlOH-2.4-Ultra-30 and AlOH-2.4-Ultra-60.

After ultrasonic treatment, the solution temperatures of AlOH-2.4-Ultra-10, AlOH-2.4-Ultra-20, AlOH-2.4-Ultra-30 and AlOH-2.4-Ultra-60 solutions were increased to 45, 55, 66 and 78 °C, respectively. It can be seen that the temperature increased with increasing reaction time because the ultrasonic treatment could induce the formation, growth and collapse of micro-bubbles in the liquid medium, releasing large amount of energy release and creating the localize high temperatures [173]. In addition, the pH value of AlOH solutions was shifted to the acidic side with the increase of temperature of AlOH solutions. The pH of AlOH-2.4-Ultra-10, AlOH-2.4-Ultra-20, AlOH-2.4-Ultra-30 and AlOH-2.4-Ultra-60 solutions were 3.91, 3.66, 3.37 and 3.14, respectively. Hence, the high reaction temperature could accelerate the formation of Al_{13}^{7+} polyoxocation as previously discussed in conventional stirring method section [86]. However, there was

no significant difference of the peak intensity at δ = 0 ppm and δ = 63 ppm between the AlOH-2.4-Ultra-30 and AlOH-2.4-Ultra-60. Therefore, the AlOH-2.4-Ultra-30 was used as Al pillaring solution for preparation of aluminum pillared montmorillonite under ultrasonic assisted method.

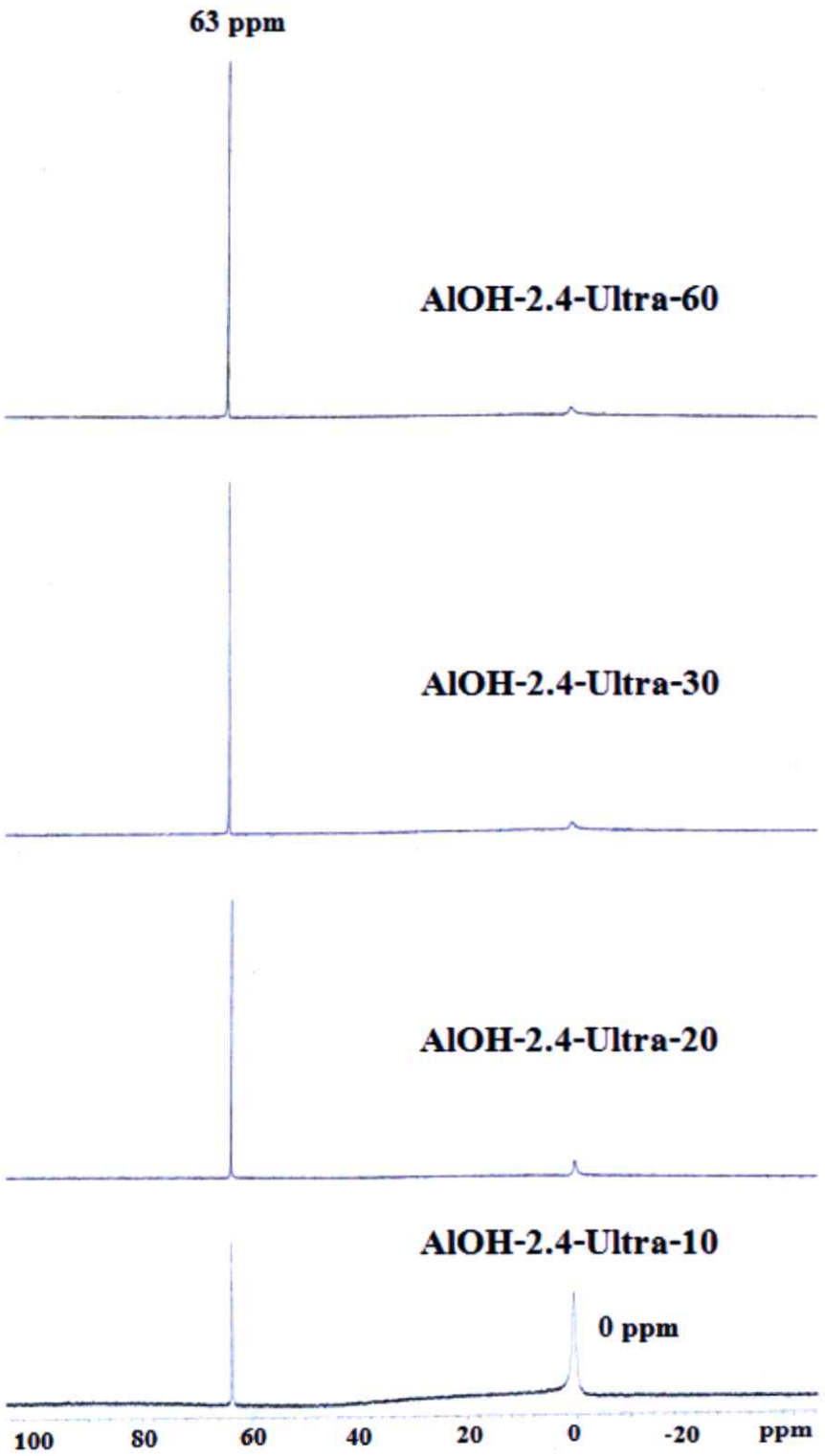

Figure 4.3 ^{27}Al NMR spectra of the AlOH solutions prepared by ultrasonic assisted method

From these results, the ^{27}Al NMR spectra indicated that the hydrated $Al(NO_3)_3$ was hydrolyzed by NaOH to $[Al(OH_2)_6]^{3+}$ monomers and then condensed to $[AlO_4Al_{12}(OH)_{24}(OH_2)_{12}]^{7+}$ tridecamers in both stirring and ultrasonic methods, however, the high power ultrasonic could enhanced the hydrolysis and condensation of AlOH species, resulting in the shortening of reaction time.

4.2 Preparation of aluminum pillared montmorillonite

In this section, the aluminum pillared montmorillonite (Alpill-MMTs) prepared by two different methods, i.e. conventional stirring and ultrasonic assisted method, were characterized in order to investigate the effects of preparation methods on the structures of Alpill-MMTs.

4.2.1 Conventional stirring method

The Na^+-MMT was modified with AlOH-2.4-60-Str solution by conventional stirring method under two different reaction temperatures i.e. room temperature and 60 °C.

Figure 4.4 shows the XRD patterns of Na^+-MMT, Alpill-MMT-2.4-60-Str-rt and Alpill-MMT-2.4-60-Str-60. The starting Na^+-MMT showed a peak at $2\theta \approx 7.12^\circ$, corresponded to d_{001} basal spacing of 1.24 nm. When the Na^+-MMT was modified with the AlOH solution, the diffraction peak of *001* plane in the Alpill-MMT-2.4-60-Str-rt and Alpill-MMT-2.4-60-Str-60 was shifted to the lower angle around 5.2° (d_{001} = 1.69 nm), indicating the great expansion of *001* interlayer distance due to the intercalation of Al_{13}^{7+} polyoxocation.

These results were in agreement with the chemical composition measured by XRF as shown in Table 4.1, in which the amount of Al_2O_3 and Al/Si molar ratio in both Alpill-MMTs were higher than the starting Na^+-MMT, insisting on the Al_{13}^{7+} polyoxocation penetration into the MMT interlayer. In addition, the amount of Na_2O in the Alpill-MMT samples significantly decreased after pillaring processes due to the cation exchange between Na^+ and Al_{13}^{7+} polyoxocation.

However, the *001* plane peak of the Alpill-MMTs was broader and significantly lower intensity than that of the starting Na^+-MMT. This result was considered to be due to the structure diversity of Al_{13}^{7+} polyoxocation intercalated MMTs as schematically shown in Fig. 4.5. In Model-(I), the random molecular orientation and inhomogeneous distribution of Al_{13}^{7+} polyoxocation in the interlayer space of MMT caused several interplanar spacing of *001* plane leading to broaden d_{001} peak. Model-(II) represented that the intercalation of Al_{13}^{7+} polyoxocation resulted in the disorder and/or

delamination of MMT tactoids in which it would create the house of card structure after calcination process [50, 74, 78].

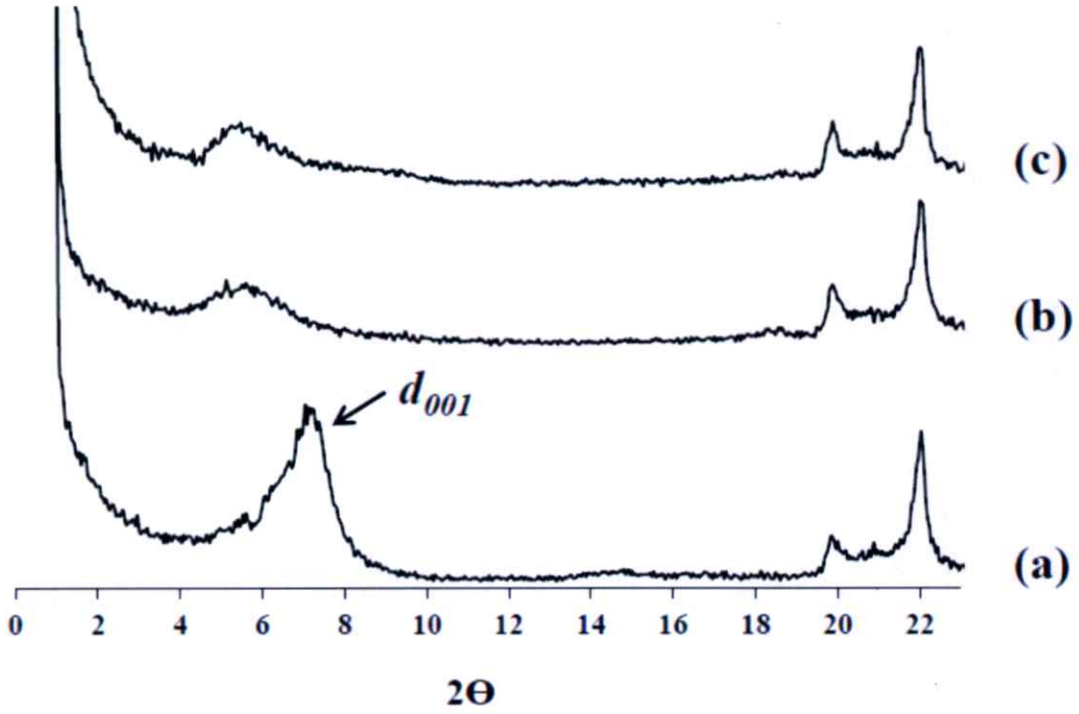

Figure 4.4 XRD patterns of (a) Na^{+} -MMT, (b) Alpill-MMT-2.4-60-Str-rt and (c) Alpill-MMT-2.4-60-Str-60

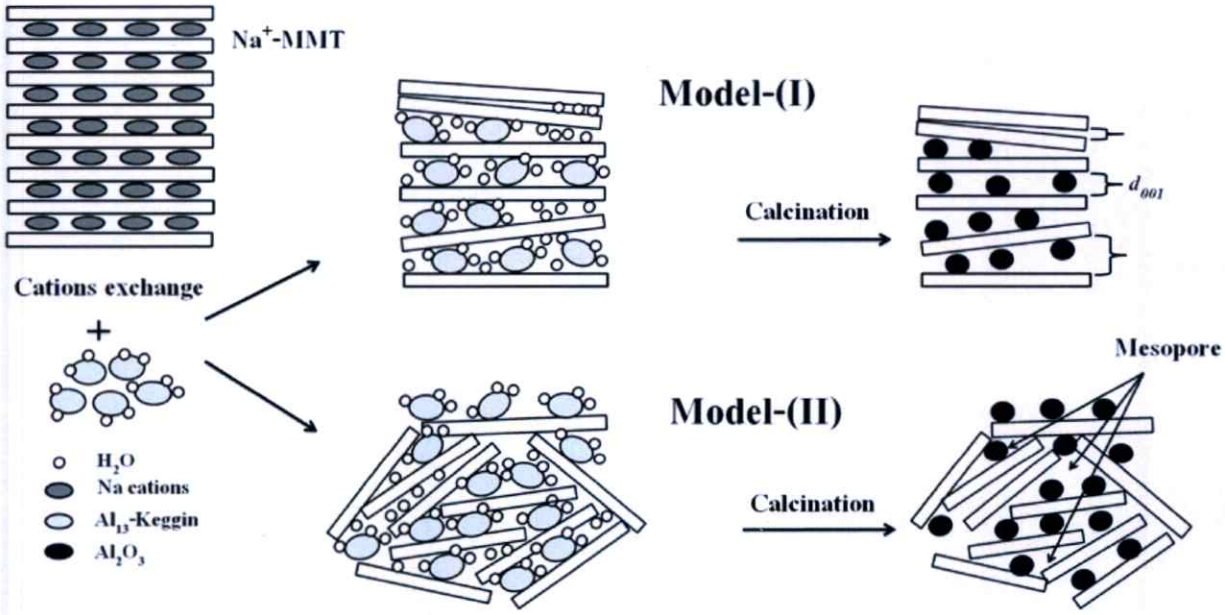

Figure 4.5 Schematic models of Al_{13}^{7+} intercalated MMTs and Alpill-MMTs structures

Table 4.1 Chemical composition, basal spacing (d_{001}), specific surface area (SSA), pore volume and BJH pore diameter of Na^+-MMT, Alpill-MMT-2.4-60-Str-rt and Alpill-MMT-2.4-60-Str-60

Sample	Chemical composition				N_2 adsorption			Basal spacing
	Al_2O_3 (wt%)	SiO_2 (wt%)	Na_2O (wt%)	Al/Si	SSA (m^2/g)	Pore volume (ml/g)	BJH pore size (nm)	d_{001} (nm)
Na^+-MMT	11.99	73.44	2.31	0.19	54	0.20	3.80	1.24
Alpill-MMT-2.4-60-Str-rt	18.46	73.57	0.56	0.29	117	0.24	3.80	1.69
Alpill-MMT-2.4-60-Str-60	19.20	71.84	0.49	0.31	120	0.23	3.82	1.69

Figure 4.6 shows the N_2 adsorption isotherms of Na^+-MMT, Alpill-MMT-2.4-60-Str-rt and Alpill-MMT-2.4-60-Str-60. The specific surface area (SSA), pore volume and pore size distribution are summarized in Table 1. The SSA values of the unmodified Na^+-MMT, Alpill-MMT-2.4-60-Str-rt and Alpill-MMT-2.4-60-Str-60a were 54, 117 and 120 m^2/g, respectively. The increase of Alpill-MMTs' SSA was considered to be due to the calcination of Al_{13}^{7+} molecules intercalated in the interplanar spacing of MMT, consisting with the XRD and XRF data.

The isotherms of both Na^+-MMT and Alpill-MMTs corresponded to type IV isotherm in the Brunauer, Deming, Dewing and Teller (BDDT) classification [91, 174], in which the adsorption curve is steep at saturation pressure and the desorption curve is at intermediate relative pressure. The hysteresis loop in both isotherms could be classified as H3 type (IUPAC classification) [175], revealing the mesoporosity (2-50 nm) of plate-like aggregates with open slit-shaped capillaries and house of card structure. These results were corroborated with the Model-(I) and Model-(II) purposed in Fig. 4.5. It can be seen that the general features of Alpill-MMT isotherms were quite similar to that of the starting Na^+-MMT, however, the amount of nitrogen adsorption in the Alpill-MMTs was significantly increased.

Figure 4.7 shows the mesopore size distributions of Na^+-MMT, Alpill-MMT-2.4-60-Str-rt and Alpill-MMT-2.4-60-Str-60. The pore size distribution of Na^+-MMT was mostly restricted to about 3.8 nm, while, two modes of distribution of about 3.8 nm and broad 6 - 30 nm were obtained in the Alpill-MMT-2.4-60-Str-rt and Alpill-MMT-2.4-60-Str-60 with higher pore volumes. These results were in consistent with the broad d_{001} peak in the XRD patterns and the proposed Model-(I) and Model-(II) as described previously in Fig. 4.5.

It can be seen that there is no significant difference in the d_{001}, SSA, pore volume and BJH pore size distribution of both Alpill-MMT-2.4-60-Str-rt and Alpill-MMT-2.4-60-Str-60, indicating high temperature was not influence on Al_{13}^{7+} polyoxocation intercalation efficiency after aging for 24 h. Hence, the Alpill-MMT-2.4-60-Str-rt was further used as an adsorbent for dye-containing waste treatment in the next section.

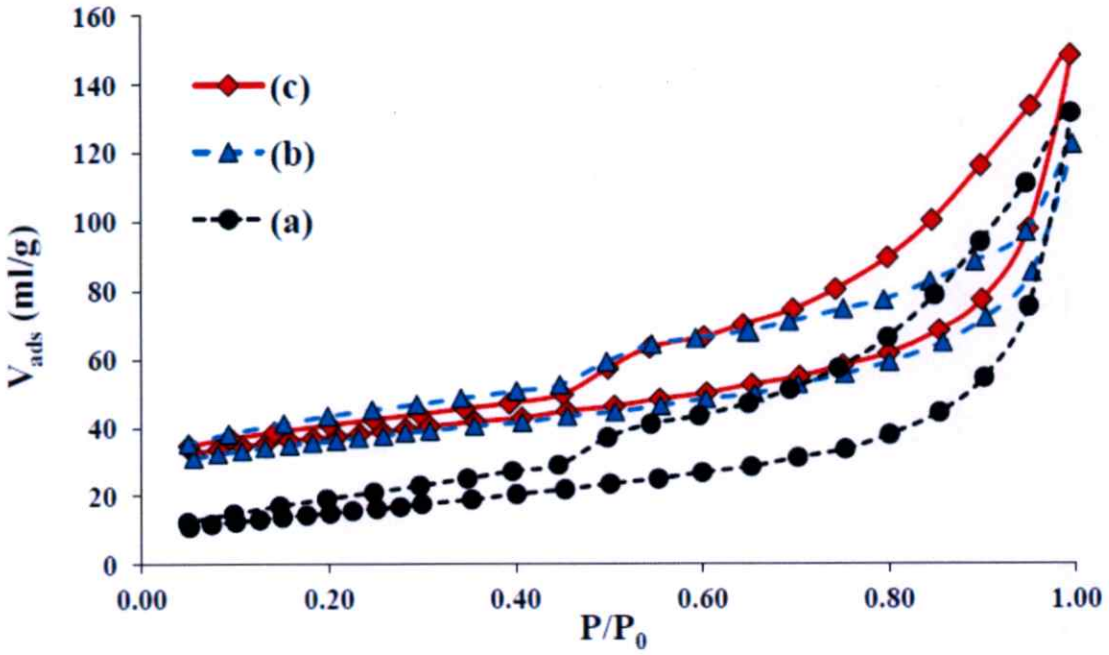

Figure 4.6 Nitrogen adsorption–desorption isotherms of (a) Na^+ -MMT, (b) Alpill-MMT-2.4-60-Str-rt and (c) Alpill-MMT-2.4-60-Str-60

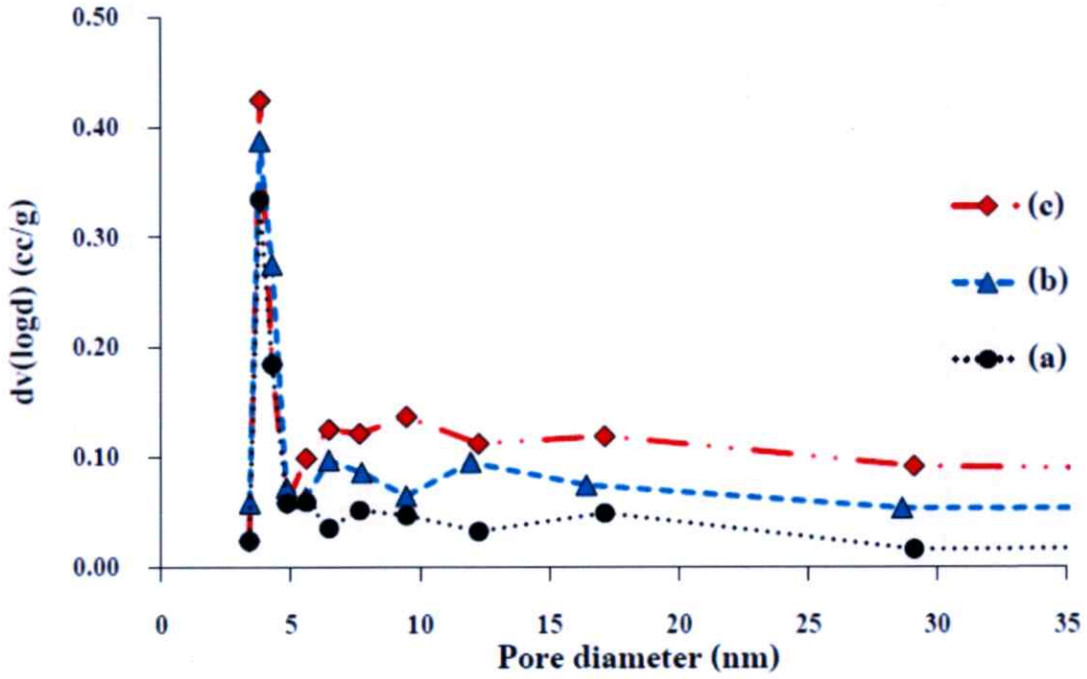

Figure 4.7 BJH pore size distribution curves of (a) Na^+ -MMT, (b) Alpill-MMT-2.4-60-Str-rt and (c) Alpill-MMT-2.4-60-Str-60

4.2.2 Ultrasonic assisted method

The Na^+-MMT was modified with AlOH-2.4-Ultra-30 solution and treated with high power ultrasonic for various treatment times, i.e. 10, 20, 30 and 60 min.

Table 4.2 shows the characterization data obtained by XRF, XRD and gas adsorption analysis of the Na^+-MMT and Alpill-MMT products. In the XRF, the Si was considered as a reference element because it is a structural element of the MMT which is not supposed to change during the pillaring process [176]. The XRF data showed the increase of the Al percentage in the Alpill-MMTs when comparing with the starting Na^+-MMT, indicating an effective penetration of Al_{13}^{7+} polyoxocation into the interlayer of Na^+-MMT. However, the Al/Si molar ratios of all Alpill-MMTs did not change with the increase of treatment time. These results suggested that the increase of treatment time could not enhance the efficiency of cation exchange between Na^+ and Al_{13}^{7+} polyoxocation. In Fig. 4.8, it can be observed from the XRD patterns of Alpill-MMTs that the *001* plane shifted to lower 2θ angles than that of Na^+-MMT, corresponding to the increase of *001* basal spacing (d_{001}), in which the Alpill-MMT-2.4-30-Ultra-20 (1.76 nm) possessed greater basal spacing than those of Alpill-MMT-2.4-30-Ultra-10 (1.69 nm), Alpill-MMT-2.4-30-Ultra-30 (1.76 nm) and Alpill-MMT-2.4-30-Ultra-60 (broad peak).

By increase of ultrasonic treatment time, the peak of *001* plane was broadened with lowering peak intensity. These results indicated that the delamination of MMT tactoids as explained previously in section 4.2.1. Since the tactoids of Na^+-MMT weakly held together by Van der Walls interaction, therefore, the strong ultrasonic force led to the formation of Alpill-MMTs with disorder and/or delaminated structures after longer ultrasonic treatment than 20 min. It was, therefore, the surface area and pore volume were initially increased after ultrasonic treatment for 10 and 20 min, but significantly decreased after 30 and 60 min treatments.

Table 4.2 Chemical composition, basal spacing (d_{001}), specific surface area (SSA), pore volume and BJH pore diameter of Na^+ -MMT, Alpill-MMT-2.4-60-Ultra-10, Alpill-MMT-2.4-60-Ultra-20, Alpill-MMT-2.4-60-Ultra-30 and Alpill-MMT-2.4-60-Ultra-60

Sample	Chemical composition				N_2 adsorption			Basal spacing
	Al_2O_3 (wt%)	SiO_2 (wt%)	Na_2O (wt%)	Al/Si	SSA (m^2/g)	Pore volume (ml/g)	BJH pore size (nm)	d_{001} (nm)
Na^+-MMT	11.99	73.44	2.31	0.19	54	0.20	3.80	1.24
Alpill-MMT-2.4-30-Ultra-10	19.81	71.99	0.70	0.32	123	0.22	3.77	1.69
Alpill-MMT-2.4-30-Ultra-20	20.48	71.71	0.54	0.34	134	0.27	3.80	1.76
Alpill-MMT-2.4-30-Ultra-30	19.68	72.92	0.45	0.32	70	0.20	3.81	1.76
Alpill-MMT-2.4-30-Ultra-60	19.24	71.53	0.43	0.32	52	0.12	3.80	Broad peak

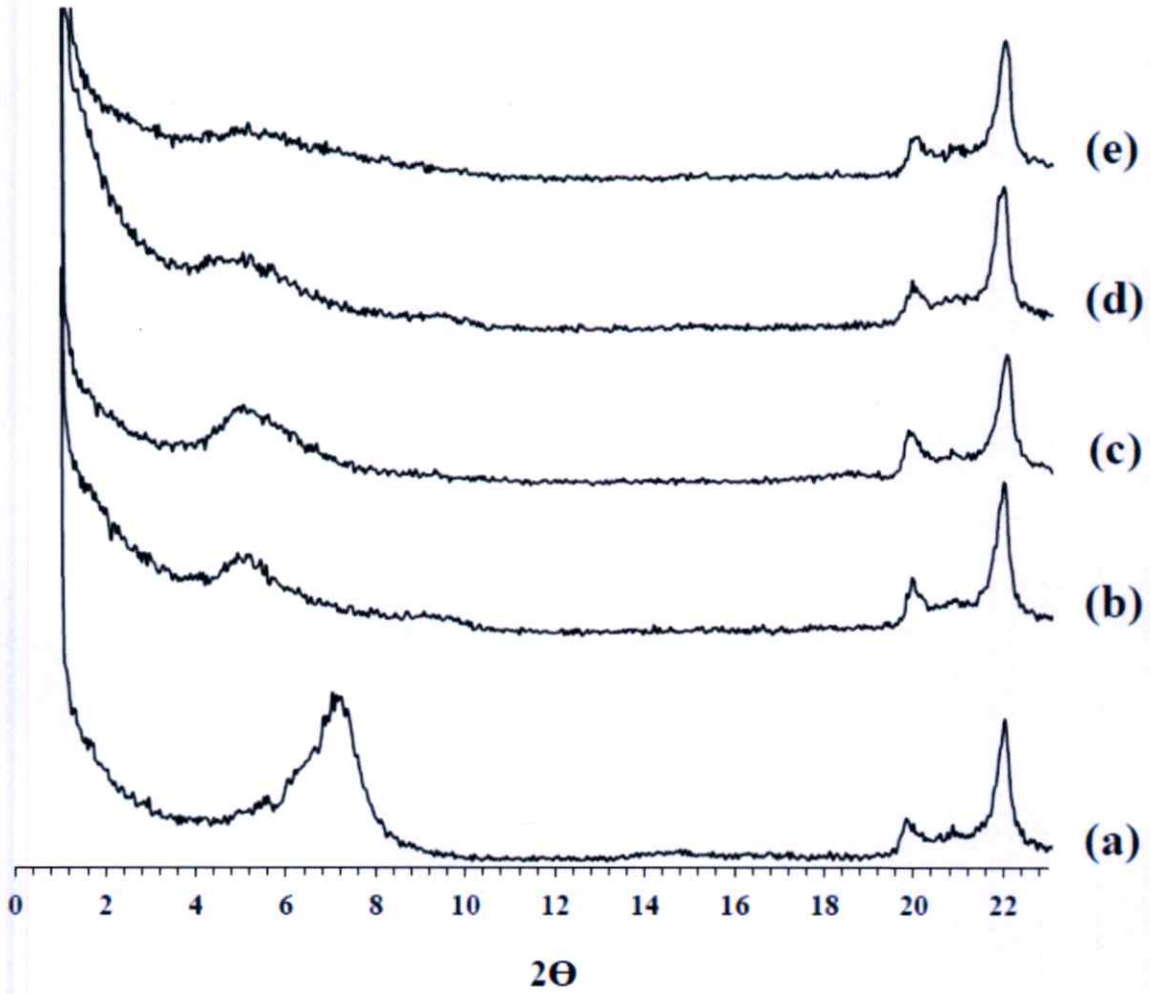

Figure 4.8 XRD patterns of (a) Na^+ -MMT, (b) Alpill-MMT-2.4-30-Uultra-10, (c) Alpill-MMT-2.4-30-Ultra-20, (d) Alpill-MMT-2.4-30-Ultra-30 and (e) Alpill-MMT-2.4-30-Ultra-60

Figure 4.9 shows the adsorption isotherms of Na^+ -MMT and all Alpill-MMTs obtained by ultrasonic method. The Alpill-MMT-2.4-30-Ultra-10 in Fig. 4.9 (b) and Alpill-MMT-2.4-30-Ultra-20 in Fig. 4.9 (c) show higher N_2 adsorption than that of the starting Na^+-MMT. Both of Na^+ -MMT and Alpill-MMTs exhibited type IV isotherms and H3 type hysteresis loop according to BDDT and IUPAC classification, respectively, in which there were the characteristics of mesopores with slit-like shape [176-178].

Figure 4.10 shows the BJH pore size distributions of Alpill-MMT-2.4-30-Ultra-10, Alpill-MMT-2.4-30-Ultra-20, Alpill-MMT-2.4-30-Ultra-30 and Alpill-MMT-2.4-30-Ultra-60. It can be observed that all of Alpill-MMT-Ultra exhibited the mesopores (2–50 nm) with mainly pore diameter of about 3.77-3.80 nm as shown in Fig. 4.10 (a)-(d). However, the

quantity of mesopore with 3.77-3.80 nm of diameter in the Alpill-MMT-ultra were initially increased after ultrasonic treatment for 10 and 20 min, but significantly decreased after 30 and 60 min treatments. These results suggested that the strong ultrasonic force led to the formation of MMT disordered staking and/or delamination of MMT tactoids as described previously. Therefore, the high mesopore sizes ranging from 5 – 35 nm were also observed in all of Alpill-MMT-Ultra.

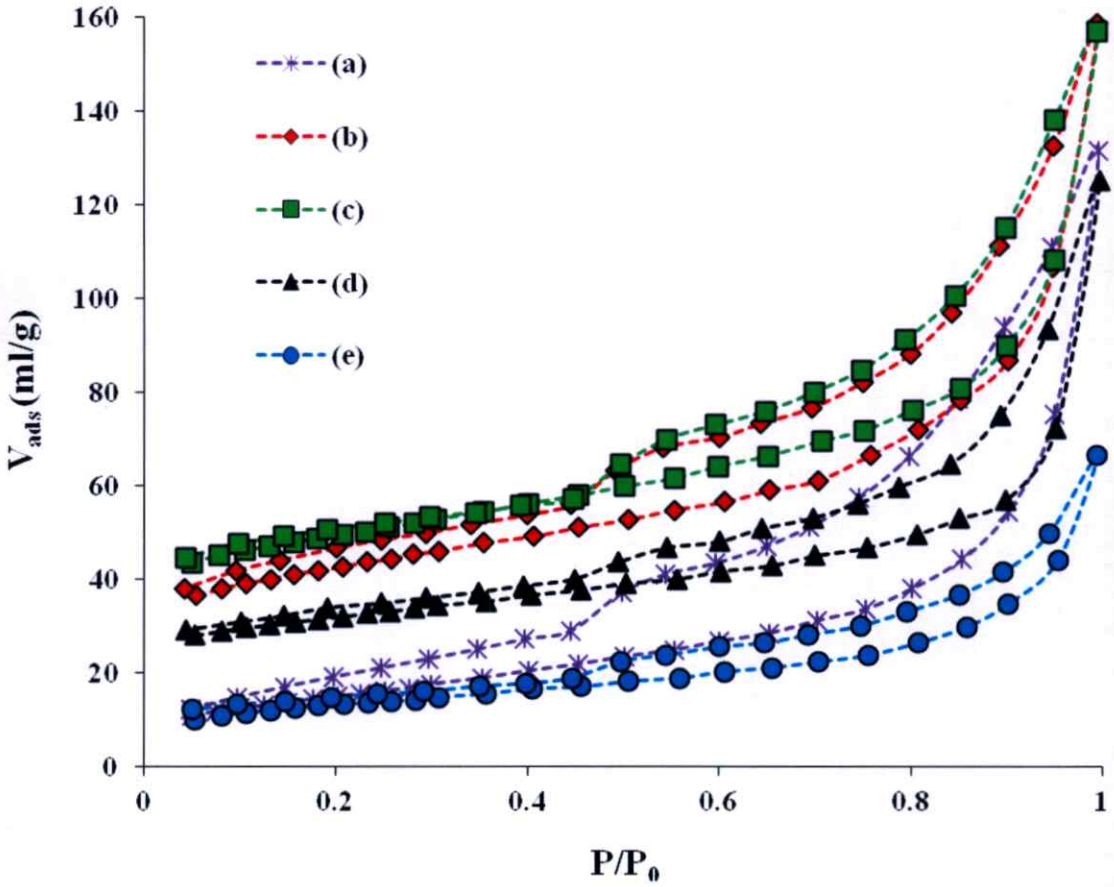

Figure 4.9 Nitrogen adsorption–desorption isotherms of (a) Na^+ -MMT (b) Alpill-MMT- 2.4-30-Ultra-10, (c) Alpill-MMT-2.4-30-Ultra-20, (d) Alpill-MMT-2.4-30-Ultra-30 and (e) Alpill-MMT-2.4-30-Ultra-60

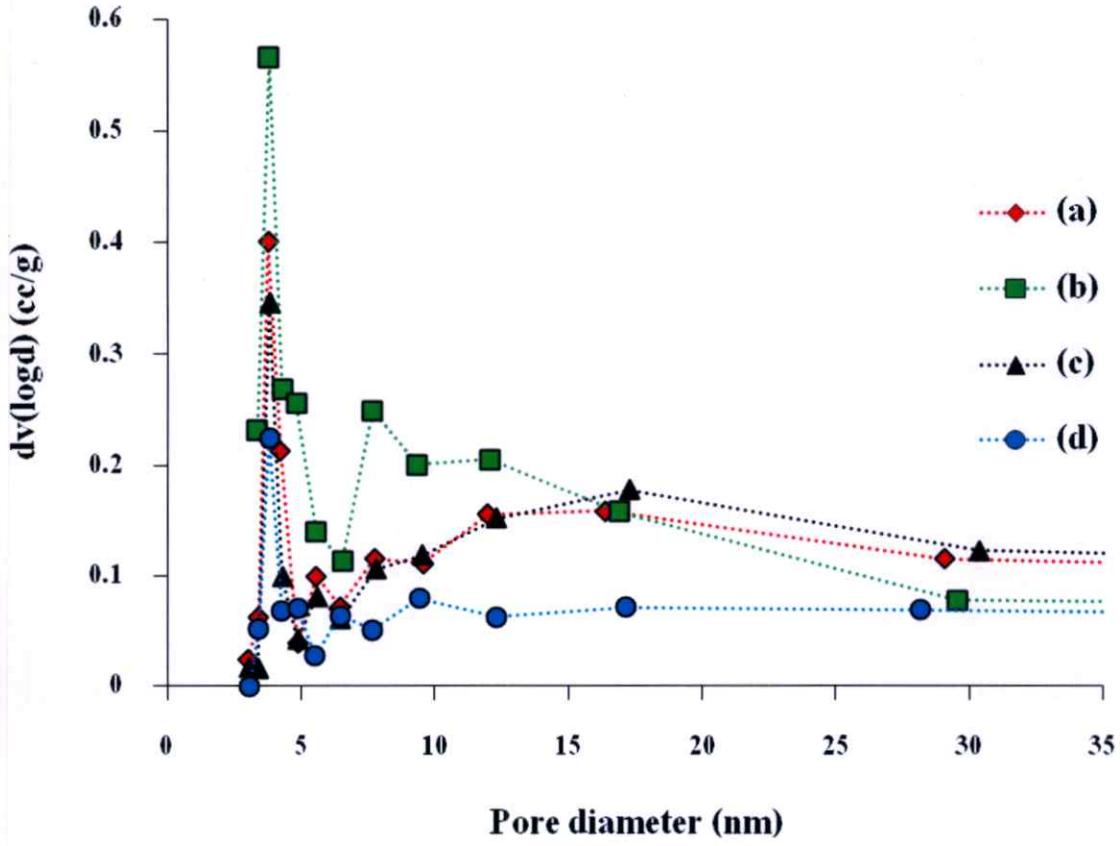

Figure 4.10 BJH pore size distribution curves of (a) Alpill-MMT-2.4-30-Ultra-10, (b) Alpill-MMT-2.4-30-Ultra-20, (c) Alpill-MMT-2.4-30-Ultra-30 and (d) Alpill-MMT-2.4-30-Ultra-60

The Alpill-MMT-2.4-30-Ultra-20 possesses high d_{001} basal spacing, SSA, pore volume and pore diameter than other Alpill-MMTs. Hence, the Alpill-MMT-2.4-30-Ultra-20 was used as an adsorbent for dye-containing waste treatment in the next step.

From the preview results, it can be concluded that the ultrasound treatment could facilitate the intercalation of Al_{13}^{7+} polyoxocation into MMT layers by inducing the formation and fracture of were bubbles in the liquid medium, in which this phenomenon created high temperature and pressure, which promoted the dispersion, expansion and delamination of the MMT tactoids. In comparison with the conventional method for synthesis of Alpill-MMTs, in section ultrasonic assisted method considerably reduced the pillaring process, in which the Alpill-MMT prepared by ultrasonic treatment for 20 min were similar to the Alpill-MMT obtained by prolonged conventional stirring method (24 hrs).

4.2.3 Dye adsorption

The dye adsorption behavior and capacity of Alpill-MMT prepared by ultrasonic assisted method (Alpill-MMT-2.4-30-Ultra-20) were determined in comparison with one prepared by conventional stirring method (Alpill-MMT-2.4-60-Str-rt). The cationic dye, i.e. Basic Yellow 1 (BY1), was used as an adsorbate model.

A. Effect of adsorbent type

Table 4.3 shows the dye adsorption abilities of Na^+-MMT, Alpill-MMT-2.4-60-Str-rt and Alpill-MMT-2.4-30-Ultra-20 using initial dye concentration of 1000 mg/L and contact time of 120 min. After adsorption treatment, the dye solution became pale yellow to clear colorless with the reduction of absorbance peak at λ_{max} of 413 nm analyzed by UV-Vis, meaning the amount of BY1 molecules was eliminated from the dye solution. The percentages of BY1 removal were 46.28, 81.34 and 94.39 % for the Na^+-MMT, Alpill-MMT-2.4-60-Str-rt and Alpill-MMT-2.4-30-Ultra-20, respectively, equaling to the adsorption capacities of 46.28, 81.34 and 94.39 mg/g. Moreover, the BY1 solutions before and after adsorption treatment were analyzed by TOC analyzer. The amount of total organic carbon (TOC) was significantly decreased from the initial concentration of 442.30 mg/L to 210.97, 102.82 and 67.07 mg/L when using the Na^+-MMT, Alpill-MMT-2.4-60-Str-rt and Alpill-MMT-2.4-30-Ultra-20 adsorbents, respectively. The TOC data suggested that the BY1 organic dye was actually removed from the dye solution by the solid adsorbents, in line with the UV-Vis analysis described previously. The percentages of TOC removal of Na^+-MMT, Alpill-MMT-2.4-60-Str-rt and Alpill-MMT-2.4-30-Ultra-20 were 52.30, 76.75 and 84.84 %, respectively. It was found that the Alpill-MMTs exhibited

higher removal percentages than the starting Na^+-MMT because the presence of Al_2O_3 intercalated molecules in the Alpill-MMTs resulted in higher SSA and pore volume, so the diffusion of BY1 molecules into the interlayer space was facilitated. In addition, the highest amount of Al_2O_3 in the interlayer of Alpill-MMT-2.4-30-Ultra-20 brought about the highest adsorption efficiency for BY1 removal.

Table 4.3 Percentage of dye removal, adsorption capacities and percentage of TOC removal of Na^+-MMT, Alpill-MMT-2.4-60-Str-rt and Alpill-MMT-2.4-30-Ultra-20

Sample	UV-Vis		TOC	
	Dye removal (%)	q_e (mg/g)	TOC (mg/L)	TOC removal (%)
BY 1	-	-	442.30	-
Na^+-MMT	46.28	46.28	210.97	52.30
Alpill-MMT-2.4-60-Str-rt	81.34	81.34	102.82	76.75
Alpill-MMT-2.4-30-Ultra-20	94.39	94.39	67.07	84.84

B. Effect of contact time

Figure 4.11 shows the adsorption data of Alpill-MMT-2.4-60-Str-rt and Alpill-MMT-2.4-30-Ultra-20 adsorbents carried out using initial BY1 concentration of 1000 mg/L under various contact times, i.e. 30, 60, 90, 120, 150, 180, 210, 240, 270 and 300 min. The adsorption capacities of Alpill-MMT-2.4-60-Str-rt and Alpill-MMT-2.4-30-Ultra-20 increased with an increase of contact time and became constant after 120 min because the number of free adsorbent surface decreased with filling of BY1 molecules and the free path in adsorbent pore was also blocked. These results represent the time at which equilibrium of BY1 adsorption (q_e) has been attained. The experimental q_e values of Alpill-MMT-2.4-60-Str-rt and Alpill-MMT-2.4-30-Ultra-20 were 83.46 and 96.36 mg/g, respectively. According to these results, the contact times for further adsorption experiments of both Alpill-MMT-2.4-60-Str-rt and Alpill-MMT-2.4-30-Ultra-20 were fixed at 120 min.

It can be seen that there are no significant difference in the adsorption capacities for both adsorbents in the first 30 min contact time because the large number of pores and free surface area were available for dye adsorption together with free pore volume for diffusion of dye molecules into the interlayer of adsorbents. However, Alpill-MMT-2.4-30-Ultra-20 showed higher adsorption capacity than the Alpill-MMT-2.4-60-Str-rt after

prolonged contact time in the period of 60 - 300 min. These results were attributed to the presence of multiple pore sizes (wide range of pore size distribution), high pore volume and high SSA in the Alpill-MMT-2.4-30-Ultra-20 as discussed previously, facilitating the penetration of more BY1 molecules into the partially occupied interlayer of Alpill-MMT-2.4-30-Ultra-20.

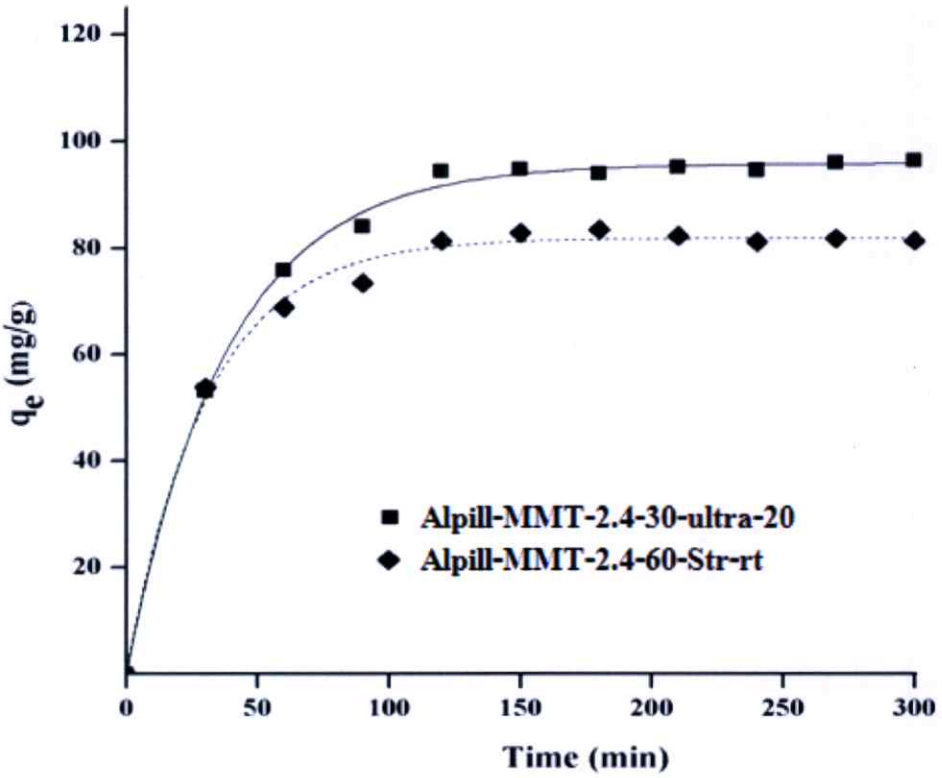

Figure 4.11 Effect of contact time on adsorption capacities of Alpill-MMT-2.4-60-Str-rt and Alpill-MMT-2.4-30-Ultra-20 for BY1 removal (initial BY1 concentration = 1000 mg/L)

C. Effect of initial dye concentration

Figure 4.12 shows the effect of initial dye concentration on the adsorption capacities of Alpill-MMT-2.4-60-Str-rt and Alpill-MMT-2.4-30-Ultra-20 using various initial concentrations, i.e. 50, 100, 300, 500, 700, 1000, 2000 and 3000 mg/L. For both adsorbents, the adsorption capacities increased when increasing the initial dye concentration and reached the maximum capacities at 1000 mg/L. When using initial dye concentration lower than 500 mg/L, the adsorption capacity of Alpill-MMT-2.4-30-Ultra-20 was equal to that of Alpill-MMT-2.4-60-Str-rt because the content of BY1 molecules

was lower than the adsorption sites in the adsorbents. Besides, the Alpill-MMT-2.4-30-Ultra-20 exhibited higher adsorption capacity than the Alpill-MMT-2.4-60-Str-rt when using high initial dye concentration (>500 mg/L) due to their higher SSA, pore size and pore volume as similarly explained in the effect of the contact time. These adsorption data were used for determination of adsorption isotherm.

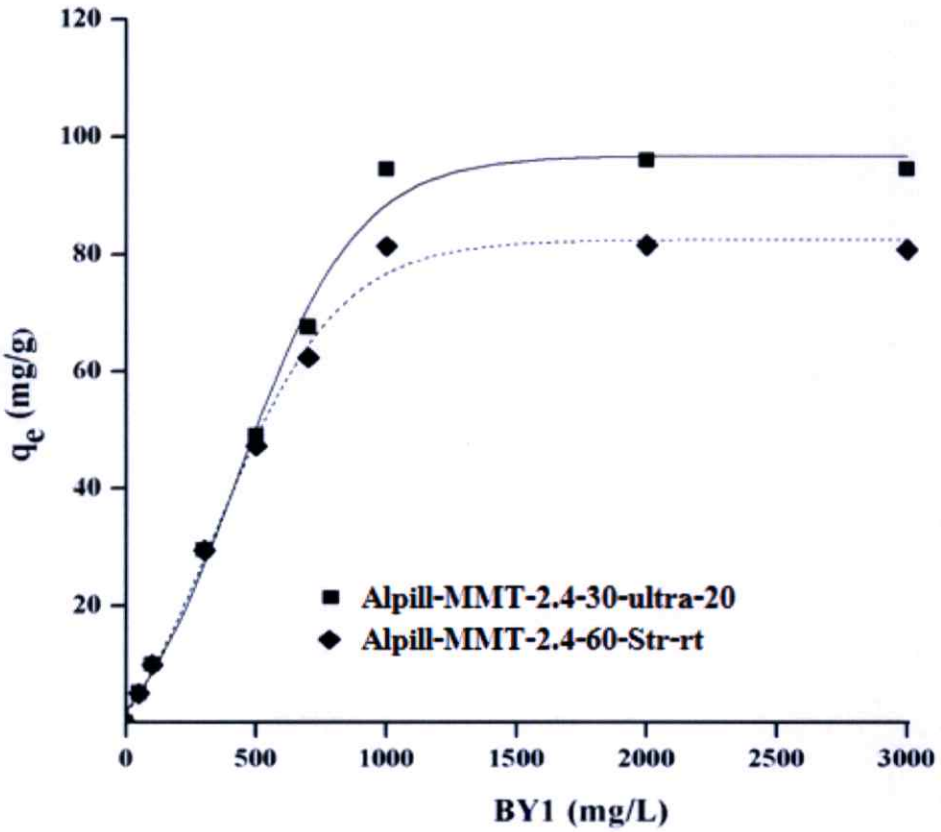

Figure 4.12 Effect of the initial dye concentration on adsorption capacities of Alpill-MMT-2.4-60-Str-rt and Alpill-MMT-2.4-30-Ultra-20 for BY1 removal (contact time = 120 min)

D. Adsorption kinetics

The experimental data from varying contact time were used to evaluate the kinetic parameters corresponding to equations (3) and (4). Figure 4.13 and 4.14 respectively show the linear plots of pseudo-first-order and pseudo-second-order models for both Alpill-MMT-2.4-60-Str-rt and Alpill-MMT-2.4-30-Ultra-20 systems. All calculated parameters from the linear plots were summarized in Table 4.4.

The pseudo-first-order rate constant (k_1) of Alpill-MMT-2.4-60-Str-rt and Alpill-MMT-2.4-30-Ultra-20 were 0.015 and 0.026 min^{-1}, respectively. It can be seen that the linear correlation coefficients (R^2) of Alpill-MMT-2.4-60-Str-rt and Alpill-MMT-2.4-30-Ultra-20 in the pseudo-first-order model were 0.1919 and 0.7164, respectively. These R^2 values were significantly lower than unity, suggesting that the adsorption mechanism of Alpill-MMT-2.4-60-Str-rt and Alpill-MMT-2.4-30-Ultra-20 did not obey to the pseudo-first order model.

In contrast, the R^2 values from the linear plots of pseudo-second-order model were close to unity for both Alpill-MMT-2.4-60-Str-rt (R^2 = 0.9970) and Alpill-MMT-2.4-30-Ultra-20 (R^2 = 0.9953) systems. It was, therefore, the calculated q_e values of Alpill-MMT-2.4-60-Str-rt and Alpill-MMT-2.4-30-Ultra-20 were matched with the experimental q_e values. It was cleared that the mechanism of BY1 adsorption on Alpill-MMT-2.4-60-Str-rt and Alpill-MMT-2.4-30-Ultra-20 corresponded to the pseudo-second-order model, implying to the chemical adsorption.

In addition, the Alpill-MMT-2.4-30-Ultra-20 possessed lower pseudo-second-order rate constant (k_2) but higher equilibrium adsorption capacity than the Alpill-MMT-2.4-60-Str-rt, indicating that the Alpill-MMT-2.4-30-Ultra-20 possessed higher BY1 adsorption efficiency.

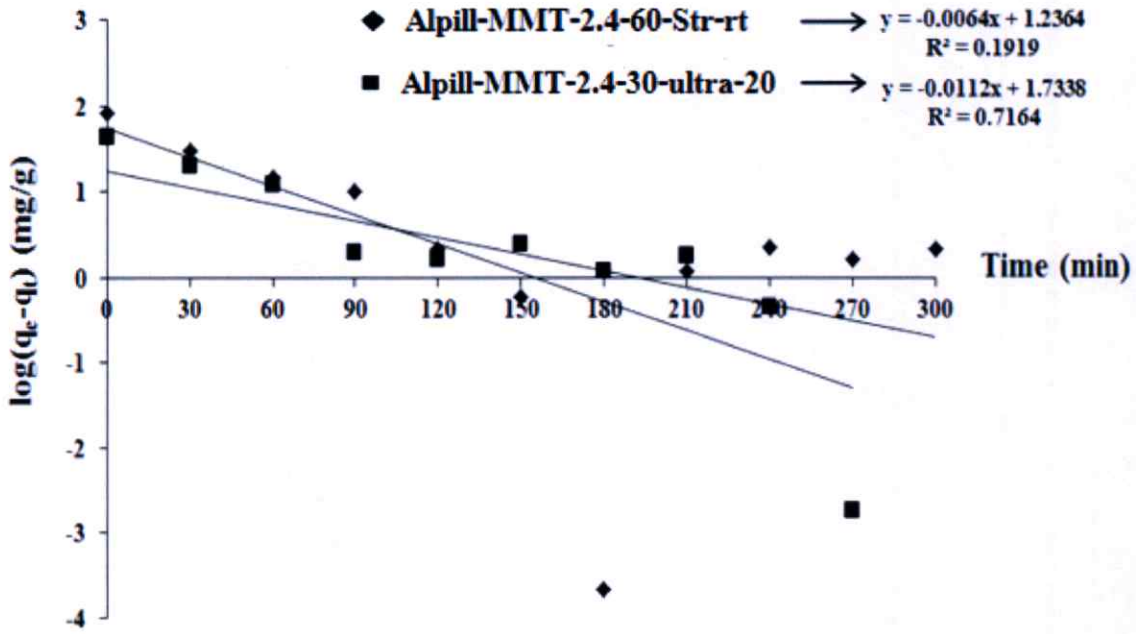

Figure 4.13 Pseudo-first-order of Alpill-MMT-2.4-60-Str-rt and Alpill-MMT-2.4-30-Ultra-20 for BY1 removal

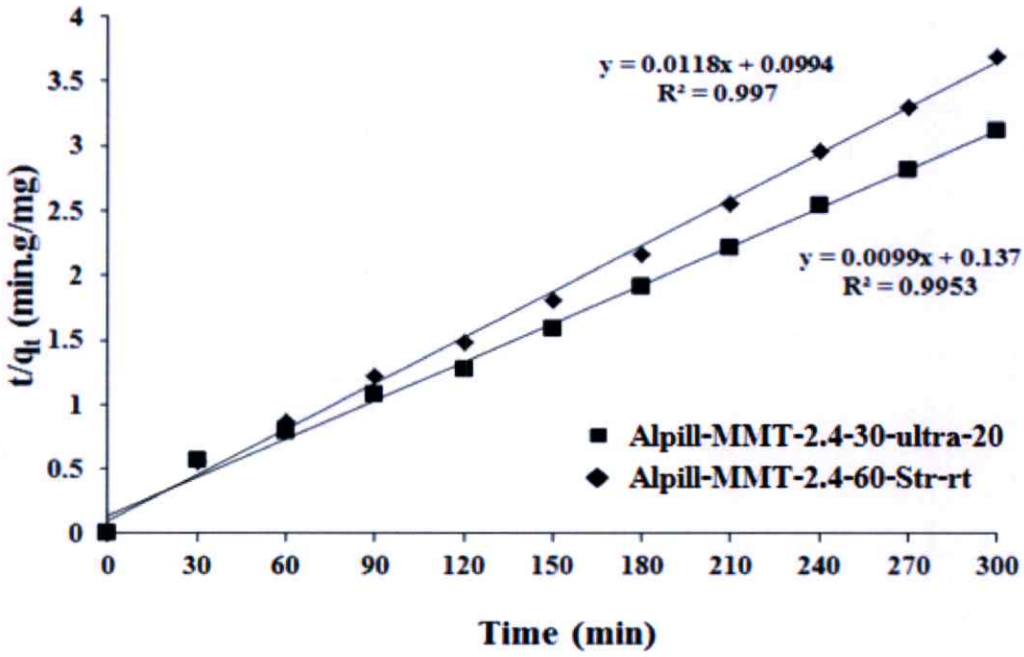

Figure 4.14 Pseudo-second-order of Alpill-MMT-2.4-60-Str-rt and Alpill-MMT-2.4-30-Ultra-20 for BY1 removal

Table 4.4 Kinetic adsorption parameters for BY1 adsorption onto Alpill-MMT-2.4-60-Str-rt and Alpill-MMT-2.4-30-Ultra-20

Adsorbent	q_e (mg/g) experimental	Pseudo-Second-Order		
		k_2 (g/mg-min)	q_e* (mg/g)	R^2
Alpill-MMT-2.4-60-Str-rt	83.46	0.0014	84.74	0.9970
Alpill-MMT-2.4-30-Ultra-20	96.36	0.0007	101.01	0.9953

* q_e was calculated from equation (4) as $\frac{t}{q_t} = \frac{1}{k_2 q_e^2} + \frac{t}{q_e}$

E. Adsorption isotherms

The adsorption isotherm data were calculated according to Langmuir and Freundlich adsorption models as their linear plots in Fig. 4.15 and 4.16, respectively. All calculated isotherm parameters were summarized in Table 4.5.

From the linear equation of Langmuir isotherm, the calculated q_m of Alpill-MMT-2.4-30-Ultra-20 was higher than that of Alpill-MMT-2.4-60-Str-rt, in which these calculated values were close to the highest adsorption capacities from experimental data as shown in Fig. 4.12. In addition, the R_L values of both adsorbents were in the range of 0 - 1, indicating favorable interaction between the BY1 molecules and both Alpill-MMTs.

In the case of Freundlich calculation, both Alpill-MMT adsorbents showed the values of n greater than 1, reflecting a strong bond between the adsorbent and the adsorbate [179]. However, the value for correlation coefficient (R^2) of linear plots for both Alpill-MMT adsorbents deviated from unity, implying that the adsorption of Alpill-MMT did not obey the Freundlich model. Therefore, these results suggested that the BY1 molecules were assumed to be monolayer adsorbed on the surface of Alpill-MMT adsorbents. It was because the molecular diameter of BY1 molecule (3.5 $\pm$ 0.5 nm) [180] is close to the average pore diameter of Alpill-MMTs (3.8 nm) as shown in Fig. 4.7 and 4.10.

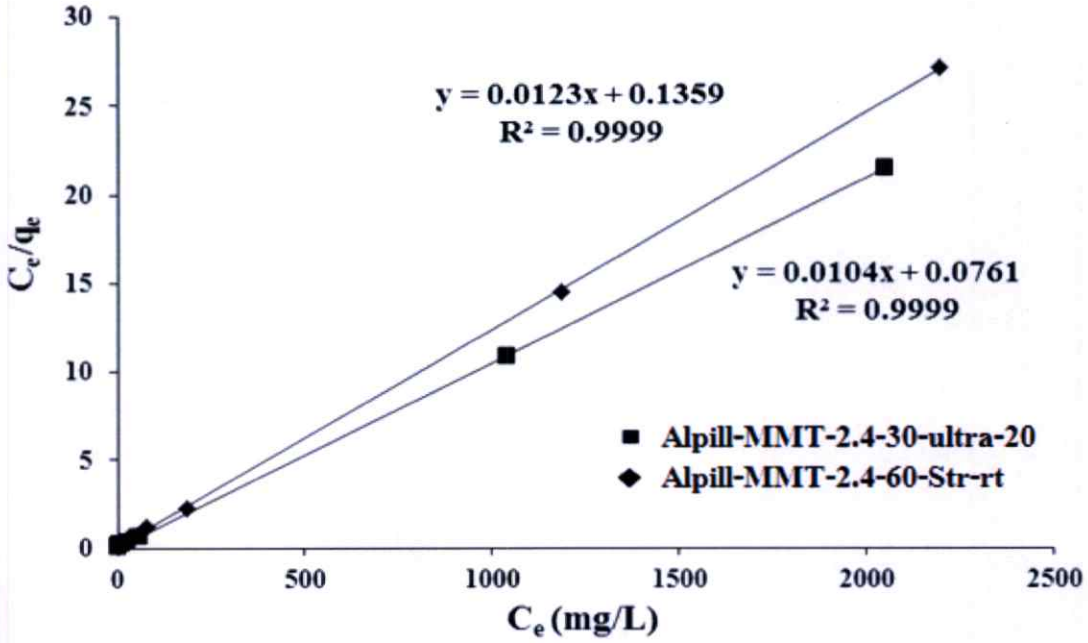

Figure 4.15 Langmuir isotherms of Alpill-MMT-2.4-60-Str-rt and Alpill-MMT-2.4-30-Ultra-20 for BY1 removal

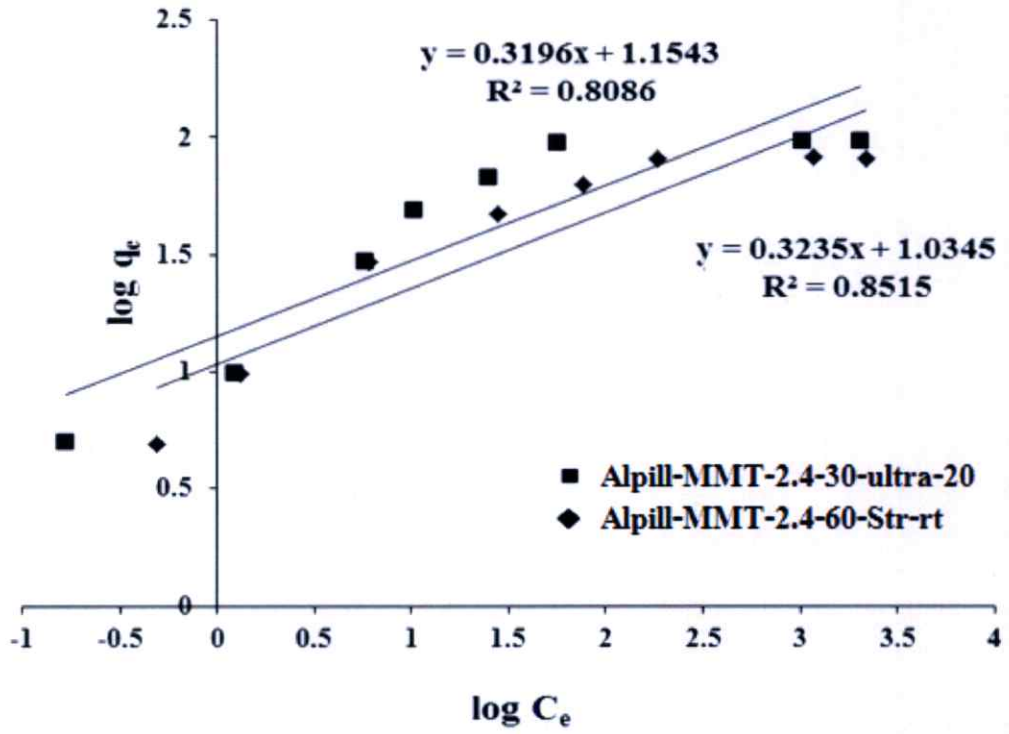

Figure 4.16 Freundlich isotherms of Alpill-MMT-2.4-60-Str-rt and Alpill-MMT-2.4-30-Ultra-20 for BY1 removal

Table 4.5 Langmuir and Freundlich parameters for BY1 adsorption onto Alpill-MMT-2.4-60-Str-rt and Alpill-MMT-2.4-30-Ultra-20

Langmuir isotherm		
Parameters	Alpill-MMT-2.4-60-Str-rt	Alpill-MMT-2.4-30-Ultra-20
Linear equation	y = 0.0123x + 0.1359	y = 0.0104x + 0.0761
q_m (mg/g)	81.30	96.15
K_L (L/mg)	0.09	0.14
R_L	0.004 - 0.18	0.002 - 0.13
R^2	0.9999	0.9999
Freundlich isotherm		
Parameters	Alpill-MMT-2.4-60-Str-rt	Alpill-MMT-2.4-30-Ultra-20
Linear equation	y = 0.3235x + 1.0345	y = 0.3196x + 1.1543
K_F (mg/g)	10.83	14.27
n	3.09	3.13
R^2	0.8515	0.8086

F. Regeneration

Table 4.6 shows the adsorption capacity of the as-prepared Alpill-MMTs for BY1 removal in comparison with those of the Alpill-MMTs after 1st and 2nd thermal regeneration, denoted as 1st-Alpill-MMTs and 2nd-Alpill-MMTs, respectively. The adsorption capacities of the Alpill-MMTs gradually decreased after thermal regeneration.

Table 4.6 Adsorption capacity (q_e) and reduction percentage of q_e of Alpill-MMT-2.4-60-Str-rt and Alpill-MMT-2.4-30-Ultra-20 after thermal regeneration

Adsorbent	Adsorption capacity (q_e, mg/g)		% reduction of q_e*	
	Alpill-MMT-2.4-60-Str-rt	Alpill-MMT-2.4-30-Ultra-20	Alpill-MMT-2.4-60-Str-rt	Alpill-MMT-2.4-30-Ultra-20
As-prepared	81.34	94.39	-	-
1st regeneration	76.63	90.14	5.8	4.5
2nd regeneration	69.95	84.22	14.0	10.8

Table 4.7 Specific surface area (SSA), pore volume and BJH pore diameter of thermally regenerated 2nd-Alpill-MMTs

Sample	N_2 adsorption		
	SSA (m^2/g)	Pore volume (ml/g)	BJH pore size (nm)
Alpill-MMT-2.4-60-Str-rt	117	0.24	3.80
2nd - Alpill-MMT-2.4-60-Str-rt	81	0.20	3.84
Alpill-MMT-2.4-30-Ultra-20	134	0.27	3.80
2nd - Alpill-MMT-2.4-30-Ultra-20	93	0.24	3.81

$$* \text{ \% reduction of } q_e = \frac{q_{e\,(as-prepared)} - q_{e\,(as-prepared)}}{q_{e\,(as-prepared)}} \; x\; 100$$

In addition, the 2nd-Alpill-MMTs were thermally regenerate at 700 °C for 2 hrs after the second adsorption experiment, and then characterized by XRD and N_2 adsorption. It was found that the SSA values of both regenerated Alpill-MMTs were lower than the as-prepared Alpill-MMTs as shown in Table 4.7. The SSA reduction of thermally regenerate Alpill-MMTs was attributed to the presence of thermally degraded residuals of BY1, i.e. carbonaceous and sulfur products, resulting in the lowering of adsorption capacities.

Besides, the d_{001} basal spacing and BJH pore size distribution of the regenerated Alpill-MMTs shown in Fig. 4.17 were not significantly different from those of the as-

prepared Alpill-MMTs. These results exhibited the unchanged pore structures of Alpill-MMTs after several cycles of adsorption and regeneration.

The thermally regenerated Alpill-MMT-2.4-30-Ultra-20 showed higher adsorption capacities than the regenerated Alpill-MMT-2.4-60-Str-rt. These results were ascribed to the effect of different pore size and pore structure between the Alpill-MMT-2.4-60-Str-rt and the Alpill-MMT-2.4-30-Ultra-20. Alpill-MMT-2.4-60-Str-rt mainly possessed the mesopores with almost average diameter of about 3.8 nm, in which they might be partially blocked with thermally degraded residuals of BY1 after regeneration. On the other hand, the multiple pore sizes ranging from 3 – 30 nm in the Alpill-MMT-2.4-30-Ultra-20 could facilitate the migration and liberation of the degraded products from the interior pores of Alpill-MMT-2.4-30-Ultra-20.

From the adsorption experiments, it can be concluded that the Alpill-MMT prepared by ultrasonic assisted method exhibited higher adsorption capacity than the Alpill-MMT prepared by the conventional stirring method when using the 2000 mg/L BY1 as the adsorbate. Hence, the Alpill-MMT-2.4-30-Ultra-20 was further applied as the adsorbent for the dye removal experiment using the continuous process in section 4.2.3 (G). In addition, we have been interested in enhancing the decolorization efficiency of the Alpill-MMT-2.4-60-Str-rt by doping with copper (II) in section 4.3.

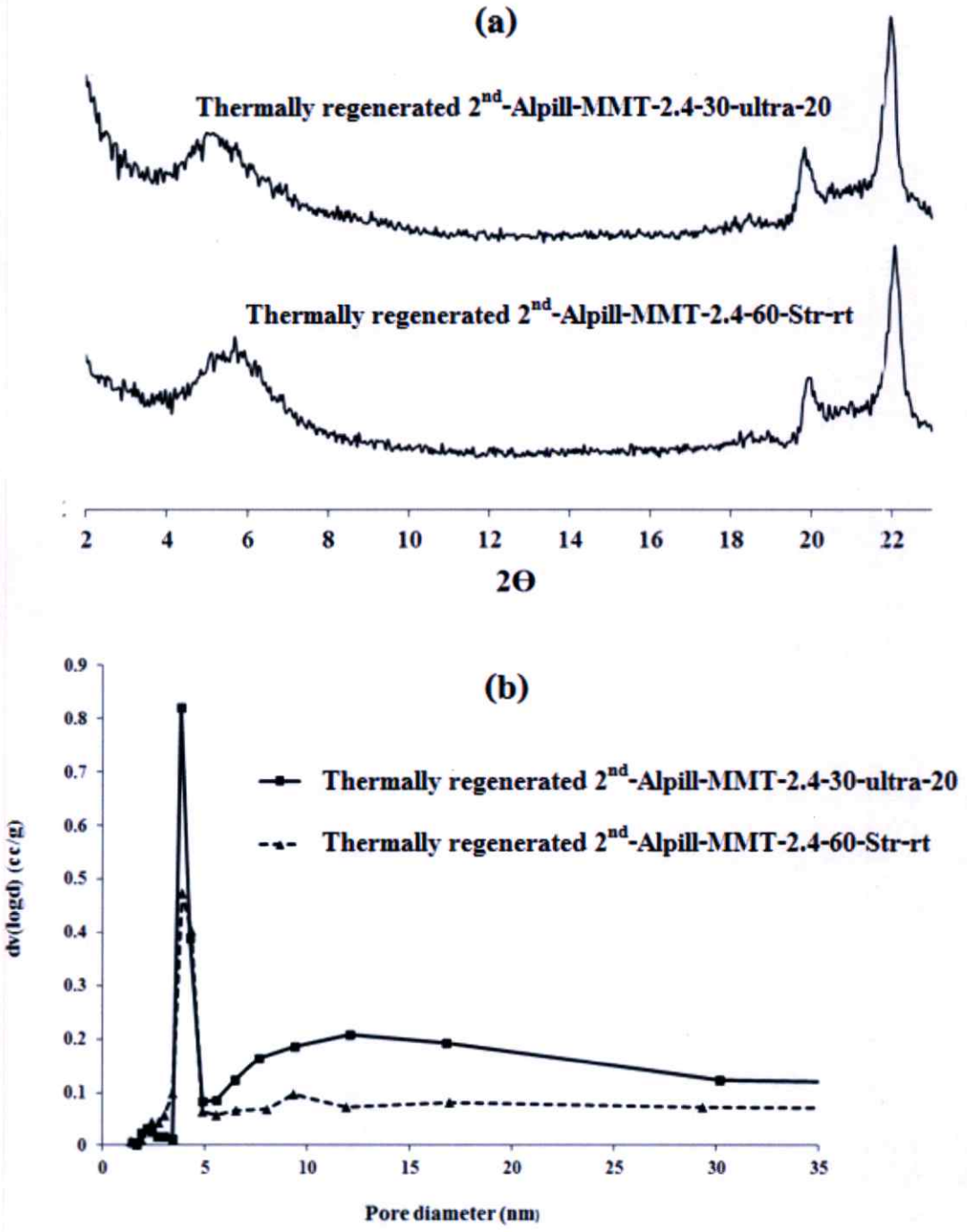

Figure 4.17 (a) XRD patterns and (b) BJH pore size distribution of thermally regenerated 2nd-Alpill-MMTs

G. Continuous process

The continuous adsorption experiment was carried out using the glass column packed with the Alpill-MMT-2.4-30-Ultra-20 adsorbent in order to evaluate the efficiency of Alpill-MMT-2.4-30-Ultra-20 for removal BY1 molecules from the aqueous solution. The 300 mg/L BY1 solution was continuously fed into the column using rate of about 2 ml/min at room temperature. The treated solution was collected at regular time intervals and further determined the BY1 concentration in the evaluate by UV-vis spectrometer. Figure 4.18 shows the break through curve for continuous BY1 removal in the fixed-bed Alpill-MMT-2.4-30-Ultra-20 column. It can be seen that there were three periods of breakthrough curve for BY1 on Alpill-MMT-2.4-30-Ultra-20. In the first period (I; 10-120 ml of evaluate), the concentration for BY1 decreased from 300 mg/L (initial concentration) to 0.3-6.0 mg/L. The percentage of BY1 removal and adsorption capacity in the period I were ~99% and ~35.78 mg/g, respectively, indicating the favorable interaction (Chemisorption) between the BY1 molecules and Alpill-MMT-2.4-30-Ultra-20.

In period II, it can be seen that there were significant difference in the concentration of treated BY1 solution when increasing the feed volume from 120 to 130 ml, in which the percentage of BY1 removal decreased from 98% to 71%. After that, the BY1 concentration in the evaluate slightly increased when increasing the feed volume to 350 ml because of the reduction of free surface area for BY1 adsorption. The BY1 removal data in period II suggested that the adsorption mechanism in period II was assumed to be mainly physical interaction (Physisorption) between the free BY1 molecules and the previously adsorbed BY1 molecules in free pore volume of Alpill-MMT-2.4-30-Ultra-20 adsorbent. This physisorption was in agreement with the presence of multiple pore sizes (6-30 nm) in the Alpill-MMT-2.4-30-Ultra-20 as discussed previously in Fig. 4.10 (b).

In period III, the BY1 concentration in the evaluate was steeply increased when the feed volume increased from 350 to 360 ml, then gradually increased when the feed volume increased from 360-570 ml and became constant after the feed volume was higher than 580 ml. It can be seen that the BY1 concentration in the evaluate between the feed volumes from 580 to 700 ml was almost equal to 300 mg/L of initial BY1 concentration. The low BY1 removal in period III was because the number of free adsorbent surface decreased with the filling of BY1 molecules and the free path in adsorbent pore was also blocked. Therefore, the adsorption mechanism in this period was mostly occurred at the void space between particles of Alpill-MMT-2.4-30-Ultra-20.

The adsorption capacities of the Alpill-MMT-2.4-30-Ultra-20 in batch and continuous adsorption processes were 96.15 and 83.83 mg/g, respectively as shown in Table 4.8. It can be seen that the adsorption efficiency in the continuous adsorption process was slightly lower than that of the batch adsorption process because the contact time between the BY1 molecules and the adsorbent in the continuous adsorption process was low.

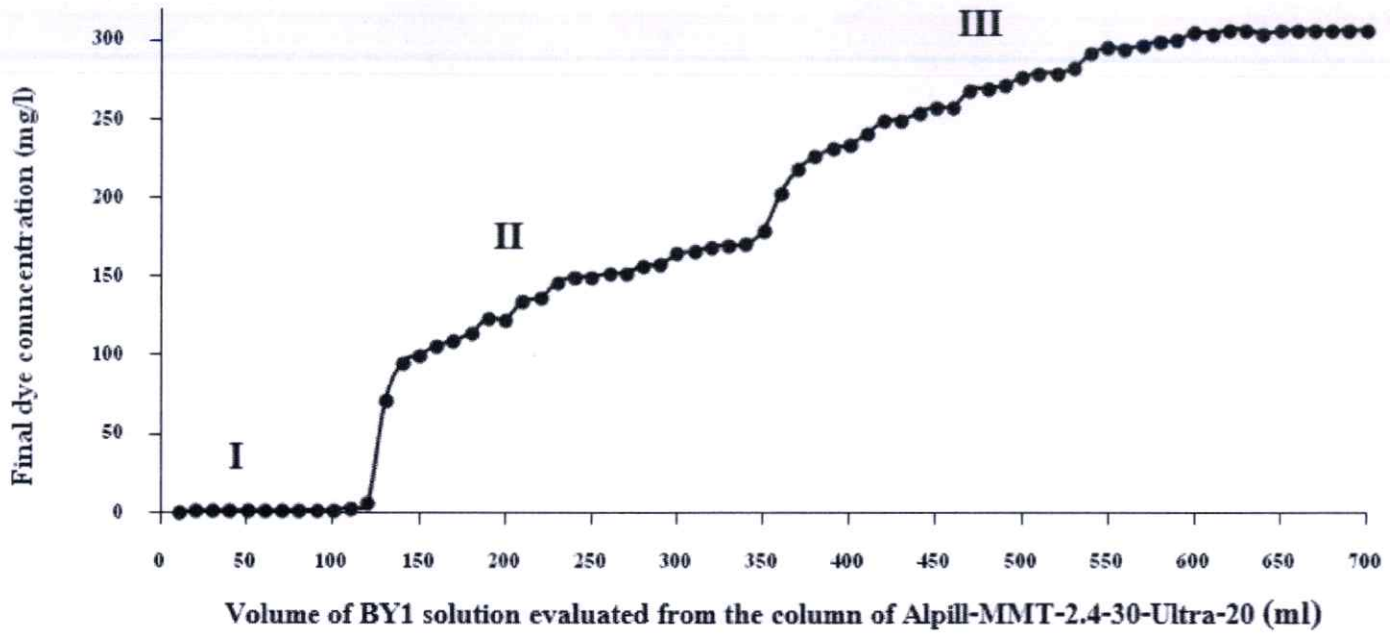

Figure 4.18 Break through curve analysis for fixed-bed adsorption of BY1 using the Alpill-MMT-2.4-30-Ultra-20 adsorbent

Table 4.8 The adsorption capacities of the Alpill-MMT-2.4-30-Ultra-20 in batch and continuous adsorption processes

Sample	Breakthrough volume (ml)	q_t (mg/g)		% Reduction	% Utilazation
		batch process	continuous process		
Alpill-MMT-2.4-30-Ultra-20	120	96.15	83.83	12.81	87.18

4.3 Preparation of copper doped aluminium pillared montmorillonite

In this section, the copper doped aluminium pillared montmorillonite (Cu-Alpill-MMTs) were prepared by two different methods, i.e. ultrasonic assisted adsorption and impregnation method, in order to study the effect of preparation method on their porosity structures and decolorization activities.

4.3.1 Ultrasonic assisted adsorption method

In this section, two different starting precursors were used for preparation of Cu-Alpill-MMTs by ultrasonic assisted adsorption, i.e. AlOH-MMT-2.4-60-Str-rt* and Alpill-MMT-2.4-60-Str-rt**.

The AlOH-MMT-2.4-60-Str-rt and Alpill-MMT-2.4-60-Str-rt precursor were dispersed in the aqueous solution of copper solution with ultrasonic treatment, and then calcined. The calcined products of AlOH-MMT-2.4-60-Str-rt and Alpill-MMT-2.4-60-Str-rt precursor were denoted as Cu-ads-Alpill-MMT1 and Cu-ads-Alpill-MMT2, respectively.

A. Characterization of copper doped aluminium pillared montmorillonite

The chemical compositions and XRD patterns of AlOH-MMT-2.4-60-Str-rt, Alpill-MMT-2.4-60-Str-rt, Cu-ads-Alpill-MMT1 and Cu-ads-Alpill-MMT2 are respectively shown in Table 4.9 and Fig. 4.19. The main components of the starting Na^+-MMT were Al_2O_3 and SiO_2 of phyllosilicate structure accompanying with a trace of Na_2O from the Na^+ interlayer counterions. In Fig. 4.8 (a), the crystalline peak at $2\theta \approx 7.12^{\circ}$ corresponded to the *001* plane interlayer spacing (d_{001}) of Na^+-MMT, in which the interlayer distance calculated from Braggs' equation was 1.24 nm.

* AlOH-MMT-2.4-60-Str-rt was prepared by conventional stirring method in section 3.4.3 (A)

** Alpill-MMT-2.4-60-Str-rt was prepared by conventional stirring method in section 3.4.3 (A)

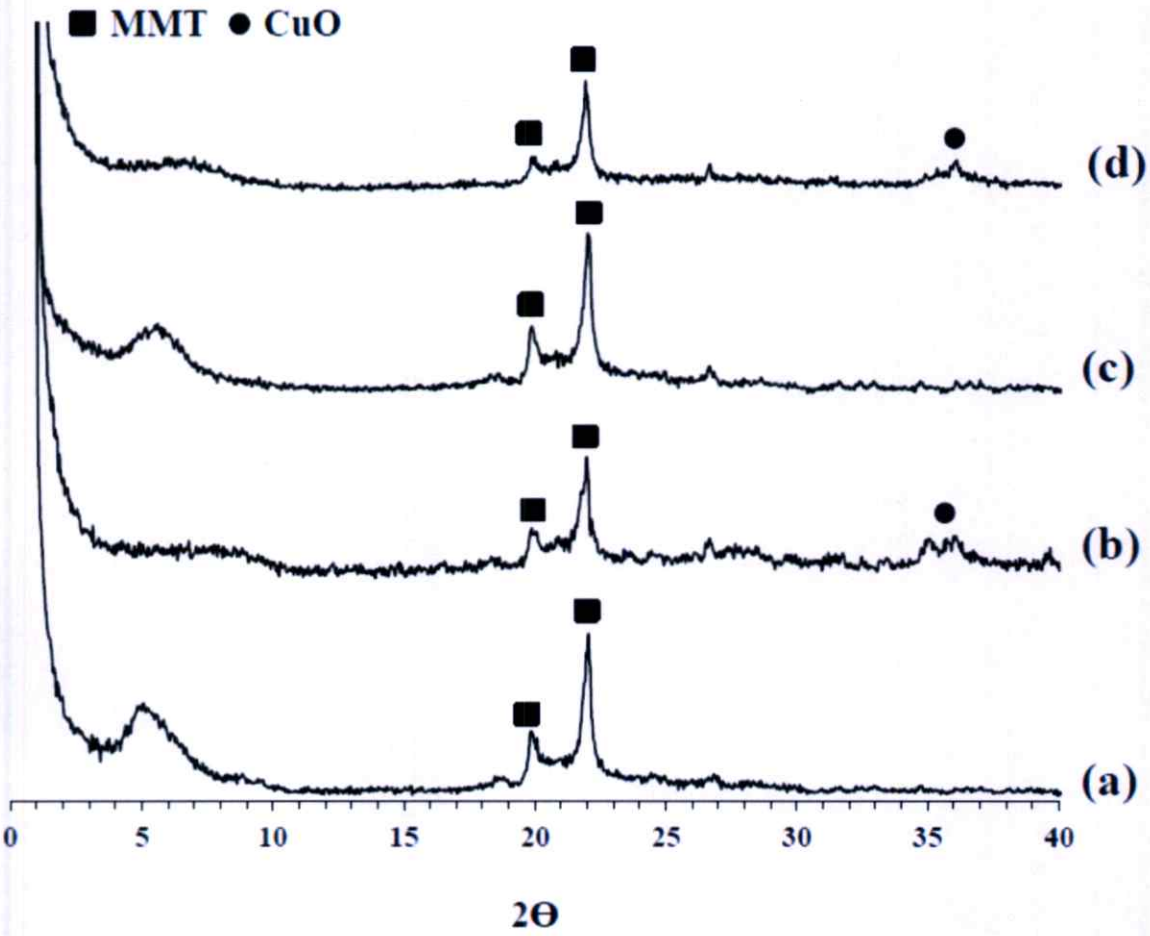

Figure 4.19 XRD patterns of (a) AlOH-MMT-2.4-60-Str-rt, (b) Cu-ads-Alpill-MMT1, (c) Alpill-MMT-2.4-60-Str-rt and (d) Cu-ads-Alpill-MMT2

Table 4.9 Chemical composition, basal spacing (d_{001}), specific surface area (SSA), pore volume and BJH pore diameter of AlOH-MMT-2.4-60-Str-rt, Alpill-MMT-2.4-60-Str-rt, Cu-ads-Alpill-MMT1 and Cu-ads-Alpill-MMT2

Sample	Chemical composition						N_2 adsorption			Basal spacing
	Al_2O_3 (wt%)	SiO_2 (wt%)	Na_2O (wt%)	CuO (wt%)	Al/Si molar ratio	Cu/Si molar ratio	SSA (m^2/g)	Pore volume (cm^3/g)	BJH pore size (nm)	d_{001} (nm)
AlOH-MMT-2.4-60-str-rt	18.44	73.68	0.50	0.00	0.29	0.00	n/a	n/a	n/a	1.74
Alpill-MMT-2.4-60-Str-rt	18.46	73.57	0.56	0.00	0.29	0.00	117	0.24	3.80	1.69
Cu-ads-Alpill-MMT1	15.50	56.20	0.43	25.50	0.32	0.34	12	0.10	4.24	Broad peak
Cu-ads-Alpill-MMT2	19.00	69.56	0.49	13.20	0.31	0.15	83	0.21	3.78	Broad peak

The d_{001} values of the AlOH-MMT-2.4-60-Str-rt and Alpill-MMT-2.4-60-Str-rt precursor were 1.74 and 1.69 nm, respectively, corresponding to the presence of Al_{13}^{7+} Keggin ions and Al_2O_3 in the starting precursors as previously discussed and shown in Fig. 4.20.

Since, the structures of AlOH-MMT-2.4-60-Str-rt and Alpill-MMT-2.4-60-Str-rt possessed the random molecular orientation and inhomogeneous distribution, resulting in multi-interplanar spacing as schematically shown in Fig. 4.20. When the Cu (II) was doped into the AlOH-MMT-2.4-60-Str-rt, Alpill-MMT-2.4-60-Str-rt using the ultrasonic treatment, the CuO component could be measured in the Cu-ads-Alpill-MMT products. Moreover, the sample prepared from the AlOH-MMT-2.4-60-Str-rt precursor (Cu-ads-Alpill-MMT1) possessed higher CuO and Cu/Si molar ratio than the sample prepared from the Alpill-MMT-2.4-60-Str-rt precursor (Cu-ads-Alpill-MMT2). The higher d_{001} value of Cu-ads-Alpill-MMT1 brought about the higher efficiency for Cu (II) adsorption, corresponding to the XRD and XRF data. However, the relative amounts of Al_2O_3 and SiO_2 and the Al/Si molar ratio in the Cu-ads-Alpill-MMTs were hardly changed in comparison with those in the AlOH-MMT-2.4-60-Str-rt and Alpill-MMT-2.4-60-Str-rt. In Fig. 4.19 (b) and (d), the d_{001} crystalline peak observed was broadened with slight declining peak intensity. In addition, a crystalline peak observed at $2\theta \approx 35.5°$ was indentified to CuO phase. These results suggested that the pillared structure of Cu-ads-Alpill-MMTs remain unchanged during the Cu (II) doping process even it was treated with the high intensity ultrasonic processor, implying to the structural stability of the as-prepared AlOH-MMT and Alpill-MMT.

The doped Cu (II) was considered to partially occupy both internal and external surfaces of the AlOH-MMT-2.4-60-Str-rt and Alpill-MMT-2.4-60-Str-rt precursor as schematically shown in Fig. 4.20. These results were in agreement with the regular distribution of Cu element observed on the surfaces of both Cu-ads-Alpill-MMT1and Cu-ads-Alpill-MMT2 as shown in SEM micrographs of Cu mapping (Fig. 4.21). It can be seen that the Cu-ads-Alpill-MMT1 possessed higher quantity of Cu in the EDX mapping than the Cu-ads-Alpill-MMT2.

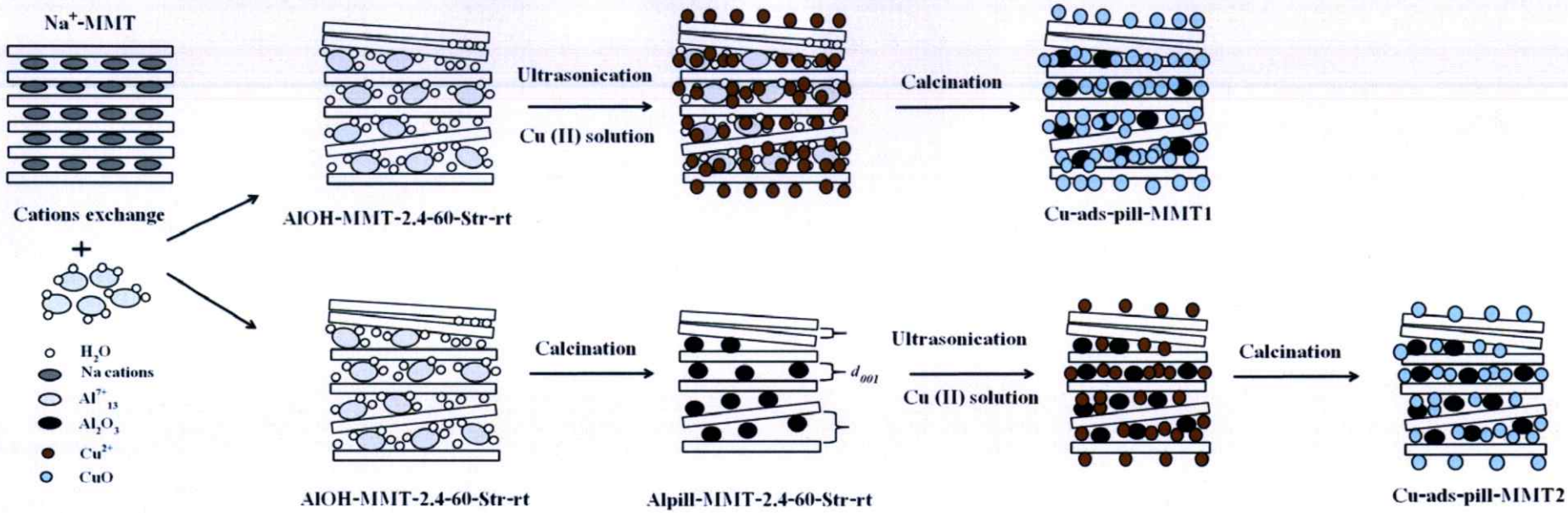

Figure 4.20 Schematic illustration of preparation of Cu-ads-Alpill-MMT1 and Cu-ads-Alpill-MMT2

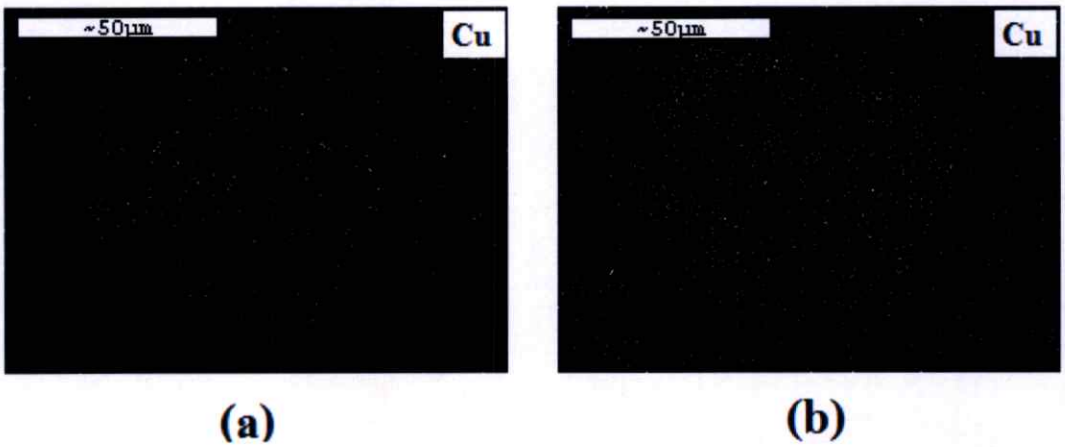

Figure 4.21 SEM micrographs of Cu mapping of (a) Cu-ads-Alpill-MMT1 and (b) Cu-ads-Alpill-MMT2

Figure 4.22 shows the N_2 adsorption isotherm of Cu-ads-Alpill-MMT1 in comparison with that of the Cu-ads-Alpill-MMT2, in which their SSA, pore volume and BJH pore diameter were summarized in Table 4.9. Both isotherms corresponded to type IV isotherm in the Brunauer-Deming-Dewing-Teller (BDDT) classification [91]. The volume of N_2 adsorption in the Cu-ads-Alpill-MMT1 was lower than that in the Cu-ads-Alpill-MMT2, in which it was in agreement with the reduction of SSA and pore volume. These results were considered to be due to the presence of CuO occupied the internal surface of Cu-ads-Alpill-MMTs samples. Moreover, the SSA and pore volume of Cu-ads-Alpill-MMT1 was lower than Alpill-MMT-2.4-60-Str-rt.

The hysteresis loop isotherms of both Cu-ads-Alpill-MMT1 and Cu-ads-Alpill-MMT2 could be classified according to the IUPAC classification as H3 type [181]. The H3 type represented the structure of mesoporosity (2-50 nm), having pore geometry of slit-like. Both of Cu-ads-Alpill-MMT1 and Cu-ads-Alpill-MMT2 possessed the mesopores with almost average diameter of about 3.8 nm in the BJH pore size distribution diagram as shown in Fig. 4.23. It can be seen that the quantity of pores with diameter of 3.8 nm in the Cu-Alpill-MMT decreased in concomitance with an increase of pores with diameter ranging from 6 to 30 nm, representing the nanoporous structure with multiple pore sizes as schematically purposed in Fig. 4.20. This result was considered to be because the pores of Cu-ads-Alpill-MMTs were encumbered with CuO.

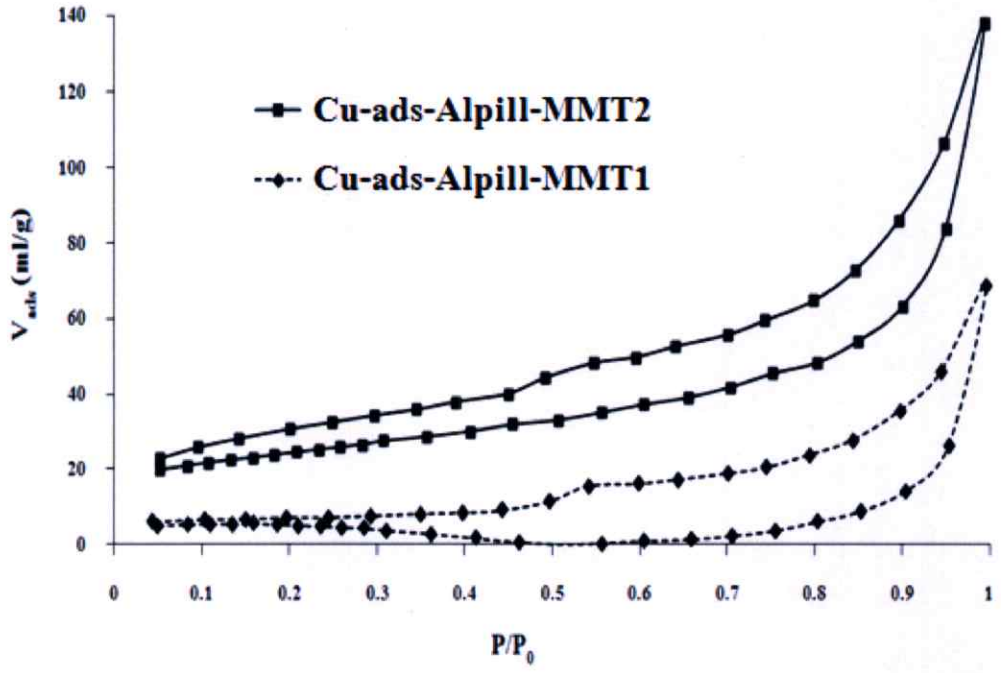

Figure 4.22 Nitrogen adsorption–desorption isotherms of Cu-ads-Alpill-MMT1 and Cu-ads-Alpill-MMT2

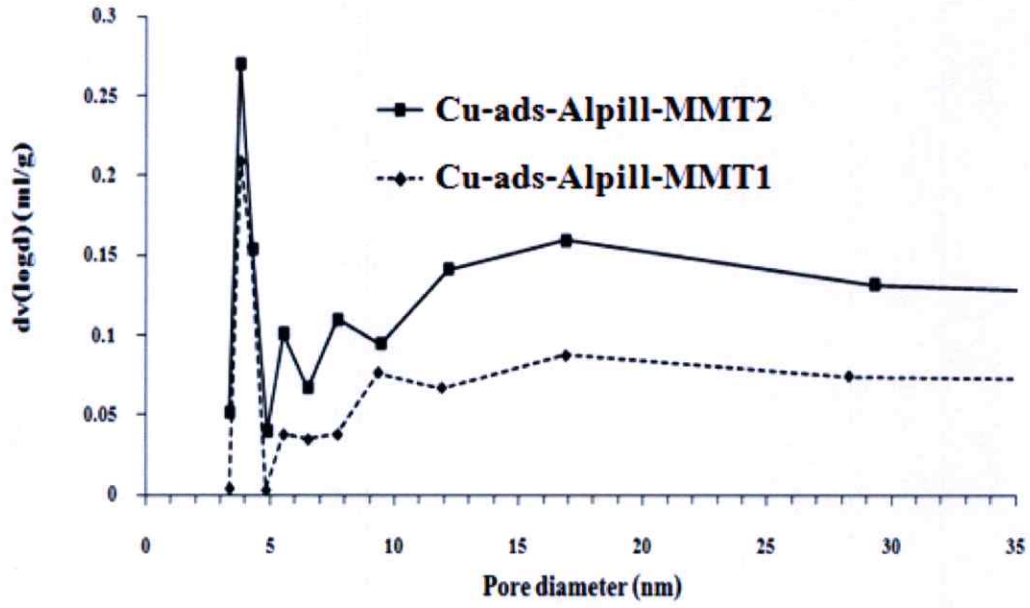

Figure 4.23 BJH pore size distribution curves of Cu-ads-Alpill-MMT1 and Cu-ads-Alpill-MMT2

B. Dye removal

B.1 Batch adsorption process

Table 4.10 shows the BY1 and RO16 removal capacities of Alpill-MMT-2.4-60-Str-rt, Cu-ads-Alpill-MMT1 and Cu-ads-Alpill-MMT2 adsorbents using batch adsorption process. It can be seen that all of adsorbents more preferably adsorbed the BY1 adsorbate than the RO16 adsorbate. Although the initial concentration of BY1 was 500 mg/L, the Alpill-MMT-2.4-60-Str-rt, Cu-ads-Alpill-MMT1 and Cu-ads-Alpill-MMT2 exhibited very high percentage of dye removal, i.e. ~94%, ~87% and ~89%, respectively. In addition, the significant reduction of TOC values was obtained after treatment the BY1 solution with all Alpill-MMT-2.4-60-Str-rt (~90%), Cu-ads-Alpill-MMT1 (~80%) and Cu-ads-Alpill-MMT2 (~85%) adsorbents, indicating the successful removal of BY1 molecules from the dye solution by the solid adsorbents. The adsorption capacities of Alpill-MMT-2.4-60-Str-rt, Cu-ads-Alpill-MMT1 and Cu-ads-Alpill-MMT2 for BY1 removal reached about 47.19, 43.95 and 44.55 mg/g, respectively. On the other hand, the percentages of dye removal and TOC removal were somewhat low in the RO16 system for all Alpill-MMT-2.4-60-Str-rt, Cu-ads-Alpill-MMT1 and Cu-ads-Alpill-MMT2 adsorbents even the initial concentration was just 300 mg/L. The adsorption capacities of Alpill-MMT-2.4-60-Str-rt, Cu-ads-Alpill-MMT1 and Cu-ads-Alpill-MMT2 were 1.09 mg/g, 1.17 mg/g and 1.16 mg/g, respectively. These results were because the Alpill-MMT-2.4-60-Str-rt, Cu-ads-Alpill-MMT1 and Cu-ads-Alpill-MMT2 possessed negative charged sites throughout their structures, in which the zeta-potential values of Alpill-MMT-2.4-60-Str-rt, Cu-ads-Alpill-MMT1 and Cu-ads-Alpill-MMT2 were -28, -5 and -5 mV, respectively. It was, therefore, the Alpill-MMT-2.4-60-Str-rt, Cu-ads-Alpill-MMT1 and Cu-ads-Alpill-MMT2 could uptake the BY1 molecules from the dye solution into their interlayer spaces and/or onto the external surfaces *via* the electrostatic interaction between the negative surfaces of adsorbents and the positive charged BY1 adsorbate. Besides, the RO16 is an anionic water soluble dye, so the RO16 molecules hardly interacted with the Alpill-MMT-2.4-60-Str-rt, Cu-ads-Alpill-MMT1 and Cu-ads-Alpill-MMT2 adsorbents. In addition, the molecular size of BY1 was smaller than that of RO16; therefore, the BY1 could easily migrate and adsorb in the nanopores of Alpill-MMT-2.4-60-Str-rt, Cu-ads-Alpill-MMT1 and Cu-ads-Alpill-MMT2 adsorbates.

Table 4.10 Percentage of dye removal, adsorption capacity (q_t), TOC and percentage of TOC removal of Alpill-MMT-2.4-60-Str-rt, Cu-ads-Alpill-MMT1 and Cu-ads-Alpill-MMT2 adsorbents in the batch adsorption process

Dye adsorbate	Adsorbent	UV-Vis		TOC	
		Dye removal (%)	q_t (mg/g)	TOC (mg/L)	TOC removal (%)
BY1 [a]	Alpill-MMT-2.4-60-Str-rt	94.39	47.19	19.03	90.18
	Cu-ads-Alpill-MMT1	87.89	43.95	33.74	82.60
	Cu-ads-Alpill-MMT2	89.10	44.55	27.90	85.61
RO16 [b]	Alpill-MMT-2.4-60-Str-rt	3.64	1.09	83.66	2.47
	Cu-ads-Alpill-MMT1	3.91	1.17	82.03	4.37
	Cu-ads-Alpill-MMT2	3.85	1.16	82.06	4.34

[a] Initial concentration of BY1 = 500 mg/L (TOC = 193.9 mg/L)

[b] Initial concentration of RO16 = 300 mg/L (TOC = 85.78mg/L)

In the BY1 system, the Alpill-MMT-2.4-60-Str-rt exhibited the superior removal capacity than the Cu-ads-Alpill-MMT1 and Cu-ads-Alpill-MMT2 because the former had higher SSA and pore volume than the latter as discussed previously. Likewise, the Cu-ads-Alpill-MMT2 with higher SSA and pore volume than the Cu-ads-Alpill-MMT1, therefore, the Cu-ads-Alpill-MMT2 exhibited the highest adsorption efficiency for BY1 removal. On the other hand, the RO16 adsorption capacity of Cu-ads-Alpill-MMTs was slightly higher than that of the Alpill-MMT-2.4-60-Str-rt. This result was attributed to the lowering of negative charge in the Cu-ads-Alpill-MMTs, so that it could adsorb higher amount of anionic RO16 molecules than the Alpill-MMT-2.4-60-Str-rt. However, the batch adsorption process using Alpill-MMT-2.4-60-Str-rt, Cu-ads-Alpill-MMT1 and Cu-ads-Alpill-MMT2 adsorbates were inappropriate for elimination of RO16 molecules from the dye solution; therefore, the catalytic oxidation system of Cu-ads-Alpill-MMTs was developed in order to enhance the efficiency of RO16 removal.

B.2 Catalytic oxidation process

B.2.1 Fenton process

Figure 4.24 present the percentages of color and TOC removals when the Alpill-MMT-2.4-60-Str-rt, Cu-ads-Alpill-MMT1 and Cu-ads-Alpill-MMT2 were used as heterogeneous reagent for elimination of RO16 in the presence of H_2O_2. In the Alpill-MMT-2.4-60-Str-rt/H_2O_2 system, the percentage of color removal gradually increased with the increase of reaction time and reached about 16.25% in 360 min. This result was attributed to the presence of H_2O_2 which could generate highly reactive •OH radicals. These radicals were then reacted with the aromatic rings and chromophores of RO16, resulting in the decolorization of RO16 solution. However, the percentage of color removal significantly increased and reached around 70-80% in the first 60 min of treatment when the Cu-ads-Alpill-MMTs/H_2O_2 were used, while the percentage of TOC removal reached around 40-60%. These results suggested that the presence of CuO in the Cu-ads-Alpill-MMTs significantly enhanced the efficiencies of color and TOC removals because the CuO could act as the heterogeneous catalyst for the decomposition of H_2O_2, in which this system was commonly known as Fenton process. The Cu^{2+} ions were considered to leach out from the CuO in the Cu-Alpill-MMT and then reacted with the H_2O_2, leading to the formation of strong oxidizing species as shown in the chemical equations (4.1) and (4.2). At the first stage (Eq.4), the H_2O_2 decomposition with Cu^{2+} resulted in the formation of hydroperoxyl radical (HOO•) and Cu^{+}, then the Cu^{+} reactive

intermediate further reacted with the H_2O_2, producing the Cu^{2+} and HO• in the second stage (Eq.4.2) [154-155].

$$Cu^{2+} + H_2O_2 \rightarrow Cu^{+} + HOO\bullet + H^{+} \qquad (4.1)$$

$$Cu^{+} + H_2O_2 \rightarrow Cu^{2+} + HO\bullet + OH^{-} \qquad (4.2)$$

These reactive radicals could oxidize the RO16 molecules which adsorbed in the nanoporous structure of Cu-ads-Alpill-MMTs and the dissolved molecules in the vicinity of Cu-ads-Alpill-MMTs. From these results, the Cu-ads-Alpill-MMT1 exhibited higher decolorization and TOC removal percentages than the Cu-ads-Alpill-MMT2 because the Cu-ads-Alpill-MMT1 possessed the highest amount of CuO occupied on both internal and external surfaces as shown in the XRF data and the SEM Cu mapping image.

In the catalytic oxidation treatment, the degradation of RO16 was considered to be the azo linkage (–N=N–) cleavage and aromatic degradation, resulting in the drastic decolorization of RO16 solution in the earlier stage of treatment. However, the percentage of TOC removal in the first 60 min of treatment was lower than that of color removal. These results suggested that the RO16 molecules were firstly degraded to smaller molecules of organic compounds and then partially mineralized to CO_2, H_2O, etc. The longer the reaction time, the higher percentages of color and TOC removals were obtained until they reached about 98% removals in 360-min treatment. These results indicate that the complete mineralization of RO16 was obtained after prolonged treatment in the Cu-Alpill-MMT/H_2O_2 system.

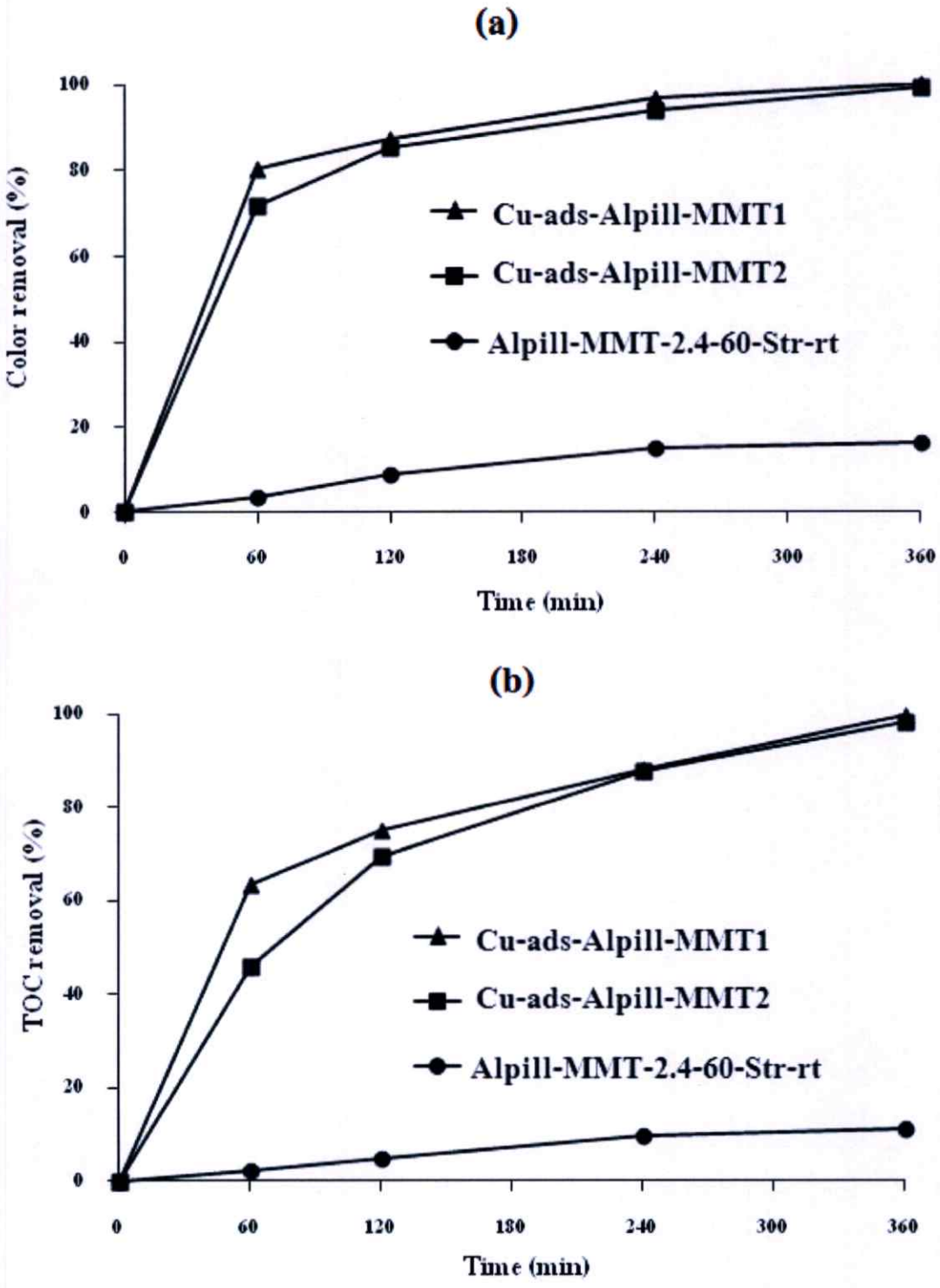

Figure 4.24 Efficiency of RO16 elimination of Cu-ads-Alpill-MMTs in Fenton process: (a) percentage of color removal and (b) percentage of TOC removal

B.2.2 Photo-Fenton process

The efficiency of Cu-ads-Alpill-MMT1 and Cu-ads-Alpill-MMT2 for RO16 elimination in the presence of H_2O_2 and UV radiation, known as photo-Fenton process, was shown in Fig. 4.25. It can be seen that the percentages of color and TOC removals rapidly increased and respectively reached around 96-98% and 91-95% even the treatment was performed for 30 min. The complete decolorization and mineralization of RO16 solution were achieved after 60-min treatment with the Cu-ads-Alpill-MMTs/H_2O_2/UV process. However, the percentage of color and TOC removals were hardly different between Cu-ads-Alpill-MMT1 and Cu-ads-Alpill-MMT2 under photo Fenton treatment.

The RO16 elimination in the Cu-ads-Alpill-MMTs/H_2O_2/UV system was six times faster than the conventional Fenton system of Cu-ads-Alpill-MMTs/H_2O_2. These results were attributed to the activation of UV radiation on the formation of more HO• radicals from the decomposition of water molecules with Cu^{2+} and the dissociation of H_2O_2 as respectively shown in the chemical equations (Eq.4.3) and (Eq.4.4) [160].

$$Cu^{2+} + H_2O \xrightarrow{h\nu} Cu^{+} + HO\bullet + H^{+} \qquad (4.3)$$

$$H_2O_2 \xrightarrow{h\nu} 2HO\bullet \qquad (4.4)$$

In addition, the Cu^{+} intermediate produced in equation (Eq.6) could further reacted with the H_2O_2 as previously shown in equation (Eq.4.2). The higher quantity of HO• radicals, the faster catalytic oxidation of RO16 was obtained in the Cu-ads-Alpill-MMTs/H_2O_2/UV system.

The capability of BY1 and RO16 elimination suggested the competency of Cu-ads-Alpill-MMTs for treatment of wastewater containing various kinds of dyestuffs.

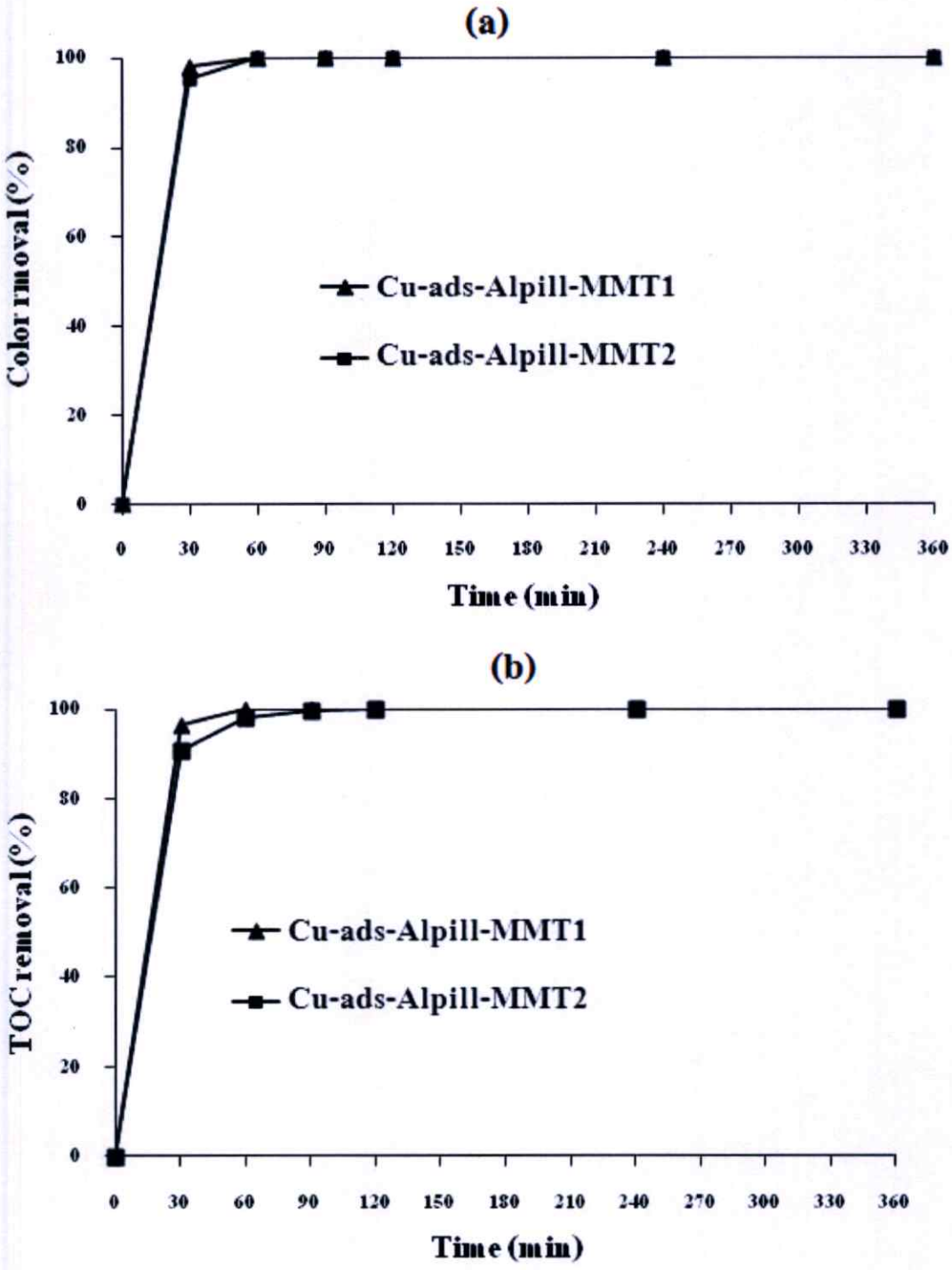

Figure 4.25 Efficiency of RO16 elimination of Cu-ads-Alpill-MMTs in photo Fenton process: (a) percentage of color removal and (b) percentage of TOC removal

4.3.2 Impregnation method

The Cu-im-Alpill-MMTs were prepared by impregnation of the copper (II) solution into the dried AlOH-MMT-2.4-60-Str-rt using various copper (II) loading, i.e. 4, 7, 10 and 13 wt%, and then calcined. The calcined products with the copper loading of 4, 7, 10 and 13 wt% were denoted as Cu-im-Alpill-MMT-4wt%, Cu-im-Alpill-MMT-7wt%, Cu-im-Alpill-MMT-10wt% and Cu-im-Alpill-MMT-13wt%, respectively.

A. Characterization of copper doped aluminium pillared montmorillonite

Figure 4.26 shows the XRD patterns of Cu-im-Alpill-MMTs are shown in comparison with the AlOH-MMT-2.4-60-Str-rt precursor. The d_{001} value of AlOH-MMT-2.4-60-Str-rt was 1.73 as summarized in Table 4.11. After Cu^{2+} impregnation into the AlOH-MMT-2.4-60-Str-rt and calcination, the d_{001} peak almost disappeared from the XRD patterns of all Cu-Im-Alpill-MMTs as shown in Fig. 4.26 (b) – 4.26 (e). These results suggested that the impregnated Cu^{2+} could penetrate into the interlayer space of AlOH-MMT-2.4-60-Str-rt, bringing about the delamination of MMT tactoids. The impregnated Cu^{2+} was calcined to CuO, therefore, the crystalline peak of CuO phase was also observed in the XRD patterns of all Cu-iAlpill-MMTs at $2\theta \approx 35.5°$. The presence of impregnated CuO in the Cu-im-Alpill-MMTs was also detected by the XRF analyses as reported in Table 1. The increases of CuO amount and Cu/Si molar ratio in the Cu-im-Alpill-MMTs were in agreement with the Cu^{2+}amount used in the impregnation process.

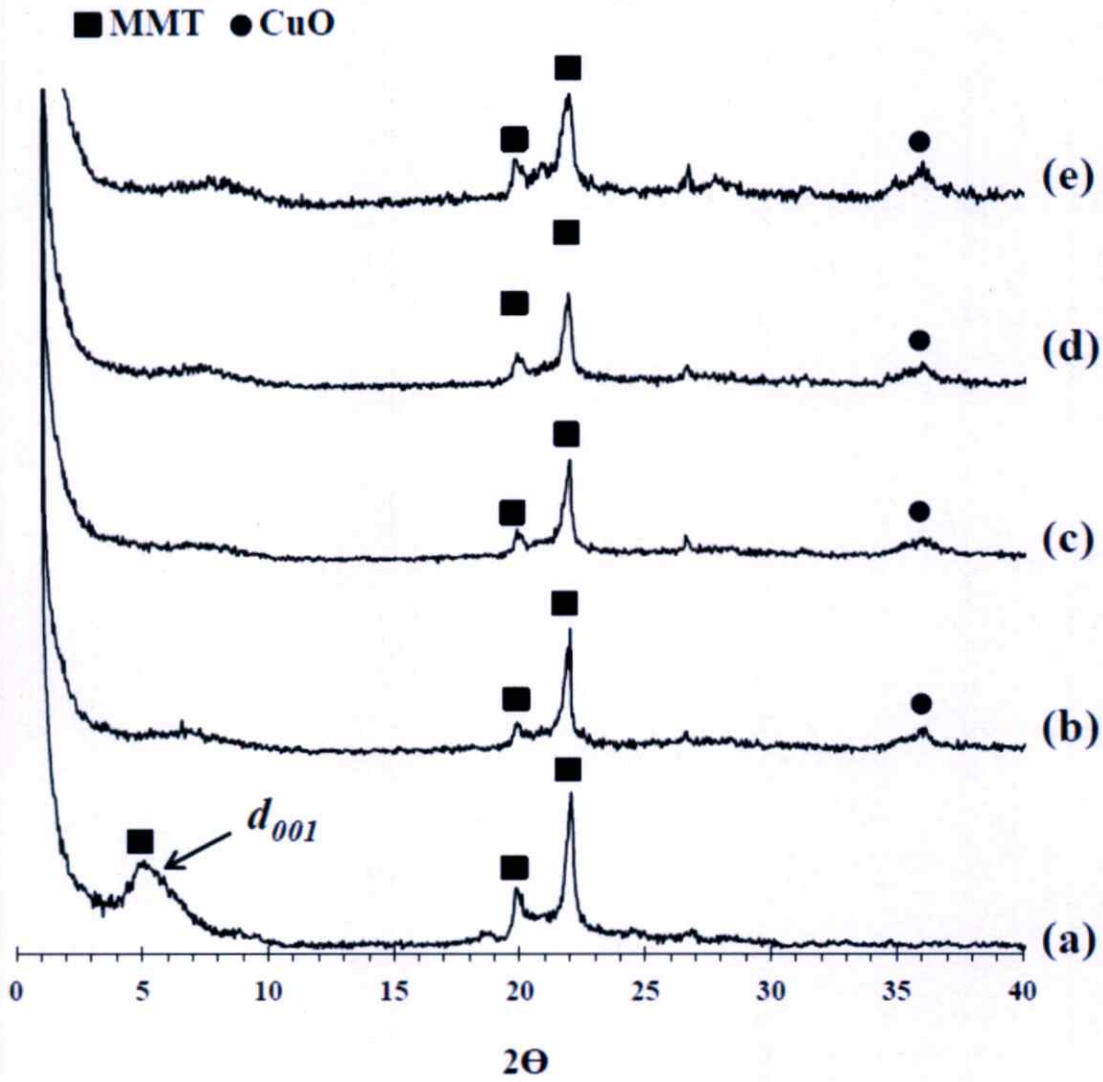

Figure 4.26 XRD patterns of (a) AlOH-MMT-2.4-60-Str-rt, (b) Cu-im-Alpill-MMT-4wt%, (c) Cu-im-Alpill-MMT-7wt%, (d) Cu-im-Alpill-MMT-10wt% and (e) Cu-im-Alpill-MMT-13wt%

Table 4.11 Chemical composition, basal spacing (d_{001}), specific surface area (SSA), pore volume and BJH pore diameter of AlOH-MMT-2.4-60-str-rt, Cu-im-Alpill-MMT-1wt%, Cu-im-Alpill-MMT-7wt%, Cu-im-Alpill-MMT-10 wt% and Cu-im-Alpill-MMT-13 wt%

Sample	Chemical composition						N_2 adsorption			Basal spacing
	Al_2O_3 (wt%)	SiO_2 (wt%)	Na_2O (wt%)	CuO (wt%)	Al/Si molar ratio	Cu/Si molar ratio	SSA (m^2/g)	Pore volume (cm^3/g)	BJH pore size (nm)	d_{001} (nm)
AlOH-MMT-2.4-60-str-rt	19.24	71.53	0.43	0.00	0.32	n/a	n/a	n/a	n/a	1.73
Cu-im-Alpill-MMT-4 wt%	16.17	66.65	0.22	4.921	0.29	0.06	87	0.19	3.79	Broad peak
Cu-im-Alpill-MMT-7 wt%	15.83	61.65	0.23	8.353	0.30	0.10	40	0.17	3.79	Broad peak
Cu-im-Alpill-MMT-10 wt%	14.98	56.23	0.14	12.132	0.31	0.16	30	0.16	3.79	Broad peak
Cu-im-Alpill-MMT-13 wt%	13.95	50.56	0.16	15.401	0.32	0.23	31	0.06	3.34	Broad peak

Figure 4.27 shows the SEM micrographs of the Cu-im-Alpill-MMT surfaces with their Cu mapping images. The regular distribution of Cu was observed on the surfaces of all Cu-im-Alpill-MMT samples, suggesting that the impregnated Cu^{2+} ions occupied not only the AlOH-MMT interlayers but also the AlOH-MMT surfaces. The quantity of Cu observed on the EDX mappings increased with the increase of Cu^{2+} amount used in the impregnation process.

Figure 4.28 shows the N_2 adsorption isotherms of the starting Na^+-MMT and all Cu-im-Alpill-MMTs. The adsorption isotherms of Na^+-MMT and Cu-im-Alpill-MMTs could be classified as type IV isotherm in the Brunauer, Deming, Dewing and Teller (BDDT) classification, having the hysteresis loop of H3 type in IUPAC classification [182]. It was, therefore, indicated that the starting Na^+-MMT and all Cu-im-Alpill-MMTs consisted of slit-like mesopore structures (2-50 nm). The Brunaur–Emmet–Teller (BET) equation and Barrett-Joyner-Halenda (BJH) method were respectively used for determination of the SSA and average diameter of mesopores as concluded in Table 4.11. It was found that the SSA and pore volume of the Cu-im-Alpill-MMTs decreased with the increase of the impregnated Cu content. These results were considered to be because the CuO occupied the interior pores of the Cu-im-Alpill-MMTs. The occupancy of CuO might occur through two main possibilities; i.e. the impregnated Cu^{2+} ions could coordinate to the oxygens of the MMT silicate layer and/or the oxygens of the aluminium polyhydroxy cations intercalated in the AlOH-MMT precursor [183].

Figure 4.29 shows the BJH pore size distributions of the starting Na^+-MMT and all Cu-im-Alpill-MMTs. It can be seen that the starting Na^+-MMT possessed the mesopores with average pore diameter of about 3.8 nm as shown in Fig.4.29 (a). On the other hand, the BJH pore size distributions of all Cu-im-Alpill-MMTs have revealed the formation of multiple mesopore sizes ranging from 3.3 – 35 nm in all Cu-im-Alpill-MMTs after intercalation and impregnation treatments as observed in Fig.429 (b) – 4.29 (e). The quantities of mesopores in the Cu-im-Alpill-MMTs gradually decreased with the increase of the impregnated Cu content due to the pore-filling with CuO.

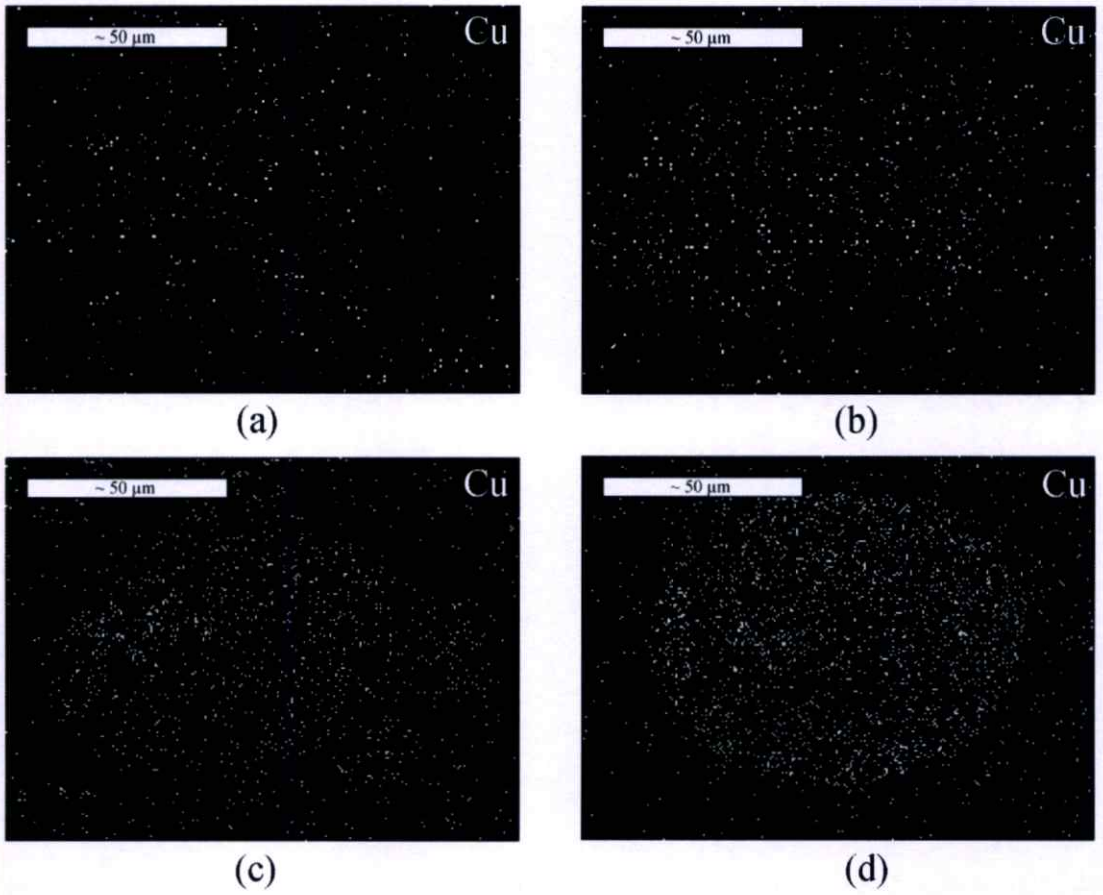

Figure 4.27 SEM micrographs mapping image with Cu of (a) Cu-im-Alpill-MMT-4wt%, (b) Cu-im-Alpill-MMT-7wt%, (c) Cu-im-Alpill-MMT-10wt% and (d) Cu-im-Alpill-MMT-13wt%

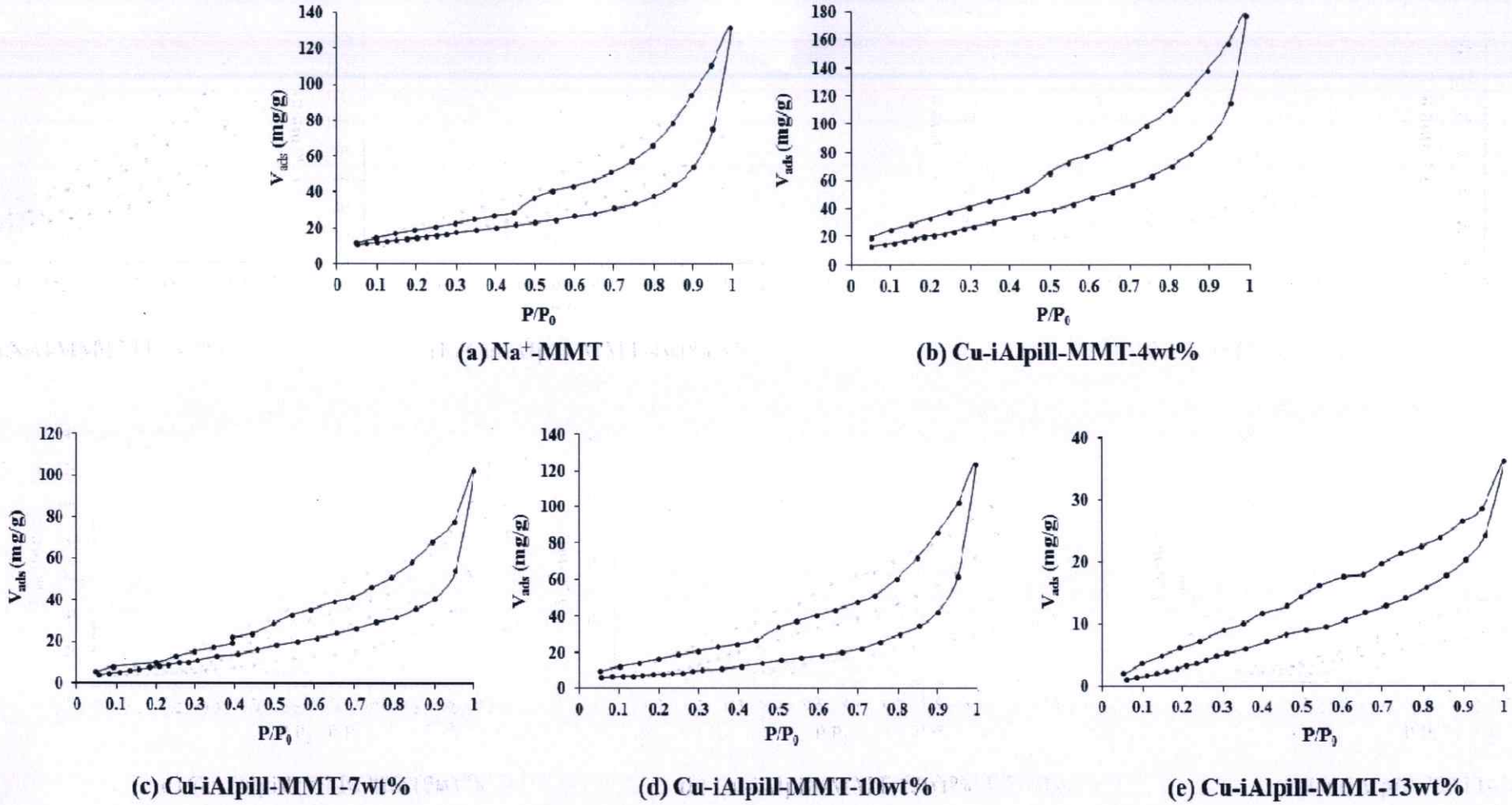

Figure 4.28 Nitrogen adsorption–desorption isotherms of Cu-im-Alpill-MMTs

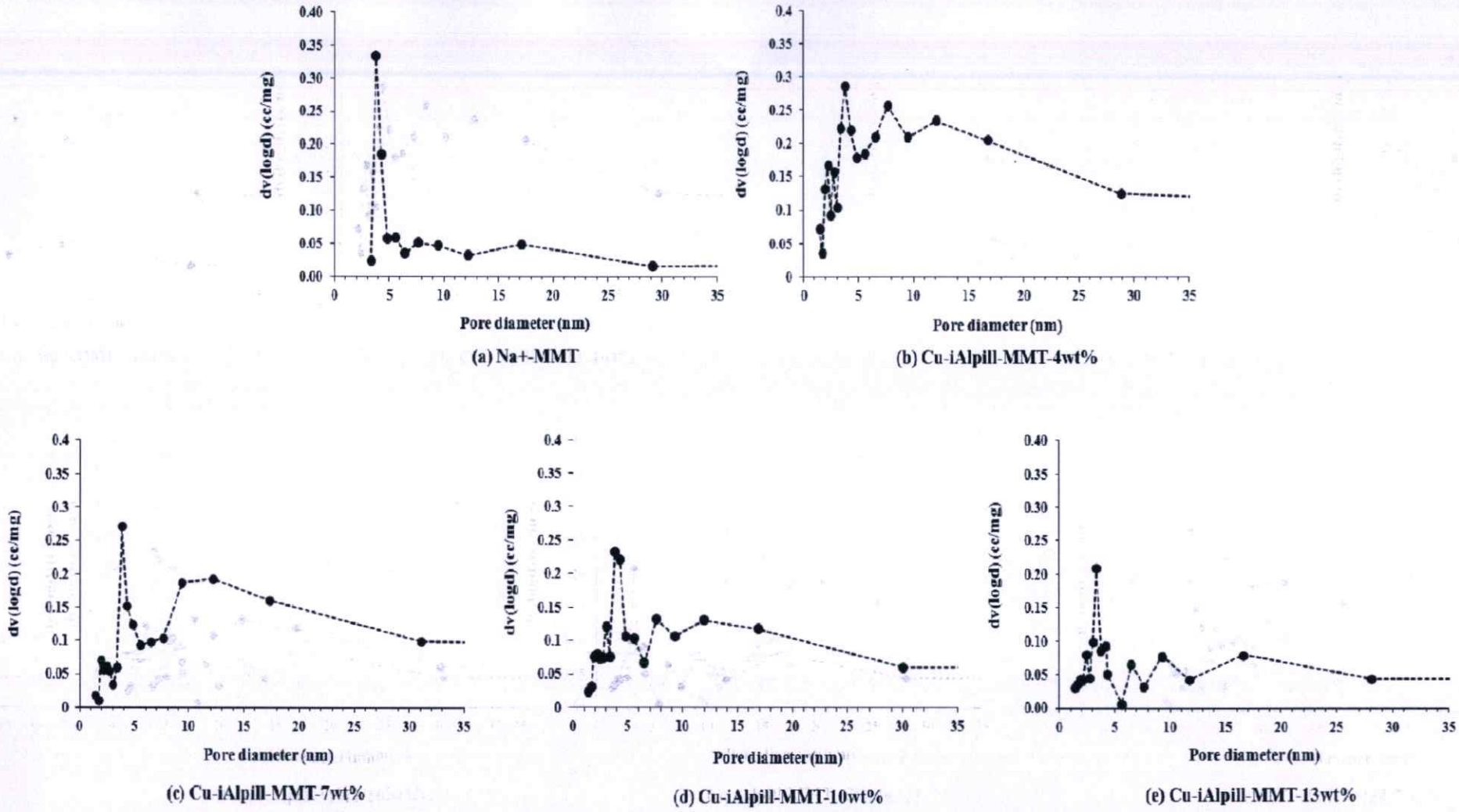

Figure 4.29 BJH pore size distribution curves of Cu-im-Alpill-MMTs

B. Catalytic oxidation system of RO16

B.1 Fenton process

Figure 4.30 (a) and 4.30 (b) respectively show the percentages of color and TOC removals of all Cu-iAlpill-MMTs in the presence of H_2O_2. It was found that the percentages of color and TOC removals gradually increased with the increases of reaction time and Cu^{2+} amount used in the impregnation process. The Cu-im-Alpill-MMT-13wt% exhibited the highest ability for RO16 removal even though it possessed the lowest pore volume, suggesting that the Cu-im-Alpill-MMTs tend to act more as the heterogeneous catalysts for the degradation of RO16 molecules than the simple adsorbents. The catalytic degradation of RO16 was considered to be initiated by the Cu^{2+} ions leached out from the CuO in both interior pores and surfaces of the Cu-im-Alpill-MMTs. The Cu^{2+} ions could promote the decomposition of H_2O_2 to strong oxidizing species, i.e. hydroperoxyl radical (HOO•) and hydroxyl (HO•) as reported elsewhere [154-155]. These reactive radicals could oxidize the RO16 molecules, causing the cleavages of azo linkage (–N=N–), C–S bond between the aromatic ring and sulfonate group, C–N bond between the naphthalene ring and azo group and aromatic ring opening [184]. These oxidation reactions resulted in the decolorization of RO16 due to the degradation of chromophore and auxochrome which are responsible for their color. In addition, the cleavage fragments of oxidized RO16 were considered to be demineralized by the reactive radicals as evidently observed in the significant increase of TOC removal.

B.2 Photo-Fenton process

Figure 4.31 (a) and 4.31 (b) respectively show the percentages of color and TOC removals of all Cu-im-Alpill-MMTs in the presence of H_2O_2 and UV radiation. Under the UV radiation, all Cu-im-Alpill-MMT catalysts exhibit significantly higher color and TOC removals than those performed without UV radiation using the same reaction time. These results were attributed to the synergistic effect of UV radiation and Cu^{2+} ions leached from the Cu-im-Alpill-MMTs on the rapid degradation of H_2O_2 and H_2O into the HO• radicals, bringing about the faster decolorization and mineralization of RO16 molecules. The systems with the higher Cu content in the Cu-im-Alpill-MMTs and/or the longer reaction time exhibited the higher percentages of color and TOC removals. However, the efficiency of RO16 removal of Cu-im-Alpill-MMT-10wt% was quite close to that of Cu-im-Alpill-MMT-13wt%, although the Cu content in the Cu-im-Alpill-MMT-10wt% was lower than that in the Cu-im-Alpill-MMT-13wt%. This result was considered to be because the excess Cu in the Cu-im-Alpill-MMT-13wt% which formed as CuO clusters on its exterior surface might partially hinder the

migration of Cu^{2+} ions leached from the interior. It was, therefore, both Cu-im-Alpill-MMT-10wt% and Cu-im-Alpill-MMT-13wt% could completely eliminate the RO16 within 60 min when using the photo-Fenton systems.

After Fenton and photo-Fenton treatments for 360 min, the Cu-ads-Alpill-MMT2 and Cu-im-Alpill-MMT-10wt% were collected, dried at 100 °C for 24 hrs and characterized by XRD. Fig. 4.32 shows the XRD patterns of Cu-ads-Alpill-MMT2 and Cu-im-Alpill-MMT-10wt% before and after treatments. It can be seen that there were not significantly different between the as-prepared Cu-Alpill-MMTs and the used Cu-Alpill-MMTs. Moreover, the crystalline peak of CuO phase was also observed in the XRD patterns of both Cu-Alpill-MMTs at $2\theta \approx 35.5°$. These results indicated that the Fenton and photo-Fenton treatments did not effect on the Cu-Alpill-MMTs structure.

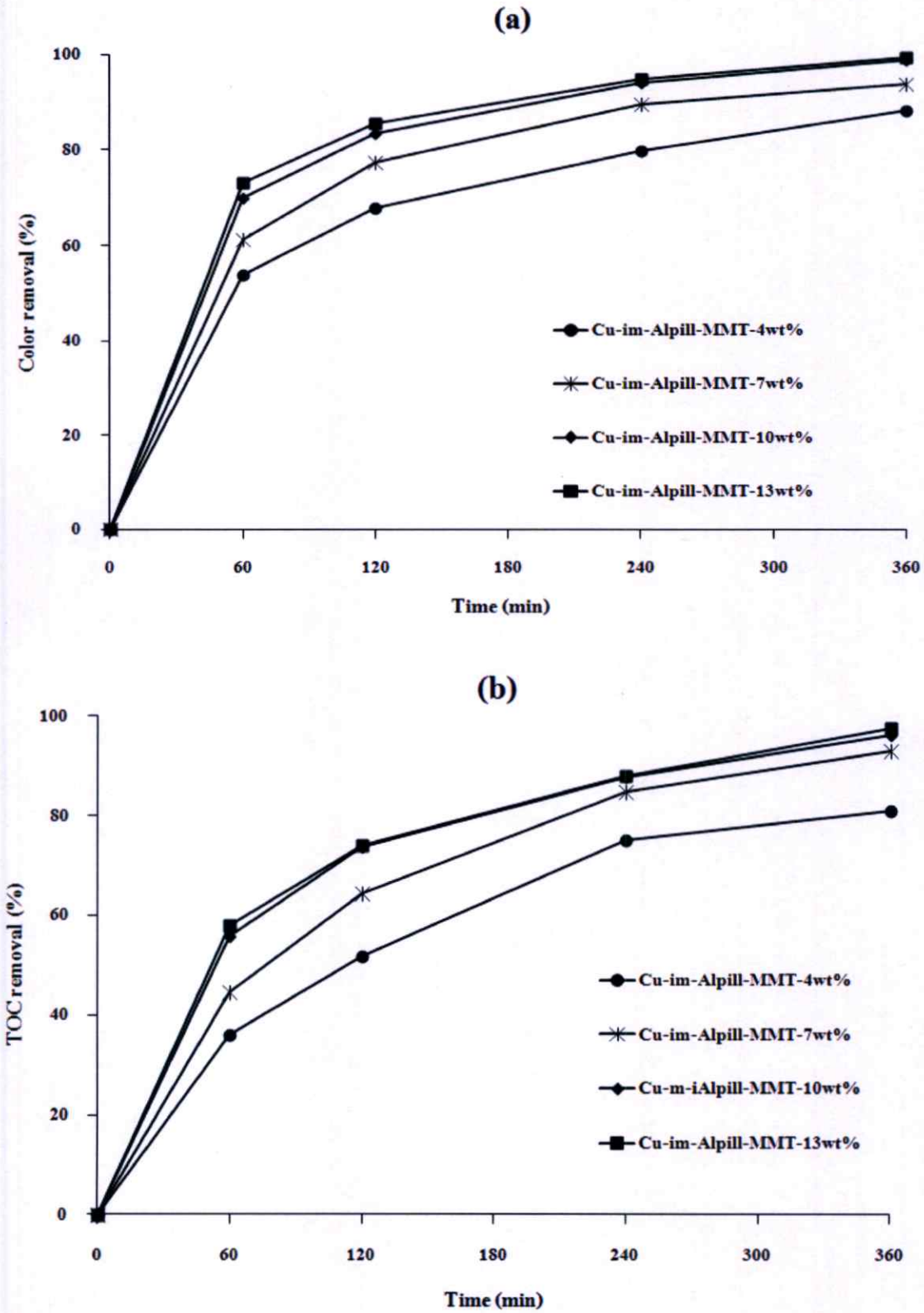

Figure 4.30 Efficiency of RO16 elimination of Cu-im-Alpill-MMTs in Fenton process: (a) percentage of color removal and (b) percentage of TOC removal

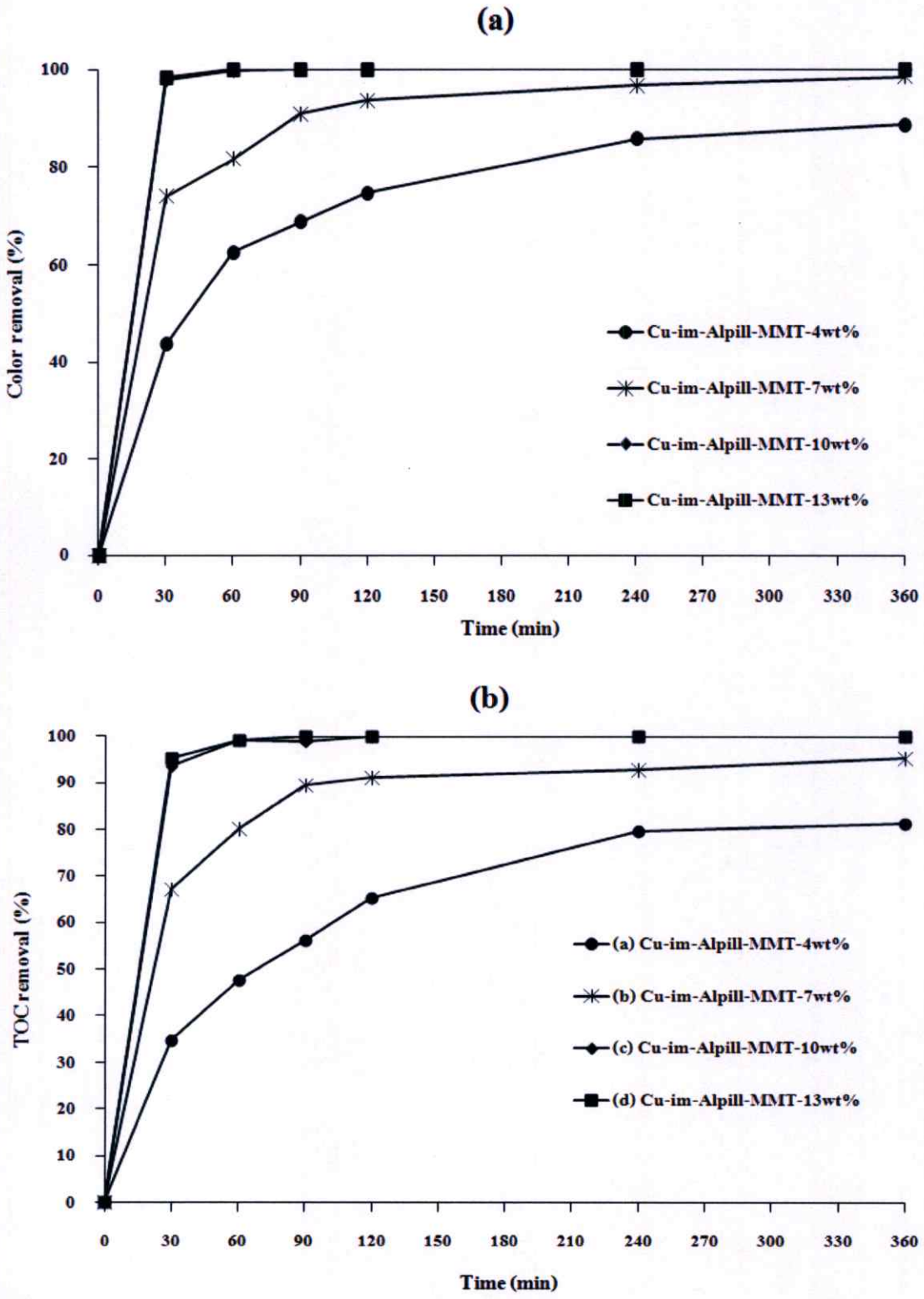

Figure 4.31 Efficiency of RO16 elimination of Cu-im-Alpill-MMTs in photo Fenton process: (a) percentage of color removal and (b) percentage of TOC removal

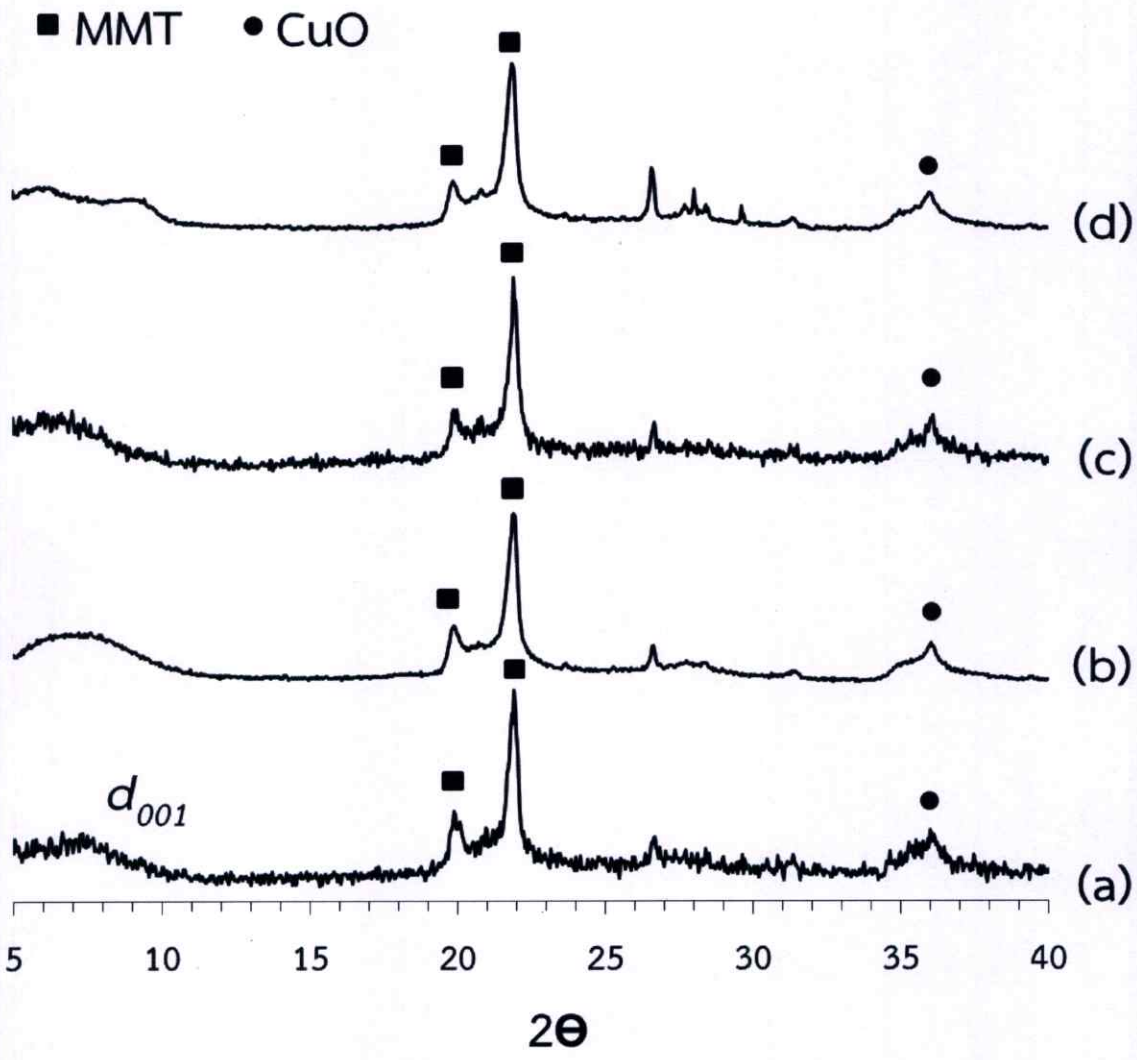

Figure 4.32 XRD patterns before and after treatments of (a) Cu-ads-Alpill-MMT2 (before) (b) Cu-ads-Alpill-MMT2 (after) (c) Cu-im-Alpill-MMT-10wt% (before) and (d) Cu-im-Alpill-MMT-10wt% (after)

4.4 Antibacterial activity

Figure 4.33 shows the antibacterial activity test of Na^{+}-MMT, Alpill-MMTs and Cu-Alpill-MMTs. It cannot observe the inhibition zone in the Na^{+}-MMT, AlOH-MMT-2.4-60-str-rt, Alpill-MMT-2.4-60-str-rt Cu-im-Alpill-MMT-4wt% and Cu-im-Alpill-MMT-7wt%, indicating that they were inactive for *E. coli*. On the other hand, Cu-ads-Alpill-MMT1, Cu-ads-Alpill-MMT2, Cu-im-Alpill-MMT-10wt% and Cu-im-Alpill-MMT-13wt% presented good antibacterial activities, with the inhibition zone diameter of 11.0, 6.0, 5.5 and 8.5 mm, respectively. The antibacterial activity of Cu-Alpill-MMTs was attributed to the catalytic activity of Cu^{2+} ions which leached out from the CuO in the Cu-Alpill-MMT, leading to the generation of highly reactive oxygen species (ROS) such as $HO^{\bullet-}$, $O_2^{\bullet 2-}$, $HO_2^{\bullet-}$ and H_2O_2 in aqueous suspensions [185]. These ROS could damage the cell integrity of *E. coli* [186]. Since the *E. coli* is a gram-negative bacterium and possesses a thin layer of peptidoglycan (about 2–3 nm) between the cytoplasmic membrane and the outer cell wall [187], therefore; the Cu^{2+} ions might be electrostatic interacted with the cell wall of *E. coli*. This phenomenon resulted in death and/or disability in replication of bacteria, in which it can be seen as the inhibition zone (clear zone) around the cylindrical pellet of sample. The diameters of clear zone formed around the Cu-Alpill-MMTs were reported in Table 4.14. The Cu-ads-Alpill-MMT1 possessed larger clear zone than those of Cu-ads-Alpill-MMT2, Cu-im-Alpill-MMT-10wt% and Cu-im-Alpill-MMT-13wt% because the Cu-ads-Alpill-MMT1 possessed high doped CuO quantity on its external as shown in Fig. 4.21 (a). Therefore, the CuO rich surfaces of Cu-ads-Alpill-MMT1 could generate high quantities of ROS species, resulting in the highest antibacterial activity.

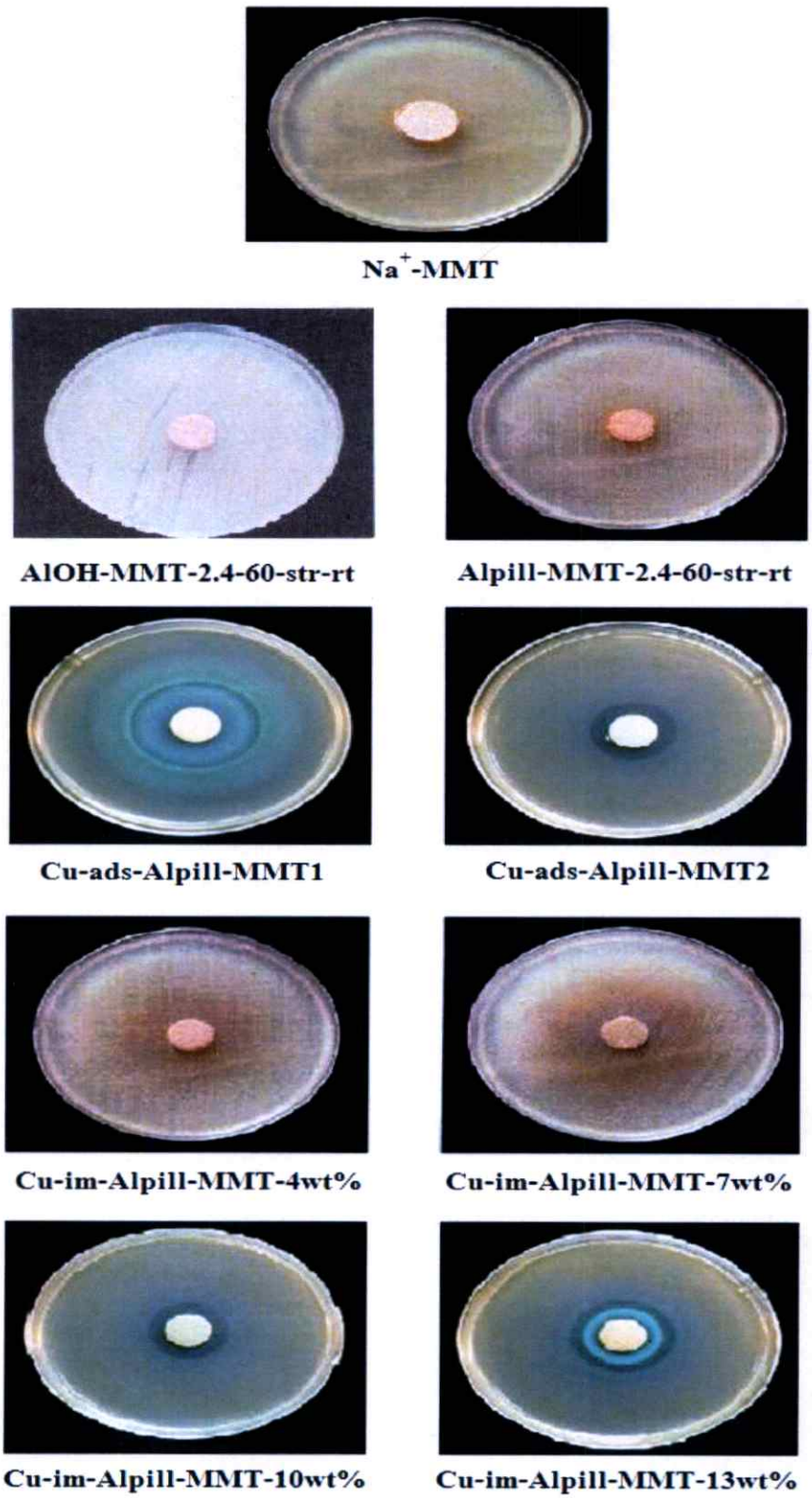

Figure 4.33 Antibacterial activities for *E. coli* growth of Na^{+}-MMT and all as-prepared samples

Table 4.12 Antibacterial activity data of Na^+-MMT, AlOH-MMT-2.4-60-str-rt, Alpill-MMT-2.4-60- str-rt, Cu-ads-Alpill-MMTs and Cu-im-Alpill-MMTs for *E. coli* growth

Sample	Clear Zone diameter (mm.)	Activity
Na^+-MMT	0.0	Inactive
AlOH-MMT-2.4-60-str-rt	0.0	Inactive
Alpill-MMT-2.4-60-str-rt	0.0	Inactive
Cu-ads-Alpill-MMT1	11.0	Active
Cu-ads-Alpill-MMT2	6.0	Active
Cu-im-Alpill-MMT-4wt%	0.0	Inactive
Cu-im-Alpill-MMT-7wt%	0.0	Inactive
Cu-im-Alpill-MMT-10wt%	5.5	Active
Cu-im-Alpill-MMT-13wt%	8.5	Active

Chapter 5
Conclusion and Recommendation

5.1 Conclusion

This research successfully prepared the nanoporous aluminum pillared montmorillonites (Alpill-MMTs) by structural modification of sodium montmorillonite clay (Na^+-MMT) with aluminum polyoxocation (AlOH). The Alpill-MMTs exhibited the excellent adsorption efficiency for cationic dye removal from aqueous solution. In addition, the copper (II) was successfully doped into the aluminum pillared montmorillonites (Cu-Alpill-MMTs) in order to create their photocatalytic activity for removal various kinds of dyestuffs. The effect of preparing conditions on the structure and properties of AlOH precursor solutions, Alpilll-MMTs and Cu-Alpill-MMTs were concluded as shown below.

5.1.1 Aluminum polyoxocation (AlOH)

The AlOH solutions were prepared by conventional stirring and ultrasonic assisted methods. It was found that the OH/Al molar ratio, system temperature and treatment time played the most important role in the formation rate of Al_{13}^{7+} polyoxocation in AlOH solutions. The AlOH solutions with monophasic Al_{13}^{7+} polyoxocation (ε-Al_{13} Keggin structure) were obtained when using the starting substances with the molar ratio of OH/Al=2.4, in which the high power ultrasonic assisted method could perform at room temperature for 30 min while the conventional stirring method had to perform at 60°C for 24 hrs. It can be concluded that the high power ultrasonic could enhance the base-hydrolysis and condensation of ε-Al_{13} Keggin ions, resulting in the shorter of reaction time.

5.1.2 Aluminum pillared montmorillonite

The Alpill-MMTs could be prepared by both conventional stirring (Alpill-MMT-Str) and ultrasonic assisted (Alpill-MMT-Ultra) methods. Since the random orientation and inhomoge-neous distribution of ε-Al_{13} Keggin ions in the interlayer space of MMT, both of Alpill-MMT-Str and Alpill-MMT-Ultra possessed the disorder and/or delaminated structures with multiple pore sizes. The Alpilll-MMT-2.4-60-Str-rt and Alpill-MMT-2.4-30-Ultra-20 showed higher of basal spacing (d_{001}), specific surface area (SSA), pore volume and pore diameter than other Alpill-MMT-Str and Alpill-MMT-Ultra products, respectively. However, the characterization results indicated that the Alpill-MMT-2.4-30-Ultra-20 possessed multiple pore sizes in the range of 3.8 – 30 nm, resulting in higher SSA than that of Alpilll-MMT-2.4-60-Str-rt, even it was prepared in

shorter processing time. The ultrasonic treatment could minimize not only the reaction time of AlOH base hydrolysis, but also the interaction time of AlOH into the MMT.

Dye removal efficiencies of Alpilll-MMT-2.4-60-Str-rt and Alpill-MMT-2.4-30-Ultra-20 adsorbents were investigated by using basic yellow 1 (BY1) and reactive orange 16 (RO16) as adsorbates. The BY1 adsorption behaviors of Alpilll-MMT-2.4-60-Str-rt and Alpill-MMT-2.4-30-Ultra-20 were corresponded to pseudo-second-order kinetic equation and Langmuir isotherm, representing the chemisorption of monolayer adsorbate on both Alpilll-MMT adsorbents. After thermal regeneration, the adsorption capacities of Alpilll-MMT-2.4-60-Str-rt and Alpill-MMT-2.4-30-Ultra-20 were slightly decreased. The higher numbers of adsorption and regeneration, the lower adsorption capacities were obtained. The Alpill-MMT-2.4-30-Ultra-20 exhibited the highest percentage of dye removal and adsorption capacity in the batch adsorption system. When the Alpill-MMT-2.4-30-Ultra-20 was used for removal 300 mg/l BY1 in the continuous adsorption system, the BY1 adsorption capacity was slightly lower than that in the batch adsorption system because the contact time between the BY1 molecules and the adsorbent in the continuous adsorption process was low. Moreover, it was found that Alpilll-MMT-2.4-60-Str-rt exhibited the highest BY1 removal capacities (>90%), but they hardly removed RO16 (<5%).

5.1.3 Copper doped aluminum pillared montmorillonite

The AlOH-MMT-2.4-60-Str-rt and Alpill-MMT-2.4-60-Str-rt were modified by doping with the copper (II) ion using ultrasonic assisted adsorption and impregnation methods.

In the ultrasonic assisted adsorption method, it was found that the amount of CuO in the porous structure of Cu-Alpill-MMT1 obtained from the AlOH-MMT-2.4-60-Str-rt was higher than that of Cu-Alpill-MMT2 obtained from the Alpill-MMT-2.4-60-Str-rt, therefore, it possessed lower SSA and pore volume than the Cu-Alpill-MMT2. In the impregnation method, the AlOH-MMT-2.4-60-Str-rt impregnated with 13 wt% Cu (Cu-im-Alpill-MMT-13wt%) possessed the highest CuO content resulted in the lowest of SSA, pore volume and pore diameter. Nevertheless, both ultrasonic assisted adsorption and impregnation methods could create the Cu doped Alpill-MMTs with multiple pore sizes ranging from 6 to 30 nm in diameter, indicating that the delamination of MMT tactoids. The regular distribution of Cu was observed on the exterior surfaces of both Cu-ads-Alpill-MMTs and Cu-im-Alpill-MMTs, suggesting that the Cu^{2+} ions occupied not only the MMT interlayers but also the MMT surfaces. During impregnation, the quantity of Cu^{2+} solution closed to the pore volume of support. Therefore, the Cu^{2+} ion tended to deposited into the internal pore structure higher than the external surface of support.

The efficiencies of Cu-ads-Alpill-MMTs and Cu-im-Alpill-MMTs for RO16 removal were performed using Fenton reaction (Cu-Alpill-MMT/H_2O_2) and photo-Fenton reaction (Cu-Alpill-MMT/H_2O_2/UV). It was found that the removal efficiency of photo-Fenton reaction was 100% using 6-fold shorter reaction time than the Fenton reaction. The Cu-ads-Alpill-MMT1 exhibited higher decolonization efficiency than the Cu-ads-Alpill-MMT2. In addition, the Cu-im-Alpill-MMT-13wt% also showed higher decolonization efficiency than other Cu-im-Alpill-MMTs. However, the efficiency of RO16 removal of Cu-im-Alpill-MMT-10wt% was quite close to that of Cu-ads-Alpill-MMT1 and Cu-im-Alpill-MMT-13wt%, although the Cu content in the Cu-im-Alpill-MMT-10wt% was lower than that in the Cu-ads-Alpill-MMT1, and Cu-im-Alpill-MMT-13wt%. This result was considered to be because the excess Cu in the Cu-ads-Alpill-MMT1 and Cu-im-Alpill-MMT-13wt% which formed as CuO clusters on its exterior surface might partially hinder the migration of Cu^{2+} ions leached from the interior pores.

Moreover, the amount of Cu^{2+} in the support can be controlled. Hence, the impregnation method for preparation of Cu-Alpill-MMT was more effective than the ultrasonic assisted adsorption method.

5.1.4 Antibacterial activity

Antibacterial activity was studied using *E.coli* ATCC®25922 under JIS L 1902: 1998 (Qualitative) test method. It was found that the Na^{+}-MMT, AlOH-MMT-2.4-60-str-rt, Alpill-MMT-2.4-60-str-rt Cu-im-Alpill-MMT-4wt% and Cu-im-Alpill-MMT-7wt% were inactive for *E. coli*. In contrast, the Cu-ads-Alpill-MMT1, Cu-ads-Alpill-MMT2, Cu-im-Alpill-MMT-10wt% and Cu-im-Alpill-MMT-13wt% could clearly inhibit the growth of *E.coli*. The Cu-ads-Alpill-MMT1 with the CuO rich surface could generate high quantities of reactive oxygen species (ROS), resulting in their high antibacterial activities. The Cu-ads-Alpill-MMT1 presented larger clear zone (11.0 mm) than the Cu-ads-Alpill-MMT2 (6.0 mm), Cu-im-Alpill-MMT-10wt% (5.5 mm) and Cu-im-Alpill-MMT-13wt% (8.5 mm).

5.2 Recommendation

5.2.1 The effect of pH and salt ions on dyes adsorption behavior of Alpill-MMTs should be studied by using batch and continuous adsorption process.

5.2.2 The efficiency of continuous adsorption process should be studied in the larger scale in order to evaluate the tendency of Alpill-MMTs and/or Cu-Alpill-MMTs usages for textile industrial applications.

5.2.3 The efficiencies of Alpill-MMTs and Cu-Alpill-MMTs for treatment of wastewater containing other contaminants such as organic compounds, toxic substances, etc., should be investigated.

5.2.4 The antibacterial activities and cytotoxicities of Cu-Alpill-MMTs should be investigated.

References

[1] Pagga, U., and Brown, D. 1986. "The Degradation of Dyestuffs." **Chemosphere.** 15(4) : 479-491.

[2] Moore, S.B., and Ausley, L.W. 2004. "Systems Thinking and Green Chemistry in the Textile Industry: Concepts, Technologies and Benefits." **J. Clean. Prod.** 12(6) : 585-601.

[3] Hayati, B., Mahmoodi, N.M., Arami, M., and Mazaheri, F. 2011. "Dye Removal from Colored Textile Wastewater by Poly (Propylene Imine) Dendrimer: Operational Parameters and Isotherm Studies." **Clean – Soil. Air. Water.** 39 (7) : 673-679.

[4] Kim, T.H., Park, C., and Kim, S. 2005. "Water Recycling from Desalination and Purification Process of Reactive Dye Manufacturing Industry by Combined Membrane Filtration." **J. Clean. Prod.** 13(8) : 779-786.

[5] Hai, F.I., Yamamoto, K., Nakajima, F., and Fukushi, K. 2008. "Removal of Structurally Different Dyes in Submerged Membrane Fungi Reactor Biosorption/PAC-Adsorption, Membrane Retention and Biodegradation." **J. Membr. Sci.** 325(1) : 395-403.

[6] Wu, J., Doan, H., and Upreti, S. 2008. "Decolorization of Aqueous Textile Reactive Dye by Ozone." **Chem. Eng. J.** 142(2) : 156-160.

[7] Muthukumar, M., Sargunamani, D., Selvakumar, N., and Venkata, R.J. 2004. "Optimisation of Ozone Treatment for Colour and COD Removal of Acid Dye Effluent Using Central Composite Design Experiment." **Dyes. Pigments.** 63(2) : 127-134.

[8] Khalid, A., Arshad, M., and Crowley, D.E. 2009. "Biodegradation Potential of Pure and Mixed Bacterial Cultures for Removal of 4-Nitroaniline from Textile Dye Wastewater." **Water. Res.** 43(4) : 1110-1116.

[9] Chakraborty, S., Basak, B., Dutta, S., Bhunia, B., and Dey, A. 2013. "Decolorization and Biodegradation of Congo Red Dye by a Novel White Rot Fungus *Alternaria Alternata* CMERI F6." **Bioresource. Technol.** 147 : 662-666.

[10] Wu, J.-S., Liu, C.-H., Chu, K.H., and Suen, S-Y. 2008. "Removal of Cationic Dye Methyl Violet 2B from Water by Cation Exchange Membranes." **J. Membr. Sci.** 309(1-2) : 239-245.

[11] Chiu, H-C., Liu, C-H., Chen, S-C., and Suen, S-Y. 2009. "Adsorptive Removal of Anionic Dye by Inorganic–Organic Hybrid Anion-Exchange Membranes." **J. Membr. Sci.** 337(1-2) : 282-290.

[12] Wang, S., Ma, Q., and Zhu, Z.H. 2008. "Characteristics of Coal Fly Ash and Adsorption Application." **Fuel.** 87(15-16) : 3469-3473.

[13] Ozdemir, O., Armagan, B., Turan, M., and Celik, M. S. 2004. "Comparison of Adsorption Characteristic of Azo-Reactive Dyes on Mezoporous Minerals." **Dyes. Pigments.** 62(1) : 49-60.

[14] Bailey, S.E., Olin, T.J., Bricka, R.M., and Adrian, D.D. 1999. "A Review of Potentially Low Costs Sorbents for Heavy Metals." **Wat. Res.** 33(11) : 2469-2479.

[15] Atun, G., Hisarli, G., Sheldrick, W.S., and Muhler, M. 2003. "Adsorptive Removal of Methylene Blue from Colored Effluents on Fuller's Earth." **J. Coll. Interf. Sci.** 261(1) : 32-39.

[16] Meshko, V., Markovska, L., Mincheva, M., and Rodrigues, A.E. 2001. "Adsorption Behavior of Basic Dyes on Granular Activated Carbon and Natural Zeolite." **Wat. Res.** 35(14) : 3357-3366.

[17] Murray, H.H. 1991. "Overview: Clay Mineral Applications." **Appl. Clay. Sci.** 5(5-6) : 379-395.

[18] Murray, H.H. 2000. "Traditional and New Applications for Kaolin, Smectite, and Palygorskite: a General Overview." **Appl. Clay. Sci.** 17(5-6) : 207-221.

[19] Liu, P., and Zhang, L. 2007. "Adsorption of Dyes from Aqueous Solutions or Suspensions with Clay Nano-Adsorbents." **Sep. Purif. Technol.** 58(1) : 32-39.

[20] Jaafar, S.N.B.S. 2006. "Adsorption Study-Dye Removal Using Cay." A report in partial fulfillment of the requirements for the award of the degree of Bachelor of Chemical Engineering, University College of Engineering & Technology Malaysia.

[21] Monvisade, P., and Siriphannon, P. 2009. "Chitosan Intercalated Montmorillonite: Preparation, Characterization and Basic Dye Adsorption." **Appl. Clay. Sci.** 42(3-4) : 427-431.

[22] Zohra, B., Aicha, K., Fatima, S., Nourredine, B., and Zoubir, D. 2008. "Adsorption of Direct Red 2 on Bentonite Modified by Cetyltrimethylammonium Bromide." **Chem. Eng. J.** 136(2-3) : 295-305.

[23] Juang, L.C., Wang, C.C., Lee, C.K., and Hsu, T.C. 2007. "Dyes Adsorption onto Organoclay and MCM-41." **J. Environ. Eng. Manage.** 17(1) : 29-38.

[24] Shen, D., Fan, J., Zhou, W., Gao, B., Yue, Q., and Kang, Q. 2009. "Adsorption Kinetics and Isotherm of Anionic Dyes onto Organo-Bentonite from Single and Multisolute Systems." **J. Hazard. Mater.** 172(1) : 99-107.

[25] Trillo, J.M., Alba, M.D., Castro, M.A., Poyato, J., and Tobías, M.M. 1993. "Alumina-Pillared Montmorillonite: Effect of Thermal and Hydrothermal

Treatment on the Accessible Micropore Volume." **J. Mater. Sci.** 28(2) : 373-378.

[26] Altunlu, M., and Yapar, S. 2007. "Effect of OH^-/Al^{3+} and Al^{3+}/Clay Ratios on the Adsorption Properties of Al-Pillared Bentonites." **Colloids. Surf. A: Physicochem. Eng. Aspects.** 306(1-3) : 88-94.

[27] Molu, Z.B., and Yurdako, K. 2010. "Preparation and Characterization of Aluminum Pillared K10 and KSF for Adsorption of Trimethoprim." **Micropor. Mesopor. Mater.** 127(1-2) : 50-60.

[28] Musil, J., Blazek, J., Zeman, P., Proksova, S., Sasek, M., and Cerstvy, R. 2010. "Thermal Stability of Alumina Thin Films Containing γ-Al_2O_3 Phase Prepared by Reactive Magnetron Sputtering." **Appl. Surf. Sci.** 257(3) : 1058-1062.

[29] Qin, Z., Yuan, P., Zhu, J., He, H., Liu, D., and Yang, S. 2010. "Influences of Thermal Pretreatment Temperature and Solvent on the Organosilane Modification of Al_{13}-Intercalated/Al-Pllared Montmorillonite." **Appl. Clay. Sci.** 50(4) : 546-553.

[30] Gil, A., Assis, F.C.C., Albeniz, S., and Korili, S.A. 2011. "Removal of Dye from Wastewater by Adsorption on Pillared Clays." **Chem. Eng. J.** 168(3) : 1032-1040.

[31] Mori, H., Miyoshi, H., Takeda, K., Yoneyama, H., Fujita, H., Iwata, Y., Otsuka, Y., and Murata, Y. 1992. "TEM Observation of Iron Oxide Pillars in Montmorillonite." **J. Mater. Sci.** 27(12) : 3197-3199.

[32] Sampieri, A. 2004. "Washing Effect on the Synthesis of Silica-Pillared Clays." **J. Porous. Mater.** 11(3) : 157-162.

[33] Lahtinen, P., Lankinen, E., Leskelä, M., and Repo, T. 2005. "Insight into Copper Oxidation Catalysts: Kinetics, Catalytic Active Species and Their Deactivation." **Appl. Catal. A-Gen.** 295(2) : 177-184.

[34] Punniyamurthy, T., and Rout, L. 2008. "Recent Advances in Copper-Catalyzed Oxidation of Organic Compounds." **Coord. Chem. Rev.** 252(1-2) : 134-154.

[35] Yu-Hao, C., Chung-Fang, H., Keng-Liang, O., and Pei-Wen, P. 2011. "Mechanical Properties and Antibacterial Activity of Copper Doped Diamond-Like Carbon Films." **Surf. Coat. Technol.** 206(6) : 1037-1040.

[36] Majzlik, P., Strasky, A., Adam, V., Nemec, M., Trnkova, L., Zehnalek, J., Hubalek, J., Provaznik, I., and Kizek, R. 2011. "Influence of Zinc(II) and Copper(II) Ions on Streptomyces Bacteria Revealed by Electrochemistry." **Int. J. Electrochem. Sci.** 6 : 2171-2191.

[37] Al-Kdas, A., Idris, A., Saed, K., and Guan, C.T. 2004. "Treatment of Textile Wastewater by Advance Oxidation Processes – A Review." **Global. Nest: the Int. J.** 6(3) : 222-230.

[38] Grrido-Ramirez, E.G., Theng, B.K.G., and Mora, M.L. 2010. "Clay and Oxide Minerals as Catalysts and Nanocatalysts in Fenton-Like Reaction – A Review." **Appl. Clay. Sci.** 47(3-4) : 182-192.

[39] Bach, A., Zelmanov, G., and Semiat, R. 2009. "Wastewater Mineralization Using Advanced Oxidation Process." **Desalin. Water. Treat.** 6(1-3) : 152-159.

[40] Tomul, F. 2011. "Effect of Ultrasound on the Structural and Textural Properties of Copper-Impregnated Cerium-Modified Zirconium-Pillared Bentonite." **Appl. Surf. Sci.** 258(5) : 1836-1848.

[41] Zhou, S., Qian, Z., Sun, T., Xu, J., and Xia, C. 2011. "Catalytic Wet Peroxide Ooxidation of Phenol Over Cu–Ni–Al Hydrotalcite." **Appl. Clay. Sci.** 53(4) : 627-633.

[42] Moore, D., and Reynolds, R.C. 1997. "X-Ray Diffraction and the Identification and Analysis of Clay Minerals." 2nd ed.: Oxford University Press, New York.

[43] **Available :** www.soilsurvey.org

[44] Kloprogge, J.T., Komarneni, S., and Amonette, E.J. 1999. "Synthesis of Smectite Clay Minerals: A Critical Review." **Clays. Clay. Miner.** 47(5) : 529-554.

[45] Asif, A.A., Kyong, Y.R., Soo, J.P., and David, H. 2012. "Epoxy Clay Nanocomposites–Processing, Properties and Applications: A Review." **Compos. Part. B-Eng.** 45(1) : 308-320.

[46] Tran, D.T., Nguyen, D.M., Nguyen, T.K.N., Ha, T.C.N., Ha, T.H., and Anne-Cecile, G. 2012. "Study Structure and Properties of Nanocomposite Material Based on Unsaturated Polyester with Clay Modified by Poly (Ethylene Oxide)." **J. Nano. Mater.** DOI:10.1155.2012.841813.

[47] Fowden, L., Barrer, R.M., and Tinker, R.B. 1984. "Clay Minerals: Their Structure, Behaviour and Use." Philoso-phical transactions of the royal society of London, Series A, mathematical and physical sciences. 311(1517) : 219-432.

[48] Grim, R.E. 1947. "Relation of Clay Mineralogy to Origin and Recovery of Petroleum." **Am. Assoc. Petroleum. Geologists. Bull.** 31(8) : 1491-1499.

[49] Haydn, H.M., and Jessica, E.K. 2005. "Engineered Clay Products for the Paper Industry." **Appl. Clay. Sci.** 29(3-4) : 199-206.

[50] Kloprogge, J.T. 1998. "Synthesis of Smectites and Porous Pillared Clay Catalysts: A Review." **J. Porous. Mater.** 5(1) : 5-41.

[51] Moreno, S., Sun, K.R., Molina, R., and Poncelet, G. 1999. "Al, Al,Zr, and Zrpillared Montmorillonites and Saponites: Preparation, Characterization, and Catalytic Activity in Heptane Hydroconversion." **J. Catal.** 182(1) : 174-185.

[52] Rytwo, G., Nir, S., and Margulies, L. 1996. "A model for Adsorption of Divalent Organic Cations to Montmorillonite." **J. Colloid. Interface. Sci.** 181(2) : 551-560.

[53] Ramakrishna, K.R., and Viraraghavan, T. 1997. "Dye Removal Using Low Cost Adsorbents." **Water. Sci. Technol.** 36(2-3) : 189-196.

[54] Al-Ani, T., and Sarapää, O. 2008. "Clay and Clay Mineralogy." Geologian Tutkuskeskus Espoo, 1-94.

[55] Gil, A., Gandia, L.M., and Vicenteb, M.A. 2000. "Recent Advances in the Synthesis and Catalytic Applications of Pillared Clays." **Catal. Rev. Sci. Eng.** 42(1-2) : 145-212.

[56] Zhang, Q-X., Yu, Z-Z., Xie, X-L., Naito, K., and Kagawa, Y. 2007. "Preparation and Crystalline Morphology of Biodegradable Starch/Clay Nanocomposites." **Polymer.** 48(24) : 7193-7200.

[57] Zohra, B., Aicha, K., Fatima, S., Nourredine, B., and Zoubi,r D. 2008. "Adsorption of Direct Red 2 on Bentonite Modified by Cetyltrimethylammonium Bromide." **Chem. Eng. J.** 136(2-3) : 295-305.

[58] Juang, L-C., Wang, C-C., Lee, C-K., and Hsu, T-C. 2007. "Dye Adsorption onto Organical and MCM-41." **J. Environ. Eng. Manage.** 17(1) : 29-38.

[59] **Li**, Y., Sun, D., Pan, X., and Zhang, B. 2009. "Kaolinite Intercalation Precursors." **Clays. Clay. Miner.** 57(6) : 779-786.

[60] Thomas, J.P., Ming-Shin, T., Steven, D.L., and Rasik, H.R. 1984. "On the Pillaring and Delamination of Smectite Clay Catalysis by Polyoxo Cations of Aluminum." **J. Mol. Catal.** 27(1-2) : 195-212.

[61] Trillo, J.M., Alba, M.D., Castro, M.A., Poyato, J., and Tobías, M.M. 1993. "Alumina-Pillared Montmorillonite: Effect of Thermal and Hydrothermal Treatment on the Accessible Micropore Volume." **J. Mater. Sci.** 28(2) : 373-378.

[62] Altunlu, M., and Yapar, S. 2007. "Effect of OH/Al^{3+} and Al^{3+}/clay Ratios on the Adsorption Properties of Al Pillared Bentonites." **Colloids. Surf. A: Physicochem. Eng. Aspects.** 306(1-3) : 88-94.

[63] Molu, Z.B., and Yurdakoc, K. 2010. "Preparation and Characterization of Aluminum Pillared K10 and KSF for Aadsorption of Ttrimethoprim." **Micropor. Mesopor. Mater.** 127(1-2) : 50-60.

[64] Musil, J., Blazek, J., Zeman, P., Proksova, S., Sasek, M., and Cerstvy, R. 2010. "Thermal Stability of Alumina Thin Films Containing γ-Al $_2O_3$ Phase Prepared by Reactive Magnetron Sputtering." **Appl. Surf. Sci.** 257(3) : 1058-1062.

[65] Qin, Z., Yuan, P., Zhu, J., He, H., Liu, D., and Yang, S. 2010. "Influence of Thermal Pretreatment Temperature and Solvent on the Organosilane Modification of Al_{13}-Interclated/Al-Pillared Montmorillonite." **Appl. Clay. Sci.** 50(4) : 546-553.

[66] Mori, H., Miyoshi, H., Takeda, K., Yoneyama, H., Fujita, H., Iwata, Y., Otsuka, Y., and Murata, Y. 1992. "TEM Observation of Iron Oxide Pillars in Montmorillonite." **J. Mater. Sci.** 27(12) : 3197-3199.

[67] Sampieri, A. 2004. "Washing Effect on the Synthesis of Silica-Pillared Clays." **J. Porous. Mater.** 11(3) : 157-162.

[68] Oliveira, L.C.A., Lago, R.M., Fabris, J.D., Solar, and C., Sapag, K. 2003. "Transition Metals Supported on Al-Pilcs as Catalysts for C_6H_5Cl Oxidation." **Braz. J. Chem. Eng.** 20(1) : 45-50.

[69] Kloprogge, J.T., Duong, L.V., and Frost, R.L. 2005. "A review of the Synthesis and Characterization of Pillared Clays and Related Porous Materials for Cracking of Vegetable Oil to Produce Bio-Fuels." **Environmental. Geology.** 47(7) : 967-981.

[70] Kloprogge, J.T. 1992. "Pillared Clays Preparation and Characterization of Clay Minerals and Aluminum-Based Pillaring Agents." **Geologica. Ultraiectina.** 91 : 1-348.

[71] Wang, M., and Muhammed, M. 1999. "Novel Synthesis of Al13-Cluster Based Alumina Materials." **Nanostruct. Mater.** 11(8) : 1219-1229.

[72] Baes, C.F., and Mesmer, R.E. 1976. "The Hydrolysis of Cations." John Wiley, New York. 112-122.

[73] Mesmer, R.E., and Baes, C.F. 1971. "Acidity Measurements at Elevated Temperatures. V. Aluminum Ion Hydrolysis." **Inorg. Chem.** 10(10) :2290-2296.

[74] Casey, W.H. 2006. "Large Aqueous Aluminum Hydroxide Molecules." **Chem. Rev.** 106(1) : 1-16.

[75] Duana, J., and Gregoryb, J. 2003. "Coagulation by Hydrolysing Metal Salts." **Advs. Colloid. Interface. Sci.** 100 –102 : 475-502.

[76] Bi, S., Wang, C., Cao, Q., and Zhang, C. 2004. "Studies on the Mechanism of Hydrolysis and Polymerization of Aluminum Salts in Aqueous Solution: Correlations Between the "Core-links" Model and "Cage-like" Keggin-Al_{13} Model." **Coord. Chem. Rev.** 248(5-6) : 441-455.

[77] Allouche, L., and Taulelle, F. 2003. "Conversion of Al_{13} Keggin into Al_{30}: a Reaction Controlled by Aluminum Monomers." **Inor. Chem. Commun.** 6(9) : 1167-1170.

[78] Pinnavaia, T.J., Ming-Shin, T., Landau, S.D., and Raythatha, R.H. 1984. "On the Pillaring and Delamination of Smectite Clay Catalysts by Polyoxo Cations of Aluminum." **J. Molec. Catal.** 27(1-2) : 195-212.

[79] Jim, D., and John, G. 2003. "Coagulation by Hydrolyzing Metal Salts." **Adv. Colloid. Interface. Sci.** 100-102 : 475-502.

[80] Baoyou, S., Guohong, Li., Dongsheng, W., and Hongxiao, T. 2007. "Separation of Al_{13} from Polyaluminum Chloride by Sulfate Precipitation and Nitrate Metathesis." **Sep. Purif. Technol.** 54(1) : 88-95.

[81] Wei-Zi, W., and Pa, H.H. 1994. "The Nature of Polynuclear OH-Al Complexes in Laboratory-Hydrolyzed and Commercial Hydroxyaluminum Solution." **Clays. Clay. Miner.** 42(3) : 356-368.

[82] Wallace, O., Parker, Jr., and Imre, K. 1995. "Aluminum Complexes in Partially Hydrolyzed Aqueous $AlCl_3$ Solutions Used to Prepare Pillared Clay Catalysts." **Appl. Catal. A.** 121(1) : L7-L11.

[83] Lionel, A., and Francis, T. 2003. "Conversion of Al_{13} Keggin **ε** into Al_{30}: a Reaction Controlled by Aluminum Monomers." **Inorg. Chem. Commun.** 6(9) : 1167-1170.

[84] Zhaoyang, C., Zhaokun, L., Jinghua, F., Zhongguo, Z., Xianjia, P., and Bin, F. 2007. "Effect of Thermal Treatment on the Formation and Transformation of Keggin Al_{13} and Al_{30} Species in Hydrolytic Polymeric Aluminum Solutions." **Colloids. Surf. A.** 292(2-3) : 110-118.

[85] Pinnavaia, T.J. 1983. "Intercalated Clay Catalysts." **Science. Magazine.** 220(4595) : 365-371.

[86] Wang, M., and Muhammed, M. 1999. "Novel Synthesis of Al-Cluster Based Alumina Materials." **Nanostruct. Mater.** 11(8) : 1219-1229.

[87] Sivaiahab, M.V., Petit, S., Brendle, J., and Patrier, P. 2010. "Rapid Synthesis of Aluminium Polycations by Microwave Assisted Hydrolysis of Aluminium *via* Decomposition of Urea and Preparation of Al-pillared Montmorillonite." **Appl. Clay. Sci.** 48(1-2) : 138-145.

[88] Mokaya, R., and Jones, W. 1995. "The Microstructure of Alumina Pillared Acid-Activated Clays." **J. Pore. Mater.** 1(1) : 97-110.

[89] Khalap, H., Bouras, O., and Perrichon, V. 1997. "Synthesis and Characterization of Al-pillared and Cationic Surfactant Modified Al-Pillared Algerian Bentonite." **Micropor. Mater.** 8(3-4) : 141-150.

[90] Maes, N., Heylen, I., Cool, P., and Vansant, E.F. 1997. "The Relation Between theS of Pillared Clays and Their Resulting Porosity." **Appl. Clay. Sci.** 12(1-2) : 43-60.

[91] Cheng, L.S., and Yang, R.T. 1997. "Tailoring Micropore Diamensions in Pillared Clays for Enhanced Gas Adsorption." **Micropor. Mater.** 8(3-4) : 177-186.

[92] Sanchez, A., and Montes, M. 1998. "Influence of the Preparation Parameters (Particle Size and Aluminum Concentration) on the Textural Properties of Al-Pillared Clays for a Scale-Up Process." **Micropor. Mesopor. Mater.** 21(1-3) : 117-125.

[93] Young-Sub, S., Seung-Geun, O., and Baik-Hyon, H. 2003. "Pore Structures and Acidities of Al-Pillared Montmorillonite." **Korea. J. Chem. Eng.** 20(1) : 77-82.

[94] Jime´nez de Haro, M.C., Pe´rez-Rodrı´guez, J.L., Poyatoa, J., Pe´rez-Maqueda, L.A., Rami´rez-Valle, V., Justo, A., Lerf, A., and Wagner, F.E. 2005. "Effect of Ultrasound on Preparation of Porous Materials from Vermiculite." **Appl. Clay. Sci.** 30(1) : 11-20.

[95] Olaya, A., Moreno, S., and Molina, R. 2009. "Synthesis of Pillared Clays with Aluminum by Means of Concentrated Suspensions and Microwave Radiation." **Catal. Commun**. 10(5) : 697-701.

[96] Vicente, M.A., Belver, C., Trujillano, R., Bañares-Muñoz, M.A., Rives, V., Korili, S. A., Gil, A., Gand´ıa, L.M., and Lambert, J.F. 2003. "Preparation and Characterisation of Vanadium Catalysts Supported Over Alumina-Pillared Clays." **Catal. Today.** 78(1-4) : 181-190.

[97] Tomul, F. 2011. "Effect of Ultrasound on the Structural and Textural Properties of Copper-Impregnated Cerium-Modified Zirconium-Pillared Bentonite." **Appl. Surf. Sci.** 258(5) : 1836-1848.

[98] Pirkanniemi, K., and Sillanpaa, M. 2002. "Heterogeneous Water Phase Catalysis as an Environmental Application: A Review." **Chemosphere.** 48(10) : 1047-1060.

[99] Barrault, J., Jean-Michel, T., and Papayannakos, N. 2000. "Catalytic Wet Peroxide Oxidation of Phenol Over Pillared Clay Containing Iron or Copper Species." **Chemistry.** 3(10) : 777-783.

[100] Zhou, S., Qian, Z., Sun, T., Xu, J., and Xia, C. 2011. "Catalytic Wet Peroxide Oxidation of Phenol Over Cu– Ni–Al Hydrotalcite." **Appl. Clay. Sci.** 53(4) : 627-633.

[101] Barrault, J., Bouchoule, C., Echachoui, K., Frini-Srasra, N., Trabelsi, M., and Bergaya, F. 1998. "Catalytic Wet Peroxide Oxidation (CWPO) of Phenol Over Mixed (Al-Cu)-Pillared Clays." **Appl. Catal. B-Environ.** 15(3-4) : 269-274.

[102] Carriazo, J.G., Guelou, E., Barrault, J., Tatibouet, J.M., and Moreno, S. 2003. "Catalytic Wet Peroxide Oxidation of Phenol Over Al-Cu or Al-Fe Modified Clays." **Appl. Clay. Sci.** 22(6) : 303-308.

[103] Achma, R.B., Ghorbel, A., Sayadi, S., Dafinov, A., and Medina, F. 2008. "A Novel Method of Copper-Exchanged Aluminum-Pillared Clay Preparation for Olive Oil Mill Wastewater Treatment." **J. Phys. Chem. Solid.** 69(5-6) : 1116-1120.

[104] Caudo, S., Centi, G., Genovese, C., and Perathoner, S. 2007. "Copper and Iron-Pillared Clay Catalysts for the WHPCO of Model and Real Wastewater Streams from Olive Oil Milling Production." **Appl. Catal. B- Environ.** 70(1-4) : 437-446.

[105] Kim, S-C., and Lee, D-K. 2004. "Preparation of Al-Cu Pillared Clay Catalysts for the Catalytic Wet Oxidation of Reactive Dyes." **Catal. Today.** 97(2-3) : 153-158.

[106] Ntampegliotis, K., Riga, A., Karayannis, V., Bontozoglou, V., and Papapolymerou, G. 2006. "Decolorization Kinetics of Procion H-exl Des from Textile Dyeing Using Fenton-Like Reactions." **J. Hazard. Mater.** 136(1) : 75-84.

[107] Garrido-Ramírez, E.G., Theng, B.K.G., and Mora, M.L. 2010. "Clays and Oxide Minerals as Catalysts and Nanocatalysts in Fenton-Like Reactions: A Review." **Appl. Clay. Sci.** 47(3-4) : 182-192.

[108] Yu-Hao, C., Chung-Fang, H., Keng-Liang, O., and Pei-Wen, P. 2011. "Mechanical Properties and Antibacterial Activity of Copper Doped Diamond-Like Carbon Films." **Surf. Coat. Technol.** 206(6) : 1037-1040.

[109] Majzlik, P., Strasky A., Adam, V., Nemec, M., Trnkova, L., Zehnalek, J., Hubalek, J., Provaznik, I., and Kizek, R. 2011. "Influence of Zinc (II) and Copper(II) Ions on Streptomyces Bacteria Revealed by Electrochemistry." **Int. J. Electrochem. Sci.** 6 : 2171-2191.

[110] Zhan, Y., Li, H., and Chen, Y. 2010. "Copper Hydroxyphosphate as Catalyst for the Wet Hydrogen Peroxide Oxidation of Azo Dyes." **J. Hazard. Mater.** 180(1-3) : 481-485.

[111] Schwarz, J. A., Contescu, C., and Contescu, A. 1995. "Method for Preparation of Catalytic Materials." **Chem. Rev.** 95(3) : 477-510.

[112] Bahranowski, K., Gasior, M., Kielski, A., Podobinski, J., Serwicka, E.M., Vartikian, L., and Wodnicka, A.K. 1999. "Copper-Doped Alumina-Pillared Montmorillonites as Catalysts for Oxidation of Toluene and Xylenes with Hydrogen peroxide." **Clay. Miner.** 34(1) : 79-87.

[113] Frini, N., Crespin, M., Trabelsi, M., Messad, D., Damme, H.V., and Bergaya, F. 1997. "Preliminary Results on the Properties of Pillared Clays by Mixed A1-Cu Solutions." **Appl. Clay. Sci.** 12(3) : 281-292.

[114] Barrault, J., Bouchoule, C., Echachoui, K., Frini-Srasra, N., Trabelsi, M., and Bergaya, F. 1998. "Catalytic Wet Peroxide Oxidation (CWPO) of Phenol Over Mixed (Al-Cu)-Pillared Clays." **Appl. Catal. B-Environ.** 15(3-4) : 269-274.

[115] Bahranowski, K., Sior, M.G., Kielski, A., Podobi, J., Serwicka, M., Vartikian, L.A., and Wodnicka, K. 1998. "Physico-Chemical Characterization and Catalytic Properties of Copper-Doped Alumina-Pillared Montmorillonite." **Clays. Clay. Miner.** 46(1) : 98-102.

[116] Ramaswamy, V., Krishnan, M.S., and Ramaswamy, A.V. 2002. "Immobilization and Characterization of Copper Chlorophthalocyanine on Alumina Pillared Montmorillonite." **J. Mol. Catal. A- Chem.** 181(1-2) : 81-89.

[117] Yuan, P., He, H., Bergaya, F., Wu, D., Zhou, Q., and Zhu, J. 2006. "Synthesis and Characterization of Delaminated Iron-Pillared Clay with Meso-Microporous Structure." **Micropor. Mesopor. Mat.** 88(1-3) : 8-15.

[118] Lin, Q., Hao, J., Li, J., Ma, Z., and Lin, W. 2007. "Copper-Impregnated Al-Ce-Pillared Clay for Selective Catalytic Reduction of NO by C_3H_6." **Catal. Today.** 126(3-4) : 351-358.

[119] Achma, R.B., Ghorbel, A., Dafinov, A., and Medina, F. 2008. "Copper-Supported Pillared Clay Catalysts for the Wet Hydrogen Peroxide Catalytic Oxidation of Model Pollutant Tyrosol." **App.l Catal. A-Gen.** 349(1-2) : 20-28.

[120] Dong-keun, L., Dul-Sun, K., and Sung-Chul, K. 2001. "Mechanistic Studied to Hydroxyl Radical-Induced Catalytic Wet Oxidation of Dyehouse Effluents at Atmospheric Pressure." **Surf. Sci. Catal.** 133 : 297-302.

[121] Available : http://www.thomasnet.com/articles/chemicals/wastewater-chemical-treatment

[122] Wang, Z., Xue, M., Huang, K., and Liu, Z. .2011 "Textile Dyeing Wastewater Treatment." Huazhong University of Science and Technology, China.

[123] Hasan, M.B. 2008. "Adsorption of Reactive Azo Dyes on Chitosan/Oil-Palm Ash Composite Adsorbent: Batch and Continuous Studied." Thesis submitted in fulfillment of the requirements for the degree of Master of Science, University Sains Malaysia.

[124] Almeida, C.A.P., Machado, C., Flores, J.A.A., Scheibe, L.F., and Debacher, N.A. . "Characterization of Mineral Waste from Coal Mining Used in the Treatment of Textile Wastewater." 4th Mercosur Congress on Process Systems Engineering.

[125] Almeida, C.A.P., Machado, C., and Debacher, N.A. 2004. "Adsorption of Methylene Blue as a Model for the Use of Barro Branco as an Alternative Adsorbent for Color Removal." **Progr. Colloid. Polym. Sci.** 128 : 278-282.

[126] Nwe, M.T. 2011. "Hydrothermal Treatment on Lignocellulosic Adsorbents for Dehydration of Ethanol-Water Mixture." presented at the ISEM, International conference program, Bangkok, Thailand, July 8 – 9, Paper 0711168.

[127] Mc-Cade, W.L. 1993. "Liquid-Liquid and Fluid- Solid Separation Processe." Unit Operation of Chemical Engineering, 6th edition, New York: McGraw Hill Co.

[128] Elaine, M.M. 2001. "Surface Chemistry." Oxford University. New York. 54-55.

[129] Mani, K., and Sivakkumar, V. 2011. Department of Textile Chemistry, SSM College of Engineering, Chemical Protective Clothing. 40-43.

[130] Sharifah, N.B.S.J. 2006. "Adsorption Study-Dye Removal Using Clay." Report in partial fulfillment of the requirements for the award of the degree of bachelor of chemical engineering.

[131] Noroozi, B., and Sorial, G.A. 2013. "Applicable Models for Multi-Component Adsorption of Dyes: A Review." **J. Environ. Sci.** 25(3) : 419-429.

[132] Samuel, D.F., and Osman, M.A. 1987. "Adsorption Process for Water Treatment." Stoneham: Butterworth, 1-100.

[133] Sanghi, R., and Bhattacharya, B. 2002. "Review on Decolorisation of Aqueous Dye Solutions by Low Cost Adsorbents." **Coloration. Technology.** 118(5) : 256-269.

[134] Kenneth, E., Gounaris, V., and Wain-Sue, H. 1992. "Adsorption Technology for Air and Water Pollution Control." Michigan, 1-45.

[135] Kyzas, G.Z., Kostoglou, M., Lazaridis, N.K., and Bikiaris, D.N. 2013. "Decolorization of Dyeing Wastewater Using Polymeric Absorbents - An Overview." DOI: 10.5772/52817.

[136] Pontius, F.W. 1990. "Water Quality and Treatment." 4th Edition, 12-17.

[137] Rahchamani, J., Mousavi, H.Z., and Behzad, M. 2011. "Adsorption of Methyl Violet from Aqueous Solution by Polyacrylamide as an Adsorbent: Isotherm and Kinetic Studies." **Desalination.** 267(2-3) : 256-260.

[138] Zhou, Y., Jin, Q., Hu, X., Zhang, Q., and MaHeavy, T. 2012. "Metal Ions and Organic Dyes Removal from Water by Cellulose Modified with Maleic Anhydride." **. Mater. Sci.** 47(12) : 5019-5029.

[139] Mittal, A., Kurup, L., and Mittal, J. 2007. "Freundlich and Langmuir Adsorption Isotherms and Kinetics for the Removal of Tartrazine from Aqueous Solutions Using Hen Feathers." **J. Hazard. Mater.** 146(1-2) : 243-248.

[140] Caliskan, N., Kul, A.R., Alkan, S., Sogut, E.G., and Alacabey, I. 2011. "Adsorption of Zinc (II) on Diatomite and Manganese-Oxide-Modified Diatomite: a Kinetic and Equilibrium Study." **J. Hazard. Mater.** 193 : 27-36.

[141] He, J., Hong, S., Zhang, L., Gan, F., and Yuh-Shan, H. 2010. "Equilibrium and Thermodynamic Parameters of Adsorption of Methylene Blue onto Rectorite." **Fresen. Environ. Bull.** 19(11) : 2651-2656.

[142] Caliskan, N., Kul, A.R., Alkan, S., Sogut, E.G., and Alacabey, I. 2011. "Adsorption of Zinc (II) on Diatomite and Manganese-Oxide-Modified Diatomite: a Kinetic and Equilibrium Study." **J. Hazard. Mater.** 193 : 27-36.

[143] Rahchamani, J., Mousavi, H.Z., and Behzad, M. 2011. "Adsorption of Methyl Violet from Aqueous Solution by Polyacrylamide as an Adsorbent: Isotherm and Kinetic Studies." **Desalination.** 267(2) : 256-260.

[144] Hema, M., and Arivoli, S. 2007. "Comparative Study on the Adsorption Kinetics and Thermodynamics of Dyes onto Acid Activated Low Cost Carbon." **Int. J. Phys. Sci.** 2(1) : 10-17.

[145] Mei-Fang, H. , Cai-Xia, M., Wei-De, Z., Xiao-Yan, T., Yan-Ning, F., and Hong-Fu, W. 2011. "Removal of Rhodamine B Using Iron-Pillared Bentonite." **J. Hazard. Mater.** 186(2-3) : 1118-1123.

[146] Eftekhari, S., Habibi-Yangjeh, A., and Sohrabnezhad, Sh. 2010. "Application of ALMCM-41 for Competitive Adsorption of Methylene Blue and Rhodamine B: Thermodynamic and Kinetic Studies." **J. Hazard. Mater.** 178(1-3) : 349-355.

[147] Dogan, M., Ozdemir, Y., and Alkan, M. 2007. "Adsorption Kinetics and Mechanism of Cationic Methyl Violet and Methylene Blue Dyes onto Sepiolite." **Dyes. pigments.** 75(3) : 701-713.

[148] Gil, A., Assis, F.C.C., Albeniz, S., and Korili, S.A. 2011. "Removal of Dyes from Wastewaters by Adsorption on Pillared Clays." **Chem. Eng. J.** 168(3) : 1032-1040.

[149] Andreozzi, R., Caprio, V., Insola, A., and Marotta, Ra. 1999. "Advanced Oxidation Processes (AOP) for Water Purification and Recovery." **Catal. Today.** 53(1) : 51-59.

[150] Goi, A. 2005. "Advance Oxidation Processes for Water Purification and Soil Remediation." Thesis on chemistry and chemical engineering. ISBN 9985-59-534-3, 1-170.

[151] Fenton, H.J.H. 1894. "Oxidation of Tartaric Acid in the Presence of Iron." **J. Chem. Soc.** 65 : 899-910.

[152] Pulgarin, C., and Kiwi, J. 1996. "Overview on Photocatalytic and Electrocatalytic Pretreatment of Industrial Non-Biodegradable Pollutants and Pesticides." **Chimia.** 50(3) : 50-55.

[153] Nancy, R.S., Rafael, M., and Sonia, M. 2012. "Development of Pillared Clays for Wet Hydrogen Peroxide Oxidation of Phenol and Its Application in the Post-Treatment of Coffee Wastewater." **Int. J. Photoenergy.** DOI:10.1155.2012.864104.

[154] Haber, F., and Weiss, J. 1934. "The Catalytic Decomposition of Hydrogen Peroxide by Ion Salts." **J. Proc. Roy. Soc. London. A.** 147 : 332-351.

[155] Timofeeva, M.N., Khankhasaeva, S.T., Talsi, E.P., Panchenko, V.N., Golovin, A.V., Dashinamzhilova, E.T., and Tsybulya, S.V. 2009. "The Effect of Fe/Cu Ratio in the Synthesis of Mixed Fe,Cu,Al-Clays Used as Catalysts in Phenol Peroxide Oxidation." **Appl. Catal. B-Environ.** 90(3-4) : 618-627.

[156] Zhan, Y., Li, H., and Chen, Y. 2010. "Copper Hydroxyphosphate as Catalyst for the Wet Hydrogen Peroxide Oxidation of Azo Dyes." **J. Hazard. Mater.** 180(1-3) : 481-485.

[157] Grrido-Ramirez, E.G., Theng, B.K.G., and Mora, M.L. 2010. "Clay and Oxide Minerals as Catalysts and Nanocatalysts in Fenton-Like Reaction – A Review." **Appl. Clay. Sci.** 47(3-4) : 182-192.

[158] Galeano, L.A., Gil, A., and Vicente, M.A. 2010. "Effect of the Atomic Active Metal Ratio in Al/Fe-, Al/Cu- and Al/(Fe-Cu)- Intercalating Solutions on the Physicochemical Properties and Catalytic Activity of Pillared Clays in the CWPO of Methyl Orange." **Appl. Catal. B-Environ.** 100(1-2) : 271-281.

[159] Ruppert, G., Bauer, R., and Heisler, G. 1993. "The Photo-Fenton Reaction-an Effective Photochemical Wastewater Treatment Process." **J. Photochem. Photobiol. A.** 73(1) : 75-78.

[160] Neamtu, M., Yediler, A., Siminicean, I., and Kettrup, A. 2003. "Oxidation of Commercial Reactive Azo Dye Aqueous Solutions by the Photo-Fenton and Fenton-Like Processes." **J. Photochem. Photobiol. A-Chem.** 161(1) : 87-93.

[161] Herney-Ramirez, J., Vicente, M.A., and Madeira, L.M. 2010. "Heterogeneous Photo-Fenton Oxidation with Pillared Clay-Based Catalysts for Wastewater Treatment: A Review." **Appl. Catal. B-Environ.** 98(1-2) : 10-26.

[162] Bouberka, Z., Kacha, S., Kameche, M., Elmaleh, S., and Derriche, Z. 2005. "Sorption Study of an Acid Dye from an Aqueous Solutions Using Modified Clays." **J. Hazard. Mater. B.** 119(1-3) : 117-124.

[163] Gurses, A., Dogar, C., Yalcin, M., Acikyildiz, M., Bayrak, R., and Karaca, S. 2006. "The Adsorption Kinetics of the Cationic Dye, Methylene Blue, onto Clay." **J. Hazard. Mater. B.** 131(1-3) : 217-228.

[164] Manohar, D.M., Noeline, B.F., and Anirudham, T.S. 2006. "Adsorption Performance of Al-Pillared Bentonite Clay for the Removal of Cobalt (II) from Aqueous Phase." **Appl. Clay. Sci.** 31(3-4) : 194-206.

[165] Ntampegliotis, K., Riga, A., Karayannis, V., Bontozoglou, V., and Papapolymerou, G. 2006. "Decolorization Kinetics of Procion H-exl Dyes from Textile Dyeing Using Fenton-Like Reactions." **J. Hazard. Mater.** 136(1) : 75-84.

[166] Baskaralingam, P., Pulikesi, M., Elango, D., Ramamurthi, V., and Sivanesan, S. 2006. "Adsorption of Acid Dye onto Organobentonite." **J. Hazard. Mater. B.** 128(2-3) : 138-144.

[167] Wang, L., and Wang, A. 2008. "Adsorption Properties of Congo Red from Aqueous Solution onto Surfactant-Modified Montmorillonite." **J. Hazard. Mater.** 160(1) : 173-180.

[168] Galeano, L.A., Gil, A., and Vicente, M.A. 2010. "Effect of the Atomic Active Metal Ratio in Al/Fe-, Al/Cu- and Al/(Fe-Cu)- Intercalating Solutions on the Physicochemical Properties and Catalytic Activity of Pillared Clays in the CWPO of Methyl Orange." **Appl. Catal. B-Environ.** 100(1-2) : 271-281.

[169] Abdullah, A.H., Yuan, W.W., and Yaziz, M.I. 2010. "Decolourisation of Reactive Orange 16 by Activated Carbon and Copper Oxide Catalysts Supported by Activated Carbon." **J. Phys. Sci.** **21**(2) : 29-40.

[170] Molu, Z.B., and Yurdakoc, K. 2010. "Preparation and Characterization of Aluminum Pillared K10 and KSF for Adsorption of Trimethoprim." **Micropor. Mesopor. Mat.** 127(1-2) : 50-60.

[171] Kaemkit, C., Monvisade, P., Siriphannon, P., and Nukeaw, J. 2013. "Water-Soluble Chitosan Intercalated Montmorillonite Nanocomposites for Removal of Basic Blue 66 and Basic Yellow 1 from Aqueous Solution." **J. Appl. Polym. Sci.** 128(1) : 879-887.

[172] Shi, B., Li, G., Wang, D., and Tang, H. 2007. "Separation of Al_{13} from Polyaluminum Chloride by Sulfate Precipitation and Nitrate Metathesis." **Sep. Purif. Technol.** 54 : 88-95.

[173] Zhang, Z., Liao, L., and Xia, Z. 2010. "Ultrasound-Assisted Preparation and Characterization of Anionic Surfactant Modified Montmorillonites." **Appl. Clay. Sci.** 50(4) : 576-581.

[174] Sapag, K., and Mendioroz, S. 2001. "Synthesis and Characterization of Micro-Mesoporous Solids: Pillared Clay." **Colloids. Surf. A: Physicochem. Eng. Aspects.** 187-188(1-3) : 141-149.

[175] Chae, H.J., Nam, I.S., Ham, S.W., and Hong, S.B. 2001. "Physicochemical Characteristics of Pillared Interlayered Clays." **Catal. Today.** 68(1-3) : 31-40.

[176] Olaya, A., Blanco, G., Bernal, S., Moreno, S., and Molina, R. 2009. "Synthesis of Pillared Clays with Al–Fe and Al–Fe–Ce Starting from Concentrated

Suspensions of Clay Using Microwaves or Ultrasound, and Their Catalytic Activity in the Phenol Oxidation Reaction." **Appl. Catal. B.** 93(1-2) : 56-65.

[177] Rouquerol, F., Rouquerol, J., and Sing, K.S.W. 2002. "Adsorption from the Gas Phase." The experimental approach. In: Handbook of porous solids, Wiley- VCH, Winheim (Germany), 1 : 236-275.

[178] Gregg, S.J., and Sing, S.W. 1982. "Adsorption, Surface Area and Porosity." **Academic Press, London**, Second edition.

[179] Okeola, F.O., and Odebunmi, E.O. 2010. "Comparison of Freundlich and Langmuir Isotherm for Adsorption of Methylene Blue by Agrowaste Derived Activated Carbon." **Adv. Environ. Biol.** 4 : 329-335.

[180] Khurana, R., Coleman, C., Ionescu-Zanetti, C., Carter, S.A., Krishna, V., Grover, R.K., Roy, R., and Singh, S. 2005. "Mechanism of Thioflavin T Binding to Amyloid Fibrils." **J. Struct. Biol.** 151(3) : 229-238.

[181] Chae, H.J., Nam, I.S., Ham, S.W., and Hong, S.B. . "Physicochemical Characteristics of Pillared Interlayered Clays." **Catal. Today.** 68(1-3) : 31-40.

[182] Tepmatee, P., and Siriphannon, P. 2013. "Effect of Preparation Method on Structure and Adsorption Capacity of Aluminum Pillared Montmorillonite." **Mater. Res Bull.** 48(11) : 4856-4866.

[183] Bahranowski, K., Gasior, M., kielski, A., Podobinski, J., Serwicka, E.M., Vartikian, L.A., and Wodnicka, K. 1998. "Physico-Chemical Characterization and Catalytic Properties of Copper-Doped Alumina-Pillared Montmorillonites." **Clays. Clay. Miner.** 46(1) : 98-102.

[184] Kumar, S.S., Muruganandham, T., and Jaabir, M.S.M. 2014. "Decolourization of Azo Dyes in a Two-Stage Process Using Novel Isolate and Advanced Oxidation with Hydrogen Peroxide / HRP System." **Int. J. Curr. Microbiol. App. Sci.** 3(1) : 514-522.

[185] Hassan, M.S., Amna, T., Yang, O-B., El-Newehy, M.H., Al-Deyab, S.S., and Khil, M-S. 2010 . "Smart Copper Oxide Nanocrystals: Synthesis, Characterization, Electrochemical and Potent Antibacterial Activity." **Colloids. Surf. B. Biointerfaces.** 97 : 201-206.

[186] Borkow, G., and Gabbay, J. 2005. "Copper as a Biocidal Tool." **Curr. Med. Chem.** 12(18) : 2163-2175.

[187] Raffi, M., Hussain, F., Bhatti, T.M., Akhter, J.I., Hameed, A., and Hasan, M.M. 2008. "Antibacterial Characterization of Silver Nanoparticles against." **J. Mater. Sci. Technol** 24(2) : 192-196.

APPENDIX A
DYE REMOVALS

A. 1 Determination of dye removal

a. UV-Visible spectrophotometer (UV-Vis)

Absorbencies of the dye solutions were measured by UV-Vis at λ_{max} of 413 nm for BY1 and 388 nm for RO16. The standard calibration curves of BY1 and RO16 were shown in Fig A.1 (a) and B.1 (b), respectively. Therefore, the dye concentration was calculated by linear regression equation from the standard calibration curve as shown in Table A.1.

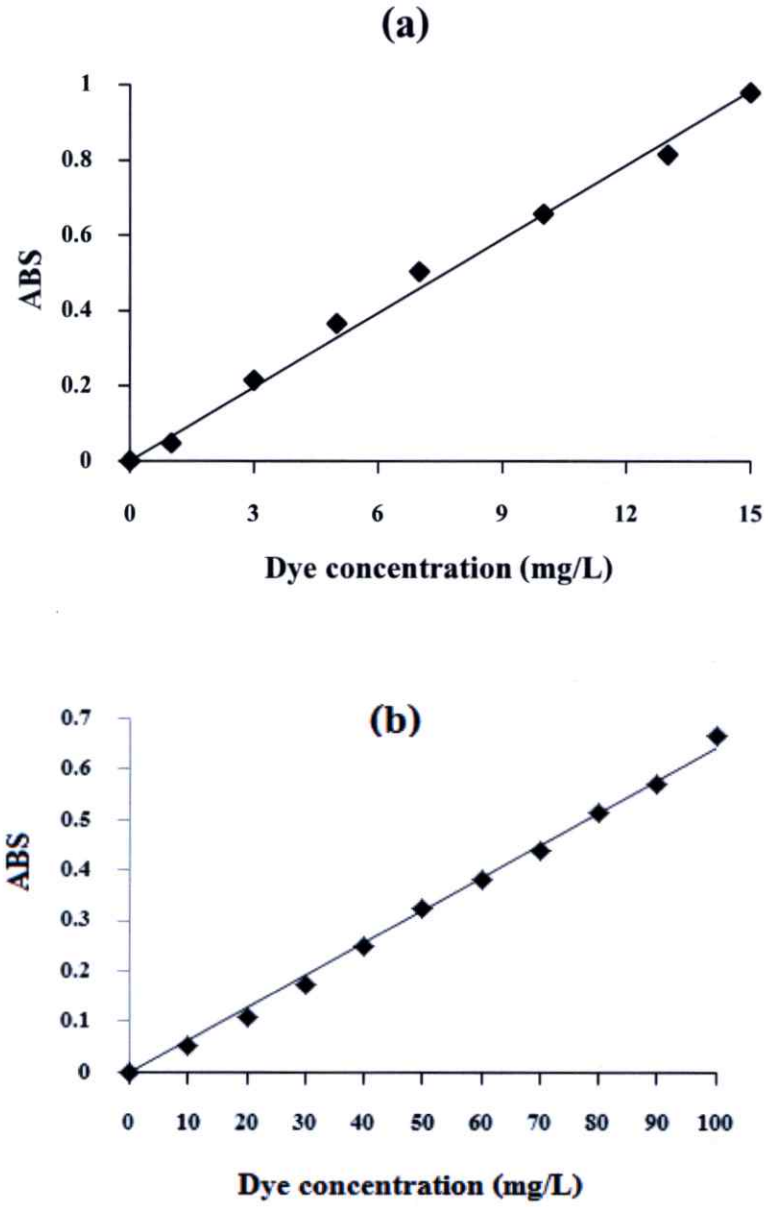

Figure A.1 Standard calibration curves of (a) BY1 and (b) RO16

Table A.1 The linear regression equations from the standard calibration curve of BY1 and RO16

Dye	Linear regression equation	R^2
Basic Yellow 1 (BY1)	y = 0.0659x	0.9997
Reactive Orange 16 (RO16)	y = 0.0064x	0.9999

Where y = UV-Vis absorbance

x = final dye concentration (mg/L).

Percentage of dye removal could be determined from equation (B.1):

$$\%\ dye\ removal = \frac{(C_I - C_f)}{C_I}\ x\ 100 \qquad \text{(B.1)}$$

The adsorption capacities of all adsorbents for each dye adsorbate (q_t, mg/g) were calculated by equation (B.2):

$$q_t = \frac{V(C_I - C_f)}{m} \qquad \text{(B.2)}$$

where C_I = Initial dye concentration (mg/L)

C_f = Final dye concentration (mg/L)

V = Volume of dye solution (L)

m = Amount of adsorbent (g)

b. Total organic carbon (TOC)

Total organic carbon (TOC) in the dye solutions before and after treatment processes was measured by TOC analyzer (Shimadzu, TOC-VCPH). Percentage of TOC removal could be determined from equation (B.4):

$$\%\ TOC\ removal = \frac{(TOC_I - TOC_f)}{TOC_I}\ x\ 100 \qquad \text{(B.3)}$$

where TOC_I = Initial concentration of total organic carbon (mg/L)

TOC_f = Final concentration of total organic carbon (mg/L)

A.2 Dye removal by adsorption process

A.2.1 Effect of adsorbent type

Table A.2 ABS and final concentration (mg/L) of dye and TOC of Na^+-MMT, Alpill-MMT-2.4-60-Str-rt and Alpill-MMT-2.4-30-Ultra-20 using BY1 concentration of 1000 mg/L and contact time of 120 min

	ABS	Final concentration	
		Dye (mg/L)	TOC (mg/L)**
Na^+-MMT	0.354*	537.17	210.97
Alpill-MMT-2.4-60-Str-rt	0.123*	186.64	102.82
Alpill-MMT-2.4-30-Ultra-20	0.037*	56.14	67.07

* 1 ml of treated BY1 solution was adjusted to 100 ml with distilled water

** Initial concentration of TOC = 442.3 mg/L

Table A.3 ABS and final concentration (mg/L) of dye and TOC of Alpill-MMT-2.4-60-Str-rt, Cu-ads-Alpill-MMT1 and Cu-ads-Alpill-MMT2 using BY1 concentration of 500 mg/L and contact time of 120 min

	ABS	Final concentration	
		Dye (mg/L)	TOC (mg/L)**
Alpill-MMT-2.4-60-Str-rt	0.185*	28.07	19.03
Cu-ads-Alpill-MMT1	0.399*	60.54	33.74
Cu-ads-Alpill-MMT2	0.359*	54.46	27.90

* 1 ml of treated BY1 solution was adjusted to 10 ml with distilled water

** Initial concentration of TOC = 193.9 mg/L

Table A.4 ABS and final concentration (mg/L) of dye and TOC of Alpill-MMT-2.4-60-Str-rt, Cu-ads-Alpill-MMT1 and Cu-ads-Alpill-MMT2 using RO16 concentration of 300 mg/L and contact time of 120 min

	ABS	Final concentration	
		Dye (mg/L)	TOC (mg/L)*
Alpill-MMT-2.4-60-Str-rt	1.851	289.08	83.66
Cu-ads-Alpill-MMT1	1.845	288.27	82.03
Cu-ads-Alpill-MMT2	1.846	288.45	82.06

* Initial concentration of TOC = 85.78 mg/L

A.2.2 Effect of initial dye concentration

Table A.5 Adsorption capacity (q_t, mg/g) of Alpill-MMT-2.4-60-Str-rt and Alpill-MMT-2.4-30-Ultra-20 using contact time of 120 min under various initial BY1 concentrations

Initial BY1 concentration (mg/L)	Adsorption capacity (q_t, mg/g)	
	Alpill-MMT-2.4-60-Str-rt	Alpill-MMT-2.4-60-Str-rt
0	0	0
50	4.95	4.98
100	9.86	9.87
300	29.38	29.41
500	47.19	48.95
700	62.33	67.49
1000	81.33	94.38
2000	81.48	95.90
3000	80.72	94.38

A.2.3 Effect of contact time

Table A.6 Adsorption capacity (q_t, mg/g) of Alpill-MMT-2.4-60-Str-rt and Alpill-MMT-2.4-30-Ultra-20 using BY1 concentration of 1000 mg/L under various contact times

Time (min)	Adsorption capacity (q_t, mg/g)	
	Alpill-MMT-2.4-60-Str-rt	Alpill-MMT-2.4-30-Ultra-20
0	0	0
30	53.71	53.11
60	68.89	75.87
90	73.44	84.06
120	81.33	94.38
150	82.85	94.68
180	83.45	93.93
210	82.24	95.14
240	81.18	94.53
270	81.79	95.90
300	81.33	96.35

Table A.7 Final concentration and percentage of dye removal of Alpill-MMT-2.4-60-Str-rt and Alpill-MMT-2.4-30-Ultra-20 after thermal regeneration using BY1 concentration of 1000 mg/L and contact time of 120 min

Adsorbent	Final dye concentration (mg/L)		Dye removal (%)	
	Alpill-MMT-2.4-60-Str-rt	Alpill-MMT-2.4-30-Ultra-20	Alpill-MMT-2.4-60-Str-rt	Alpill-MMT-2.4-30-Ultra-20
As-prepared	186.64	56.14	81.34	94.39
1st regeneration	233.68	98.63	76.63	90.14
2nd regeneration	300.45	157.81	69.95	84.22

A.2.4 Adsorption kinetics

Table A.8 Pseudo-first-order kinetics for dye adsorption onto Alpill-MMT-2.4-60-Str-rt and Alpill-MMT-2.4-30-Ultra-20 using BY1 concentration of 1000 mg/L

Time (min)	$\log(q_e-q_t)$ (mg/g)	
	Alpill-MMT-2.4-60-Str-rt	Alpill-MMT-2.4-30-Ultra-20
0	1.92	1.98
30	1.47	1.63
60	1.16	1.31
90	1.00	1.08
120	0.32	0.29
150	-0.21	0.22
180	-3.67	0.38
210	0.08	0.08
240	0.35	0.26
270	0.22	-0.33
300	0.32	-2.72

Table A.9 Pseudo-second-order kinetics for BY1 adsorption onto Alpill-MMT-2.4-60-Str-rt and Alpill-MMT-2.4-30-Ultra-20 using BY1 concentration of 1000 mg/L

Time (min)	t/q_t (mim.g/mg)	
	Alpill-MMT-2.4-60-Str-rt	Alpill-MMT-2.4-30-Ultra-20
0	0	0
30	0.55	0.56
60	0.87	0.79
90	1.22	1.07
120	1.47	1.27
150	1.81	1.58
180	2.15	1.91
210	2.55	2.20

Table A.9 (cont.)

Time (min)	t/q_t (mim.g/mg)	
	Alpill-MMT-2.4-60-Str-rt	Alpill-MMT-2.4-30-Ultra-20
240	2.956262	2.538684
270	3.301113	2.815348
300	3.688433	3.113386

A.2.5 Adsorption isotherms

Table A.10 Langmuir isotherms for BY1 adsorption onto Alpill-MMT-2.4-60-Str-rt and Alpill-MMT-2.4-30-Ultra-20 using contact time of 120 min

Alpill-MMT-2.4-60-Str-rt		Alpill-MMT-2.4-30-Ultra-20	
C_e (mg/L)	C_e/q_e	C_e (mg/L)	C_e/q_e
0.48	0.09	0.16	0.03
1.30	0.13	1.24	0.12
6.10	0.20	5.82	0.19
28.07	0.59	10.45	0.21
76.63	1.22	25.03	0.370
186.64	2.29	56.14	0.59
1185.12	14.54	1040.97	10.85
2192.71	27.16	2048.55	21.53

Table A.11 Freundlich isotherms for BY1 adsorption onto Alpill-MMT-2.4-60-Str-rt and Alpill-MMT-2.4-30-Ultra-20 using contact time of 120 min

Alpill-MMT-2.4-60-Str-rt		Alpill-MMT-2.4-30-Ultra-20	
$\log C_e$	$\log q_e$	$\log C_e$	$\log q_e$
-0.31	0.69	-0.77	0.69
0.11	0.99	0.09	0.99
0.78	1.46	0.76	1.46
1.44	1.67	1.01	1.682
1.88	1.79	1.39	1.82

Table A.11 (cont.)

Alpill-MMT-2.4-60-Str-rt		Alpill-MMT-2.4-30-Ultra-20	
$\log C_e$	$\log q_e$	$\log C_e$	$\log q_e$
2.27102	1.910279	1.749316	1.974905
3.073766	1.911089	3.017439	1.981832
3.340982	1.907026	3.311448	1.978382

A.2.6 Continuous adsorption

Table A.12 Continuous BY1 adsorption onto Alpill-MMT-2.4-30-Ultra-20 using initial dye concentration of 300 mg/L

No.	Volume (ml)	ABS	Final concentration (mg/l)**	Dye removal (%)	Dye elimination (mg)
1	10	0.021	0.31	99.89	2.99
2	10	0.079	1.19	99.60	2.98
3	10	0.082	1.24	99.59	2.98
4	10	0.081	1.22	99.59	2.98
5	10	0.083	1.25	99.58	2.98
6	10	0.088	1.33	99.56	2.98
7	10	0.089	1.35	99.56	2.988
8	10	0.094	1.42	99.53	2.98
9	10	0.118	1.79	99.41	2.98
10	10	0.123	1.86	99.39	2.98
11	10	0.201	3.05	99.00	2.97
12	10	0.382	5.79	98.11	2.94
13	10	0.094*	71.32	76.76	2.30
14	10	0.126*	95.59	68.86	2.06
15	10	0.132*	100.15	67.37	2.02
16	10	0.14*	106.22	65.40	1.96
17	10	0.144*	109.25	64.41	1.93
18	10	0.151*	114.56	62.68	1.88

Table A.12 (cont.)

No.	Volume (ml)	ABS	Final concentration (mg/l)**	Dye removal (%)	Dye elimination (mg)
19	10	0.163*	123.67	59.71	1.79
20	10	0.162*	122.91	59.96	1.79
21	10	0.177*	134.29	56.25	1.68
22	10	0.18*	136.57	55.51	1.66
23	10	0.193*	146.43	52.30	1.56
24	10	0.197*	149.46	51.31	1.53
25	10	0.198*	150.22	51.06	1.53
26	10	0.2*	151.74	50.57	1.51
27	10	0.201*	152.50	50.32	1.50
28	10	0.207*	157.05	48.84	1.461
29	10	0.208*	157.81	48.59	1.45
30	10	0.217*	164.64	46.37	1.39
31	10	0.219*	166.16	45.87	1.37
32	10	0.223*	169.19	44.88	1.34
33	10	0.224*	169.95	44.64	1.33
34	10	0.2258	170.71	44.39	1.33
35	10	0.237*	179.81	41.42	1.24
36	10	0.268*	203.33	33.76	1.01
37	10	0.288*	218.51	28.82	0.86
38	10	0.298*	226.10	26.35	0.79
39	10	0.305*	231.41	24.62	0.73
40	10	0.308*	233.68	23.88	0.71
41	10	0.318*	241.27	21.40	0.64
42	10	0.328*	248.86	18.93	0.56
43	10	0.329*	249.62	18.69	0.56
44	10	0.335*	254.17	17.20	0.51
45	10	0.34*	257.96	15.97	0.47
46	10	0.34*	257.96	15.97	0.47

Table A.12 (cont.)

No.	Volume (ml)	ABS	Final concentration (mg/l)**	Dye removal (%)	Dye elimination (mg)
47	10	0.354*	268.58	12.51	0.37
48	10	0.355*	269.34	12.26	0.36
49	10	0.358*	271.62	11.52	0.34
50	10	0.364*	276.17	10.04	0.30
51	10	0.368*	279.21	9.05	0.27
52	10	0.368*	279.21	9.05	0.27
53	10	0.3728*	282.24	8.06	0.24
54	10	0.384*	291.35	5.09	0.15
55	10	0.3898*	295.14	3.86	0.11
56	10	0.388*	294.38	4.10	0.12
57	10	0.391*	296.66	3.36	0.10
58	10	0.394	298.93	2.62	0.07
59	10	0.395*	299.69	2.37	0.07
60	10	0.402*	305.00	0.64	0.01
61	10	0.401*	304.24	0.89	0.02
62	10	0.404*	306.52	0.15	0.00
63	10	0.404*	306.52	0.15	0.00
64	10	0.401*	304.24	0.89	0.02
65	10	0.403*	305.76	0.40	0.01
66	10	0.404*	306.52	0.15	0.00
67	10	0.404*	306.52	0.15	0.00
68	10	0.403*	305.76	0.40	0.01
69	10	0.404*	306.52	0.15	0.00
70	10	0.403*	305.76	0.40	0.01
					83.83***

* 1 ml of treated BY1 solution was adjusted to 50 ml with distilled water

** Initial dye concentration of BY1 = 307 mg/L

*** Total dye adsorption capacity

A.3 Dye removal by oxidation process

Table A.13 Percentage of dye and TOC removal when using Alpill-MMT-2.4-60-Str-rt in the Fenton process (Alpill-MMT-2.4-60-Str-rt /H_2O_2) and Cu-ads-Alpill-MMTs in the Fenton (Cu-ads-Alpill-MMTs/H_2O_2) and photo Fenton process (Cu-ads-Alpill-MMTs/H_2O_2/UV)

Processes	Dye removal (%)						TOC removal (%)					
	Time (min)						Time (min)					
	30	60	90	120	240	360	30	60	90	120	240	360
Alpill-MMT-2.4-60-Str-rt /H_2O_2	-	4	-	9	15	16	-	2	-	5	10	11
Cu-ads-Alpill-MMT1/ H_2O_2	-	80	-	87	97	100	-	63	-	74	88	100
Cu-ads-Alpill-MMT2/ H_2O_2	-	72	-	85	94	99	-	46	-	69	88	98
Cu-ads-Alpill-MMT1/ H_2O_2/UV	98	100	100	100	100	100	91	98	99	100	100	100
Cu-ads-Alpill-MMT2/ H_2O_2/UV	95	100	100	100	100	100	91	98	99	100	100	100

Table A.14 Percentages of dye and TOC removals of Cu-im-Alpill-MMT in the Fenton (Cu-im-Alpill-MMT/H_2O_2) and photo Fenton systems (Cu-im-Alpill-MMT/H_2O_2/UV)

Systems	Dye removal (%)						TOC removal (%)					
	Time (min)						Time (min)					
	30	60	90	120	240	360	30	60	90	120	240	360
Cu-im-Alpill-MMT-4wt%/H_2O_2	-	54	-	68	80	88	-	36	-	52	75	81
Cu-im-Alpill-MMT-4wt%/H_2O_2/UV	44	63	69	75	86	89	35	48	56	65	80	81
Cu-im-Alpill-MMT-7wt%/H_2O_2	-	61	-	77	89	94	-	45	-	64	85	93
Cu-im-Alpill-MMT-7wt%/H_2O_2/UV	74	82	91	94	97	98	67	80	89	91	93	95
Cu-im-Alpill-MMT-10wt%/H_2O_2	-	70	-	83	94	99	-	56	-	74	88	96
Cu-im-Alpill-MMT-10wt%/H_2O_2/UV	98	99	100	100	100	100	93	99	98	100	100	100
Cu-im-Alpill-MMT-13wt%/H_2O_2	-	73	-	85	95	99	-	58	-	74	88	97
Cu-im-Alpill-MMT-13wt%/H_2O_2/UV	98	100	100	100	100	100	95	99	100	100	100	100

APPENDIX B

SEM-EDX

B.1 Copper doped aluminium pillared montmorillonite

B.1.1 Ultrasonic assisted adsorption method

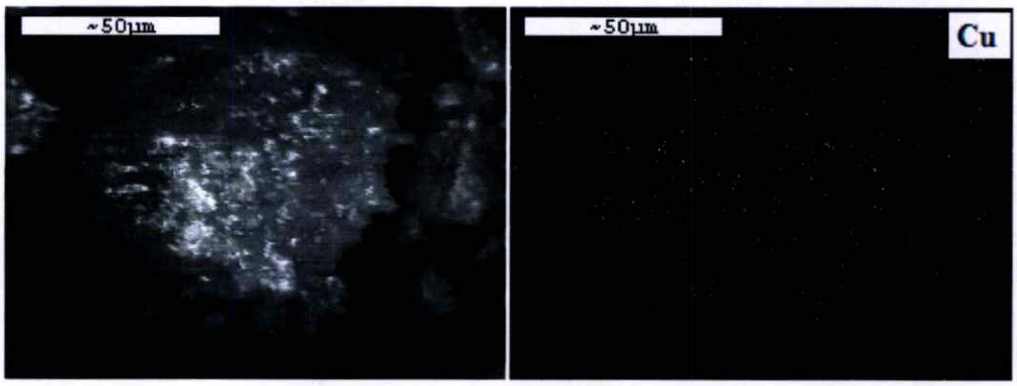

Cu-ads-Alpill-MMT1

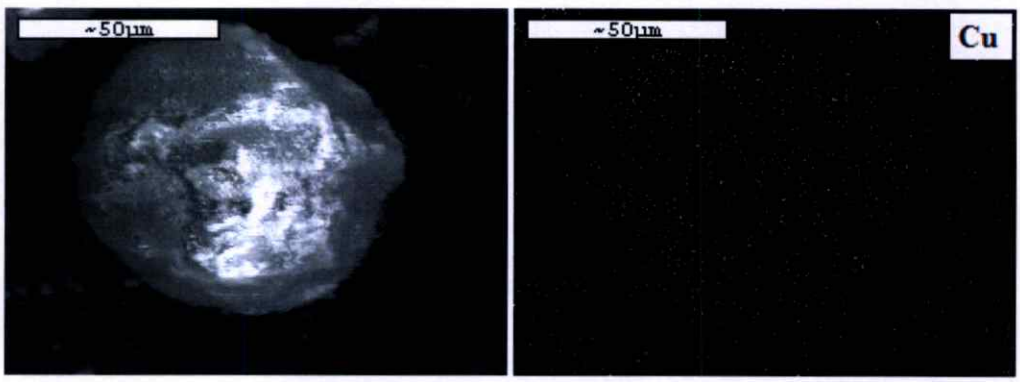

Cu-ads-Alpill-MMT2

Figure B.1 SEM micrographs mapping image with Cu of Cu-ads-Alpill-MMTs

Table B.1 Percentage of Cu atomic in Cu-asd-Alpill-MMTs

Sample	Atomic of Cu (%)			
	1	2	3	average
Cu-ads-Alpill-MMT1	1.17	1.94	1.31	1.47
Cu-adsAlpill-MMT2	0.38	0.57	0.85	0.60

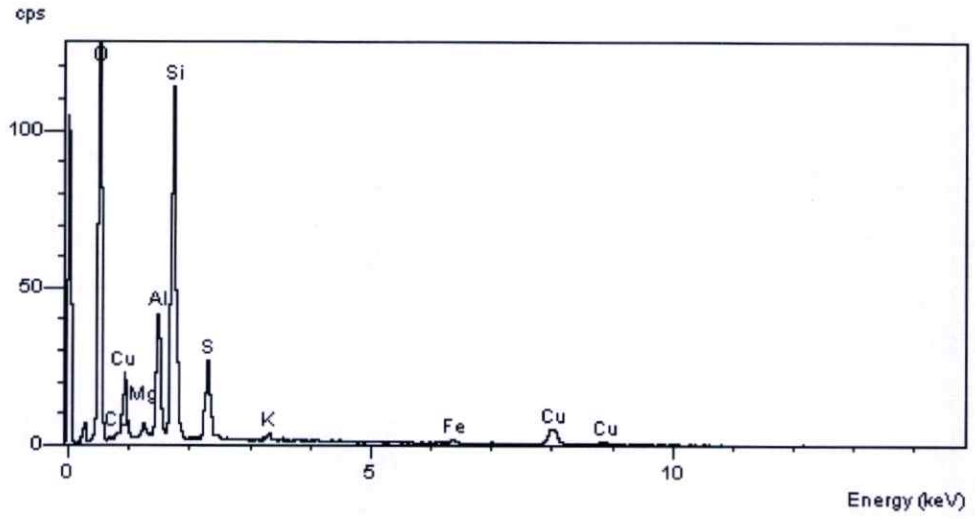

Position 1

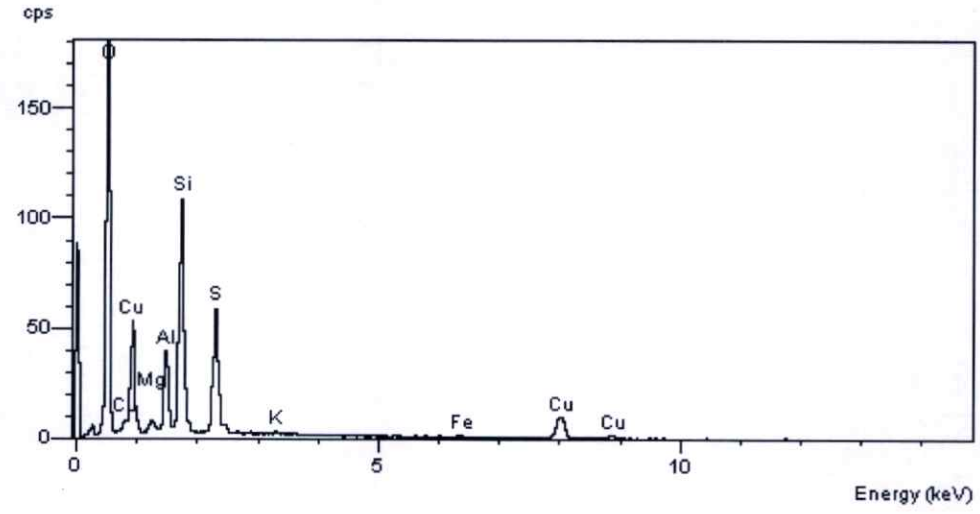

Position 2

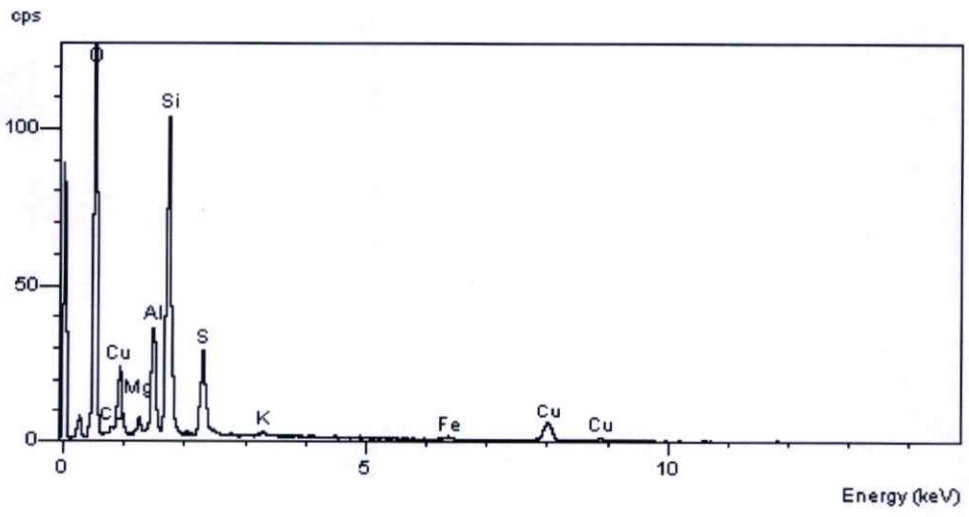

Position 3

Figure B.2 EDX spectrum of Cu-ads-Alpill-MMT1

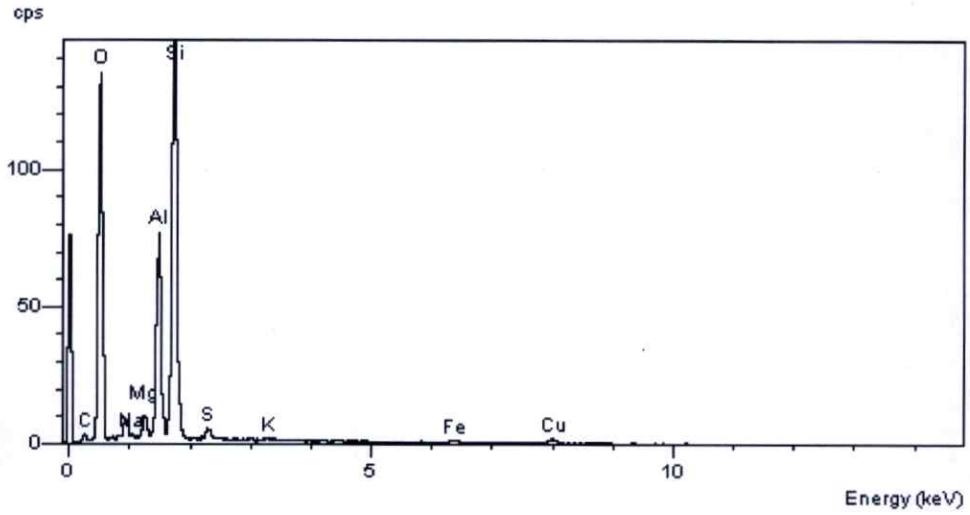

Position 1

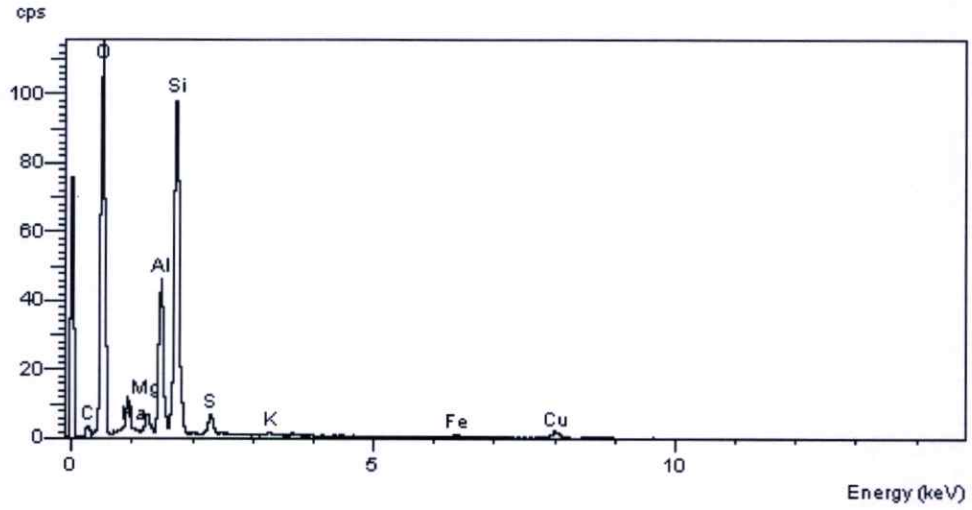

Position 2

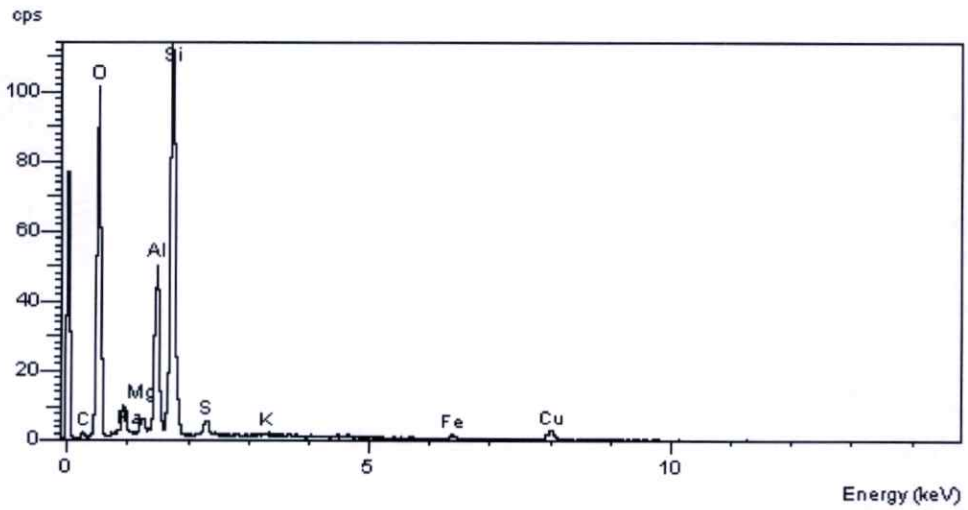

Position 3

Figure B.3 EDX spectrum of Cu-ads-Alpill-MMT2

B.1.2 Impregnation method

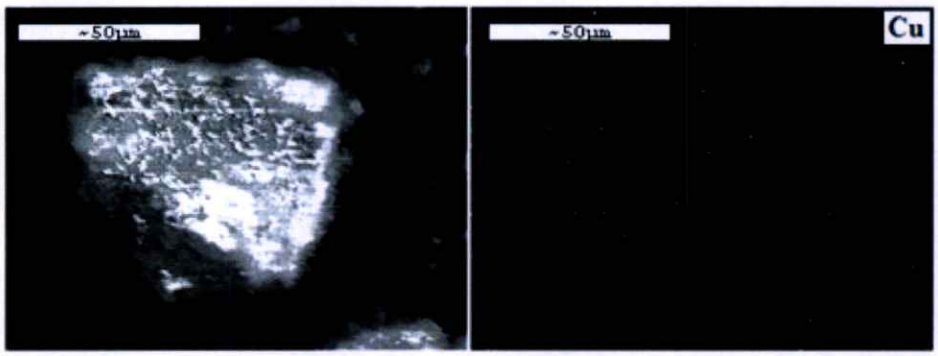

Cu-im-Alpill-MMT-4wt%

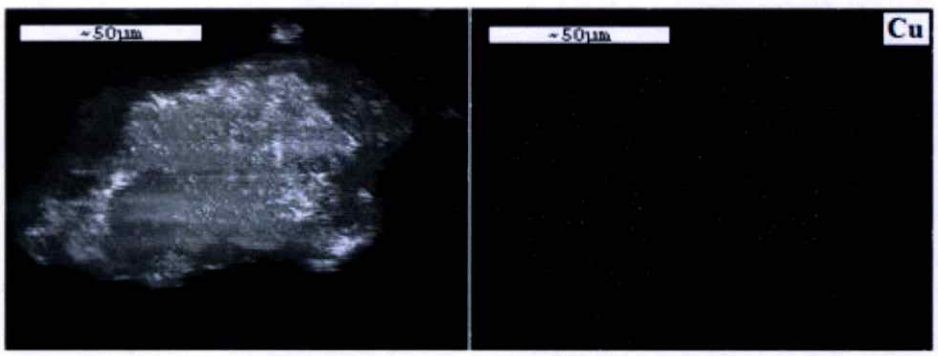

Cu-im-Alpill-MMT-7wt%

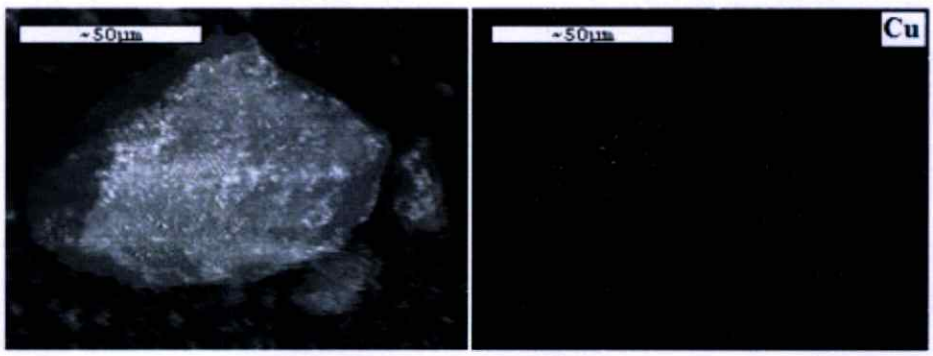

Cu-im-Alpill-MMT-10wt%

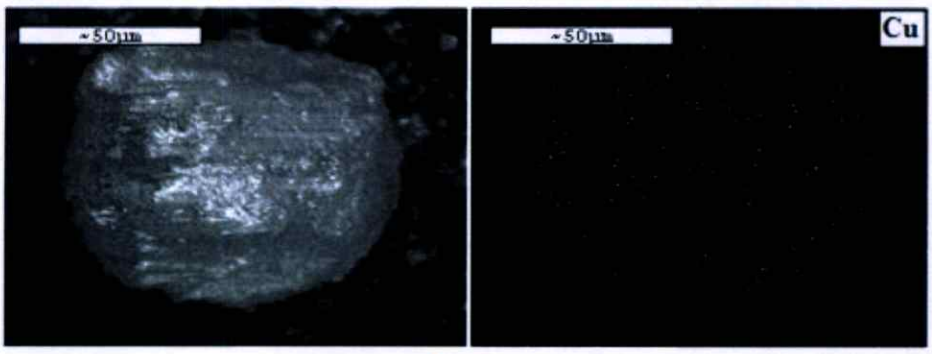

Cu-im-Alpill-MMT-13wt%

Figure B.4 SEM micrographs mapping image with Cu of Cu-ads-Alpill-MMTs

Table B.2 Percentage of Cu atomic in Cu-im-Alpill-MMTs

Sample	Atomic of Cu (%)			
	1	2	3	average
Cu-im-Alpill-MMT-4wt%	0.22	0.15	0.33	0.23
Cu-im-Alpill-MMT-7wt%	0.30	0.23	0.34	0.29
Cu-im-Alpill-MMT-10wt%	0.67	0.32	0.26	0.42
Cu-im-Alpill-MMT-13wt%	0.85	0.67	1.00	0.84

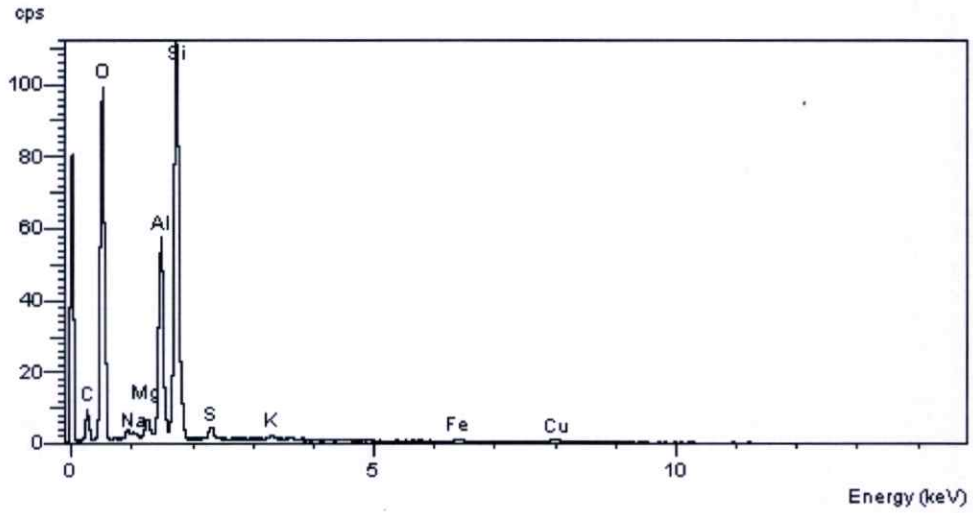

Position 1

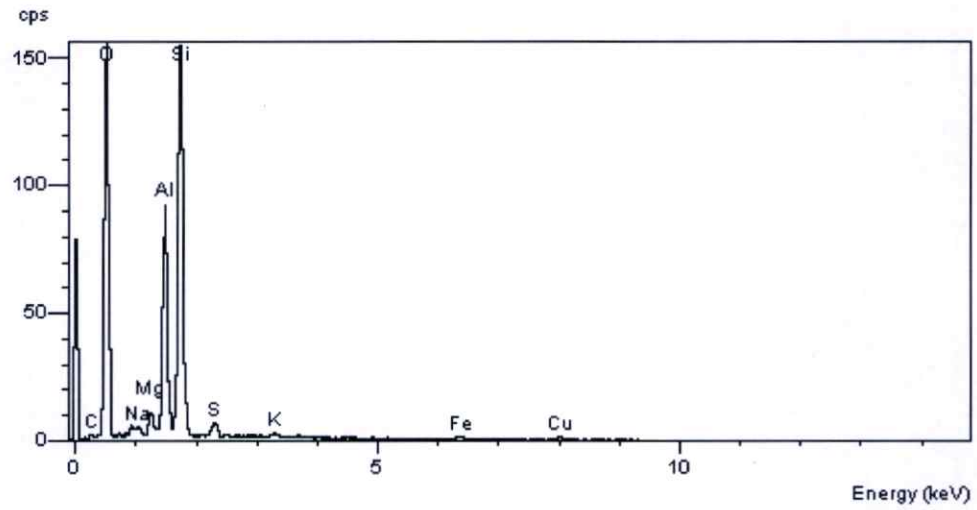

Position 2

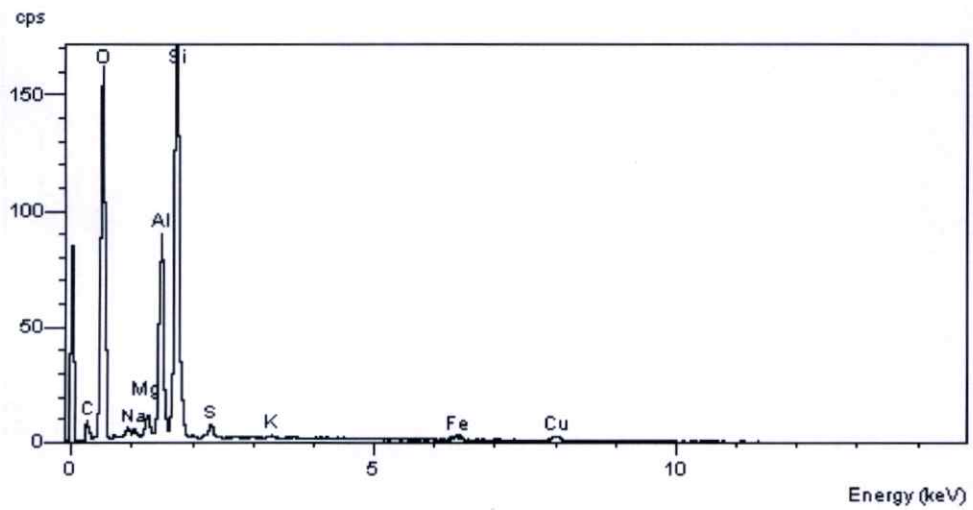

Position 3

Figure B.5 EDX spectrum of Cu-im-Alpill-MMT-4wt%

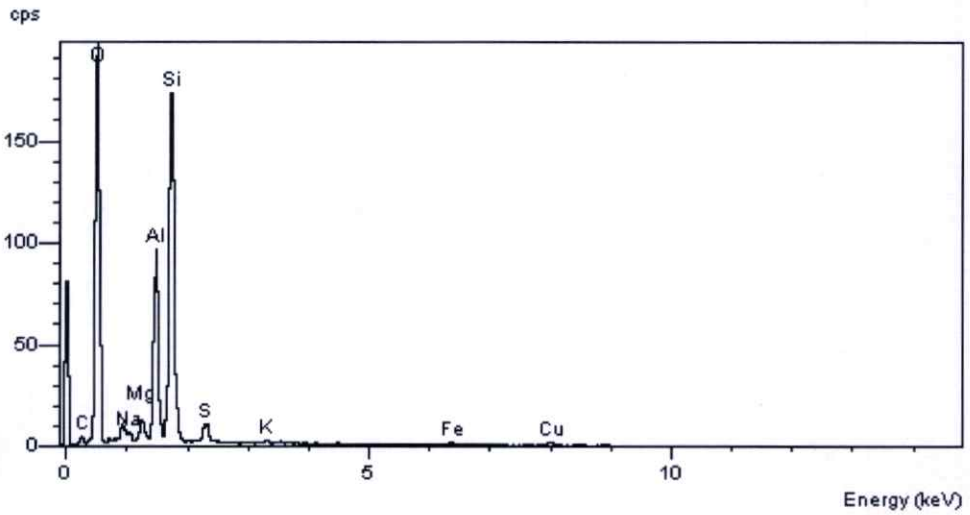

Position 1

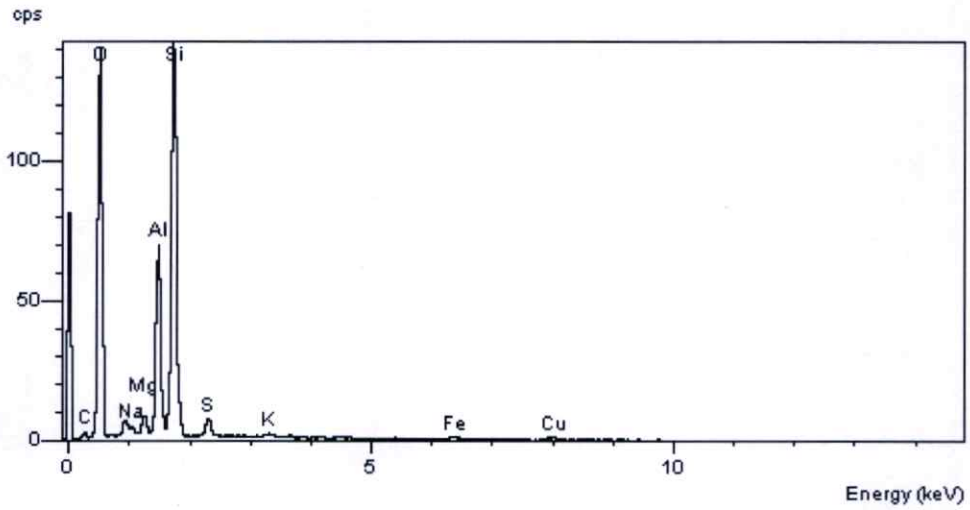

Position 2

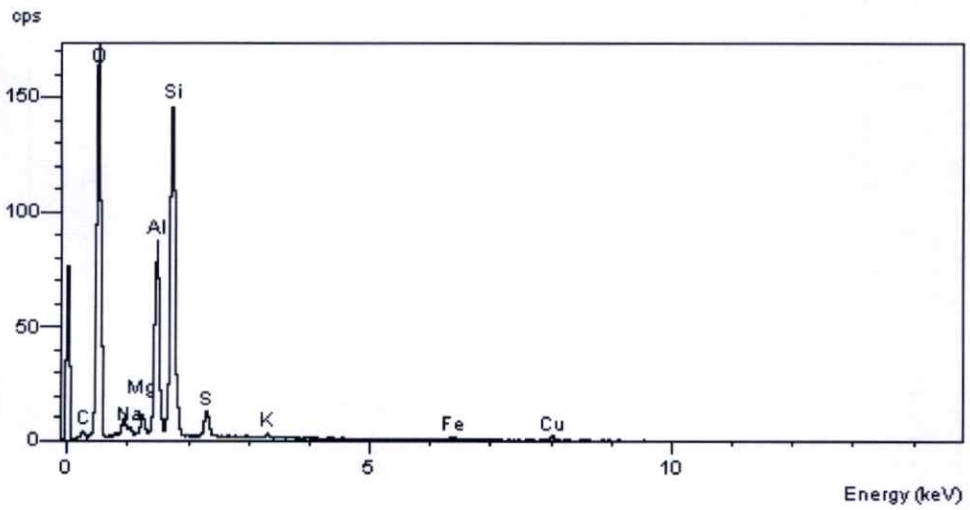

Position 3

Figure B.6 EDX spectrum of Cu-im-Alpill-MMT-7wt%

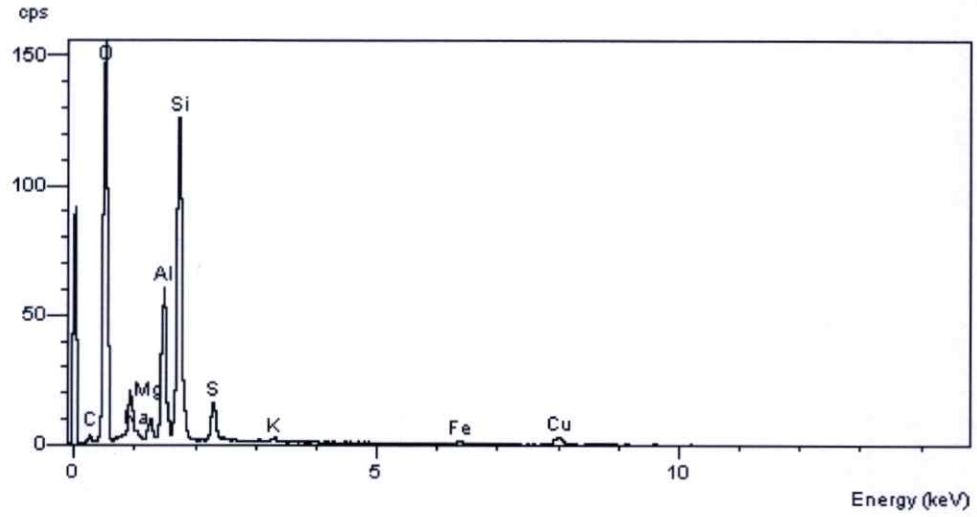

Position 1

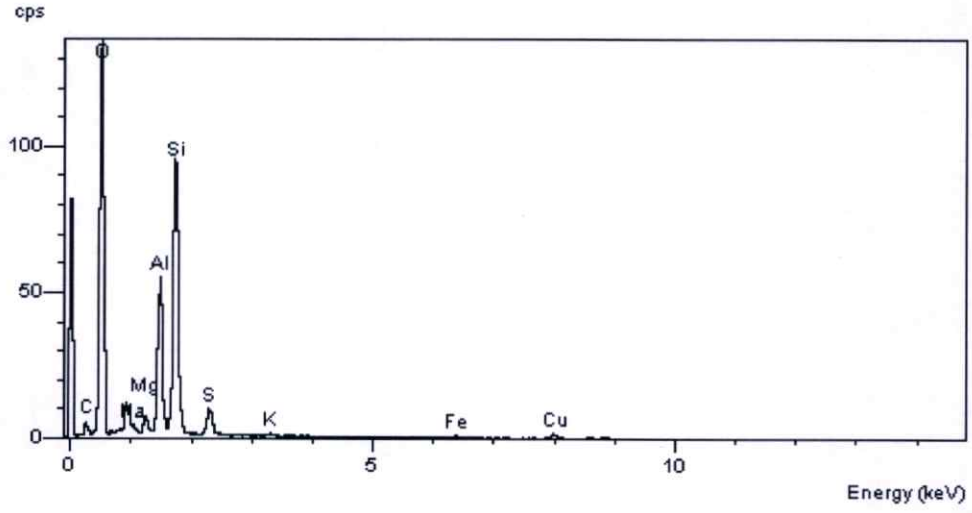

Position 2

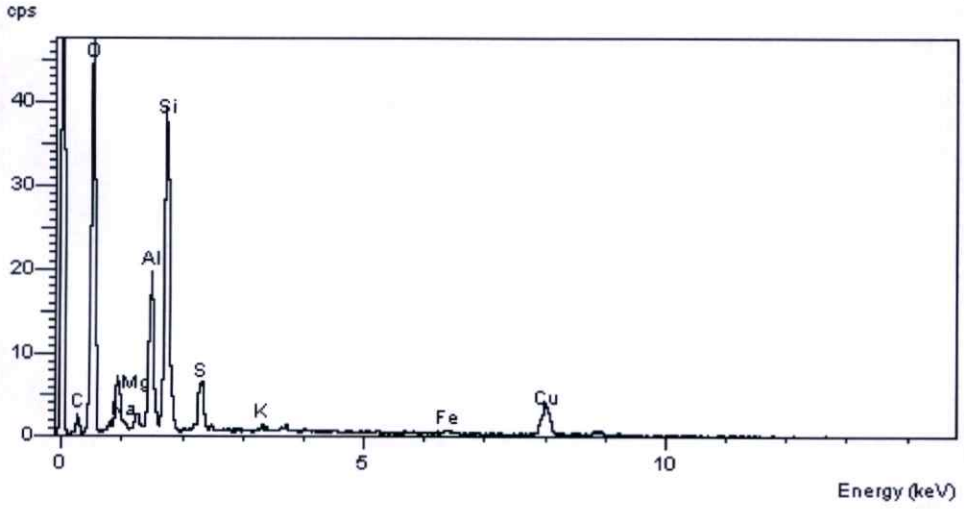

Position 3

Figure B.7 EDX spectrum of Cu-im-Alpill-MMT-10wt%

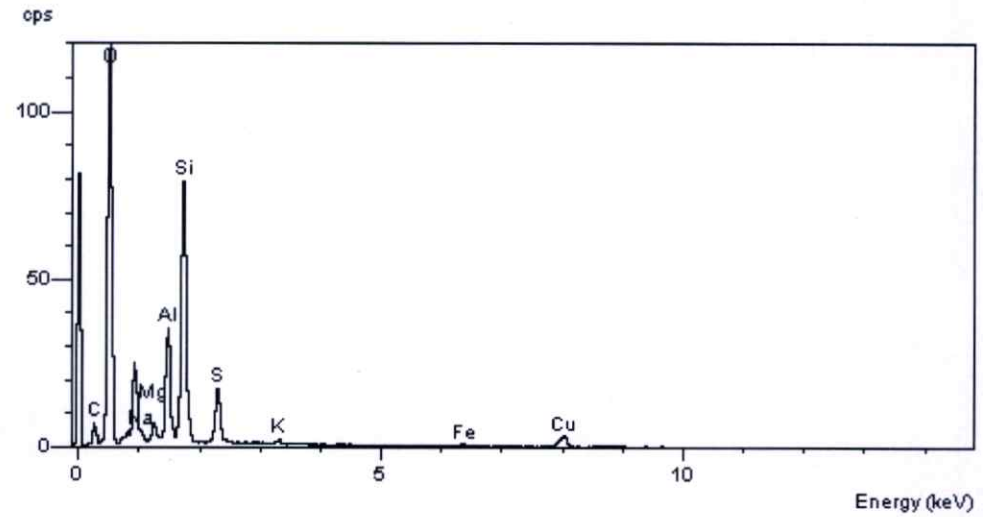

Position 1

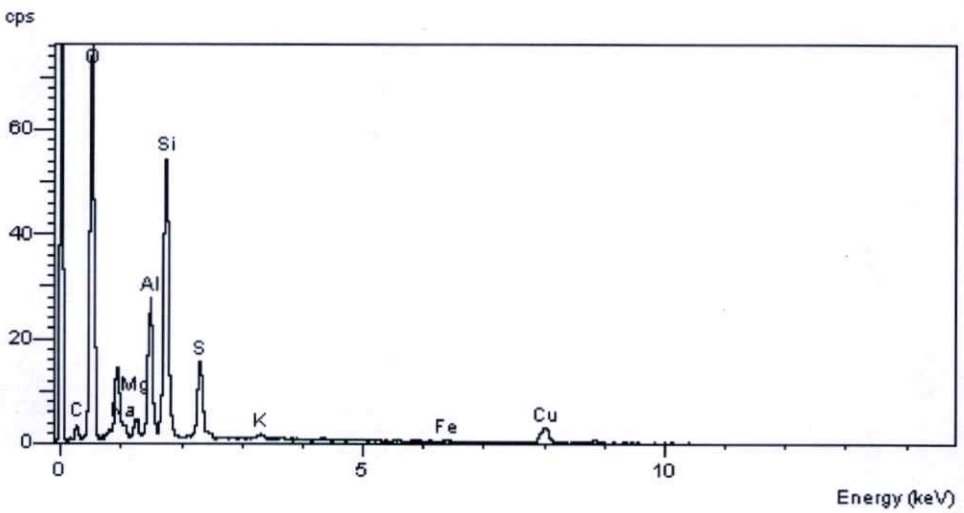

Position 2

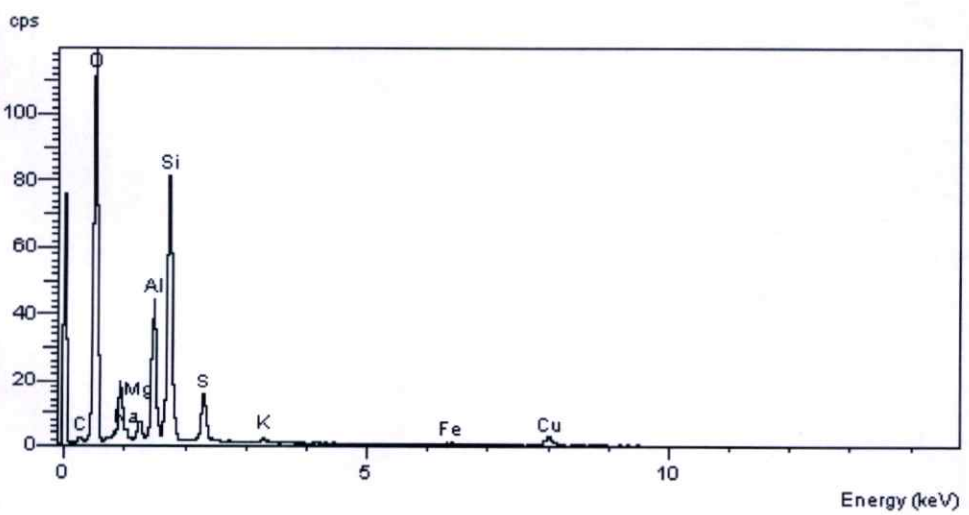

Position 3

Figure B.8 EDX spectrum of Cu-im-Alpill-MMT-13wt%

APPENDIX C
ZETA POTENTIALS

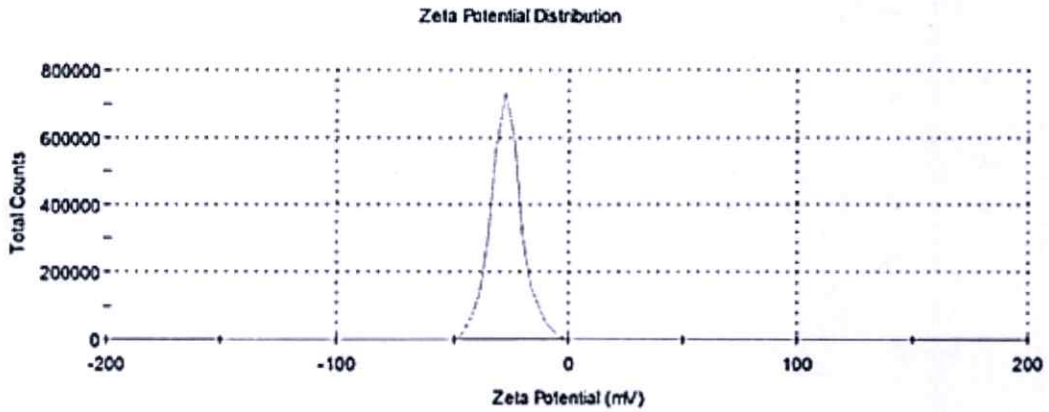

Alpill-MMT-2.4-60-Str-rt

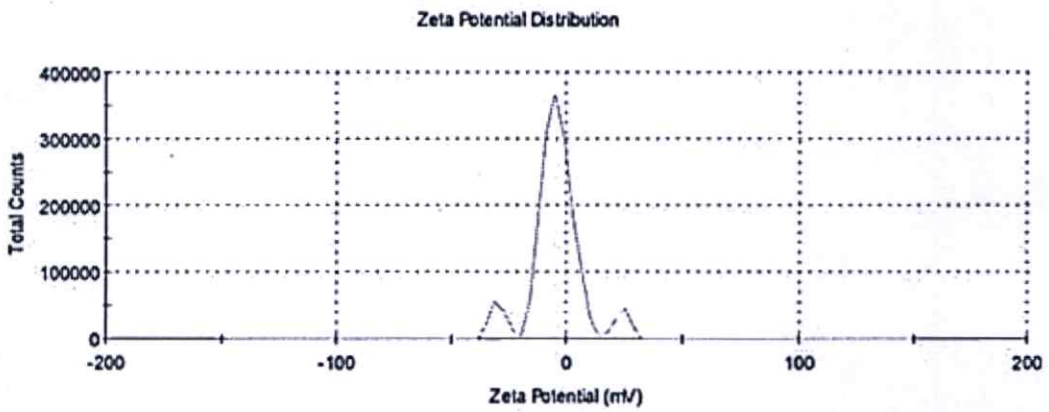

Cu-ads-Alpill-MMT1

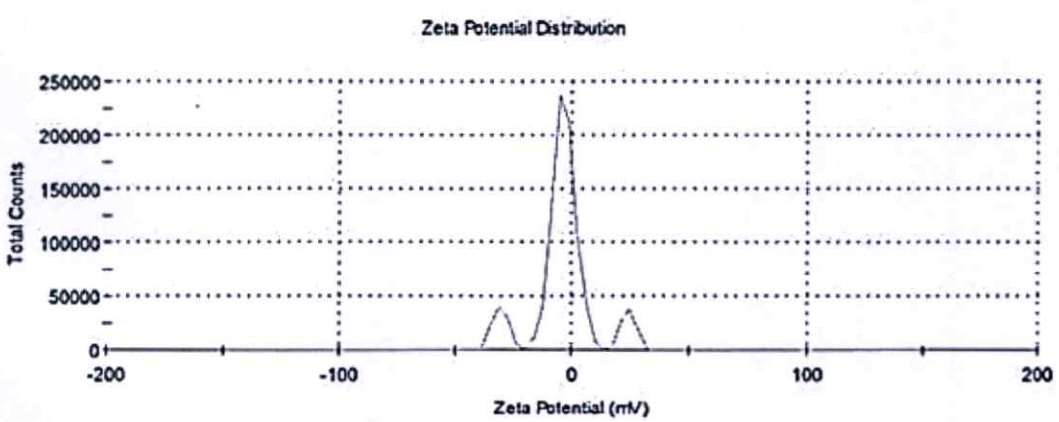

Cu-ads-Alpill-MMT2

Figure C.1 Zeta potential distribution of Alpill-MMT-2.4-60-Str-rt and Cu-ads-Alpill-MMTs

Author Biography

Name: Miss Pratyaporn Tepmatee

Date of Birth: February 12, 1984

Nationality: Thai

University Education:

2004 - 2007 **Bachelor Degree:** Bachelor of Engineering, Chemical Engineering Burapha University

2007 - 2009 **Master Degree:** Master of Engineering, Chemical Engineering Chulalongkorn University

2009 - 2015 **Doctor of Philosophy Degree:** Doctor of Philosophy of Science, Nanoscience and Nanotechnology
King Mongkut's Institute of Technology Ladkrabang

Work experiences:

2011 - 2013 Researcher Assistant, Development of nanoporous aluminium - pillared clay and copper doped alumlnium-pillared clay for dye-containing wastewater treatment.

Conferences:

2011 Pratyaporn Tepmatee, and Punnama Siriphannon
Proceeding: "Development of Nanoporous Aluminium-pillared montmorillonite adsorbents for dye containing wastewater treatment",
The 6 th PACCON Chemstry for Materials & Nanotechnology (MNT).

Journals:

2013 Pratyaporn Tepmatee, and Punnama Siriphannon
Published: "Effect of preparation method on structure and adsorption capacity of aluminum illared montmorillonite",
Materials Research Bulletin; Vol 48; pp 4856-4866.

2015 Pratyaporn Tepmatee, and Punnama Siriphannon
Published: "Nanoporous Copper Doped Aluminium Pillared Montmorillonite for Dye-containing Wastewater Treatment",
Water Environment Federation; DOI:
10.2175/106143015X14362865227076